

①

AFIT/DS/ENP/92-1

**AD-A256 568**



**MULTI-ION AMBIPOLAR DIFFUSION**

**DISSERTATION**

**Thomas E. Gist  
Major, USAF**

AFIT/DS/ENP/92-1

**92-28141**



## MULTI-ION AMBIPOLAR DIFFUSION

**DISSERTATION**

**Presented to the Faculty of the School of Engineering  
of the Air Force Institute of Technology**

# Air University

**In Partial Fulfillment of the  
Requirements for the Degree of  
Doctor of Philosophy**

**Thomas E. Gist, B.S., M.S.**

**Major, USAF**

**July 1992**

DTIC OADR 14 JAN 1969

**Aproved for public release; distribution unlimited**

AFIT/DS/ENP/92-1

MULTI-ION AMBIPOLAR DIFFUSION

Thomas E. Gist, B.S, M.S  
Major, USAF

Approved:

Tom F. Bailey

20 July '92

Alan Hawsadden

20<sup>th</sup> July 1992

Dennis Lavin

20 July 1992

[Signature]

20 JULY 1992

JM & Shang

20 17 192

Accepted:

Robert Alabur L 20 July '92  
Dean, School of Engineering

## Acknowledgments

I have had a lot of help in this effort. First, I would like to thank the present and past members of my committee. Dr Donn Shankland's guidance and advice were instrumental in my finding a dissertation topic. Dr William Bailey's willingness to take over as Chairman after Dr Shankland's retirement, and his continual support, was one of the things that made completion possible. The willingness of Capt Glen Perram, Dr Dennis Quinn, and Dr Joseph Shang to join the committee late in the effort, and then respond quickly with cogent advice, were essential to the final success of my research.

I would also like to thank my close friends, Majors Jamie and Diane Varni, for their unflagging encouragement, and a number of coworkers who were vital in this project. Special thanks go to Major Jamie Varni, Dr Charles DeJoseph, Dr Court Bohn, Dr Biswa Ganguly, Dr Peter Bletzing, Lt Col Rich Durham, Lt Col John Souders, Dr Ken Boyer, and Capt Dave Bell, whose suggestion of the relaxation algorithm led to the success of my numerical solutions.

One man did more to help me complete this dissertation than any other. Dr Alan Garscadden was my guiding light throughout this entire eleven year project. I cannot list all the areas where his support and help was vital.

Finally, and most importantly, I want to thank my children; Andi, Stephanie, and Michael; and most of all my wife, Karen, for allowing me to play absentee father and husband for the years it took to finish this task.

Thomas E. Gist



## *Table of Contents*

<b>Acknowledgments</b> .....	<b>iii</b>
<b>List of Figures</b> .....	<b>ix</b>
<b>List of Tables</b> .....	<b>xi</b>
<b>List of Symbols</b> .....	<b>xii</b>
<b>Abstract</b> .....	<b>xiv</b>
<b>I. Introduction and Background</b> .....	<b>1-1</b>
<b>Introduction</b> .....	<b>1-1</b>
<b>Rationale for Investigation</b> .....	<b>1-1</b>
<b>Summary of the Investigation</b> .....	<b>1-2</b>
<b>Momentum and Continuity Equations</b> .....	<b>1-5</b>
<b>II. Historical Perspective of the Theory of Multi-Ion Discharges</b> .....	<b>2-1</b>
<b>Introduction</b> .....	<b>2-1</b>
<b>Single-ion Models</b> .....	<b>2-2</b>
<b>Schottky's Model of Ambipolar Diffusion</b> .....	<b>2-3</b>
<b>Rationale for Ambipolar Diffusion</b> .....	<b>2-3</b>
<b>Single-ion Ambipolar Diffusion</b> .....	<b>2-5</b>
<b>Derivation of Schottky's Model</b> .....	<b>2-6</b>
<b>Schottky's Solutions</b> .....	<b>2-7</b>
<b>Tonks and Langmuir</b> .....	<b>2-9</b>
<b>Ecker</b> .....	<b>2-13</b>
<b>Allis and Rose</b> .....	<b>2-13</b>
<b>Summary for Single Ion Models</b> .....	<b>2-14</b>
<b>Multi-ion Ambipolar Diffusion</b> .....	<b>2-15</b>
<b>Proportional Solutions</b> .....	<b>2-16</b>
<b>Oskam</b> .....	<b>2-16</b>
<b>Other Proportional Solutions</b> .....	<b>2-19</b>
<b>Nonproportional Solutions</b> .....	<b>2-20</b>
<b>Edgley and von Engel</b> .....	<b>2-20</b>
<b>Ferreira, Gousset, and Touzeau.</b> .....	<b>2-21</b>
<b>Valentini</b> .....	<b>2-22</b>
<b>Wunderer</b> .....	<b>2-25</b>
<b>Conclusions Drawn from Comparison of the Various Models</b> .....	<b>2-25</b>
<b>Problems To Be Addressed</b> .....	<b>2-27</b>
<b>Proportionality</b> .....	<b>2-27</b>
<b>Analytic Solutions</b> .....	<b>2-27</b>
<b>Scaling Relationships</b> .....	<b>2-28</b>
<b>III. New Ambipolar Diffusion Model</b> .....	<b>3-1</b>
<b>Introduction</b> .....	<b>3-1</b>

General Formulation .....	3-1
Time-Independent Formulation, Positive Ions .....	3-6
Dimensionless Differential Equations .....	3-9
Justification for Dimensionless Form .....	3-9
Definition of the Dimensionless Variables .....	3-10
Dimensionless Equations .....	3-11
Conclusions .....	3-13
 IV. Implications of Proportionality .....	 4-1
Introduction .....	4-1
Definitions of the Concept of Proportionality .....	4-2
Proportionality for the Normalized Equations .....	4-2
Other Expressions for Proportionality .....	4-2
Physical Implications .....	4-3
Ratio of the Fluxes .....	4-4
Source Term Proportionality .....	4-5
Case Studies of Proportionality for Particular Source Terms .....	4-6
Volume Ionization .....	4-7
External Ionization .....	4-9
External and Volume Ionization .....	4-10
Using Proportionality to Determine Solutions .....	4-11
Multi-ion Ambipolar Diffusion Coefficient .....	4-11
Summary of Results .....	4-13
 V. Analytic Solutions to the Model .....	 5-1
Introduction .....	5-1
Definition of Cases of Interest .....	5-1
Geometries. ....	5-1
Sources .....	5-2
Boundary Conditions .....	5-3
Small-e-Flux Approximation .....	5-4
Summary of Solutions .....	5-7
External Ionization. ....	5-7
PX .....	5-8
PE .....	5-8
CX .....	5-9
Volume Ionization. ....	5-9
PV .....	5-10
CV .....	5-10
PT .....	5-10
Exact Solutions .....	5-11
External Sources .....	5-11
Planar Geometry .....	5-11
PX Case .....	5-14
PE Case .....	5-18
Cylindrical Geometry .....	5-21
CX Case .....	5-23
General Self-Ionization Sources .....	5-24

Planar Geometry. ....	5-25
PV Case. ....	5-25
PT Case ....	5-32
Cylindrical Geometry ....	5-35
CV Case ....	5-35
Summary ....	5-37
 VI. Numerical Solutions to the Model ....	 6-1
Introduction ....	6-1
Rationale ....	6-1
Cases To Be Examined ....	6-2
Measure of Nonproportionality ....	6-3
External Ionization ....	6-6
Volume Ionization ....	6-7
Algorithmic Method ....	6- 8
Comparisons ....	6-10
Comparison to Wunderer's Results ....	6-10
Temperature As an Eigenvalue ....	6-17
Comparison to Schmidt ....	6-21
Basis for Comparison with the New Model ....	6-23
$N_2^+ - N_4^+$ Systems ....	6-25
$N_2^+ - HN_2^+$ System ....	6-33
Summary of Verification Results ....	6-41
Investigation of Generic Plasma Systems ....	6-41
External Sources ....	6-42
External Source plus Recombination ....	6-43
High-Recombination Example ....	6-46
Nonproportionality ....	6-59
Conclusions ....	6-66
External Sources plus Charge Transfer ....	6-66
High Charge Transfer Example ....	6-68
Nonproportionality ....	6-74
Similarity Parameters ....	6-75
Summary of Charge Transfer Results ....	6-77
Volume Sources ....	6-78
Volume Source plus Recombination ....	6-78
High-Recombination Example ....	6-82
Electron Temperature versus Recombination ....	6-85
Deviations from Proportionality ....	6-90
Conclusions ....	6-91
General Result ....	6-92
Summary of Results ....	6-95
Comparisons ....	6-95
General Plasma Systems ....	6-97
 VII. Conclusions and Recommendations ....	 7-1
Introduction ....	7-1
Regime of Validity of Ambipolar Diffusion ....	7-2

Criteria for Determining an Appropriate Multi-Ion Model .....	7-6
Basis for Evaluating Decisions .....	7-8
Implementation of the Decision Tree .....	7-11
Results of the Investigation .....	7-21
Summary of Results .....	7-21
Proportionality .....	7-22
Requirements for Proportionality .....	7-22
Applications of the Proportionality Conditions .....	7-24
Analytic Solutions .....	7-26
Influence of Charge Transfer on Plasma Balance .....	7-28
Recommendations for Future Research .....	7-31
New Investigations Suggested by the Present Model .....	7-31
N2 -H2 Investigations .....	7-32
Multi-ion Effects on Sheaths .....	7-33
Extensions of the Present Model .....	7-36
Additional Ion Species .....	7-36
More Accurate Kinetic Coefficients .....	7-36
Expansion of Sources .....	7-36
Magnetic Fields .....	7-39
Spatial Temperature Variations .....	7-43
Conclusions .....	7-46
 Appendix A. Derivation of the Dimensionless Equations .....	 A-1
 Appendix B. Integration of the Equation for N .....	 B-1
 Appendix C. Numerical Algorithms .....	 C-1
Introduction .....	C-1
Relaxation Method .....	C-2
Previous Methods .....	C-2
Relaxation Method Overall Methodology .....	C-3
Explanation of the Relaxation Method .....	C-3
Strengths and Weaknesses of Relaxation .....	C-5
Brent Algorithm .....	C-6
 Appendix D. Source Codes and Documentation .....	 D-1
Introduction .....	D-1
General Discussion .....	D-1
DISSOC .....	D-2
DISSOC.F .....	D-3
GETPARMS.F .....	D-5
DEFPRMS.F .....	D-6
DIFEQ.F .....	D-12
TIFUNC.F .....	D-15
OUTHEADER.F .....	D-16
OUTPARMS.F .....	D-17
OUTPUT.F .....	D-17
MAKEFILE .....	D-18

EXT .....	D-20
EXT.F .....	D-20
GETPARMS.F .....	D-21
DEFPRMS.F .....	D-22
DIFEQ.F .....	D-25
OUTHEADER.F .....	D-27
OUTPARMS.F .....	D-28
OUTPUT.F .....	D-28
TIFUNC.F .....	D-29
MAKEFILE .....	D-30
HENE .....	D-30
HENE.F .....	D-30
GETPARMS.F .....	D-32
FREQCOMPLEX.F .....	D-33
DEFPRMSN.F .....	D-34
NEWPARAMS.F .....	D-36
OUTPARMS.F .....	D-38
OUTPUT.F .....	D-38
TIFUNC.F .....	D-39
VON.F .....	D-39
YNG.F .....	D-39
MAKEFILE .....	D-40
WUNDERER .....	D-42
EXT.F .....	D-43
COMMONS.F and COMPARM.F .....	D-44
GETPARMS.F .....	D-44
DEFPRMS.F .....	D-45
DIFEQ.F .....	D-46
OUTHEADER.F .....	D-48
OUTPUT.F .....	D-48
TIFUNC.F .....	D-49
Bibliography .....	BIB-1
Vita .....	VITA-1

## *List of Figures*

Figure 6-1. Normalized Number Densities and External Source Term For Wunderer's Example System .....	6-15
Figure 6-2. Comparison of Calculated and Measured Values of Electron Temperature at Selected Discharge Currents .....	6-30
Figure 6-3. Comparison of Calculated and Measured Electron Wall Flux .....	6-32
Figure 6-4. Effect on Temperature of Small Amounts of H <sub>2</sub> in N <sub>2</sub> ...	6-37
Figure 6-5. Influence of Hydrogen on Particle Fluxes .....	6-38
Figure 6-6. Comparison of H <sub>2</sub> <sup>+</sup> and N <sub>2</sub> <sup>+</sup> Fluxes with Changing Gas Mix	6-39
Figure 6-7. Particle Densities for High Recombination .....	6-47
Figure 6-8. Effect of Increasing Recombination on On-Axis Curvature	6-51
Figure 6-9. Fluxes with External Sources and High Recombination .	6-55
Figure 6-10. Radial Profiles of Recombining Ions for Recombination Rates Ranging from 10 <sup>-6</sup> to 10 <sup>-14</sup> cm <sup>3</sup> /s in a 2-Torr Discharge .....	6-56
Figure 6-11. Ratio of Non-recombining to Recombining Field .....	6-58
Figure 6-12. Deviation from Proportionality as Recombination Increases, Equal Sources .....	6-64
Figure 6-13. Deviation from Proportionality As Recombination Increases, Nonequal Sources .....	6-65
Figure 6-14. Number Densities with High Charge Transfer Present .	6-69
Figure 6-15. Particle Fluxes with High Charge Transfer .....	6-72
Figure 6-16. Deviation from Proportionality As Charge Transfer Increases, Species 1 .....	6-75
Figure 6-17. Deviation from Proportionality As Charge Transfer Increases, Species 2 .....	6-75
Figure 6-18. N versus r, Maximum Recombination .....	6-83
Figure 6-19. Particle Fluxes for High Recombination and Volume Sources .....	6-84

Figure 6-20. Effect of Increasing Recombination on Electron Temperature for Single and Multi-Ion Models .....	6-90
Figure 6-21. Deviation From Proportionality <i>versus</i> Recombination; 1 T	6-92
Figure 6-22. Deviation From Proportionality <i>versus</i> Recombination; 1T	6-93
Figure 7-1. Initial Decision Tree for Multi-Ion Models .....	7-12
Figure 7-2. Decision Tree for Multi-Ion Recombining Systems .....	7-16
Figure 7-3. Decision Tree for Multi-Ion Charge Transfer Systems ...	7-18
Figure 7-4. Effect of Changing Diffusion Coefficient on Electron Temperature and Ionization Frequency .....	7-30

*List of Tables*

Table 2-1. Comparison of Various Models .....	2-26
---	------



# *List of Symbols*

$\alpha$	Recombination rate [ $\text{cm}^3/\text{s}$ ]
$\beta_i$	Ion nonproportionality parameter $\equiv \frac{\frac{S_i}{S_e}}{\frac{\Gamma_i}{\Gamma_e}}$
$\epsilon$	Ratio of electron to ion characteristic energy $\equiv \frac{\frac{\mu_e}{D_e}}{\frac{\mu_+}{D_+}} = \frac{T_+}{T_e}$
$\vec{\Gamma}$	Particle current density [ $\text{cm}^{-2}\text{-s}^{-1}$ ]
$\vec{\gamma}$	Dimensionless particle current density
$\lambda$	Eigenvalue for volume source terms (dimensionless)
$\Lambda$	Characteristic physical dimension of the plasma or discharge
$\mu$	Mobility [ $\text{cm}^2/\text{V/s}$ ]
$\nu$	Frequency (Ionization, and so forth) [Hz]
$\vec{\mathcal{E}}$	Dimensionless electric field
$\rho$	Dimensionless spatial coordinate ( = $x/d$ or $r/R$ )
$\rho$	Net electric charge density
$S_i$	Proportional source term; used in the definition of $\beta_i$
$\sum_j$	Sum over species. Species involved can be all positive, all negative, or all species, depending on context.
$D$	Diffusion coefficient [ $\text{cm}^2/\text{s}$ ]
$d$	Half-width of planar discharge [cm]
$\vec{E}$	Electric field [V/cm]

<b>e</b>	<b>Fundamental unit of charge (<math>1.602 \times 10^{19}</math> Coulombs)</b>
<b>f</b>	<b>Dimensionless frequency ( = <math>vd^2/D</math> or <math>vR^2/D</math>)</b>
<b><math>k_b</math> or <math>k</math></b>	<b>Boltzmann constant</b>
<b>k</b>	<b>Reaction rate constant for associative charge transfer [<math>\text{cm}^6/\text{s}</math>]</b>
<b><math>K_i</math></b>	<b>Proportionality constant; <math>N_i/N_e</math></b>
<b>l</b>	<b>d or R, depending on geometry</b>
<b>N</b>	<b>Particle number density [<math>\text{cm}^{-3}</math>]</b>
<b>n</b>	<b>Dimensionless number density</b>
<b>R</b>	<b>Radius of cylindrical discharge [cm]</b>
<b>r</b>	<b>Distance from discharge axis, cylindrical geometry [cm]</b>
<b>S</b>	<b>Source term [<math>\text{cm}^{-3}\text{-s}^{-1}</math>]</b>
<b>s</b>	<b>Dimensionless source term</b>
<b><math>t_{+,i}</math></b>	<b>The value of some parameter t for positive species i</b>
<b><math>t_{-,j}</math></b>	<b>The value of some parameter t for negative species j</b>
<b>t</b>	<b>The value of some parameter t for negative or positive species</b>
<b>x</b>	<b>Distance from discharge axis of symmetry, planar geometry [cm]</b>

*Abstract*

The continuity and momentum equations for electrons and multiple ion species are solved analytically and numerically using a new model for ambipolar diffusion. The general form of the model is valid for any quasi-neutral plasma for which the diffusion approximation is appropriate, including positive or negative ions, arbitrary geometries, and time dependence. The model provides criteria for determining when single ion diffusion theory is appropriate for describing multi-ion discharges, when a multi-ion proportional model is appropriate, and when a multi-ion nonproportional model must be used. The constant of proportionality for proportional discharges is shown to be the ratio of the source term for each species to the sum of the source terms for all species, with the source term normalized by the respective free diffusion coefficient.

Proportional analytic solutions are determined for uniform external ionization in planar and cylindrical geometries, double-exponential external ionization in planar geometries, ionization by the bulk electrons in planar and cylindrical geometries, and bulk ionization and nonresonant charge transfer in planar geometries. Numerical comparisons to previous experimental and theoretical determinations of electron temperature verify earlier simpler models. Previous results from a model by Wunderer are duplicated for a nonproportional case (Wunderer, 1978). Comparison to experimental results of Schmidt provide explanations for features of his results (Schmidt, 1965). Numerical solutions for generic two-ion plasmas with recombination or charge transfer as volume losses and external or

**AFIT/DS/ENP/92-1**

**electron impact ionization sources provide scaling relationships for the effects of multiple ions on discharge parameters.**

## ***MULTI-ION AMBIPOLAR DIFFUSION***

### ***I. Introduction and Background***

#### ***Introduction***

***Rationale for Investigation.*** One of the more difficult and interesting problems in plasma physics is incorporating the electric field into the description of the plasma in a self-consistent manner. This problem is especially difficult if the field involved is generated by the separation of charges within the plasma itself. Its intractability, as we will see in Chapter II, is related to the sensitivity of the electric field to very small changes in charge densities, and the fact that the problem must be solved self-consistently. The first successful attempt to address such problems was Schottky's ambipolar diffusion model, which took advantage of the nearly neutral conditions present in many plasmas to describe the electric field (Schottky, 1924).

We will fully describe the rationale and derivation of Schottky's model in the next chapter. In brief, he addressed a single-ion plasma by assuming the charge densities and fluxes of the two species to be equal. This allowed him to develop a closed-form expression for the electric field without the necessity of solving Poisson's equation. This expression, in turn, allowed him to express the momentum (or diffusion) equation as a form of Fick's law.

Since then, many authors have extended Schottky's model to include multiple positive ions, negative ions, and additional ionization mechanisms. However, previous attempts to apply Schottky's ambipolar model to multiple ions have led to extremely complicated systems that required additional assumptions or were impossible to solve analytically, and often difficult to solve numerically. (Phelps and Brown, 1952; Oskam, 1958; Thompson, 1959; Golubovskii and Lyagushchenko, 1977; Wunderer, 1978; Ferreira, Gousset, and Touzeau, 1988). Only in the simplest cases, corresponding to what we will later describe as simple volume ionization, or analytically simple external sources such as uniform ionization, was solution possible. Even then the theoretical basis of the solutions was of limited applicability. Typical of the solutions is Brown, who stated solutions for very simple cases without any limitations on the validity of those solutions at all (Brown, 1966: 67-68).

In this document, we will develop a new model of multi-ion ambipolar diffusion in weakly ionized plasmas. The new model, while similar in many respects to Schottky's model of single-ion ambipolar diffusion, uses a slightly different and less restrictive set of physical assumptions that enables simple descriptions of multi-ion ambipolar diffusion. For single-ion plasmas, it reverts to Schottky-based models. For multi-ion plasmas, it allows analytic solutions for physically realistic systems without restrictive assumptions, and easy formulation and development of numerical solutions.

*Summary of the Investigation.* In the remainder of this chapter we will briefly discuss the momentum and continuity equations, including the

simplifications applicable to the regime of our interest. This will provide a starting point for the remainder of the work, and allow us to point out the assumptions inherent in any diffusion model.

In Chapter II we discuss previous ambipolar diffusion models, their limitations, and proposed resolution of some of those limitations. We start with a detailed exposition of Schottky's model, so that we can see clearly the justification for and foundations of the model. This is useful both to understand the extensions of other authors, and to understand the differences between those models and the new model being developed here. Next, we examine a number of works that addressed various aspects of the system we are investigating. Finally, we discuss some of the shortcomings of previous multi-ion models, and what this investigation will do to address those shortcomings.

In Chapter III we formulate the new model. We start by explaining the difference in assumptions between the present model and Schottky-based models, and show how the assumptions lead to the new model for ambipolar diffusion. We then develop a simplified form useful for systems containing only positive ions. Finally, we develop a normalized form of the system for use in developing and investigating analytic solutions.

In Chapter IV we use the model to examine the phenomenon of proportionality: the existence of multi-ion systems where the species number densities have the same spatial dependence. In such systems, each ion density can be written as a constant times the electron density, and so can be said to be proportional to the electron density; hence, the name. We are primarily concerned with systems consisting of positive ions only. We are

able to derive a necessary and sufficient condition for proportionality to occur, and a more general necessary condition. We discuss the implications of the necessary condition for a number of source terms, predicting the results for the analytic solutions obtained later.

In Chapter V we develop analytic solutions for a number of cases. In particular, we examine cylindrical and planar geometries, with source terms representing uniform ionization, non-resonant charge transfer, ionization by the electrons in the plasma, and ionization produced by particles incident from both sides of a planar discharge. We include the multi-ion equivalent of the system described by Schottky in the original expositions of his model. We discuss the implications the solutions have for overall scaling of the particle densities, fluxes, and electric field for the various cases.

In Chapter VI we use numerical solutions to investigate systems not amenable to analytic solution. We look at two classes of systems. One class is comprised of fairly realistic systems. In these cases, the purpose of the examinations is to compare the model to experiment or other authors' calculations. The other class is comprised of quasi-realistic systems, sometimes not fully attainable in reality. However, these systems allow us to isolate and examine particular aspects of such processes as recombination and charge transfer.

In Chapter VII we present the results of the investigation, including a summary of the significant results of the individual chapters, how the investigation addressed the problems discussed in Chapter II, and suggestions for continued research.



In the Appendices we discuss several areas that are important, but need not be in the main body of the work. In particular, we include the derivation of the dimensionless form of the differential equation system, the details of an important but tedious integration, description of the basic numerical algorithms used, and complete documentation and listings of the programs used.

### *Momentum and Continuity Equations*

We will be examining a fluid model of a plasma using the first two moment equations. The first moment equation is the continuity equation:

$$\frac{\partial N}{\partial t} + \nabla \cdot \vec{\Gamma} = S(\vec{r}, t) \quad (1-1)$$

where  $N$  is the particle density as a function of position and time,  $\vec{\Gamma}$  is the particle flux defined by  $\vec{\Gamma} = N\vec{u}$ ,  $S$  is the net production rate of the particles, and  $\vec{u}$  is the average velocity of the particles as a function of position and time.

The second moment is the momentum equation:

$$mN \left( \frac{\partial \vec{u}}{\partial t} + (\vec{u} \cdot \nabla) \vec{u} \right) = qN\vec{E} - \nabla p + mN \frac{\delta \vec{u}}{\delta t} \quad (1-2)$$

This form of the momentum equation is appropriate for collisional systems where viscosity forces are negligible, and where there is no magnetic field. Here,  $\delta \vec{u} / \delta t$  refers to the change in the average velocity due to collisions.

Let us now examine the changes in Equation 1-2 that produce the form of the momentum equation appropriate for these investigations.

The  $\partial \vec{u}/\partial t$  term in the momentum equation can be neglected if the characteristic time of variation of plasma parameters (such as particle density, fluxes, electron temperature) greatly exceeds the time between collisions (Golant, Zhilinsky, Sakharov, and Brown, 1980:193). At best, the characteristic time of variation can be no shorter than the time it takes to propagate a disturbance across the plasma. Therefore, we can approximate  $\partial u/\partial t$  by noting that it is comparable to  $u/\tau$ , where  $\tau$  is the time for propagation of disturbances across the plasma. In a diffusive plasma, this time is  $\Lambda^2/D$ , where  $\Lambda$  is the characteristic scale length of the plasma and  $D$  is the diffusion coefficient. On the other hand,  $\delta u/\delta t$  may be approximated by  $u\nu_c$ , where  $\nu_c$  is the total collision frequency. Therefore, we may neglect the  $\partial \vec{u}/\partial t$  term if the plasma response frequency  $\nu_p = D/\Lambda^2$  (not to be confused with the plasma frequency  $\omega_p$ ) is significantly smaller than the total collision frequency. This condition is true for the plasmas of interest in this paper. We can also define a generalized ionization frequency as the ratio of species net source to the number density for that species:  $\nu_i \equiv S_i/N_i$ . If the total number density in the plasma is slowly varying, then the net gain in particles described by  $\nu_i$  must be comparable to the flux loss to the walls, characterized by  $D/\Lambda^2$ . Under those circumstances  $\partial u/\partial t$  may be neglected if  $\nu_i$  is small compared to  $\nu_c$ .

Even though the explicit time dependence in the momentum equation can be neglected for a particular system, it still may be necessary to retain the  $\partial N/\partial t$  term in the continuity equation. The reason is that the collision term in the continuity equation involves the net source frequency  $\nu_i$  (as defined immediately above), not the total momentum transfer collision frequency  $\nu_c$ . As a result, time-dependent plasmas can often be described with explicit time dependence appearing only in the continuity equation.

The second term within the parentheses on the left hand side of Equation 1-2 is denoted as the inertia term. For collisional plasmas it is generally smaller than the pressure gradient term. In situations where collisions can be neglected in describing the motion of the ions (commonly called collisionless, or free fall), the inertia term dominates the pressure term. The relationship required to justify neglect of the inertia term is

$$mN(\vec{u} \cdot \nabla)\vec{u} < \nabla p = kT\nabla N \quad (1-3)$$

The magnitude of  $(\vec{u} \cdot \nabla)\vec{u}$  may be approximated as  $u^2/\Lambda$ , while the magnitude of  $\nabla N$  may be approximated as  $N/\Lambda$ . Using those relationships produces

$$u^2 < \frac{kT}{m} \quad (1-4)$$

This implies that the inertia term may be neglected if  $u$  is small compared the thermal velocity  $v_{th}$ , where  $v_{th}$  is defined by  $mv_{th}^2/2 = kT$ .

To evaluate Equation 1-4, we approximate  $u$  as  $\Lambda/\tau$ , with  $\tau$  defined as  $D/\Lambda^2$ , just as before. With these approximations, Equation 1-4 becomes

$$\left(\frac{D}{\Lambda}\right)^2 < \frac{kT}{m} \quad (1-5)$$

Using the definition of  $D$  as  $kT/mv_c$  produces

$$kT < m(v_c \Lambda)^2 \quad (1-6)$$

If we then utilize the definition of  $v_{th}$ , we find

$$v_{th} < \sqrt{2} v_c \Lambda \quad (1-7)$$

Finally, expressing  $v_{th}$  in terms of the definition of mean free path and collision frequency as  $v_{th} = v_c \lambda_{mfp}$  produces

$$\lambda_{mfp} < \Lambda \sqrt{2} \quad (1-8)$$

In other words, the inertia term may be neglected if the mean free path for collisions is small compared to the characteristic scale length of the plasma.

We neglect the inertia term in describing diffusional plasmas in the model we are developing. Note, however, that several of the papers we discuss in the next chapter retain it, at least for some of the species. It must be retained for ions in the regime approaching free fall.

The last term on the right-hand side of the equation is the change in momentum of the particles due to collisions with other species. One effect present in this term is the change in momentum associated with the creation or loss of particles, such as might occur in ionization. Such a creation or loss represents not only a change in total number of particles as described in the continuity equation, but also a change in momentum for the species due to the momentum possessed by the particle that is produced or lost. It is difficult to make general statements about when this effect may

be neglected, since the particle produced (or lost) may represent either a loss or gain of momentum for the species. For instance, electron impact ionization produces two electrons, one generally of considerably lower energy than the other. Furthermore, the total energy of the two is less than the initial energy of the incident electron, since energy was needed for the ionization itself. This can represent a net loss of momentum to the electrons. However, every collision of an electron with a background particle represents a change in the net momentum of the electrons. In general, it is safe to say that if the collision frequency associated with a particular reaction is negligible compared to a suitably defined total collision frequency, it is possible to neglect the momentum change associated with particle creation or loss. Such a situation usually exists for weakly ionized collisional plasmas. The other effect present in this term is the change in momentum that particles undergo when colliding with the background gas. This change in momentum is generally not negligible. Therefore, we retain only that term. In that case, the collision term can be written in terms of a suitably defined collision frequency as  $-v_m N \vec{u}$ .

We express the pressure in terms of temperature:

$$p = NkT \quad (1-9)$$

This gives a  $\nabla(NkT)$  factor in the second term of the right hand side of Equation 1-2. If thermal gradients are small, we can remove the temperature from within the gradient operator. Otherwise, a temperature diffusion term must be included. If we then define the diffusion coefficient:

$$D = \frac{kT}{mv} \quad (1-10)$$

and mobility:

$$\mu = \frac{|q|}{mv} \quad (1-11)$$

We obtain the momentum equation in the form we will use in our analysis:

$$\vec{\Gamma} = \pm \mu N \vec{E} - DVN \quad (1-12)$$

where the  $\pm$  takes into account the sign of the charge.

Other authors, depending on the conditions they are describing, may retain terms we have neglected. However, this form is the appropriate expression for a collision-dominated weakly ionized plasma.

Before we leave the question of simplifications to the momentum equation, we should note that there are effects present in the discharge that are produced by interactions between the charged particles and the neutral background gas. We will consider briefly two of these; cataphoresis and electrophoresis. Cataphoresis is the process whereby transport of ions causes gradients in the background number density. The process of creation of ions, their transport to a different location in the discharge, and their recombination (either in the gas or at the wall) represents a net transport of neutral particles, as well. In general, cataphoresis may be neglected if the ion density is much less than the particle density. For the weakly ionized plasmas being investigated here, that condition is true. Electrophoresis is the process whereby the differing momenta of the ions and electrons as they arrive at the walls of the discharge results in a net momentum transfer to the walls of the discharge. The result, of course, is a net momentum transfer to the discharge, as well. The details are related

to the momentum gained or lost by the creation or loss of charged species. Therefore, electrophoresis may be ignored in discharges where the collision term in the momentum equation need only include simple momentum transfer collisions, and not particle production or losses. Such is the case for the discharges we are investigating.

In summary, the assumptions and restrictions inherent in the form of the momentum equation we use in this analysis are that there are no temperature gradients present, that the collision frequency is independent of position, that the inertia term can be neglected, and that the explicit time derivative of the particle velocity is small compared to the collision term.

Finally, if there is no electric field, the momentum equation reduces to a form called Fick's law:

$$\vec{\Gamma} = -DVN \quad (1-13)$$

As we shall discuss in the next chapter, Fick's law is much easier to deal with than the form that includes the electric field.

## *II. Historical Perspective of the Theory of Multi-Ion Discharges*

### *Introduction*

In this chapter we will discuss some of the previous works that addressed the collisional positive column. Our intent is to examine the difficulties in describing diffusion in the presence of electric fields, see how various authors addressed those difficulties, and point out areas where improvement is needed.

We first briefly describe the historical background of the theory of single-ion ambipolar diffusion. We discuss Schottky's original theory, which assumed quasi-neutrality in the body of the plasma, but ignored the sheath (Schottky, 1924). We include solutions for cylindrical and planar geometries. Next, we discuss Ecker's paper, which extended Schottky's theory to non-neutral plasmas, but retained congruence (Ecker, 1954). We also consider the paper of Tonks and Langmuir, who used an approach more general than Schottky's to describe quasi-neutral plasmas in the expanded regime of ambipolar diffusion to free fall (Tonks and Langmuir, 1929). Finally, we discuss Allis and Rose, who described diffusional plasmas over the entire regime from the free diffusion of plasmas whose number densities were too low to enforce quasi-neutrality to ambipolar diffusion (Allis and Rose, 1954).

Earlier works on multi-ion ambipolar diffusion, including Oskam's paper (Oskam, 1959) are then considered. We use the difficulties in justifying the assumptions required to produce solutions to Oskam's model



as an example of general difficulties that occur in Schottky-based models. We also discuss other multi-ion plasma models, with an emphasis on the limitations and applicability of the models, and the differences between those models and the present one.

We finish by discussing problem areas that still need to be addressed, and how they will be addressed in the remaining chapters of this document.

### *Single-ion Models*

First, we will discuss single-ion diffusion, starting with Schottky's theory of single-ion ambipolar diffusion. In particular, we will examine the difficulties inherent in modeling the diffusion of charged particles with the self-consistent field explicitly included. These difficulties will demonstrate why Schottky was interested in taking advantage of the physical characteristics of diffusional, quasi-neutral plasmas to develop a model that did not include an explicit field dependence. We will describe Schottky's derivation, the assumptions used, the resulting model, and typical solutions.

We will then continue with three other single ion models, those of Tonks and Langmuir (Tonks and Langmuir, 1929), Ecker (1954), and Allis and Rose (Allis and Rose, 1954). Tonks and Langmuir developed a more general model of plasmas that recovers Schottky's model in the collisional quasi-neutral case, but which also includes the free fall case. Their model addresses non-neutral plasmas in the sheath region, providing values for the sheath thickness. Allis and Rose extended Schottky's model to include

the transition to free diffusion, where the Debye length is no longer much smaller than  $\Lambda$ .

*Schottky's Model of Ambipolar Diffusion.*

*Rationale for Ambipolar Diffusion.* Recall the momentum equation for a collisional plasma (Equation 1-9):

$$\vec{\Gamma} = -D\nabla N \pm \mu N \vec{E} \quad (2-1)$$

If  $\vec{E}$  is produced by external means, independent of the plasma conditions, the changes that  $\vec{E}$  produces have no effect on  $\vec{E}$ . Under these circumstances the diffusion and continuity equations form a system that can usually be dealt with in a straightforward manner. In general, however, the charged particles in the generation of the electric field, or at least a significant part of it. Under these circumstances, the problem of describing the motion of the species in the plasma must include the field in a self-consistent fashion. To do so requires another relationship to determine the electric field. In principle, that relationship should be based directly or indirectly on Maxwell's equations. In particular, we can use Gauss's law for the electric field, or its more commonly used equivalents; Poisson's equation and the definition of the field in terms of the scalar potential:

$$\begin{aligned} -\nabla^2 \phi &= \frac{\rho}{\epsilon_0} \\ \vec{E} &= -\nabla \phi \end{aligned} \quad (2-2)$$

where  $\rho$  here is used to represent the volume charge density,  $\phi$  is the electric scalar potential, and  $\epsilon_0$  is the permittivity of free space. Un-

fortunately, Equation 2-2, along with the continuity and momentum equations, produces a system of differential equations that can be extremely difficult to solve.

The difficulty arises because of the extremely large fields that can be produced by very small net charge densities. For instance, consider the numerical problem of describing a near-neutral plasma typical of those found in the positive column of a glow discharge. We will assume a charged particle density of  $10^9$  particles/cm<sup>3</sup>, which is well within the range typical of laboratory plasmas (von Engel, 1965:241). We will also assume that the numerical errors are on the order of only one part in  $10^6$ . The numerical errors are equivalent to a charge density that would produce a change in the electric field of more than 0.18 V/cm. If we assume a reasonable value of 1.0 eV for the electron temperature, and also assume that the electrons can be described in terms of the electric potential  $\phi(r)$  by the Boltzmann relation  $N_e(r) = N_{e0} \exp(e\phi(r)/kT_e)$ , we find that the electron density changes almost 20% in one cm. Obviously, such a drastic change invalidates the description of the plasma as quasi-neutral and renders the numerical model useless.

Similar difficulties occur in trying to make simplifying assumptions to allow analytic solutions. As can be seen from the discussion in the previous paragraph, an assumption that allows errors in the number densities of only one part in  $10^6$  can lead to faulty values for the electric field that produce gross errors in the solutions.

The difficulties in finding analytic solutions to this system led to Schottky's development of a model that took advantage of quasi-neutrality to eliminate the need to explicitly include the electric field.

*Single-ion Ambipolar Diffusion.* Schottky first introduced the concept of ambipolar diffusion to describe conditions in the volume of the plasma (Schottky, 1924). He established an analytic solution using the assumptions of quasi-neutrality and congruence. The basic principle of quasi-neutrality is that the extremely strong fields produced by any charge separation in a plasma tend to eliminate that charge separation. As a result, the plasma has a near-zero net charge density. The role of congruence can be established by recalling the continuity equation (which, for convenience, we use in the time-independent form):

$$\nabla \cdot \vec{\Gamma} = S(\vec{r}) \quad (2-3)$$

for each of the two species (positive and negative). Conservation of charge implies that  $S(r)$  for the positive species is equal to that for the negative, since we cannot create one charge polarity without creating the other. Therefore, we conclude that the divergences of the positive and negative species are equal.

Now consider a one-dimensional system. If there is any point where the fluxes are equal, then they will be equal at every point. This condition is referred to as congruence. From this, the system of coupled sets of moment equations plus Poisson's equation can be reduced to a single set of moment equations. Note that we are not requiring a planar single-dimensional plasma. All that is necessary is that variations in the plasma be single-

dimensional. An example would be a cylindrical plasma with symmetry in the longitudinal and azimuthal directions. Such a plasma can be described by a one-dimensional model with radial variations only.

*Derivation of Schottky's Model.* An exposition of Schottky's original derivation for time-independent diffusion can be found in most basic plasma texts (e. g., Mitchner and Kruger, 1973: 146-149. von Engel, 1965; 143-145. Chen, 1984:159-160). Schottky's original development considered a one-dimensional cylindrical case. We will treat the more general case, paralleling the development given by Chen. Consider the time-independent diffusion and continuity equations for electrons and positive ions:

$$\begin{aligned}\vec{\Gamma}_i &= -D_i \nabla N_i + \mu_i N_i \vec{E} \\ \vec{\Gamma}_e &= -D_e \nabla N_e - \mu_e N_e \vec{E} \\ \nabla \cdot \vec{\Gamma}_i &= S_i \\ \nabla \cdot \vec{\Gamma}_e &= S_e\end{aligned}\tag{2-4}$$

As did Schottky, we assume  $N_i = N_e \equiv N$ . We also assume congruence;

$\vec{\Gamma}_i = \vec{\Gamma}_e$  at every point in the plasma. From congruence, we obtain

$$-D_i \nabla N_i + \mu_i N_i \vec{E} = -D_e \nabla N_e - \mu_e N_e \vec{E}\tag{2-5}$$

which, when coupled with quasi-neutrality, yields

$$\vec{E} = \left( \frac{\nabla N}{N} \right) \frac{(D_i - D_e)}{(\mu_i + \mu_e)}\tag{2-6}$$

This leads to

$$\begin{aligned}\vec{\Gamma} &= -\nabla N \left( \frac{\mu_i D_e + \mu_e D_i}{\mu_i + \mu_e} \right) \\ &= -D_a \nabla N\end{aligned}\tag{2-7}$$

where  $D_a$  is the "ambipolar diffusion coefficient."

We no longer have a system containing an explicit dependence on the electric field. Instead, by assuming quasi-neutrality and congruence we have eliminated the electric field from the system entirely.

*Schottky's Solutions.* The system generally referred as a "Schottky" system contains source terms of the form

$$\nabla \cdot \vec{\Gamma} = \nu N_e\tag{2-8}$$

for each species. We take the divergence of the simplified momentum Equation 2-7, and substitute for  $\nabla \cdot \vec{\Gamma}$  using Equation 2-8 as appropriate. The following boundary conditions are then applied to obtain:

$$\begin{aligned}\Gamma(0) &= 0 \\ N(L) &= 0\end{aligned}\tag{2-9}$$

where  $L$  is the radius or half-width of the plasma, depending on the geometry chosen. The following solutions result. For planar geometry:

$$\begin{aligned}N_e &= N_{e0} \cos\left(\frac{\pi}{2d} r\right) \\ \vec{\Gamma} &= \frac{2d}{\pi} \nu N_{e0} \sin\left(\frac{\pi}{2d} r\right)\end{aligned}\tag{2-10}$$

For cylindrical geometry:

$$\begin{aligned}N_e &= N_{e0} J_0\left(\lambda_0 \frac{r}{R}\right) \\ \vec{\Gamma} &= \frac{R}{\lambda_0} \nu N_{e0} J_1\left(\lambda_0 \frac{r}{R}\right)\end{aligned}\tag{2-11}$$

where  $d$  is the half-width of the planar discharge,  $R$  the radius of the cylindrical discharge, and  $\lambda_0$  is the first zero of the zero-order Bessel function  $J_0$ , and  $J_1$  is the second-order Bessel function. Inherent in each of these solutions is an eigencondition on  $D_a$  and  $v$  (we discuss these conditions in a later chapter in a more general context):

$$\begin{aligned}\frac{vd^2}{D_a} &= \left(\frac{\pi}{2}\right)^2 \\ \frac{vR^2}{D_a} &= \lambda_0^2\end{aligned}\tag{2-12}$$

We should note that this model, as is true for all models based upon quasi-neutrality, is only valid away from the boundary of the plasma. Near this boundary, in what is generally termed the plasma sheath, large charge differences are developed that invalidate the assumption of quasi-neutrality. For these reasons, other models that explicitly deal with the non-neutral regime must be used to calculate sheath potential and thickness.

Before we leave Schottky's model, it is important to clearly restate the assumptions Schottky made.

1. He assumed quasi-neutrality.
2. He assumed equal fluxes (or "congruence").
3. And, although this point is usually ignored in discussions of Schottky diffusion, Schottky implicitly assumed (but did not take advantage of)  $\nabla N_i = \nabla N_e$ .

This third assumption will assume more significance later, when the new model of multi-ion ambipolar diffusion is presented. In fact, we shall see that the new model, which uses assumptions 1 and 3 explicitly, reveals assumption 2 as a consequence in those physical situations where it is

valid. For the moment, we will merely note that 3 is implicit in Schottky's replacing the separate ion and electron densities with a single  $N$ , and then describing the system in terms of  $\nabla N$  instead of in terms of  $\nabla N_e$  and  $\nabla N_i$ .

*Tonks and Langmuir.* Tonks and Langmuir used a totally different approach to the problem of describing discharges (Tonks and Langmuir, 1929). First, they assumed that the ions started from rest, with their only velocity being that produced by the field. Furthermore, instead of using the momentum equations *per se*, they made two explicit assumptions:

1. The electrons were in equilibrium with the scalar potential, such that the electron distribution could be described by the Boltzmann relation as (Tonks and Langmuir, 1929: 883)

$$\frac{N_e}{N_0} = \exp\left(\frac{e\phi}{kT_e}\right) \quad (2-13)$$

2. The discharge can be entirely described in terms of Poisson's equation, where the charge density is expressed as the difference between an electron charge density derived from Equation 2-13 and an ion charge density whose definition varied according to the particular situation, but which could always be written in terms of an ion velocity.

Depending on how they expressed Poisson's equation, Tonks and Langmuir could describe a wide variety of discharge phenomena. They examined a parameter space that spanned two characteristic effects:

1. Mean free path for collision. They examined the cases where the mean free path for collision was much longer ("free fall") or much shorter ("diffusion") than  $\Lambda$ , as well as the intermediate case.
2. Effect of the electric field. Although their terminology was somewhat different, they divided the discharge into two regions; the plasma, where quasi-neutrality held, and the sheath, where it did not hold.

They developed a variety of solutions for the plasma region, including source terms for both uniform ionization and ionization proportional to the



electron number density. Their principal result in the sheath region was an expression for the sheath thickness, in the free fall limit. Although most of their development was based on assuming that the ions' thermal velocity was negligible compared to the field-induced motion, they did examine cases where the thermal velocity was small but non-zero. They also examined solutions for geometries corresponding to probes inside the plasma.

Tonks and Langmuir used Poisson's equation as the basic equation of their system (Tonks and Langmuir, 1929:883):

$$\nabla^2 \phi - 4\pi e N_0 \exp\left(\frac{e\phi}{kT_e}\right) + 4\pi e r^\beta \int_0^r \frac{N_z z^\beta}{v_z(r)} dz = 0 \quad (2-14)$$

where  $N_0$  is the electron density at the origin,  $\beta$  is a parameter with value 1, 2, or 3 in planar, cylindrical, or spherical geometry, respectively,  $N_z$  is the number of ions produced per  $\text{cm}^{-3}\text{-s}$  at  $z$ , and  $v_z(r)$  is the velocity of ions which were generated at  $z$  but are now at  $r$ .

The key to solving this equation is the proper determination of  $N_z$  and  $v_z$ . For uniform external ionization,  $N_z$  is a constant. For ionization dependent on the electron density,  $N_z = \nu N_e(z)$ . For free fall,  $v_z$  is determined by the difference in potential the ion has been subjected to in traveling from  $z$  to  $r$ . For diffusion,  $v_z$  is the drift velocity determined by the sum of the field-induced and gradient-induced fluxes (Tonks and Langmuir, 1929:887):

$$v_z = -\{D/N_p\}dN_p/dr - (eD/kT_g)dV/dr \quad (2-15)$$

This is recognizable, of course, as the momentum equation for ions, with  $N_p(r)$  as the ion particle density.

Tonks and Langmuir divide the discharge into two regions. For the plasma volume, they assume that the Laplacian of  $\phi$  is negligible (Tonks and Langmuir, 1929:883). In the region they define as the sheath, they assume no curvature in the system (*i. e.*, they assume planar geometry for all systems), they assume that the ion current density in the sheath is constant, and they drop the electron charge term from the generalized plasma-sheath equation "when it becomes negligible" (Tonks and Langmuir, 1929:905)

Tonks and Langmuir recover Schottky's description for plasmas with ionization proportional to the electron density and mean free path much less than  $\Lambda$ . In order to explain this, we need to examine the consequences of Equation 2-13 more closely. If we take the logarithm of that equation, and then the gradient, we find

$$\frac{\mu_e}{D_e} \nabla \phi = \frac{\nabla N_e}{N_e} \quad (2-16)$$

where we have used the Einstein relationship to express  $e/kT_e$  in terms of  $\mu$  and  $D$ . We can then use the definition of the field in terms of the scalar potential to express Equation 2-16 in a suggestive form:

$$\mu_e N_e \vec{E} = -D_e \nabla N_e \quad (2-17)$$

But, this is the time independent momentum equation for electrons, for the case where the electron flux is approximately zero. (See Equation 2-4.)

Let us examine the concept of zero electron flux more closely, especially in the context of ambipolarity. We note that the electron mobility and diffusion coefficients significantly exceed that of the ion. Ambipolarity is

the condition that a self-consistent field in the plasma will develop so as to equalize the ion and electron fluxes in a quasi-neutral plasma. Given the relative magnitudes of  $\mu$  and  $D$  for the two species, this equalization arises by the electric field achieving a necessary value to reduce the electron flux to match the ion flux. The result is that the field-induced flux of electrons is oppositely directed, and essentially equal to, the gradient-induced flux. This is described by Equation 2-17. Therefore, Tonks and Langmuir's assumption of the Boltzmann relation for the electrons and the assumption of quasi-neutrality implies that the radial electric field is equivalent to the ambipolar field. We will revisit this result in the next chapter, when we discuss the new ambipolar diffusion model. In that chapter we will examine exactly under what circumstances the Boltzmann relation follows from ambipolarity for circumstances where the electron mobility and diffusion coefficients are much greater than the ion mobility and diffusion coefficients.

Since Tonks and Langmuir's results produce ambipolar diffusion in certain cases, Schottky's theory is a limiting case of Tonks and Langmuir's for the regime in which Schottky's theory is applicable:

1. In assuming that the Laplacian of the potential is negligible in the plasma, Tonks and Langmuir set the expressions for ion and electron density as defined in our Equation 2-14 equal to each other, which implies quasi-neutrality.
2. Tonks and Langmuir assume an expression for the electron number density that requires the electric field in a quasi-neutral plasma to be equivalent to the ambipolar field.
3. Tonks and Langmuir incorporate the momentum equation for ions to determine the ion velocity.

*Ecker.* Ecker examined a subnormal discharge in mercury by assuming congruence in a development similar to Schottky's, except that he did not assume quasi-neutrality (Ecker, 1954). Instead, he explicitly distinguished between the positive and negative charge densities to obtain a more general form of Schottky's model. For quasi-neutral plasmas he obtained Schottky's model exactly. In general, his model did not require any particular relationship between the positive and negative number densities. In order to formulate approximate solutions, however, he assumed that the two densities had the same spatial dependence (this is equivalent to the proportionality condition for multi-ion models, which we will discuss shortly). His technique produced those solutions for which the spatial dependence of ions and electrons was the same, and which also minimized the total error in the differential equations.

*Allis and Rose.* Allis and Rose addressed the transition regime between free and ambipolar diffusion (Allis and Rose, 1954). They also used congruence without assuming quasi-neutrality. Their approach relies on modifying their expression equivalent to the Schottky eigencondition in Equation 2-12. That eigencondition applies to free diffusion, ambipolar diffusion, and the transition regime, if the proper definition of the diffusion coefficient  $D$  is used. Schottky's  $D_a$  is the appropriate form for ambipolar diffusion; Allis and Rose sought the appropriate form for other regimes. They produced analytic solutions applicable to various situations by several methods. First, they assumed that the ratio of positive ions to electrons was constant in defining the equivalent to the ambipolar diffusion coefficient. They investigated a discharge with the electron temperature much greater

than the ion temperature by dividing it into an interior region and a sheath. They also made approximations appropriate to a plasma near the quasi-neutral limit. These methods allowed them to produce analytic solutions for the problem. They also produced a numerical solution for a hydrogen discharge between parallel plates, primarily to investigate the range of validity of their analytic approximations. They found that the spatial profiles were only crudely approximated by the theory, but that various integrals over the number densities were reasonably accurate.

*Summary for Single Ion Models.* We have presented only four of the many single ion models that have been developed to describe discharges. We chose these four because they are representative of work in this area. Schottky's is the seminal work on ambipolar diffusion, but only examines ionization generated by the electrons in the plasma volume, without including external sources or recombination. In contrast, the theory of Tonks and Langmuir covers a very broad range of systems, in three different geometries, for both volume and external sources, and spans the regime from highly collisional plasmas to free fall plasmas. Ecker, as does Allis and Rose, only considers collisional systems, but includes the entire regime of ambipolar to free diffusion. Although Ecker's formulation is slightly more general, Allis and Rose are able to produce solutions for a wider range of cases.

All these single-ion models, of course, share one failing for the present purpose; by definition, they do not include multiple ions. This is not to say that they could not be extended to address multi-ion discharges, but only that the authors did not do so. The multi-ion models we will shortly present

are, in many cases, extensions of the single-ion models presented here, with varying levels of success. Other single-ion models could be included in this summary, but they would merely fill in various portions of the parameter space from free fall to collisional plasmas, and from free diffusion to ambipolar diffusion. They would still not address the fundamental problem of multiple ion species.

Phelps has written a particularly thorough, critical, and tutorial review of diffusion in plasmas, including a number of different regimes in single-ion diffusion (Phelps, 1990). He reviews contributions of Schottky, Tonks and Langmuir, and Allis and Rose in greater detail than we do here, and includes works by other authors that are variations of the above approaches.

### *Multi-ion Ambipolar Diffusion*

We now address situations where there are more than two species in the plasma. The reason for doing this is quite simple; a number of realistic systems cannot be accurately described without accounting for the effects of more than one ion species. The various species can be positive or negative, and can be formed by a variety of processes, including ionization, charge transfer, attachment, and dissociative attachment. For the purposes of this chapter, however, the exact details of the formation processes for the various species are unimportant.

Approaches to the problem of multi-ion diffusion may be divided into two classes: those that assume proportionality and those that do not. We note that, in many cases in which proportionality is involved, this assumption is

made with no other justification than facilitating a solution. We address proportional models first. Next, we examine models where the assumption of proportionality is not made. Generally, (except for the model developed in this effort) these models allow only numeric solutions.

*Proportional Solutions.* Numerous investigations of ambipolar diffusion assume that the various particle densities have the same dependence on position. This assumption is called proportionality. We will discuss one such investigation (Oskam, 1958) in detail, and briefly describe others.

*Oskam.* An early multi-ion ambipolar diffusion model was Oskam's (Oskam, 1958). We choose to review the work of Oskam because of the thoroughness with which he delineated the system, and to demonstrate the errors proportionality can produce when applied to nonproportional plasmas. Oskam was seeking to provide the theoretical underpinnings to experimental work he had performed in microwave-driven plasmas. He was interested in two regimes:

1. The discharge plasma. Here, the microwave fields are providing a continuous source of ionization and excitation. The electron temperature is much higher than the gas or ion temperatures, and the plasma is in a steady-state condition. (The microwave field changes too rapidly for the plasma to follow.)
2. The afterglow plasma. Here, the microwave excitation has stopped, so the plasma density is decreasing with time, due primarily to diffusion losses. All species in this particular discharge have equilibrated to the temperature of the background gas, so the electrons and ions are at the same temperature.

Oskam used a multi-ion version of the momentum and diffusion equations, which he wrote as:

$$\begin{aligned}
\vec{\Gamma}_{+,i} &= -D_{+,i} \nabla N_{+,i} + \mu_{+,i} N_{+,i} \vec{E} \\
\vec{\Gamma}_{-,j} &= -D_{-,j} \nabla N_{-,j} + \mu_{-,j} N_{-,j} \vec{E} \\
\nabla \cdot \vec{\Gamma}_{+,i} + \frac{\partial N_{+,i}}{\partial t} &= S_{+,i} \\
\nabla \cdot \vec{\Gamma}_{-,j} + \frac{\partial N_{-,j}}{\partial t} &= S_{-,j}
\end{aligned}
\tag{2-18}$$

Here, the  $+,i$  subscripts refer to the various positive species, and the  $-,j$  subscripts refer to the negative species. We will maintain this notation for the moment.

Following the assumptions in Schottky's derivation, Oskam assumed that the total current density and the total charge density were both zero, which is equivalent to

$$\begin{aligned}
\sum_i q_{+,i} \vec{\Gamma}_{+,i} &= \sum_j q_{-,j} \vec{\Gamma}_{-,j} \\
\sum_i q_{+,i} N_{+,i} &= \sum_j q_{-,j} N_{-,j}
\end{aligned}
\tag{2-19}$$

Using these two equations, he eliminated the electric field in exactly the same manner as Schottky. This led to the following system of equations:



$$\begin{aligned}
\vec{\Gamma}_{+,i} &= -D_{+,i}\nabla N_{+,i} + \mu_{+,i}N_{+,i} \left( \frac{\sum_k D_{+,k}\nabla N_{+,k} - \sum_k D_{-,k}\nabla N_{-,k}}{\sum_k \mu_{+,k}N_{+,k} + \sum_k \mu_{-,k}N_{-,k}} \right) \\
\vec{\Gamma}_{-,j} &= -D_{-,j}\nabla N_{-,j} - \mu_{-,j}N_{-,j} \left( \frac{\sum_k D_{+,k}\nabla N_{+,k} - \sum_k D_{-,k}\nabla N_{-,k}}{\sum_k \mu_{+,k}N_{+,k} + \sum_k \mu_{-,k}N_{-,k}} \right) \quad (2-20) \\
\nabla \cdot \vec{\Gamma}_{+,i} + \frac{\partial N_{+,i}}{\partial t} &= S_{+,i} \\
\nabla \cdot \vec{\Gamma}_{-,j} + \frac{\partial N_{-,j}}{\partial t} &= S_{-,j}
\end{aligned}$$

We see that the momentum equation that relates  $\Gamma_{+,j}$  to  $\nabla N_{+,i}$  also includes all the other  $\nabla N$ 's, and similarly for the equation relating  $\Gamma_{+,j}$  to  $\nabla N_{-,j}$ . Oskam found the resulting system extremely difficult to solve. His approach to the problem involved assuming proportionality in order to be able to find solutions:

$$\begin{aligned}
N_{+,i} &= K_{+,i} N_e \\
N_{-,j} &= K_{-,j} N_e \quad (2-21)
\end{aligned}$$

Oskam admits in his paper that this assumption is not always justified (Oskam, 1958:368-369). In particular, he notes that it was not appropriate to his time-varying afterglow plasma, where the various diffusion modes present had different characteristic decay times. Only after the plasma had decayed to the fundamental diffusion mode was proportionality valid. However, he also addresses negative ions, which also render proportionality invalid. As we shall see shortly, the difficulties are not specific to

Oskam; the assumption of proportionality is very common among authors wishing to find analytic solutions to this problem.

*Other Proportional Solutions.* To this date, although many authors have addressed diffusion in quasi-neutral gases, we have seen no papers that use a multi-ion ambipolar diffusion model without using Schottky's assumption of congruence. None of the authors has been able to solve the system analytically without restrictions of some kind. Usually those restrictions are as severe as those imposed by Equation 2-21, or are exactly the same restrictions as Equation 2-21. In some cases, the assumption is perfectly valid for the reactions being modeled (although Schottky-based models do not lend themselves to predicting that validity *a priori*). For instance, Phelps and Brown assume proportionality when investigating  $\text{He}^+$  and  $\text{He}_2^+$  in an afterglow discharge (Phelps and Brown, 1952). The only sources and losses they include are single-step ionization by the electrons in the plasma, charge transfer, and diffusion. In addition, all the species are at the same temperature. As we will see in later chapters, if they were dealing only with the fundamental diffusion mode, then for such plasmas, proportionality holds.

Occasionally, the assumptions required are not explicitly stated. For example, Thompson found analytic solutions for the case of a single negative and a single positive ion species, plus electrons (Thompson, 1959). However, Clouse points out that to do so, he made a quasi-proportional assumption (Clouse, 1985:7)

$$\frac{\nabla N_e}{\nabla N_i} = \epsilon \frac{N_e}{N_i} \quad (2-22)$$

where  $\epsilon$  is the ratio of the gas to electron temperatures, equivalent to  $1/\gamma$  in Thompson's notation. This is an extremely severe assumption, equivalent to requiring  $N_e$  to vary as  $(N_e)^\epsilon$  (Clouse, 1985:15). Furthermore, the assumption is never explicitly stated. Instead, it can be shown to be a consequence of the form Thompson derives for his ambipolar diffusion coefficients (Clouse, 1985:57-59).

We could continue with other examples. However, doing so would add little to the discussion. Rather, we again refer the interested reader to the review article of Phelps, who provides a fairly thorough discussion of proportional multi-ion diffusion (Phelps, 1990.)

*Nonproportional Solutions.* A number of authors have produced numerical solutions to various problems involving multiple ions. We will give some examples; this list is not, and is not intended to be, exhaustive. Rather, we concentrate on articles that have importance, either to the field as a whole, or to this work in particular.

*Edgley and von Engel.* Edgley and von Engel performed a comprehensive analysis of the theory of the positive column in electronegative gases (Edgley and von Engel, 1980). They did not use ambipolarity, but kept the electric field as a separate dependent variable, and explicitly included positive ion inertia in the momentum equation. This inclusion allowed them to model free fall, where the charged particles undergo no collisions; free diffusion, where the particles undergo collisions, but the plasma density is low and therefore electric field effects are small enough that the particles diffuse as if uncharged; and ambipolar diffusion, where both

collisions and electric field must be taken into account. The resulting system of seven differential equations and eight boundary conditions was solved numerically. Their analysis was very thorough, but produced an extremely wide parameter space to search. As a result, they were only able to find numerical solutions for a restricted range of their parameter space. They were unable to find any analytic solutions.

*Ferreira, Gousset, and Touzeau.* Ferreira, Gousset, and Touzeau adapted Edgley and von Engel's results by assuming quasi-neutrality and ignoring positive ion inertia (Ferreira *et alia*, 1988). They applied the model to the oxygen positive column. The resulting system was solved numerically. Of interest is their critique and comparison of previous works in this area, which was concerned with validity of boundary conditions in their own and previous authors' work. In particular, they pointed out that previous authors had overlooked the requirement for the proper number of eigenconditions to produce physically realistic solutions. One of the two eigenconditions they chose is equivalent to Schottky's eigencondition in Equation 2-12. They also establish a second eigencondition relating the magnitude of the on-axis particle densities for electrons and negative ions. Although this eigencondition is valid for their system of differential equations, its appearance as a condition for successful solution instead of a consequence of the solution is due to the normalizations they have chosen for their system, not to the physics of the problem. This point will be addressed in detail Chapter V when we discuss analytic solutions to the model developed here. However, we point out that their approach and ours represent different paths to the same result: they determined the on-axis

ratio that the solutions had to have, and then found solutions that had that ratio, and we found solutions that met all the boundary conditions, and then from those solutions found the on-axis ratio.

*Valentini.* Valentini authored or coauthored a number of works involving multi-ion discharges (e. g., Valentini, 1979. Valentini, 1980a. Valentini, 1980b. Valentini, 1988. Shapiro and Valentini, 1991). These examined various combinations of diffusional and free-fall plasmas, low and high ionization fractions, quasi-neutral and non-neutral plasmas, and single and multiple ion species. Valentini differs from others in that he retains the inertia term for the ion momentum equation, even in diffusional plasmas.

We will consider three examples. First is Valentini's 1980 article on discharges containing excited and multiply charged ions (Valentini, 1980b). Valentini examined "...positive columns at low pressure containing several species of ions..."; in particular, he included singly charged ions and either doubly charged ions or singly charged excited ions, as well as electrons (Valentini, 1980b; 243). Since the discharge was at low pressures, the momentum equations for ions contained the inertia term, but no pressure term. He stated that this neglect of the pressure term "...is applicable if the ion temperature is considerably smaller than the electron temperature." (Valentini, 1980b:245). This is appropriate for the conditions he is interested in. The pressure term can be neglected if the average particle velocity is greater than the thermal velocity. In the regimes Valentini was investigating, the electron transport was dominated by diffusion but the ions were in free fall. This implies that the average electron velocity is determined by

the electron thermal velocity. Since Valentini assumed congruence and quasi-neutrality, the electron and ion average velocities were equal. As a result, comparing the ion average and thermal velocities is equivalent to comparing the electron and ion temperatures, which justifies the statement quoted above. Valentini also claimed that inclusion of both the pressure and inertia terms leads to mathematical divergence in the system. He assumed quasi-neutrality except near the edge of the plasma, and congruence, and then used these assumptions to eliminate the electric field from the continuity and momentum equations for the electrons and ions. Various types of power series expansions produced values for the variables at the axis of symmetry, and numerical integration then produced solutions. In all cases, the solutions he presented "...are...for discharges in argon in free-fall conditions..." (Valentini, 1980b;243,257). Although he claims to extend Tonks and Langmuir to plasmas containing two species of ions, he actually does so only for the case where two ions exist, one singly charged and one doubly charged, and where the singly charged ion dominates the discharge; other cases are outside the regime of his analysis (Valentini, 1980b; 243, 262).

Valentini's 1988 paper discusses the mathematical difficulties that arise for very high drift velocities if both the inertia and pressure terms are retained (Valentini, 1988). He develops a single-ion model that retains both terms, and then uses a number of different power series methods to obtain solutions without assuming quasi-neutrality. He then extends this to a multi-ion model that explicitly includes quasi-neutrality. He provides no solutions for the multi-ion case.

Finally, consider Shapiro and Valentini (Shapiro and Valentini, 1991). This is an extension of the article just discussed to include high ionization rates in multiply charged ion plasmas "...under free-flight conditions." (Shapiro and Valentini, 1991:391). The authors treat electrons, single and doubly-ionized ions, and neutral gases in a cylindrical quasi-neutral positive column at very low pressure. They consider very high degrees of ionization, so that the background gas density can no longer be considered constant, but must be included in the differential equation system. The ion inertia terms are included in the momentum, and the pressure terms are discarded. To solve this system, they assume congruence and quasi-neutrality. This allows them to eliminate the electric field from their system. They then establish boundary conditions based on the symmetry of the system, the normalization of the electron density, and the requirement that the derivatives of the variables be bounded. They use a power series expansion about the axis of symmetry to establish the starting values for the system, and then numerically integrate the system. They present results for a number of cases involving variations in the ratio of ionization rates for the two species, the fractional ionization, and the importance of Coulomb collisions.

Examination of Valentini's works reveals that they are all similar and are based on retention of the inertia term in the ion momentum equation, generally to the exclusion of the pressure term. Although his theoretical models are very general, addressing the entire regime of the free-fall discharge and approaching the diffusion regime, his solutions tend to rely on power series or purely numerical methods to solve the systems. He

addresses the extremes of the regimes, beyond the interest of other authors. The articles discussed above are typical in this regard; phenomena addressed in one, the other, or both include ionization fraction much higher than the typical positive column (although not out of line for ion lasers), multiply-charged or excited ions, or nonuniform background gas density and temperatures. With situations of such complexity, only numerical solutions are possible.

*Wunderer.* Wunderer derived a model for plasmas containing multiple positive ions using Schottky's assumptions (Wunderer, 1978). In addition, he expanded the electric field in a power series to allow for easier numerical solutions. He obtained only numerical solutions, but concentrated more on showing the general failure of the assumption of proportionality. We will discuss his model in much more detail in Chapter VI, when we compare the results of our model with previous efforts. Of general note, however, is that he is one of the few authors to address external ionization sources for multi-ion discharges.

### *Conclusions Drawn from Comparison of the Various Models*

Table 2-1 summarizes the various features of the models discussed, including the model to be developed in this paper. Several conclusions can be drawn from the works described above. First, analytic solutions are not obtained for models that retain Poisson's equation. Second, none of the models produced multi-ion analytic solutions without assuming proportionality or some other condition equally restrictive. Third, based on the difficulties Edgley and von Engel found in producing numerical solutions,



**Table 2-1. Comparison of Various Models**

<b>Article</b>	<b>Additional Assumptions</b>	<b>Major Area of Applicability</b>	<b>Solutions</b>
Schottky, 1224	Quasi-neutrality, congruence, zero charge gradient	Single-ion Diffusion	Analytic
Tonks and Langmuir, 1929	Quasi-neutrality, congruence	Single ion, free-fall to diffusion	Analytic
Ecker, 1954	Congruence, proportionality	Single ion free diffusion	Numerical
Allis and Rose, 1954	Congruence	Single ion free diffusion	Numerical
Oskam, 1958	Quasi-neutrality, congruence, proportionality	Multi-ion, diffusion	Analytic
Edgley & von Engel, 1980	None	Multi-ion, free to ambipolar diffusion, free fall to diffusion	Limited numerical
Ferreira <i>et alia</i> , 1988	Quasi-neutrality, congruence	Multi-ion, diffusion	Numerical
Valentini <i>et alia</i> , various	Free fall	Multi-ion, free fall	Numerical
Present Model	Quasi-neutral, zero charge gradient	Multi-ion, diffusion	Analytic and numerical

it is difficult to model multi-ion systems by brute force techniques. Instead, it is generally necessary to take advantage of the physical properties of the discharge to justify a simplifying assumption such as quasi-neutrality.

In Table 2-1, "Additional Assumptions" refers to assumptions beyond those necessary to produce the final form of the momentum and continuity

equations shown in Chapter I. "Zero charge gradient" refers to the assumption that the gradient of the net charge density is zero.

### *Problems To Be Addressed*

A number of problems in describing multi-ion ambipolar diffusion have not yet been addressed by other authors. The remaining chapters will address many of them. At this point, we will describe exactly what those problems are.

*Proportionality.* Proportionality has been widely used to describe multi-ion plasmas, both in theoretical analyses and in interpretation of experimental data. To date there has been no analysis of when it will be valid, and when it will not. Furthermore, the assumption of proportionality under present theories does not provide any information about the form of possible analytic solutions, except for the fact of proportionality itself. Finally, there are no descriptions of the difficulties in defining and using measurements of proportionality. All these issues will be addressed in Chapters IV, V, and VI.

*Analytic Solutions.* At present there is no multi-ion diffusion model that produces analytic solutions without assuming proportionality, or some other constraint equally restrictive. Present theories can only produce analytic solutions by first assuming proportionality (or some other restrictive constraint), finding the solutions, and then seeing if the assumption is valid. In Chapter V we will see analytic solutions developed in most cases without the assumption of proportionality or any other restrictive constraint. Even when a solution cannot be found without the assumption of propor-

tionality, the results of the analysis in Chapter IV can be used to determine the form of the solution and verify the validity of the assumption, prior to determination of the solutions.

*Scaling Relationships.* Although scaling relationships for single-ion ambipolar diffusion are well-known, the lack of analytic solutions has made development of additional scaling relationships for multi-ion diffusion difficult to date. In Chapters IV, V, and VI, expressions will be developed that quantitatively or qualitatively describe the scaling of such parameters as on-axis densities, species fractions, particle fluxes, and electron temperature.

### *III. New Ambipolar Diffusion Model*

#### *Introduction*

Recall that Schottky's model of ambipolar diffusion relies on the assumption of congruence, and leads to multi-ion models that cannot produce analytic solutions without restrictive assumptions. Even though congruence is very often a valid assumption, it is not universally so. It would be useful to develop a model that is based on a more general assumption than congruence, and which allows analytic solutions without restrictions as severe as proportionality. The model presented here does that.

We will develop the model in a completely general formulation. We will then look at the form the model takes when used to investigate time-independent systems containing only positive ions. Finally, we will transform the system into a dimensionless form that is more convenient for theoretical analysis than a form using the physical variables.

#### *General Formulation*

As did Schottky, we assume charge neutrality:

$$\sum_i q_{+i} N_{+i} = \sum_j q_{-j} N_{-j} \quad (3-1)$$

We also assume that the gradient of the net charge density is zero, which is equivalent to assuming that the charge-weighted sum of the gradients of the particles densities are equal:

$$\sum_i q_{+i} \nabla N_{+i} = \sum_j q_{-j} \nabla N_{-j} \quad (3-2)$$

This is the implicit assumption that Schottky made, but did not explicitly use. It cannot be justified on purely mathematical grounds; as long as we have quasi-neutrality, and not exact neutrality, it is possible for Equation 3-1 to be valid, without Equation 3-2 being valid. For example, let us look at a hypothetical example, chosen not because it is realistic, but because it illuminates the mathematical possibilities. We will assume that  $N_i$  and  $N_e$  may be defined as follows:

$$\begin{aligned} N_i &= N_0 x \\ N_e &= N_0 (x + \delta \cos \lambda x) \end{aligned} \tag{3-3}$$

If we have  $\delta \ll 1$ , then quasi-neutrality is valid. However, note that we obtain the following results for the gradients of the number densities:

$$\begin{aligned} \nabla N_i &= N_0 \\ \nabla N_e &= N_0 (1 - \lambda \delta \sin \lambda x) \end{aligned} \tag{3-4}$$

Depending on the relative magnitudes of  $\lambda$  and  $\delta$ , the difference between  $\nabla N_e$  and  $\nabla N_i$  can be very large, thus violating the assumption.

At first, it would seem that the relatively poor mathematical justification for Equation 3-2 casts doubts on the model we are developing. However, as von Engel has pointed out, there are very strong physical grounds to believe that such a pathological case cannot occur in practice; if there were differences between the gradients, strong fields would be created that would eliminate the differences (von Engel, 1965:143). (It should be pointed out that von Engel makes this assumption, and justifies it, but does not use it.

Equation 3-2 is the crucial assumption for the new model. Because of its importance, we should discuss the general validity of this assumption, as

opposed to the assumption of congruence that Schottky used. Congruence ultimately rests on Equation 3-1 and the continuity equations. From conservation of charge, we know that the sum of net source terms for the positive species must equal the sum of the negative terms. From quasi-neutrality, we know that the sum of  $\partial N/\partial t$  for the positive terms must equal the same sum for the negative terms. Therefore, summing the continuity equations implies that the sums of the  $\nabla \cdot \Gamma$ 's of the two charge polarities must be equal also. In a one-dimensional system, this implies that the fluxes themselves are equal. However, in systems of more than one dimension, it is possible to maintain quasi-neutrality without having the fluxes equal. Rather, it is sufficient for the magnitudes of the fluxes to be equal: their directions can be different. For example, consider the common textbook problem of diffusion in the presence of a magnetic field. The cyclotron frequency of ions is much lower than that of the electrons. As a result, it is possible for situations to arise where the ions undergo many collisions in a single orbit, while the electrons do not. Since collisions tend to disrupt the coherent cyclotron orbiting, electron diffusion across the field is restrained by the magnetic field more than the ion diffusion. As a result, it is possible for the electrons to leave only by diffusing along the magnetic field while the ions can diffuse across the field. (For a detailed exposition, see Golant, Zhilinsky, Sakharov, and Brown, Mitchner and Kruger, or Chen (Golant, Zhilinsky, Sakharov, and Brown, 1980:305-308. Mitchner and Kruger, 1973: 173-182, 179. Chen, 1984: 173-175).) In consequence, we see that congruence is generally valid only for one-dimensional plasmas.

Equation 3-2 rests on much firmer grounds than congruence. First, the very presence of diffusion itself tends to eliminate small-scale gradients in particle density. This tendency reduces the gradients in charge density that could invalidate Equation 3-2. Second, as was noted above, any gradients that did exist would produce fields that would also tend to eliminate the gradients. In a real plasma, such gradients imply changes over a distance on the order of the Debye length at the most. But the fact that we are describing quasi-neutral plasma is sufficient to ensure that the Debye length is much smaller than the characteristic physical length  $\Lambda$  of the plasma for almost all cases of interest. Therefore, we conclude that using Equation 3-2 to describe features of size comparable to  $\Lambda$  for a quasi-neutral plasma is quite appropriate.

To continue, if we rearrange the first two equations of the system in Equation 2-8, we get

$$\begin{aligned}\vec{\nabla} N_{+,i} &= -\frac{\vec{\Gamma}_{+,i}}{D_{+,i}} + \frac{\mu_{+,i}}{D_{+,i}} N_{+,i} \vec{E} \\ \vec{\nabla} N_{-,j} &= -\frac{\vec{\Gamma}_{-,j}}{D_{-,j}} - \frac{\mu_{-,j}}{D_{-,j}} N_{-,j} \vec{E}\end{aligned}\tag{3-5}$$

We now multiply these equations by their charge, sum over  $i$  or  $j$ , as appropriate, and set them equal, in accordance with Equation 3-2. It is then straightforward to use the result to find the electric field:

$$\vec{E} = \frac{\sum_i \frac{q_{+,i} \vec{\Gamma}_{+,i}}{D_{+,i}} - \sum_j \frac{q_{-,j} \vec{\Gamma}_{-,j}}{D_{-,j}}}{\sum_i \frac{q_{+,i} \mu_{+,i}}{D_{+,i}} N_{+,i} + \sum_j \frac{q_{-,j} \mu_{-,j}}{D_{-,j}} N_{-,j}}\tag{3-6}$$

Note that the sums are over all positive or negative species.

Upon substituting Equation 3-6 into Equation 3-5 we obtain

$$\begin{aligned} \nabla N_{+,i} &= -\frac{\vec{\Gamma}_{+,i}}{D_{+,i}} + \frac{\mu_{+,i}}{D_{+,j}} N_{+,i} \left( \frac{\sum_k q_{+,k} \frac{\vec{\Gamma}_{+,k}}{D_{+,k}} - \sum_j q_{-,j} \frac{\vec{\Gamma}_{-,j}}{D_{-,j}}}{\sum_k q_{+,k} \frac{\mu_{+,k}}{D_{+,k}} N_{+,k} + \sum_j q_{-,j} \frac{\mu_{-,j}}{D_{-,j}} N_{-,j}} \right) \\ \nabla N_{-,j} &= -\frac{\vec{\Gamma}_{-,j}}{D_{-,j}} - \frac{\mu_{-,j}}{D_{-,j}} N_{-,j} \left( \frac{\sum_i q_{+,i} \frac{\vec{\Gamma}_{+,i}}{D_{+,i}} - \sum_k q_{-,k} \frac{\vec{\Gamma}_{-,k}}{D_{-,k}}}{\sum_i q_{+,i} \frac{\mu_{+,i}}{D_{+,i}} N_{+,i} + \sum_k q_{-,k} \frac{\mu_{-,k}}{D_{-,k}} N_{-,k}} \right) \end{aligned} \quad (3-7)$$

$$\nabla \cdot \vec{\Gamma}_{+,i} + \frac{\partial N_{+,i}}{\partial t} = S_{+,i}$$

$$\nabla \cdot \vec{\Gamma}_{-,j} + \frac{\partial N_{-,j}}{\partial t} = S_{-,j}$$

Note the significant differences between this form and, for instance, Oskam's. In Oskam's form, each equation for  $\nabla N$  included  $\vec{\Gamma}$  for the same species, plus all the other  $\nabla N$ 's. In this model, each  $\nabla N$  equation includes all the  $\vec{\Gamma}$ 's, but no other  $\nabla N$ 's. Note also that Oskam's form had, in the denominator, sums over terms of the form  $q\mu N$ . Even if we have singly-charged ions, all at the same temperature, we cannot simplify these sums. However, Equation 3-7 has sums over terms of the form  $qN\mu/D$ . As we will see shortly, this form allows for tremendous simplification for certain conditions.



Both the new model and Schottky-based models are equally valid for any system where ambipolar diffusion itself is valid. The differences are that Schottky-based models use all the assumptions of the new model plus congruence and that in many cases the new model is much easier to solve, both analytically and numerically. In the next section we will develop the formalism for such cases.

### *Time-Independent Formulation, Positive Ions*

It is especially fruitful to examine time-independent cases involving positive ions. In our formulation, only the continuity equations had explicit time dependence. If we consider stationary conditions and assume that the only negative species present are electrons, Equation 3-7 becomes

$$\begin{aligned} \nabla N_e &= -\frac{\vec{\Gamma}_e}{D_e} - \frac{\mu_e}{D_e} N_e \left( \frac{\sum_j \frac{\vec{\Gamma}_j}{D_j} - \frac{\vec{\Gamma}_e}{D_e}}{\sum_j q_j \frac{\mu_j}{D_j} N_j + \frac{\mu_e}{D_e} N_e} \right) \\ \nabla N_i &= -\frac{\vec{\Gamma}_i}{D_i} + \frac{\mu_i}{D_i} N_i \left( \frac{\sum_j \frac{\vec{\Gamma}_j}{D_j} - \frac{\vec{\Gamma}_e}{D_e}}{\sum_j q_j \frac{\mu_j}{D_j} N_j + \frac{\mu_e}{D_e} N_e} \right) \end{aligned} \quad (3-8)$$

$$\nabla \cdot \vec{\Gamma}_i = S_i$$

$$\nabla \cdot \vec{\Gamma}_e = S_e$$

Now, recall the Einstein relationship for ions:

$$\frac{\mu_i}{D_i} = \frac{q_i}{kT_i} \quad (3-9)$$

In almost all plasmas where sufficient collisions occur to make diffusion a reasonable model, the ions will be in thermal equilibrium with the background gas, which means that all the ion species will have the same temperature. Therefore, we see that  $\mu_j/D_j$  is equal to  $q_j/kT_+$  for all ion species, where "+" refers to the values common to all the ions.. So, we see that  $\sum(\mu_j/D_j)N_j$  now becomes  $1/kT_+\sum q_jN_j$ . But, from the assumption of quasi-neutrality, we have  $\sum q_jN_j = eN_e$ , for positive ions. Therefore, the momentum equations become

$$\begin{aligned} \nabla N_e &= -\frac{\vec{\Gamma}_e}{D_e} - \frac{\mu_e}{D_e} \left( \frac{\sum_j \frac{\vec{\Gamma}_j}{D_j} \cdot \frac{\vec{\Gamma}_e}{D_e}}{\frac{\mu_+}{D_+} + \frac{\mu_e}{D_e}} \right) \\ \nabla N_i &= -\frac{\vec{\Gamma}_i}{D_i} + \frac{\mu_i}{D_i} \frac{N_i}{N_e} \left( \frac{\sum_j \frac{\vec{\Gamma}_j}{D_j} \cdot \frac{\vec{\Gamma}_e}{D_e}}{\frac{\mu_+}{D_+} + \frac{\mu_e}{D_e}} \right) \end{aligned} \quad (3-10)$$

Here, we have defined  $\mu_+/D_+$  as equal to  $e/kT_+$ . For singly charged ions, we note that  $\mu_+/D_+ = \mu_j/D_j$  precisely. For multiply charged ions, we have  $\mu_+/D_+ = \mu_j/(D_jZ_j)$ , where  $Z_j$  is the multiplicity of the charge.

We immediately discover that this form is much simpler than those based on the assumption of congruence in Schottky's model. The equation for  $N_i$  no longer depends on any other ion density. In addition, the equation for  $N_e$  does not depend on any particle density at all. In Chapter V we will see how to take advantage of these relationships to produce analytic

solutions. We do so for singly charged ions, but note that much of the analysis would apply to multiply charged ions, as well.

We note that in some instances a similar transformation might be used to model systems containing negative species. If the electrons are at the same temperature as the negative ions (as might occur in an afterglow plasma, for instance), then the arguments given above would apply to the negative species, producing a similar simplification. We will not go into these systems in detail. However, consider such a system with a single positive species, denoted by "+", a single negative species, denoted by "-", and electrons, denoted by "e". The analog to Equation 3-10 would be

$$\begin{aligned}
 \nabla N_e &= -\frac{\vec{\Gamma}_e}{D_e} - \frac{\mu_e N_e}{D_e N_+} \left( \frac{\vec{\Gamma}_+}{D_+} - \frac{\vec{\Gamma}_e}{D_e} - \frac{\vec{\Gamma}_-}{D_-} \right) \\
 \nabla N_- &= -\frac{\vec{\Gamma}_-}{D_-} - \frac{\mu_- N_-}{D_- N_+} \left( \frac{\vec{\Gamma}_+}{D_+} - \frac{\vec{\Gamma}_e}{D_e} - \frac{\vec{\Gamma}_-}{D_-} \right) \\
 \nabla N_+ &= -\frac{\vec{\Gamma}_+}{D_+} + \frac{\mu_+}{D_+} \left( \frac{\vec{\Gamma}_+}{D_+} - \frac{\vec{\Gamma}_e}{D_e} - \frac{\vec{\Gamma}_-}{D_-} \right)
 \end{aligned} \tag{3-11}$$

Here,  $\mu/D$  denotes both electron and negative ion values. We point out that this system, although appearing to be analogous to that described in Equation 3-10, does have a significant difference. For the system described in Equation 3-10, the most common source term depends on  $N_e$ , which is the only negative species. As we will see in the next chapter, that allows us to find analytic solutions in some cases. Here,  $N_e$  is not the only negative

species. That renders the solution techniques of the next chapter less useful. We will discuss this somewhat further when the analogous cases arises in the next chapter.

### *Dimensionless Differential Equations*

At this point we will transform the system of equations from the physical variables to a new set of dimensionless variables. Note that this will not necessarily result in normalized forms. Normalization is the process of defining the units by which we will measure a quantity so that the value of the quantity at some convenient point is 1. Although this may make numerical calculations easier, it does not necessarily make the physics any simpler. When we transform into dimensionless form, we rescale the quantities to make them all dimensionless. This generally involves dividing or multiplying them by some number characteristic of the system. As a result, the scale parameters are of physical significance, whereas in a brute force normalization they may not be.

*Justification for Dimensionless Form.* The use of a dimensionless system gives us several advantages:

1. Simplifies the equations by reducing the number of parameters. This allows an easier understanding of the underlying structure of the differential equation system.
2. Replaces the physically observable parameters in the original equations with parameters that are more significant to the physical processes occurring in the system. This highlights the most important of those processes and clarifies the scaling of the system.

The dimensionless form was found most useful for the present model in forming and evaluating analytic solutions. For purely numerical solutions, it is often just as easy to use the physical quantities. For this particu-

lar formulation, introducing dimensionless forms led to a numerically less stable system. We will discuss that point further when we discuss numerical solutions.

*Definition of the Dimensionless Variables.* First consider the spatial coordinate,  $x$  or  $r$ . We divide that coordinate by the distance from the center of the plasma to the edge:

$$\begin{aligned}\rho &= \frac{x}{d} \\ \rho &= \frac{r}{R}\end{aligned}\tag{3-12}$$

The form we choose depends on whether we are using cylindrical or spherical geometry. Here  $R$  is the radius of a cylindrical plasma, and  $d$  the half-width of a planar plasma. This gives us a spatial coordinate that ranges from  $\rho = 0$  at the axis or plane of symmetry of the system to  $\rho = 1$  at the edge of the plasma.

Next, we consider the particle densities. We define

$$n = NL^3\tag{3-13}$$

where  $L$  is either  $R$  or  $d$ , depending on whether we have cylindrical or planar geometry. Notice that the dimensionless particle densities still satisfy quasi-neutrality:

$$\sum n_i = n_e\tag{3-14}$$

Now, we define particle current densities:

$$\vec{\gamma} = \frac{\vec{\Gamma}}{D} L^4\tag{3-15}$$

Notice that the  $\vec{\gamma}$ 's do not satisfy congruence, even if the  $\vec{\Gamma}$ 's do. Rather, we find

$$\sum \tilde{\gamma}_i D_i = \tilde{\gamma}_e D_e \quad (3-16)$$

For the source term, we define

$$s = \frac{S}{D} L^5 \quad (3-17)$$

This definition is for the most general form of  $S$ . We will define other quantities related to more specific source terms later. Note that, although we have

$$\sum S_i = S_e \quad (3-18)$$

we do not obtain the same result for the dimensionless form. Instead we see

$$\sum s_i D_i = s_e D_e \quad (3-19)$$

We define the dimensionless field as

$$\vec{\mathcal{E}} = \frac{\mu_+}{D_+} L \vec{E} \quad (3-20)$$

Finally, we define

$$\epsilon \equiv \frac{\frac{\mu_e}{D_e}}{\frac{\mu_+}{D_+}} = \frac{kT_+}{kT_e} \quad (3-21)$$

*Dimensionless Equations.* With the definitions above, the dimensionless equations become (see Appendix A):

$$\begin{aligned}
\nabla n_i &= -\vec{\gamma}_i + \frac{n_i}{n_e} \frac{\sum_j \vec{\gamma}_j - \vec{\gamma}_e}{1 + \epsilon} \\
\nabla n_e &= -\frac{\epsilon \sum_j \vec{\gamma}_j + \vec{\gamma}_e}{1 + \epsilon} \\
\nabla \cdot \vec{\gamma}_i &= s_i \\
\nabla \cdot \vec{\gamma}_e &= s_e \\
\vec{\mathcal{E}} &= \frac{\sum_j \vec{\gamma}_j - \vec{\gamma}_e}{n_e(1 + \epsilon)} = -\left( \frac{\nabla n_e + \gamma_e}{\epsilon n_e} \right)
\end{aligned} \tag{3-22}$$

Note that the gradient operator is now with respect to  $\rho$ , not  $r$ . We will maintain that definition when using the dimensionless formulation throughout the remainder of this paper, unless specified otherwise.

Before we leave these equations, we will exploit the last expression in Equation 3-22 to recover the well-known Boltzmann relation. First, we note that, in most cases,  $D_e$  is several orders of magnitude greater than  $D_i$  for any of the ions. This implies that  $\gamma_i$  is much greater than  $\gamma_e$  for at least one species. (This is the essence of the small-e-flux approximation, to be addressed in more detail in Chapter 5.) Since  $\nabla n_e$  is of the approximate order of  $\epsilon \sum \gamma_i + \gamma_e$ , we conclude that  $\gamma_e$  can be neglected compared to  $\nabla n_e$ . We then express the electric field in terms of the scalar potential and integrate, to obtain the Boltzmann relation:

$$N_e = N_{e0} \exp(e\phi/kT_e) \tag{3-23}$$

The significant conclusion is not the recovery of the Boltzmann relation, since it is commonly used to describe the electron density in ambipolar

diffusion plasmas (Tonks and Langmuir, 1929: 883). Rather, it is the limits of the validity that the new model places on the use of the Boltzmann relation in describing ambipolar diffusion. The Boltzmann relation is the solution of the ambipolar diffusion equations for the electron density only in those cases where the electrons are much more mobile than the ions.

### *Conclusions*

We have now developed a new model describing diffusion in quasi-neutral plasmas. The fundamental difference between this model and those based on Schottky's is the substitution of Equation 3-2 for congruence. However, even though Equation 3-2 mathematically does not necessary follow from quasi-neutrality, we find physical grounds for believing it to be valid in situations where congruence is not. In addition, the model that results has a form that will prove to make analytic solutions possible in situations where other models cannot.



## *IV. Implications of Proportionality*

### *Introduction*

This chapter examines the concept of proportionality and its implications for multi-ion ambipolar diffusion. We have several reasons to do so. First, we wish to find conditions under which the assumption of proportionality is valid. Second, we wish to be able to predict the relative scaling of the number densities for the proportional analytic solutions that we will develop in the next chapter. Third, we wish to apply those predictions to finding analytic solutions for systems where proportionality is not necessarily valid.

We will introduce proportionality more formally than we have before, including various ways of expressing it. We will then determine a set of necessary conditions for proportionality to hold, and examine the physical consequence of those conditions. We will examine some typical plasma systems, (including the ones we will discuss in Chapter V), and use the conditions determined in this chapter to explain why proportionality does or does not hold.

Note that we do not address in this chapter the question of how far a system can deviate from true proportionality before proportional solutions no longer provide an adequate description of the system. The reason is that the main emphasis of this chapter is on analytic solutions. Such questions are appropriate for the various numerical cases examined in Chapter VI.

### *Definitions of the Concept of Proportionality*

Proportionality in the most limited usage of this document is the condition that all the particle number densities have the same spatial dependence, differing only by a multiplicative factor. More general usages include proportionality of the fluxes, and of the source functions. Regardless of the exact usage, the important concept is that some function has the same spatial dependence for all the species.

Proportionality is usually defined in terms of the various ion densities being proportional to the electron density:

$$N_i(\vec{r}) = K_i N_e(\vec{r}) \quad (4-1)$$

There are other formulations as well. Those which we found useful in this research will be discussed in the next sections.

*Proportionality for the Normalized Equations.* Recall the definition of the normalized number density:

$$n = NL^3 \quad (4-2)$$

Since  $L$  is a constant, independent of  $r$ , we immediately see that a formulation of proportionality exactly equivalent to Equation 4-1 is

$$n_i(\vec{\rho}) = K_i n_e(\vec{\rho}) \quad (4-3)$$

This is the form we will use henceforth.

*Other Expressions for Proportionality.* There are several ways to express proportionality, which are totally equivalent to the definition given above. First, let us take the gradient of that definition to obtain

$$\nabla n_i(\vec{\rho}) = K_i \nabla n_e(\vec{\rho}) \quad (4-4)$$

Mathematically, we know that any functions that satisfy Equation 4-3 must also satisfy Equation 4-4. Therefore, Equation 4-4 is a necessary condition

for proportionality. Let us now show that it is generally sufficient, as well. Note that Equation 4-4 implies

$$n_i(\vec{\rho}) = K_i n_e(\vec{\rho}) + C \quad (4-5)$$

where  $C$  is some constant, as yet undetermined. However, we note that the Schottky boundary condition  $n = 0$  at the boundary of the plasma is valid to a very high accuracy for diffusion-dominated plasmas. This boundary condition cannot be met for  $C \neq 0$ . Therefore, we determine that  $C$  is identically zero, and proportionality holds.

From these arguments we see that proportionality of the gradients is a necessary and sufficient condition for proportionality of the number densities themselves. Therefore, for a particular situation, if we have shown the validity of Equation 4-3, we have shown the validity of Equation 4-4, and *vice-versa*.

Finally, we will mention another formulation. Since the constant  $K_i$  is the same whether we are discussing the number densities or their gradients, we have

$$\frac{\nabla n_i(\vec{\rho})}{\nabla n_e(\vec{\rho})} = K_i = \frac{n_i(\vec{\rho})}{n_e(\vec{\rho})} \quad (4-6)$$

or, equivalently,

$$\frac{\nabla n_e(\vec{\rho})}{n_e(\vec{\rho})} = \frac{\nabla n_i(\vec{\rho})}{n_i(\vec{\rho})} \quad (4-7)$$

### *Physical Implications*

The conclusions we have drawn so far rely on mathematical manipulation of very general conditions. Therefore, although they are very broad in application, they also lack somewhat in immediate utility and physical

relevance. We will now include the results of the model of ambipolar diffusion developed in Chapter III to produce more useful expressions.

*Ratio of the Fluxes.* We will develop an expression for the ratio of the ion flux to the electron flux by first considering the ratio of the gradients again:

$$\frac{\nabla n_i(\vec{\rho})}{\nabla n_e(\vec{\rho})} = K_i \quad (4-8)$$

From Equation 3-22 we find expressions for  $\nabla n_e$  and  $\nabla n_i$ . With those expressions, Equation 4-8 becomes

$$\frac{-\vec{\gamma}_i + \frac{n_i}{n_e} \left( \frac{\sum_j \vec{\gamma}_j - \vec{\gamma}_e}{1 + \epsilon} \right)}{\left( \frac{\epsilon \sum_j \vec{\gamma}_j + \vec{\gamma}_e}{1 + \epsilon} \right)} = K_i \quad (4-9)$$

With some algebraic manipulation, and taking advantage of the relationship  $n_i/n_e = K_i$ , we can simplify this to

$$\frac{\vec{\gamma}_i}{\sum_j \vec{\gamma}_j} = K_i \quad (4-10)$$

Note that this simple form is not due to any simplifying assumptions, but rather reflects the inherent symmetry of the equations themselves.

With this relationship, we can write

$$\frac{\vec{\gamma}_i}{K_i} = \sum_j \vec{\gamma}_j \quad (4-11)$$

The right hand side of this equation is independent of the particular ion species denoted by the subscript  $i$ . Therefore, all the  $\gamma_i$ 's have the same spatial dependence, or are proportional. Note that this does not imply that

the proportionality constant for the dimensionless fluxes is  $K_i$  , or equivalently,  $\gamma_i = K_i \gamma_o$  . In order to have  $\gamma_i = K_i \gamma_o$  , we would need  $\gamma_o = \sum \gamma_j$  . Instead, we have  $\gamma_o = \sum D_j \gamma_j$  .

Since Equation 4-10 is a direct consequence of proportionality, we see that it is a necessary condition for proportionality to hold. In fact, we can state that a necessary condition for proportionality is simply for that ratio to be a constant with respect to spatial variation; if it is not constant, it certainly cannot be equal to  $K_i$  .

Note that neither Equations 4-10 nor 4-11 are sufficient conditions: in deriving them, we used proportionality in the form  $n_i/n_o = K_i$  to simplify the equation. This prevents us from reversing the argument to show sufficiency.

*Source Term Proportionality.* Expressing Equation 4-10 as

$$\vec{\gamma} = K_i \sum_j \vec{\gamma}_j \quad (4-12)$$

we take the divergence of both sides and then divide to obtain

$$\frac{\nabla \cdot \vec{\gamma}}{\sum_j \nabla \cdot \vec{\gamma}_j} = K_i \quad (4-13)$$

Therefore, this relationship is a necessary (but again not sufficient) condition for proportionality. This is the relationship that is, in fact, the most useful, for it allows us to determine that proportionality solutions do not exist for a particular case without knowing the solutions. As before,

Equation 4-13 is still a necessary condition even if the constant is not known to be  $n_i/n_e$ .

In fact, we will henceforth express Equation 4-13 and its variants using  $C_i$  instead of  $K_i$ , to emphasize that the necessary condition is that the ratio be a constant, whether we know that constant to, indeed, be  $K_i$  or not. In practice, this position is probably overly conservative. However, we wish to keep in mind that, since Equation 4-13 is only a necessary condition, it is in principle possible to have a system that satisfies Equation 4-13 and yet is still nonproportional. Only after we determine the solutions can we verify proportionality. The importance of Equation 4-13 lies in being able to determine the allowed form of the proportionality constant before we have the solutions available to us.

#### *Case Studies of Proportionality for Particular Source Terms*

Our emphasis now turns to discovering how the conditions for proportionality we just developed can be used in finding solutions for systems. To that end, we first define a generalized source term:

$$\nabla \cdot \gamma_k = s_k(\rho) + Q_k(n_e, n_i) \quad (4-14)$$

where  $Q_k$  is a multivariate polynomial in  $n_e$  and all the  $n_i$ 's. We note that here the "k" subscripts refer to either electrons or ions. This source term can be used to describe any dependence on position,  $n_e$ , or the various  $n_i$ 's, as long as the dependence on the  $n_i$ 's is itself independent of position. (As an example, if a particular term in  $Q_k$  were of the form  $\alpha n^m$ , then neither  $\alpha$  nor  $m$  could be a function of position.) We refrain from express-

ing  $Q_k$  more explicitly; since it could include all combinations of all powers of all the species, such an expression would be extremely cumbersome. Also, for convenience, we exclude from  $Q_k$  any constant terms; any such term could be more conveniently expressed as part of  $s_k$ .

Let us now examine specific cases. We shall come back afterwards and draw further conclusions, guided by the results of the examples.

*Volume Ionization.* First, we examine the case where a generalized volume ionization is the only ionization term present. Then, the necessary condition for proportionality becomes

$$\frac{Q_i}{\sum_j Q_j} = C_i \quad (4-15)$$

We will express Equation 4-15 in a different form:

$$\frac{Q_i}{C_i} = \sum_j Q_j = P \quad (4-16)$$

where we have defined  $P = \sum_j Q_j$ .

Equation 4-16 is equivalent to stating the equality of two polynomial functions:  $Q_i/C_i$  and  $P$ . In order for any two polynomial functions to be equal, they must be equal on a term-by-term basis. But,  $P$  is independent of  $i$ . Therefore we would not, in general, expect proportionality to hold. As a result, our conclusion is that proportionality generally does not occur for systems with arbitrary volume ionization source terms.

This, of course, does not eliminate the possibility of particularly simple but still physically realistic cases where proportionality may hold. Let us now consider some of those cases. We will consider a specific example of the source term above:

$$\nabla \cdot \vec{\gamma}_i = \alpha_{ie} n_e^{m_i} + \sum_j \alpha_{ij} n_j^{m_{ij}} \quad (4-17)$$

where  $\alpha_{ik}$  is the rate constant for formation (or loss) of species  $i$  due to species  $k$ ,  $m_i$  refers to the dependence of the source term on the electron density,  $m_{ik}$  refers to the dependence of species  $i$  on the particle density for ionic species  $k$ , and where  $k$  represents either ionic species or electrons. From Equation 4-13, we know that for proportionality to be a possibility at all, we must have

$$\frac{\nabla \cdot \vec{\gamma}_i}{\sum_j \nabla \cdot \vec{\gamma}_j} = C_i \quad (4-18)$$

This leads to

$$\frac{\alpha_{ie} n_e^{m_i} + \sum_j \alpha_{ij} n_j^{m_{ij}}}{\sum_k \left( \alpha_{ke} n_e^{m_k} + \sum_j \alpha_{kj} n_j^{m_{kj}} \right)} = C_i \quad (4-19)$$

where  $k$  now refers to ionic species only. At first glance it is not apparent whether this expression allows for proportionality or not. Proportionality would be possible if each  $Q_i$  depends on the same species, and has the same dependence on that species. The simplest such cases are where that source term depends linearly on  $n_e$  for each species, which leads to the analytic volume ionization cases in the next chapter. Such a source term may be written as

$$\nabla \cdot \vec{\gamma}_i = f_i n_i \quad (4-20)$$



where  $f_i$  is a dimensionless ionization frequency defined as  $v_i L^2 / D_i$ . In such a case, Equation 4-13 predicts the following relationship between  $n_e$  and  $n_i$ :

$$n_i = \frac{f_i}{\sum_j f_j} n_e \quad (4-21)$$

Indeed, the solutions presented in the next chapter give identical results.

Consider next a slightly more complicated system where the source terms depend on more than one species, but depend on all species in the same manner. An example would be a system where all ions had ionization sources as described in Equation 4-20, and where charge transfer from one species to another at a rate proportional to the charged particle number density was present as well. The charge transfer case of the next chapter is an example.

A typical plasma system, slightly more complicated than the last example, would be one with volume ionization, depending linearly on  $n_e$ , and recombination, proportional to  $n_i n_e$ . Such a system would have the following source term:

$$\nabla \cdot \vec{n}_i = f_i n_e - f_{ri} n_i n_e \quad (4-22)$$

Here,  $f_i$  is the dimensionless ionization frequency for species  $i$ , and  $f_{ri}$  is the dimensionless recombination rate for species  $i$ . For proportionality to hold, all ion species must have this dependence, and furthermore, the ratio  $f_i / f_{ri}$  must be the same, regardless of species. We find this highly unlikely, and in fact would not expect proportionality to hold in any such system.

*External Ionization.* In this case, we have the following form for the continuity equations:

$$\nabla \cdot \vec{\gamma}_i = s_i(\rho) \quad (4-23)$$

Then, the necessary condition for proportionality becomes

$$C_i = \frac{s_i}{\sum_j s_j} \quad (4-24)$$

Here, the determination is straightforward. Again, we can rewrite this as

$$s_i = C_i \sum_j s_j = C_i s \quad (4-25)$$

where  $s = \sum_j s_j$ . This says that, for proportionality to be possible, the sources themselves must be proportional. If they are, proportionality may indeed occur, with  $K_i$  equal to  $C_i$  given by Equation 4-24. In the next chapter we will find the general solution for the particular cases of planar and cylindrical geometry with the sources proportional, and show that the solutions are proportional also. Here, we have shown that at the least the proportionality is possible as long as the sources are proportional, independent of geometry.

*External and Volume Ionization.* We will consider a source term that includes both the self and external ionization sources described before. The resulting expression for the necessary condition is

$$C_i = \frac{s_i(\rho) + Q_i}{\sum_j s_j(\rho) + Q_j} \quad (4-26)$$

or

$$s_i(\rho) + Q_i = C_i (S + P) \quad (4-27)$$

where  $S$  and  $P$  are as defined previously. Again, we see that the source terms for each species can differ only by a multiplicative constant, or proportionality cannot hold. Such a condition is extremely unlikely to be

met: even if proportionality holds for the  $s$ 's and  $Q$ 's individually, it is unlikely that the ratio  $s/Q$  would be the same for all species.

### *Using Proportionality to Determine Solutions*

Next, we wish to see how to use our results on proportionality to find solutions. The rationale for the assumption of proportionality by previous authors was to describe multi-ion ambipolar diffusion in cases that could not be described otherwise (See, for example, Oskam) (Oskam, 1958:368). For systems that involve electrons as the only negative species and ions all at the same temperature, we can now state with certainty that it is no longer necessary to make an *a priori* assumption of proportionality. Instead, we can divide all such systems of interest into three areas.

1. For some systems, we can find analytic solutions without having to assume proportionality. Examples of such systems include external ionization where the spatial dependence of the ionization is the same for all species, and simple volume ionization.
2. For some systems, we can show that the solutions are not proportional. Examples of such systems are investigated in the Chapter VI by means of numerical solutions.
3. For some systems, we can show that proportionality is possible, and can then use that possibility to investigate possible analytic solutions. The charge transfer case of the next chapter is an example. There, we used Equation 4-13 for two purposes. First, we used it to determine that proportionality was at least possible. Second, we used it to determine the constraints on the possible proportional solutions.

### *Multi-ion Ambipolar Diffusion Coefficient*

We now have sufficient information to verify an often-used form of an ambipolar diffusion coefficient for proportional systems (for example,

Brown: 1966, 68). Substituting the momentum equation for electrons into Equation 4-4, and with the approximation  $\gamma_i \gg \gamma_e$  we find:

$$\nabla n_i = K_i \nabla n_e = -K_i \left( \frac{\epsilon}{1+\epsilon} \right) \sum_j \gamma_j \quad (4-28)$$

The approximation is based on the common condition  $\mu_e \gg \mu_i$  and will be discussed in more detail in the next chapter as the "small-e-flux approximation."

We use Equation 4-11 to evaluate  $\sum_j \gamma_j$ , producing

$$\nabla n_i = -K_i \left( \frac{\epsilon}{1+\epsilon} \right) \frac{\gamma_i}{K_i} = \frac{\epsilon}{1+\epsilon} \gamma_i \quad (4-29)$$

Expressing this relationship in terms of the physical variables and rearranging terms produces

$$\Gamma_i = -\nabla n_i D_i \left( 1 + \frac{T_e}{T_i} \right) \quad (4-30)$$

This is equivalent to defining an individual ion ambipolar diffusion coefficient as

$$D_{ai} = D_i \left( 1 + \frac{T_e}{T_i} \right) \quad (4-31)$$

From this expression and congruence (which holds for one-dimensional proportional systems, among others), it is straightforward to show the validity of the following definition of an ambipolar diffusion coefficient for the electrons:

$$D_{ae} = \sum_j K_j D_{aj} \quad (4-32)$$

Note the implications of these expressions: first, for proportional systems where the small-e-flux approximation holds (that is, where the electron mobility is much higher than the ion mobility), ambipolar diffusion coefficients can be defined for each ion species that depend on the free diffusion coefficient for that species only, and second, the momentum equation can be expressed as Fick's first law, for both ions and electrons.

Because of the lack of a usable model of multi-ion ambipolar diffusion, previous usages of the diffusion coefficients defined in Equations 4-31 and 4-32 did not clearly state the limits of the definition. For instance, Brown gives the equivalent of Equation 4-31 but never discusses that it applies only for proportional systems, and only for cases where the electron mobility or diffusion coefficient is much higher than the corresponding ion value. In addition, although his definition of the electron ambipolar diffusion coefficient correctly describes it in terms of weighted sums of the ion coefficients, he is unable to provide values for  $N_i/N_e$  (Brown, 1966:67,68). As a result, his expression is of limited utility compared with Equation 4-32, which evaluates  $N_i/N_e$  explicitly.

### *Summary of Results*

Consider a multidimensional "source space" consisting of all possible source functions. Somewhere contained in that space is the subspace of sources that produce proportional solutions. We now have algorithmic methods for determining bounds for that subspace. In some cases we can find the fluxes and determine that such cases are proportional. However, even if we cannot find the fluxes we can often still make determinations of

limits on that subspace from the behavior of the source terms. In particular, we can generally determine the limits without knowing any more than the source terms themselves. This allows us to clearly determine that a particular system or class of systems will not produce proportional solutions, without needing to find the solutions first. To summarize our results more precisely:

1. An necessary condition for proportionality, is

$$\frac{\nabla n_i}{\nabla n_e} = K_i \quad (4-33)$$

For any system for which the Schottky boundary conditions are a reasonable choice, the condition is sufficient as well.

2. For those systems which contain electrons and positive ions only, and for which the Schottky boundary conditions are a reasonable choice, a sufficient condition for proportionality is

$$\frac{\nabla \cdot \gamma_i}{\sum_j \nabla \cdot \gamma_j} = K_i \quad (4-34)$$

3. The only non-pathological cases where proportionality will occur are either those where the only ionization source is an external source, and that source is proportional, or where the only ionization source is generalized volume ionization, with all terms having the same dependence on the number densities.
4. In systems involving positive ions only, if an analytic solution exists, either it can be found without assuming proportionality, or the form of the source term can be used to show that proportionality is allowed and what the constant of proportionality must be.
5. For proportional systems where the small-e-flux approximation is appropriate, ambipolar diffusion coefficients can be defined that allow formulation of the problem in terms of Fick's first law, with  $D$  not a function of position:

$$\Gamma = -D \nabla N \quad (4-35)$$

## *V. Analytic Solutions to the Model*

### *Introduction*

In this chapter we will discuss various analytic solutions of the model developed in Chapter 3. We will emphasize several features of the model in finding those solutions. First, we will demonstrate the advantages the present model has in being able to obtain analytic solutions where other models cannot. Second, we will show that those solutions are consistent with our physical understanding of plasma discharges. Finally, we will use the solutions to confirm the predictions about proportional discharges that we made in Chapter IV.

We emphasize analytic solutions for several reasons:

1. They allow us to describe a wide variety of plasma conditions in a single expression. This lets us see clearly the effect of changing the parameters in the system.
2. They allow us to see the underlying physics of the system more clearly.
3. They allow us to develop solutions more easily, using less time. This allows us to rapidly examine a number of different physical situations.

*Definition of Cases of Interest.* First, we will define the cases we wish to examine. Those cases will be defined by variations in two regimes; geometry and type of source. In addition, all the systems have certain characteristics in common; none of them contain negative ions and they all are systems where all the ions are at the same temperature.

*Geometries.* We will examine two different geometries. The first will be planar geometry. Cases examined using this geometry will consist of

one-dimensional systems, with a plane of symmetry at  $r = 0$ . In such systems, we need only examine one side of the system; we will choose positive values of  $\rho$ . Therefore, we end up with a rectilinear coordinate system, with the only variation being along the  $\rho$  axis, with the plasma confined in the region  $-1 < \rho < 1$ , and where we look only at the region for  $\rho > 0$ . We shall call such systems "P" (for planar) systems.

The second geometry we will examine is cylindrical. We will examine axi-symmetric systems, with no variation with  $z$ . The normalized coordinate  $\rho$  corresponds to the radius from the axis of symmetry. The plasma again consists of a one-dimensional system, confined to the region  $0 < \rho < 1$ . We shall call such systems "C" (for cylindrical) systems.

*Sources.* We will look at two possible ionization sources. One will be external. The  $\rho$  dependence of the external source term is unrestricted, however it is independent of any species densities:

$$\nabla \cdot \vec{\gamma} = s(\rho) \quad (5-1)$$

Although the normalized source function  $s$  depends on the diffusion coefficient  $D$  as well as the actual source function  $S$ , our intent here is to examine cases where the spatial dependence is caused by variations in  $S$ , not  $D$ . Including spatially varying  $D$ s would require additional terms in the momentum equations. Such terms are not addressed here.

We will address very general external sources, including formally solving the system in many cases. In particular, we will find analytic



closed-form solutions for uniform external ionization (designated as "X"), and for a particular double-exponential source (designated as "E").

The other ionization source represents a generalized form of ionization due to the charged species:

$$\nabla \cdot \vec{\gamma} = Q_k(n_e, n_j) \quad (5-2)$$

Here,  $Q_k$  represents a multivariate polynomial in the electron density  $n_e$ , the various ion densities  $n_j$ , and (through the appropriate definition of the coefficients of the terms in  $Q_k$ ) the neutral number density. Clearly, this formalism can accommodate any dependence of the ionization rate on the various particle densities. In addition, the formalism could be easily extended to include dependencies on neutral species, such as excited species, by adding them as addition variables in  $Q_k$ , and including the appropriate continuity and momentum equations.

Chapter IV used the full formalism in discussing proportionality. The cases discussed here will be those where there is only a linear dependence of the generalized ionization on  $n$ . Such cases are designated by "V", identifying an ionization dependence on  $n_e$  only, and "T" when charge transfer is present as well. For brevity of discussion, such sources will be referred to as volume ionization sources. Granted, this is not a completely standardized definition. However, we know of no accepted term that can refer to all possible particle density-dependent sources.

*Boundary Conditions.* The dependent variables in our system of equations are the particle densities and fluxes. Each of these is determined by a first order differential equation. Therefore, each needs a single boundary condition. The boundary condition for the fluxes is determined by sym-

metry, and by the fact that they are vector quantities. That boundary condition is that these quantities must be identically zero at the center of the system, where  $\rho = 0$ . There are a number of realistic boundary conditions appropriate for the particle densities. The common choice of  $n(1) = 0$  will be used. To a very good approximation, this is the appropriate boundary condition for a completely absorbing boundary (Cohen and Kruskal, 1963:921. Phelps, 1990:414). The choice of this boundary condition versus more realistic ones amounts to displacing the boundary by a small amount (See, for instance, Allis and Rose, 1954:84).

*Small-e-Flux Approximation.* We will provide a summary of all the solutions momentarily. Before that, however, a discussion of the small-e-flux approximation mentioned in Chapter IV would be appropriate. This approximation states that the normalized electron flux is much smaller than the total normalized ion flux. In addition, whenever the small-e-flux approximation is valid, a similar approximation for the source terms will be valid also. The term "small-e-flux approximation" will be used indiscriminately (albeit somewhat simplistically), to refer to all of these approximations. They can be stated as

$$\begin{aligned} \frac{\gamma_e}{\sum_j \gamma_j} &<< 1 \\ \frac{s_e}{\sum_j s_j} &<< 1 \\ \frac{f_e}{\sum_j f_j} &<< 1 \end{aligned} \tag{5-3}$$

where  $s$  can refer either to a generalized source or a specific external source function, and  $f$  refers to the dimensionless ionization frequency for the V or T cases. Nowhere does the validity of the model developed in this paper depend on these approximations. However, they are very well justified, and they allow simplification of a number of expressions. This allows us both to obtain a better understanding of the essential physics, and also to more easily make a number of numerical order-of-magnitude estimates.

We will not show the exact justification for all three assumptions. All three are based on the fact that both the fluxes and the source terms are normalized by factors of  $1/D$ . Since  $D_e$  is much greater than  $D_i$  for any ion (typically by several orders of magnitude), the normalized electron quantities are much smaller than their ion counterparts. We will examine the flux case in detail.

Let us consider the justification of the first approximation:

$$\frac{\gamma_e}{\sum_j \gamma_j} \ll 1 \quad (5-4)$$

The definition of the normalized flux produces

$$\frac{\gamma_e}{\sum_j \gamma_j} = \frac{\frac{\Gamma_e}{D_e}}{\sum_j \frac{\Gamma_j}{D_j}} < \frac{\frac{\Gamma_e}{D_e}}{\left( \sum_j \frac{\Gamma_j}{\max_j D_j} \right)} \quad (5-5)$$

which simplifies to

$$\frac{\gamma_e}{\sum_j \gamma_j} < \frac{\max_j D_j}{D_e} \frac{\Gamma_e}{\sum_j \Gamma_j} \quad (5-6)$$

But, congruence implies

$$\frac{\Gamma_e}{\sum_j \Gamma_j} = 1 \quad (5-7)$$

(In fact, since we only need Equation 5-6 to hold for the magnitudes of the fluxes, strict congruence is not even necessary. Quasi-neutrality is sufficient to justify the relationship.)

Hence,

$$\frac{\gamma_e}{\sum_j \gamma_j} < \frac{\max_j D_j}{D_e} \quad (5-8)$$

For typical plasmas,  $D_i$  is on the order of  $100 \text{ cm}^2 \text{ s}^{-1}$  or less, while  $D_e$  is in excess of  $10^6 \text{ cm}^2 \text{ s}^{-1}$  (von Engel, 1965: 140, 141). . As a result, in almost all cases  $D_e \gg D_i$  . Therefore, we see that

$$\frac{\gamma_e}{\sum_j \gamma_j} < \frac{\max_j D_j}{D_e} \ll 1 \quad (5-9)$$

which proves Equation 5-4. Exactly similar arguments are used to justify the other two assumptions in Equation 5-3. The only difference is that charge conservation ensures that the relationship analogous to Equation 5-7 will hold true, instead of congruence.

Note that Equation 5-9 is based on the electron diffusion coefficient being much higher than the ion diffusion coefficient, or equivalently, the electron mobility being much higher than the ion mobility. Therefore, the small-e-flux approximation is equivalent to assuming that the electrons are much more mobile than the ions. It is not equivalent to assuming that the ion

temperature is zero, or that the ions are immobile. On the other hand,  $D$  is proportional to  $T$ . Therefore, assuming that the ion temperature is zero is trivially implies  $D_e \gg D_i$ .

The small-e-flux approximation is often invoked, although not as explicitly as in this document. For instance, Tonks and Langmuir assume the Boltzmann relation for the electrons and electric potential (Tonks and Langmuir, 1929:883). As was pointed out at the end of Chapter III, the Boltzmann relation correctly describes an ambipolar plasma only when the small-e-flux approximation is valid. Therefore, Tonks and Langmuir's work relies on this approximation.

### *Summary of Solutions*

Before we go into a detailed explication of the solution methods and the resulting solutions, it would be helpful to present a summary of the solutions themselves. Note that they are in the simplified form that results from the use of the small-e-flux assumption. In this summary, we do not present the moment or continuity equations appropriate to the solutions. Rather, we save those for the complete development of the solutions, later in the chapter.

We will now describe each of the solution sets, starting with the external ionization cases and then continuing to the self ionization cases.

*External Ionization.* In these cases we assume that the only source of ionization is an external ionization, imposed by some mechanism outside the plasma. This ionization is completely independent of any phenomena occurring inside the plasma.

**PX.** First, we have the PX case; planar geometry, uniform external ionization only:

$$\begin{aligned}
 n_e &= \frac{1-\rho^2}{2(1+\epsilon)} \epsilon \sum_j s_j \\
 n_i &= \frac{1-\rho^2}{2(1+\epsilon)} \epsilon s_i \\
 \gamma &= s\rho \\
 \mathcal{E} &= \frac{2\rho}{(1-\rho^2)\epsilon}
 \end{aligned}
 \tag{5-10}$$

**PE.** The PE case combines planar symmetry with external ionization decaying exponentially from each boundary. Examples where this might arise include a time-averaged description of planar RF reactors, where in the so-called  $\gamma$  regime secondary emission produces beams of high-energy electrons from each electrode (e.g. Godyak and Khamneh, 1986), or cases where photo-ionization from each side provides the ionization source. (We note that, to model the RF reactor with complete fidelity, we would have to account for the presence of the high-energy electrons in satisfying quasi-neutrality near the boundary, where  $n_e$  is small. However, for the present case we will assume that the secondary electron emission coefficient is small enough, and the beam electron velocity high enough, that the particle density due to the high energy electrons can be neglected.) For this case, we find the following solutions for the small-e-flux approximation:

$$\begin{aligned}
n_e &= \frac{\epsilon \sum_j s_j}{\Lambda^2(1+\epsilon)} (\cosh \Lambda - \cosh \Lambda \rho) \\
n_i &= \frac{\epsilon s_i}{\Lambda^2 \sum_j s_j (1+\epsilon)} (\cosh \Lambda - \cosh \Lambda \rho) \\
\gamma &= \frac{s}{\Lambda} \sinh \Lambda \rho
\end{aligned}
\tag{5-10}$$

$$\mathcal{E} = \Lambda \frac{\sinh \Lambda \rho}{(\cosh \Lambda - \cosh \Lambda \rho)}$$

**CX.** Finally, we have the CX case, which combines cylindrical geometry with external ionization:

$$\begin{aligned}
n_e &= \frac{1-\rho^2}{4(1+\epsilon)} \epsilon \sum_j s_j \\
n_i &= \frac{1-\rho^2}{4(1+\epsilon)} \epsilon s_i \\
\gamma &= \frac{s\rho}{2} \\
\mathcal{E} &= \frac{2\rho}{(1-\rho^2)\epsilon}
\end{aligned}
\tag{5-11}$$

**Volume Ionization.** In these cases, the ionization source for both species is single-step impact ionization by the electrons in the plasma. We assume that the ionization frequency is constant throughout the plasma.

The solutions below would have the same form, with or without the small-e-flux approximation being applied to the dimensionless frequencies  $f$ . The various  $f$ 's only appear in the definition of the eigencondition that is produced in all these solutions. The approximation produces slight changes in the values of the various  $f$ 's, but does not otherwise change the

eigencondition. As a result, we see no change in the structure of the solutions.

*PV.* The PV case involves planar symmetry, with volume ionization:

$$\begin{aligned}
 n_e &= n_0 \cos \frac{\pi \rho}{2} \\
 n_i &= \frac{f_i}{\sum_j f_j} n_0 \cos \frac{\pi \rho}{2} \\
 \gamma &= \frac{2}{\pi} \sum_j f_j n_0 \sin \frac{\pi \rho}{2} \\
 \mathcal{E} &= \frac{2}{\pi(1+\epsilon)} \sum_j f_j \tan \frac{\pi \rho}{2}
 \end{aligned} \tag{5-12}$$

*CV.* We refer to the cylindrical geometry, volume ionization case as "CV":

$$\begin{aligned}
 n_e &= n_0 J_0(\lambda_0 \rho) \\
 n_i &= \frac{f_i}{\sum_j f_j} n_0 J_0(\lambda_0 \rho) \\
 \gamma &= n_0 \sum_j f_j \frac{J_1(\lambda_0 \rho)}{\lambda_0} \\
 \mathcal{E} &= \frac{\sum_j f_j}{\lambda_0(1+\epsilon)} \frac{J_1(\lambda_0 \rho)}{J_0(\lambda_0 \rho)}
 \end{aligned} \tag{5-13}$$

where  $\lambda_0$  is the first zero of the Bessel function  $J_0$ .

*PT.* Finally, we have the PT case, with self ionization and charge transfer. In this system, species 1 gains by charge transfer from species 2, plus all species have ionization sources proportional to  $n_e$ . Formally, the



solutions are similar to the PS case, except with a different definition of  $\lambda$  and a slight difference for the  $n_j$ 's:

$$\begin{aligned} n_0 &= n_0 \cos \frac{\pi \rho}{2} \\ n_i &= K_i n_0 \cos \frac{\pi \rho}{2} \\ \gamma &= \frac{2}{\pi} \int n_0 \sin \frac{\pi \rho}{2} \\ \mathcal{E} &= \frac{2}{\pi} \sum_j f_j \tan \frac{\pi \rho}{2} \end{aligned} \tag{5-14}$$

We will point out the difference in  $\lambda$  and describe " $K_j$ " when we discuss this solution in more detail, later.

### *Exact Solutions*

Next, we will develop the complete solutions, starting with the formalism for arbitrary external or volume sources, and continuing to exact solutions for a number of cases. We will also describe the implications of the solutions, as each solution is discussed. We will start with the external source cases, and then continue with the volume sources.

*External Sources.* We will examine arbitrary external source functions, in both planar and cylindrical geometry. We will first obtain a general form for the solutions, then examine sources that are proportional (in the same sense that Oskam defined particle densities as being proportional), and finally solve the system for particular external sources.

*Planar Geometry.* Consider the continuity equation in planar geometry, for an arbitrary external source term:

$$\frac{\partial \gamma}{\partial \rho} = s(\rho) \quad (5-15)$$

Here, the lack of subscripts implies that this equation is valid for any species.

Immediately, we see that the solution for the particle flux densities is given by

$$\gamma = \int_0^{\rho} s(\rho') d\rho' \quad (5-16)$$

When we use this expression in the electron momentum equation, we obtain the following form for the electron number density:

$$n_e = - \int_1^{\rho} \frac{\int_0^{\rho'} \left( \sum_j s_j(\rho'') + s_e(\rho'') \right) d\rho''}{1+\epsilon} d\rho' \quad (5-17)$$

The formal integral expression for  $n_i$  then becomes:

$$n_i = - \int_1^p \int_0^{p'} s_i(\rho'') d\rho'' \quad (5-18)$$

$$\times \exp \left( \frac{\int_0^{p''} \left( \sum_j s_j(\rho''') - s_e(\rho''') \right) d\rho'''}{\int_1^{p''} \int_0^{p'''} \left( \epsilon \sum_j s_j(\rho''''') + s_e(\rho''''') \right) d\rho'''' d\rho'''} \right) d\rho'' d\rho'$$

In general, this form is not integrable. However, let us consider sources of the following form:

$$s_k(\rho) = s_k g(\rho) \quad (5-19)$$

That is, we will consider proportional sources. This is a fairly reasonable restriction. For instance, consider a situation where the background gas mixture is homogeneous, and an same external source of high energy electrons is providing the ionization for all species. If the electron energy is high enough so that differences in ionization potential can be ignored, then the ionization rate is a function of total beam intensity. In such a case conditions such as Equation 5-19 would be true. That produces the following form for  $n_e$ :

$$n_e = - \frac{\epsilon \sum_j s_j + s_e}{1 + \epsilon} \int_1^p \int_0^{p'} g(\rho'') d\rho'' d\rho' \quad (5-20)$$

This solution can then be used to obtain the following solution for  $n_i$  (see Appendix B for details):

$$n_i = - \frac{s_i \sum_j \frac{\epsilon s_j + s_e}{1 + \epsilon}}{\sum_j s_j} \int_1^p \int_0^{p'} g(p'') dp'' dp' \quad (5-21)$$

We will not present the expression for  $\mathcal{E}$  at this time. It is too complex to be worthwhile for such a general case. Instead, we will wait until we examine specific cases. However, note that the general definition of  $\mathcal{E}$  in terms of  $n_e$  and  $\gamma$  still applies.

*PX Case.* As an example of a particular proportional external source, we shall first use a uniform external source, with

$$s_k(p) = s_k \quad (5-22)$$

This is the case referred to earlier as "PX". This source produces the following solutions for the fluxes:

$$\gamma_k = s_k \rho \quad (5-23)$$

For  $n_e$ , the result is

$$n_e = \frac{\epsilon \sum_j s_j + s_e}{2(1 + \epsilon)} (1 - \rho^2) \quad (5-24)$$

And for  $n_i$ ,

$$n_i = s_i \frac{\epsilon \sum_j s_j + s_e}{2 \sum_j s_j (1 + \epsilon)} (1 - \rho^2) = \frac{s_i}{\sum_j s_j} n_e \quad (5-25)$$

From these, we obtain the following expression for the normalized electric field:

$$\mathcal{E} = \frac{2\rho \left( \sum_j s_j - s_0 \right)}{(1-\rho^2) \left( \epsilon \sum_j s_j + s_0 \right)} \quad (5-26)$$

The small-e-flux approximation produces the following forms for the solutions (  $\gamma$  is unchanged):

$$\begin{aligned} n_e &= \frac{1-\rho^2}{2(1+\epsilon)} \epsilon \sum_j s_j \\ n_i &= \frac{1-\rho^2}{2(1+\epsilon)} \epsilon s_i = \frac{s_i}{\sum_j s_j} n_e \end{aligned} \quad (5-27)$$

$$\mathcal{E} = \frac{2\rho}{\epsilon(1-\rho^2)}$$

Let us consider some of the implications of these solutions. For convenience, we first examine situations where the small-e-flux approximation is valid.

First, consider the particle fluxes. The plasma has no volume losses. Therefore, the fluxes depend only on the external source. Since the external source is not linked to the species densities, the fluxes are also independent of these densities. For this system, with the fluxes all zero and therefore equal at the axis, congruence holds despite any changes in the plasma conditions. This result is the same for the physical fluxes or the non-dimensional fluxes.

Next, consider the expression for the physical field,  $E$ :

$$E = \frac{2x}{(d^2-x^2)} \frac{kT_e}{q} = \frac{2x}{(d^2-x^2)} \frac{D_e}{\mu_e} \quad (5-28)$$

The electric field depends only on  $T_e$ , not on  $T_i$  or the source terms. This should not be totally surprising, and in fact is identical to the results obtained from a single-ion ambipolar model. From the results on the multi-ion diffusion coefficient presented in Chapter IV, or from similar results from Schottky's definition of  $D_a$ , it follows that the field increases the field-free ion flux by a factor of  $D_a/D_i = (1+T_e/T_i)$ . At the same time it reduces the field-free electron flux by a factor of approximately  $D_e/D_a$ . Even though  $D_a$  is larger than  $D_i$ ,  $D_e$  is so much larger still that the field-induced change in the ion flux is still much smaller than that of the electron flux. The field serves to constrain the electron flux to match the ion fluxes, but has little effect on the ions, at least in those regimes where the small-e-flux approximation holds. See, for example, Phelps, who discusses the fact that the electron diffusive and field-induced fluxes balance each other (Phelps, 1990:412). This implies that the field produced is determined by the electron properties, not the ion properties. The field necessary to constrain the electrons depends on the ratio of  $\mu_e$ , which determines how well the electrons respond to the field, to  $D_e$ , which determines how well the electrons respond to diffusive forces. But that ratio is  $q/kT_e$ , and is determined solely by the electron temperature.

Finally, consider the particle densities. The field is proportional to  $T_e$ , and the fluxes are independent of the plasma characteristics.  $\nabla N$  can be expressed as approximately  $N/\Lambda$ , where  $\Lambda$  is the scale length of the discharge. Recall the momentum equation with the electric field still includ-

ed:  $\Gamma = -DVN \pm \mu NE$  . With a fixed  $\Gamma$  , if the field goes up,  $\nabla N$  and  $N$  must go down. This implies that  $N$  varies as some increasing function of  $1/T_e$  . Measuring  $T_e$  in units of  $T_i$  produces  $N$  varying as  $\varepsilon$  , consistent with Equation 5-27.

In addition,  $N$  depends on  $s$  which is equivalent to the ratio  $S/D$ . This is not surprising; number density should increase as the source strength increases. Furthermore, increased values for  $D$  imply higher diffusion losses. Therefore,  $N$  should decrease as  $D$  increases.

These results are exactly equivalent to the results from the single species theory of Schottky, as applied to this system, with the exception that Schottky's theory, which deals with only a single species, cannot address the relative magnitude of two species. In addition, they are the same that would result from applying Oskam's model to this physical situation. Note the significant difference, however; Oskam had to assume proportionality to find any solutions. We found the solutions, and then showed that they were proportional.

Changes occur when the small-e-flux approximation is not invoked. There are no significant differences for  $\gamma$  or  $n$ . However, there is a significant difference in the electric field. Consider the full expression for  $E$ :

$$E = \frac{2x}{(d^2 - x^2)^{3/2}} \frac{kT_e}{q} \left( \frac{\sum_j \frac{S_j}{D_j} + \frac{S_e}{D_e}}{\varepsilon \sum_j \frac{S_j}{D_j} + \frac{S_e}{D_e}} \right) \quad (5-29)$$

Expanding the last terms in the right hand side and dropping terms second order and higher in  $S_e/D_e$  produces

$$E = \frac{2x}{(d^2 - x^2)^q} \frac{kT_e}{q} \left( 1 - \frac{T_e}{T_i} \frac{\frac{S_e}{D_e}}{\sum_j \frac{S_j}{D_j}} \right) \quad (5-30)$$

Although there is a change in the form of  $E$ , it is small. The second term is of the form  $1-\delta$ , where  $\delta$  is dominated by the ratio  $D_j/D_e$ . This ratio is typically so small that  $\delta \ll 1$ . As a result, the additional dependence on  $T_i$ , the sources, and the diffusion coefficients is only a perturbation to the expression seen in the small-e-flux case. This higher order effect is due primarily to the fact that we are now taking into account the ions' response to the field. With the small-e-flux approximation, we neglect that response. In most practical cases, this higher order effect is insignificant. As will be shown in the next chapter,  $D_j/D_e$  is typically of the order of  $10^{-4}$  or smaller, and the second and higher order terms can be ignored.

*PE Case.* As another example, consider a case where the external source of ionization is introduced from both sides of the plasma. This might arise with photo-ionization from sources on each side of a planar discharge. It could also arise in a transverse e-beam pumped discharge using dual opposed e-beams. Another example would be a  $\gamma$ -regime RF discharge. The electrons, produced by ion secondary emission at each electrode, are accelerated in the large sheaths generated. In some pressure regimes, the ionization produced by these electrons become the major ionization source for the discharge (Godyak and Khamneh, 1986).

The resulting source function is the sum of two exponential decays, and can be described as



$$\frac{\partial \gamma_k}{\partial \rho} = s_k \cosh(\Lambda \rho) \quad (5-31)$$

where  $1/\Lambda$  represents a dimensionless decay length and is the same for every species. The  $k$  subscript explicitly denotes any species, to distinguish the species-dependent quantities  $\gamma$  and  $s$  from the species-independent quantity  $\Lambda$ . That definition produces

$$\begin{aligned} \gamma_k &= \frac{s_k}{\Lambda} \sinh(\Lambda \rho) \\ n_e &= \frac{\epsilon \sum_j s_j + s_e}{\Lambda^2 (1 + \epsilon)} (\cosh(\Lambda) - \cosh(\Lambda \rho)) \\ n_i &= \left( \frac{s_i}{\Lambda^2 (1 + \epsilon)} \right) \frac{\epsilon \sum_j s_j + s_e}{\sum_j s_j} (\cosh(\Lambda) - \cosh(\Lambda \rho)) \\ &= \frac{s_i}{\sum_j s_j} n_e \\ \mathcal{E} &= \frac{\Lambda \left( \sum_j s_j - s_e \right) \sinh(\Lambda \rho)}{\left( \epsilon \sum_j s_j + s_e \right) (\cosh(\Lambda) - \cosh(\Lambda \rho))} \end{aligned} \quad (5-32)$$

The small- $\epsilon$ -flux approximation implies

$$\gamma_k = \frac{s_k \sinh(\Lambda \rho)}{\Lambda}$$

$$n_e = \frac{\epsilon \sum_j s_j}{\Lambda^2 (1 + \epsilon)} (\cosh(\Lambda) - \cosh(\Lambda \rho))$$

$$n_i = \frac{s_i}{\Lambda^2 (1 + \epsilon)} (\cosh(\Lambda) - \cosh(\Lambda \rho)) \quad (5-33)$$

$$= \frac{s_i}{\sum_j s_j} n_e$$

$$\mathcal{E} = \frac{\Lambda \sinh(\Lambda \rho)}{\epsilon (\cosh(\Lambda) - \cosh(\Lambda \rho))}$$

Except for the different dependence of the source term on  $\rho$  (which leads both to the presence of the  $\Lambda$  and  $\Lambda^2$  terms, and to the cosh and sinh dependencies), these solutions are equivalent to the PX case. Therefore, the same discussion of consequences of the solutions applies.

These results can be compared to Godyak and Khanneh's work directly (Godyak and Khanneh, 1986). These authors are examining an RF plasma reactor in the regime where ionization by the secondary electrons emitted from the electrode at each end of the discharge are a significant portion of the total ionization of the system. They derive an ionization function for the beam electrons that is identical in form to Equation 5-31, and also include volume ionization by the electrons in the plasma, all for a single ion species. They address both the radial and longitudinal diffusion. Their solutions for the longitudinal diffusion, in the case where the volume

ionization is negligible compared to the beam ionization, have exactly the same form as the single-ion version of Equation 5-33.

*Cylindrical Geometry* Now, let us repeat the analysis of external sources for a cylindrical geometry. Again, the source term depends only on position. However, the cylindrical geometry introduces some changes. In that geometry, the continuity equations become

$$\frac{\gamma}{\rho} + \frac{\partial \gamma}{\partial \rho} = s(\rho) \quad (5-34)$$

The solution for the fluxes is

$$\gamma = \frac{1}{\rho} \int_0^{\rho} \rho' s(\rho') d\rho' \quad (5-35)$$

This differs from the planar case by a factor of  $1/\rho$  before the integral and a factor of  $\rho'$  inside the integral. This produces the following form for  $n_e$ :

$$n_e = - \frac{1}{(1+\epsilon)} \int_1^{\rho} \frac{1}{\rho'} \int_0^{\rho'} \rho' \left[ \epsilon \sum_j s_j(\rho'') + s_e(\rho'') \right] d\rho'' d\rho' \quad (5-36)$$

Again, these formal solutions produce the formal solution for  $n_i$ :

$$n_i = - \int_1^p \frac{1}{\rho'} \int_0^{p'} s_i(\rho'') d\rho'' \quad (5-37)$$

$$\times \exp \left[ \int_p^{p'} \frac{1}{\rho''} \frac{\int_0^{p''} \rho''' \left( \sum_j s_j(\rho''') - s_e(\rho''') \right) d\rho'''}{\int_1^{p''} \frac{1}{\rho'''} \int_0^{p'''} \rho'''' \left( \epsilon \sum_j s_j(\rho''''') + s_e(\rho''''') \right) d\rho'''' d\rho'''} d\rho'' \right] d\rho'$$

As in the planar case, this expression is, in general, far from integrable.

However, assuming proportional sources produces

$$s_k(\rho) = s_k g(\rho) \quad (5-38)$$

The results are the following forms for the particle fluxes:

$$n_e = - \frac{\epsilon \sum_j s_j + s_e}{(1+\epsilon)} \int_1^p \frac{1}{\rho'} \int_0^{p'} \rho'' g(\rho'') d\rho'' d\rho' \quad (5-39)$$

Another algebraic manipulation, essentially equivalent to that described in Appendix B, produces the following form for  $n_i$ :

$$\begin{aligned}
n_i &= - \frac{s_i \left( \epsilon \sum_j s_j + s_e \right)}{\sum_j s_j (1 + \epsilon)} \int_1^{\rho} \frac{1}{\rho'} \int_0^{\rho'} \rho'' g(\rho'') d\rho'' d\rho' \\
&= \frac{s_i}{\sum_j s_j} n_e
\end{aligned}
\tag{5-40}$$

The exact form for the electric field is readily obtainable, but again it does not seem worthwhile to present it in such a general case. Instead, we will look at the field in the example presented next.

*CX Case.* Consider the specific example of uniform external ionization. This leads to the following form for the particle fluxes:

$$\gamma = \frac{s}{2} \rho \tag{5-41}$$

Notice that this differs from the PX case only by a factor of two in the denominator. The momentum equations have exactly the same form as for the PX case. Therefore, the factor of two difference in the fluxes carries throughout to produce

$$\begin{aligned}
n_e &= \frac{\epsilon \sum_j s_j + s_e}{4(1 + \epsilon)} (1 - \rho^2) \\
n_i &= s_i \frac{\epsilon \sum_j s_j + s_e}{4 \sum_j s_j (1 + \epsilon)} (1 - \rho^2) \\
\mathcal{E} &= \frac{2\rho \left( \sum_j s_j - s_e \right)}{(1 - \rho^2) \left( \epsilon \sum_j s_j + s_e \right)}
\end{aligned}
\tag{5-42}$$

The small- $\epsilon$ -flux assumptions gives

$$\begin{aligned}
n_e &= \frac{\epsilon \sum_j s_j}{4(1+\epsilon)} (1-\rho^2) \\
n_i &= s_i \frac{\epsilon}{4(1+\epsilon)} (1-\rho^2) \\
\gamma &= \frac{s_p}{2} \\
\mathcal{E} &= \frac{2\rho}{\epsilon(1-\rho^2)}
\end{aligned} \tag{5-43}$$

Once more, the conclusions of the PX case apply here.

*General Self-Ionization Sources.* Next are three cases where the only ionization term is self ionization. We will first approach the solution using a very general formulation. This general formulation will help determine the bounds of practical application of the analytic method. The less general examples that follow still produce results of broad utility.

First, assume a source term as follows:

$$\nabla \cdot \vec{\gamma}_k = Q_k(n_e, n_i) \tag{5-44}$$

Here, the "k" subscripts refer to either electrons or ions.  $Q$  is a general polynomial in its arguments  $n_e$  and  $n_i$ , in the sense that it can include not only powers of those arguments, but products of those powers as well. For example, ordinary electron impact ionization produces a source term that depends linearly on  $n_e$ , but depends on no other species. On the other hand, recombination adds a source term (that is actually negative, and therefore a loss term) that depends on the product of the electron density and the appropriate ion density:

$$\nabla \cdot \vec{\gamma}_i = f_i n_e - f_r n_e n_i \tag{5-45}$$

Here, the first term on the right hand side represents electron impact ionization, and the second represents recombination.

The formulation using  $Q_k$  is sufficient to cover every case of interest where the ionization rate depends only on the number densities of the charged species. This formulation was used in Chapter IV in the discussion of proportionality, and will be used it in Chapter VI in the discussion of numerical solutions. Unfortunately, sources of this form, other than the very simplest, do not lend themselves to analytic solutions. Therefore, for the present we shall consider only electron impact ionization, and will look only at loss terms that are also proportional to  $n_e$ .

#### *Planar Geometry.*

*PV Case.* In planar geometry, and with electron ion imoact ionization as the only source, the continuity equation is

$$\frac{\partial \gamma}{\partial \rho} = f n_e \quad (5-46)$$

Here,  $f$  is a normalized ionization frequency given by  $f = v d^2 / D$ , where  $d$  is the half-width of the discharge.

The momentum equation for electrons is

$$\frac{\partial n_e}{\partial \rho} = - \frac{\epsilon \sum_j \gamma_j + \gamma_e}{1 + \epsilon} \quad (5-47)$$

Taking the divergence of this equation, and substituting the expressions for  $\partial \gamma / \partial \rho$  from the continuity equations, produces

$$\frac{\partial^2 n_e}{\partial \rho^2} = - n_e \frac{\epsilon \sum_j f_j + f_e}{1 + \epsilon} \quad (5-48)$$

Defining

$$\lambda^2 = \frac{\epsilon \sum_j f_j + f_e}{1 + \epsilon} \quad (5-49)$$

Produces the following expression for  $n_e$ :

$$\frac{\partial^2 n_e}{\partial \rho^2} + \lambda^2 n_e = 0 \quad (5-50)$$

This has, as its most general solution,

$$n_e = a \cos \lambda \rho + b \sin \lambda \rho \quad (5-51)$$

where the values of the  $a$  and  $b$  are chosen to meet the boundary conditions.

With an exact form for  $n_e$ ,  $\gamma$  is given by

$$\gamma = f\left(\frac{a}{\lambda} \sin \lambda \rho + \frac{b}{\lambda} \cos \lambda \rho\right) \quad (5-52)$$

The boundary condition  $\gamma(0) = 0$  implies that the coefficient  $b$  must be zero. That value plus the condition that  $n(1) = 0$  implies that either  $a$  is zero, or  $\cos \lambda$  is zero. But, to this point  $\lambda$  is determined by the properties of the plasma, not the solutions to the differential equation. Therefore, in the general case  $\cos \lambda$  is not zero. Thus,  $b$  is zero, and the only solution is the trivial solution.

The answer to this apparent dilemma is that the value of  $\lambda$  is not really independent of the differential equations. The requirement for physically meaningful solutions forces  $n_e$  to have a non-zero value somewhere. Assume that the non-zero value occurs at  $n_e(0) = 1$ . For  $M$  separate ion species, the  $M+1$  continuity and  $M+1$  momentum equations form a system



of  $2M+2$  first order differential equations. Each of the  $M+1$  fluxes has a boundary condition of  $\gamma(0) = 0$ . Similarly, each of the  $M+1$  number densities has a boundary condition  $n(1) = 0$ . Finally, the assumption above provides one additional boundary condition. The result is a system of  $2M+2$  first order differential equations with  $2M+3$  boundary conditions. This over-constrained system constitutes an eigenvalue problem that has solutions only for particular values of the parameters.

From a mathematical standpoint, any non-zero value at any position other than  $\rho = 1$  would suffice. From a physical standpoint, of course, the value for  $n_e(0)$  represents the on-axis electron number density and is determined by the interaction of the longitudinal electric field and the external circuit parameters. The existence of the eigencondition enforces a particular value for the ionization frequency, and hence for the electron temperature. On the other hand, the external circuit parameters enforce a particular value for the longitudinal current. To accommodate both of these enforced values,  $n_e(0)$  will change until the longitudinal flux, given by  $n_e \mu E$ , is appropriate for the total longitudinal current. For the particular case at hand, the value is truly arbitrary, but must be positive.

A number of different but related quantities could be chosen as the eigenvalue. Because of its explicit appearance in the differential equations, we chose to use the electron temperature,  $kT_e$ . All the ionization frequencies depend on the electron energy distribution, and  $\lambda$  depends on the ionization frequencies. For Maxwellian distributions, the distribution is characterized by the electron temperature  $kT_e$ . Therefore, adjusting the

value of  $kT_e$  allows non-trivial solutions. Equivalent operations could be performed for more complicated electron energy distributions, but without the simplicity of a single parameter.

In general, there are a number of allowable values for  $\lambda$  ;  $\pi/2$ ,  $3\pi/2$ , and so forth. Expressing the solution as a sum over all the possible values of  $\lambda$  produces what amounts to a Fourier expansion of the solutions, with each value of  $\lambda$  representing a different diffusion mode. This analysis examines only the simplest mode, the so-called fundamental diffusion mode. For that mode, the boundary conditions force the following value for  $\lambda$  :

$$\lambda = \frac{\pi}{2} \quad (5-53)$$

This produces the following expression for  $n_e$ :

$$n_e = n_{e0} \cos \frac{\pi \rho}{2} \quad (5-54)$$

Here,  $n_{e0}$  had the value of 1 in the example above.

In fact, this eigencondition determines the electron temperature in plasmas that depend on self-ionization. We will return to this point later, while examining numerical solutions. At that time, we will show that the present model gives results that are consistent with Schottky's model of single ion ambipolar diffusion.

Various authors have treated the eigenvalue nature of this system. For a good review, see Ferreira (Ferreira *et alia*, 1988). Note, however, that Ferreira claims his system must have two eigenvalues. One of Ferreira's eigenvalues is indeed forced by the physics of the situation, and is in fact the same as we use here. However, the other is a consequence of Ferreira's

normalization. Ferreira uses the electron number density  $n_e$  as one of his two dependent variables. For the other, he uses  $\alpha$ , defined as the ratio of the negative ion density  $n_n$  to  $n_e$ . He then normalizes the electron density, defining  $g_e = n_e/n_{e0}$ . He also normalizes his ion density ratio by defining  $g_\alpha = \alpha/\alpha_0$ . In both cases, he is dividing by the on-axis value of the variable, thus setting the value of the normalized variable on axis to 1. The result is the following normalized system of differential equations:

$$\begin{aligned} \frac{1}{X} \frac{d}{dX} \left( X(1+\alpha_0 g_\alpha) \frac{dg_e}{dX} \right) + \lambda g_e &= 0 \\ \frac{1}{X} \frac{d}{dX} \left( X\alpha_0 g_\alpha \frac{dg_e}{dX} \right) - \lambda(P-Q\alpha_0 g_\alpha) g_e &= 0 \end{aligned} \tag{5-55}$$

This is a system of two 2nd-order ordinary differential equations, which would ordinarily require four boundary conditions. In this regard it is equivalent to the system of two continuity and two momentum equations that we are using. In addition, the normalization conditions force two additional boundary conditions:  $g_\alpha(0) = g_e(0) = 1$ . The condition on  $g_e$  is exactly equivalent to the eigencondition used here. The condition on  $g_\alpha$  is a consequence of the normalization of  $g_\alpha$ . Note that  $g_\alpha$  never appears in the system separate from  $\alpha_0$ . The combination could be replaced with the single function  $\alpha(X)$  with no change to the same system. The only difference would be the loss of the boundary condition on  $\alpha$ . This would remove Ferreira's second boundary condition.

This does not imply that the condition forced by the normalization is not a consequence of the physics of the situation. Rather, Ferreira's normalization changes the on-axis ion density from a consequence of the solutions

into a requirement for solutions to exist. The present choice of boundary conditions and normalizations allows the value of the on-axis densities to appear as a natural consequence of the system.

The eigencondition on  $\lambda$  quickly produces an expression for  $\gamma$  for the electrons and each of the ions:

$$\gamma = f_{e0} \frac{2 \sin \frac{\pi \rho}{2}}{\pi} \quad (5-56)$$

For the ions, the momentum equation produces the following solution for the fundamental mode:

$$n_i = \frac{f_i}{\sum_j f_j} n_{e0} \cos \frac{\pi \rho}{2} \quad (5-57)$$

The electric field is given by

$$\mathcal{E} = \frac{2}{\pi} \frac{\left( \sum_j f_j - f_e \right)}{1 + \epsilon} \tan \frac{\pi \rho}{2} \quad (5-58)$$

Notice that we still have not determined  $f_j$ . However, the original definition of  $\lambda$  and the requirement that  $\lambda = \pi/2$  together imply

$$\left( \frac{\pi}{2} \right)^2 = \frac{\epsilon \sum_j f_j + f_e}{1 + \epsilon} \quad (5-59)$$

This single constraint is not sufficient to determine each  $f_j$  ; it only concerns the sum of the frequencies, not each individual one. Other expressions must be found to relate the individual frequencies to each other. In a real discharge, those expressions involve the ionization potential and cross-section for each species. Given the form of the electron energy distribution, the potential and cross-section are sufficient to uniquely determine the

ionization frequency associated with a particular electron temperature. This approach is exercised in Chapter VI when examining the temperature dependence of a Ne/He plasma. Presently, we will make some simple assumptions that will allow us to continue, while still modeling fairly realistic situations.

First, we will assume

$$\nu_1 = \nu_2 = \nu_3 = \nu_4 = \dots \quad (5-60)$$

for all ionic species.

Second, we make the small-e-flux approximation. Doing so allows simplification of the form of the eigencondition. The error this introduces in the final solution is negligible; because of the vastly different ion and electron mobilities, the small-e-flux approximation is valid for any system with  $kT_e \geq kT_i$ . It does not change the form of the particle or fluxes at all. In fact, the only expressions that change are those for the normalized field and for  $\lambda$ , which become

$$\mathcal{E} = \frac{2}{\pi} \sum_j \frac{f_j}{1+\epsilon} \tan \frac{\pi}{2} \rho$$

$$\left(\frac{\pi}{2}\right)^2 = \frac{\epsilon \sum_j f_j}{1+\epsilon} \quad (5-61)$$

Using the relationship in Equation 5-60 and the definition of the dimensionless sources to determine the relationship of the various  $f_i$ 's, substituting that relationship into the second half of Equation 5-61, and solving for  $f_i$  produces

$$f_i = \frac{\pi^2}{\epsilon_0 4D_i \sum_j \frac{1}{D_j}} \quad (5-62)$$

We can then use conservation of charge, which implies that  $v_e$  is equal to  $\sum v_i$  to determine  $f_e$  :

$$f_e = \frac{\sum_j f_j D_j}{D_e} \quad (5-63)$$

We then use the values for  $f_i$  and  $f_e$  to evaluate the solutions.

These results are analogous to the results Schottky's theory produces for the equivalent single-ion case. In fact, Equations 5-54 and 5-56 are identical to the dimensionless form of the Schottky solutions for a single ion plasma. Furthermore, Equation 5-57 is identical to Schottky's result for the ions, except for the normalizing factor  $n_i/\sum n_j$  , which reduces to the value identically 1 for the single ion case. The eigencondition expressed in Equation 5-49 becomes in the single ion case

$$\left(\frac{\pi}{2d}\right)^2 = v \frac{(\mu_e + \mu_+)}{(\mu_e D_+ + \mu_+ D_e)} \quad (5-64)$$

which is identical to Schottky's result. The electric fields in the two models are equivalent; in the single-ion case Equation 5-58 gives Schottky's results identically.

*PT Case.* As the last example of analytic solutions for planar systems, it would be illuminating to examine a system where this model's ability to predict the possibility of proportionality is useful in finding solutions. We will do so in the context of finding solutions for systems involving nonresonant charge transfer. Consider a generic two-ion system,

with volume source terms for each species, and nonresonant charge transfer only from species 2 to species 1:

$$\begin{aligned}\nabla \cdot \vec{\gamma}_1 &= f_1 n_e + f_{t1} n_2 \\ \nabla \cdot \vec{\gamma}_2 &= f_2 n_e - f_{t2} n_2 \\ \nabla \cdot \vec{\gamma}_e &= f_e n_e\end{aligned}\tag{5-65}$$

where  $f_{ti} = v_t d^2/D_i$ , and  $v_t$  is the non-resonant charge transfer frequency.

(Note  $v_t$  is not the resonant charge transfer frequency that has such a strong effect on the total collision frequency of ions in their parent gases.)

This gives the following relationship:

$$f_{t2} = \frac{D_2}{D_1} f_{t1}\tag{5-66}$$

We see immediately that this system is considerably more complicated than those we have considered earlier. At first glance, it appears that the complexity of this system precludes the methods used in the PV case to produce analytic solution. For that case we were able to take the divergence of the electron momentum equation to produce a diffusion equation that depended only on  $n_e$ . Here, the diffusion equation depends on the ion densities as well. However, let us examine the validity of the assumption of proportionality in this case:

$$\begin{aligned}n_1 &= K_1 n_e \\ n_2 &= K_2 n_e\end{aligned}\tag{5-67}$$

As stated in Equation 5-67, proportionality is valid if  $K_1$  and  $K_2$  are constants, independent of position. We will determine if such is the case. Equation 5-67 implies the following equation for  $n_e$ :

$$\frac{\partial^2 n_e}{\partial \rho^2} = - \frac{[\epsilon(f_1 + f_{t1} K_2 + f_2 - f_{t2} K_2) + f_e]}{1+\epsilon} n_e \quad (5-68)$$

Next, it follows that  $\lambda$  is given by:

$$\lambda^2 = \frac{[\epsilon(f_1 + f_{t1} K_2 + f_2 - f_{t2} K_2) + f_e]}{1+\epsilon} \quad (5-69)$$

The constraint on  $\lambda$  is unchanged:

$$\lambda = \frac{\pi}{2} \quad (5-70)$$

We also have constraints on  $K_1$  and  $K_2$ . In particular their definition implies

$$K_1 + K_2 = 1 \quad (5-71)$$

Furthermore, the conditions on proportionality developed in Chapter IV ensure that  $K_1$  and  $K_2$ , as proportionality constants, must satisfy the following relationship:

$$K_1 = \frac{\nabla \cdot \vec{h}}{\sum_j \nabla \cdot \vec{h}} \quad (5-72)$$

We use the continuity equations to evaluate the source terms in Equation 5-72 in terms of  $K_1$ ,  $K_2$ ,  $f_1$ ,  $f_2$ ,  $f_{t1}$ , and  $f_{t2}$ . Solving the algebraic system consisting of Equations 5-71 and 5-72 produces find the following value for  $K_2$ :

$$K_2 = \frac{-(f_1 + f_2 + f_{t2}) \pm \sqrt{(f_1 + f_2 + f_{t2})^2 + 4f_2(f_{t1} - f_{t2})}}{2(f_{t1} - f_{t2})} \quad (5-73)$$

And for  $K_1$ :

$$K_1 = 1 - K_2 \quad (5-74)$$



The ratio  $n_i/n_e = K_i$  for each species, as given by Equations 5-73 and 5-74, is independent of position. The conclusion is that the assumption of proportionality is valid. This implies solutions for the particle densities and fluxes that formally are the same as the PV case:

$$\begin{aligned}\gamma &= f n_{e0} \frac{2}{\pi} \sin \frac{\pi}{2} \rho \\ n_e &= n_{e0} \cos \frac{\pi}{2} \rho \\ n_i &= K_i n_{e0} \cos \frac{\pi}{2} \rho\end{aligned}\tag{5-75}$$

Note that we were able to show that proportional solutions existed prior to determining those solutions. This is the significant difference between this model and Schottky-based models, which must use proportionality to find solutions without any indications of whether the solutions produced satisfy the assumption necessary to produce them.

Unfortunately, analysis of these solutions (beyond the characteristics that all the volume ionization cases share) depends very strongly on the specifics of the relative magnitude of the four frequencies,  $f_1$ ,  $f_2$ ,  $f_{t1}$ , and  $f_{t2}$ . At the moment, we are more concerned with the implications that existence of the solutions has on proportionality than we are in discussing extremely case-specific results. Therefore, we will forego further discussion of these expressions.

*Cylindrical Geometry.* Finally, we will address volume sources in cylindrical geometry, using a single example.

*CV Case.* The cylindrical self-ionization case formally is almost identical to the planar case, with the substitution for Bessel functions for trigonometric functions, and with the replacement of  $\pi/2$  with  $\lambda_0$ , the first

zero of  $J_0$ . That being the case, we will forego the details of the derivation, and present the solutions for the fundamental mode:

$$\begin{aligned}
 n_e &= n_{e0} J_0(\lambda_0 \rho) \\
 n_i &= \frac{f_i}{\sum_j f_j} n_{e0} J_0(\lambda_0 \rho) \\
 \gamma &= \frac{f n_{e0}}{\lambda_0} J_1(\lambda_0 \rho) \\
 \mathcal{E} &= \frac{\left( \sum_j f_j - f_e \right) J_1(\lambda_0 \rho)}{\lambda (1+\epsilon) J_0(\lambda_0 \rho)} \\
 \lambda_0^2 &= \frac{\epsilon \sum_j f_j + f_e}{1+\epsilon}
 \end{aligned} \tag{5-76}$$

As mentioned above in the PS case, the small-e-flux approximation produces a new expression for  $\mathcal{E}$ , and  $\lambda_0$  but no other changes in the solutions:

$$\begin{aligned}
 \mathcal{E} &= \frac{\sum_j f_j J_1(\lambda_0 \rho)}{\lambda (1+\epsilon) J_0(\lambda_0 \rho)} \\
 \lambda_0^2 &= \frac{\epsilon \sum_j f_j}{1+\epsilon}
 \end{aligned} \tag{5-77}$$

As before, we must determine the ionization frequencies. Making the same approximations as before results in

$$f_i = \frac{\lambda_0^2}{\epsilon D_i \sum_j \frac{1}{D_j}} \quad (5-78)$$

$$f_e = \frac{\sum_j f_j D_j}{D_e}$$

### *Summary*

This chapter examined the analytic solutions of systems containing external or volume source terms. We were able to develop general solution forms for arbitrary source terms, and show that these forms could be used to find analytic, closed form solutions for sources that were proportional but otherwise fairly general.

We actually developed solutions for two different external sources, in two different geometries. One source described idealized systems involving completely uniform ionization in either planar or cylindrical geometries. The other source modeled a spatially varying source of ionization typical of that produce by externally introduced fluxes of particles.

We also developed solutions for various systems involving volume source terms, including one where the volume term included both a source proportional to the electron density, and charge transfer. We used this latter case to highlight the difference between previous analytic models that assumed proportionality in the hopes of finding solutions, and the present model which predicted the possible existence of proportionality and then used knowledge about the constraints on proportional solutions to find those solutions.

## *VI. Numerical Solutions to the Model*

### *Introduction*

*Rationale.* The analytic results from the new ambipolar model have given insight into charged particle diffusion phenomena. However, there are a number of physical situations which can only be addressed by numerical methods. Typically, such situations involve kinetic processes such as recombination, non-resonant charge transfer, or other source or loss terms of higher nonlinearity than the simple processes we investigated in Chapter V. In particular, we will use numerical methods to investigate nonproportional plasmas whose net sources and losses have varying spatial dependence, or whose net sources and losses do not all depend the same way on charged particle number density. Such sources and losses invalidate the proportional solutions of Chapter V. In addition, we will investigate systems where numerical methods are necessary to determine the electron temperature, even though the fluxes and densities can be found analytically.

We conduct these investigations with two purposes in mind:

1. We wish to compare the new model to previous results of other authors. We do this to demonstrate that the model is suitable to describe such systems. We compare to theoretical results of Wunderer, of Young, and of von Engel, and to experimental results of Labuda and Gordon, and of Schmidt. (Wunderer, 1978; Young, 1965; von Engel, 1965; Labuda and Gordon, 1964; Schmidt, 1965)
2. We wish to discover new physical relationships from the solutions, such as variation of the electric field with nonlinear source terms, onset of nonproportionality, spatially increasing or decreasing particle densities, and dominance of the discharge by a single ion. Such relationships are easier to discover if the physics is as simple as possible. For this reason, most of the systems examined for this

purpose will be simplified, to allow concentration on the physics revealed.

*Cases To Be Examined.* The cases to be examined can be categorized by two different source terms: external sources of ionization and volume sources. All systems used cylindrical geometry, as in the CX and CV cases of Chapter V. In Equation 6-1 we show the form of the diffusion and continuity equations appropriate for all the cases examined, as well as the definition of the ambipolar electric field.

$$\begin{aligned}
 \frac{\partial N_i}{\partial r} &= -\frac{\Gamma_i}{D_i} + \frac{N_i}{N_e} \frac{kT_e \sum_j \frac{\Gamma_j}{D_j}}{(kT_e + kT_i)} \\
 \frac{\partial N_e}{\partial r} &= -\frac{kT_i \sum_j \frac{\Gamma_j}{D_j}}{kT_e + kT_i} \\
 \frac{\partial \Gamma_1}{\partial r} &= S_1 - \frac{\Gamma_1}{r} \\
 \frac{\partial \Gamma_2}{\partial r} &= S_2 - \frac{\Gamma_2}{r} \\
 \frac{\partial \Gamma_e}{\partial r} &= S_e - \frac{\Gamma_e}{r} \\
 E &= \frac{kT_e}{e} \frac{kT_i \left( \frac{\Gamma_1}{D_1} + \frac{\Gamma_2}{D_2} \right)}{N_e (kT_e + kT_i)}
 \end{aligned}
 \tag{6-1}$$

Here,  $S_1$ ,  $S_2$  and  $S_e$  refer to the most general form of the source terms, including external ionization and volume terms proportional to arbitrary powers of the number densities. As we discuss each individual system, we will repeat the system above with the specific source/loss terms entered for the particular system being considered. Note that we are using the small-e-

flux approximation. In addition, we use the actual physical quantities themselves, not the dimensionless version. Many of the arguments for using non-dimensionalized functions pertain to the ability to more easily investigate the features of analytic solutions. For numeric solutions, the connection between the input parameters and the final solutions is not as clear. As a result, these arguments are not as strong for numeric solutions as they are for analytic solutions. Furthermore, the use of physical solutions for this particular system of equations allowed for slightly increased numerical stability. The reasons for this increased stability are not perfectly clear, as stability analysis of a numerical system this complex is extremely complicated.

*Measure of Nonproportionality.* One of the phenomena we wish to investigate is nonproportionality. We are interested in determining how far a particular solution deviates from a proportional solution and what are the implications of the deviation. Such a determination is possible only if we have a metric for nonproportionality.

A usable measure should have the following characteristics:

1. It should measure deviation in some fashion from proportional solutions. From Chapter IV, we saw that nonproportionality is determined by the form of the source. If we have proportional sources (as we defined them in Chapters IV and V), we find proportional solutions. As we add nonproportional sources, we deviate from proportional solutions. It is these deviations that we wish to measure.
2. A value of 1.0 for solutions that match the Schottky solutions is convenient for comparison from one discharge to another.
3. It should be experimentally useful. One possibility would be that the quantities involved are experimentally accessible. This allows for easier and more accurate comparison to experiment. Another possibility would be a measure that allows comparison of experimen-

tal values to analytic predictions. This allows for determination of the validity of correlation between experiment and theory.

4. The measure should be general enough to address a wide variety of physical systems.

One complication is the uncertain usage of the term "Schottky solutions". In this research, "Schottky Solutions" is used to refer to those solutions produced by Schottky's ambipolar model when the only kinetic processes are volume ionization by plasma electrons, given by  $S_i = \nu_i N_e$ . Such processes give trigonometric solutions for planar geometry, and Bessel functions for cylindrical geometry. Other systems may give proportional solutions, but these will not be referred to as Schottky solutions.

There are a number of possible measures. None of them completely meet all the requirements above. In particular, it is difficult to meet the first three requirements and maintain complete generality. We chose to use a perfectly general measure, and accept the limitations that result. We define our chosen measure as

$$\beta_i = \frac{\left. \frac{S_i}{S_e} \right|_{r=0}}{\left. \frac{\Gamma_i}{\Gamma_e} \right|_{r=d}} \quad (6-2)$$

In this expression, the "i" subscript refers to the ion species.  $S_i$  is used as a measure of the source term that would give rise to proportional solutions, evaluated on axis. For example, for uniform external ionization, it would be the external source term. For volume sources, it would be the ionization frequency.  $\Gamma$  is the particle flux, evaluated at the wall.  $S_i$  can be considered a measure the behavior that would exist if the nonproportional

process were absent, while  $\Gamma$  is a measure of the behavior that exists with the nonproportional process present. As an example, if the discharge involved volume ionization plus recombination,  $\beta$  would be given by the expression  $\beta = (v_i/v_e)(\Gamma_i/\Gamma_e)$ , with each  $\Gamma$  evaluated with the effects of recombination included.

This is not a perfect measure of nonproportionality. For instance, it only uses values on-axis and at the edge of the discharge. It can also give misleading results for systems where one ion dominates the discharge. In such cases,  $\beta$  can seem to indicate proportionality for the dominant ion, when in fact the discharge as a whole is highly nonproportional. However, its generality and its independence of system-specific effects makes it a worthwhile parameter.

The measure chosen meets our criteria. First, proportional solutions predict a particular relationship between the on-axis source terms and the wall fluxes, which determines  $\beta$ . As the solutions move away from proportionality, that relationship, and  $\beta$ , changes. Second, it does have a value of 1.0 for Schottky solutions. Third, it is experimentally accessible. For instance, a value of  $\beta = 2.0$  means that the proportional source terms are twice what the ion fluxes at the wall would predict them to be. As a result, using a proportional model to determine the on-axis ionization from the wall fluxes would also be in error by that same factor of 2.

There are other measures we could use. One would be to calculate the integral of  $(N_i(r)/N_e(r) - N_i(0)/N_e(0))^2$ , as  $r$  goes from 0 to  $R$ . For a propor-



tional discharge, this would be exactly zero for each species. However, it would be very difficult to compare this measurement to experiment. Furthermore, it does not relate to any of the external or internal parameters of the discharge, which restricts its utility. It would also be difficult to devise a scale for this measurement; that is, is a value of 2.0 nearly proportional or very nonproportional?

Because of the difficulties that arise with other measures, we choose to use  $\beta$ , knowing full well that for different situations there may be other choices.

*External Ionization.* Three systems will be examined that use external ionization sources. The first is investigated in the verification of the model. The other two are addressed in the last part of the chapter, when we use generic plasmas to investigate the effect of recombination and charge transfer in nonproportional discharges. We will briefly describe each system below. Fuller descriptions will be provided as we address each individual system.

The first system examined duplicates the system described in Wunderer (Wunderer, 1978). It uses a pseudo-Gaussian external source for the first species, nonresonant charge transfer from the first species to the second, and recombination for both species. The entire purpose for examining this system is to demonstrate that the present model produces results consistent with previous theoretical analyses, in a regime where both the previous analysis and the present one are applicable. Because of the contrived nature of Wunderer's system, we do not attempt to draw any general conclusions.

A second system uses uniform external ionization for two species, diffusion as a loss for both species, and recombination as an additional loss for the second species. Here, we are interested in examining deviations from proportionality and discovering scaling relationships for recombining multi-ion plasmas. That being the case, we use quasi-realistic gases, in the sense that their parameters are reasonably close to those of real gases, but are chosen more for convenience in demonstrating the desired effects.

Another system also uses uniform external ionization for both sources, but includes nonresonant charge transfer from the first species to the second species instead of recombination. We are interested in examining deviations from proportionality and discovering scaling relationships, and so we again use quasi-realistic gases, still in the sense that their parameters are reasonably close to those of real gases, but are chosen more for convenience in demonstrating the desired effects.

*Volume Ionization.* Three systems were examined that used volume ionization sources. The first two are used to demonstrate the applicability of the new model to physical systems. The last is a generic system used to investigate recombination and volume sources in a discharge.

One system models a helium-neon mixture, at various mixture ratios. The new model is used to calculate the electron temperature required to meet the eigencondition of a volume-ionized discharge. The electron temperatures calculated are shown to agree with previous theoretical results for pure gases and mixtures, and to experimental results for mixtures.

In a second case, the new model is used to calculate electron temperatures and electron wall fluxes for two different systems based on an impurity-contaminated  $N_2$  discharge. The first system considers an  $N_2^+ - N_4^+$  discharge model. This system has a volume source term for  $N_2^+$ , charge transfer from  $N_2^+$  to  $N_4^+$  as the only source for  $N_4^+$ , and dissociative recombination of  $N_4^+$  as a loss term. The second system uses an  $N_2^+ - HN_2^+$  discharge model, with direct ionization of  $N_2^+$  and charge transfer from  $N_2^+$  to  $HN_2^+$ . The  $N_2^+ - N_4^+$  system models dissociative recombination, which is not present in the  $N_2^+ - HN_2^+$  system, and provides information about the relative importance of the two species. However, the  $N_2^+ - HN_2^+$  system allows us to see the effects of small admixtures of a more mobile ion. This example demonstrates the ability of the model to use only two ion species to describe systems to a fair degree of accuracy, when those systems have more than two ion species. The results are compared to experimental data of Schmidt (Schmidt, 1965).

A third system uses volume ionization for both species, and recombination as a loss term for the second species. As in the corresponding external ionization case, the primary purpose is to discover more about the deviations from proportionality and establish scaling relationships. That being the case, the system once again uses quasi-realistic gases, still in the sense that their parameters are reasonably close to those of real gases, but are chosen more for convenience in demonstrating the desired effects.

*Algorithmic Method.* An algorithm usually described as the relaxation method was used to solve the two-point boundary value problems arising from this investigation. This is a boundary value problem-solving algo-

rithm based on recasting the problem as a minimization of the error between the finite differenced form of the derivatives, and the functional form that the derivatives are equal to. This error is evaluated over the entire region, and then an iterative process is used to approach the correct solutions. The code used to implement the relaxation algorithm itself is from *Numerical Recipes the Art of Scientific Computing (FORTRAN Version)* (Press, *et alia*, 1989). For complete details on the programs, see Appendices C and D. Appendix C describes the overall structure of the programs, including a more complete explanation of the relaxation method. Appendix D describes each separate program, including listings of the various source codes and makefiles.

All solutions were produced on a Commodore Amiga 3000UX computer using the NKR, Inc Fortran-77 compiler and Unix System V, Release 4, Version 1.1. The maximum resolution allowed in the code was 201 mesh points, determined primarily by the balance between the need to have sufficient accuracy to describe physically pertinent detail and speed of solution. At the maximum resolution used (201 points), five to ten iterations were performed per second. This was fast enough to allow interactive operation of the program. Since the time required scales approximately as the square of the mesh size, increasing the mesh size dramatically slows the algorithm. Therefore, higher resolutions were not used. This 201-point resolution was generally used for all calculations of final results. Floating point calculations were performed using 64-bit reals to ensure that roundoff error did not affect the results.

## Comparisons

At this point the process of comparing the new model developed in this effort to the results of other authors begins. The goal is to show that the new model can accurately depict diffusive plasma discharges containing multiple ions. We do that by comparing our results with calculations from previous models, and with experimental results.

*Comparison to Wunderer's Results.* Wunderer developed a multiple ion model using an initial derivation based on Schottky's assumption of congruence, much as previous authors such as Oskam did (Wunderer, 1978; Oskam, 1958). The result is the following system of differential equations, one for each ion species:

$$\frac{\partial n_i}{\partial t} = \mu_i \left[ U_i \left( n_i \left( \frac{\nabla^2 n_e}{n_e} - \frac{|\nabla n_e|^2}{n_e^2} \right) + \frac{\nabla n_e \cdot \nabla n_i}{n_i} \right) + U_i \nabla^2 n_i \right] + \left. \frac{\delta n_i}{\delta t} \right|_{\text{coll}} \quad (6-3)$$

Here,  $\mu$  is the particle mobility, and  $U$  is the particle energy (corresponding to  $kT$ ). The collision term represents the net source or loss of each species due to ionization, charge transfer, recombination, and so forth. This result is dependent on an expansion of the electric field corresponding to the small-e-flux approximation.

Wunderer discusses extensively the validity of the assumption of proportionality. However, since the validity of that assumption has already been addressed in Chapter IV, Wunderer's numerical solution is more germane to the matter at hand.

Wunderer gives one example of a complete solution. This example is for a time independent system with cylindrical geometry, with an external source for the first ion species only, charge transfer from that species to the

second species, and recombination for both species. There is no pretense made that this model is a good representation of any particular realistic gas. However, the geometry is readily realizable, and the gas parameters correspond approximately to those appropriate for  $H_3^+$  and  $H_3O^+$ . Wunderer's primary purpose was attempting to model a system where he was certain that proportionality would not hold. The utility for this investigation is in comparing two different approaches (ours and Wunderer's) to the same system, and seeing how they compare.

In the present model, the continuity equations for this case become:

$$\begin{aligned}\frac{\partial \Gamma_1}{\partial r} &= f_1(r) - v_c n_1 - \alpha_1 n_1 n_e \\ \frac{\partial \Gamma_2}{\partial r} &= v_c n_1 - \alpha_2 n_2 n_e\end{aligned}\tag{6-4}$$

Species 1 ( $n_1$ ) corresponds to  $H_3^+$ , and species 2 ( $n_2$ ) to  $H_3O^+$ , formed by an associative charge transfer reaction with  $H_2O$ . Wunderer used values appropriate for a pressure of about 0.1 T. Note that "n" in this case is not the normalized "n" used earlier, but rather is the physical variable. This matches Wunderer's notation. Note also that the right hand side of each equation is the same form that Wunderer uses for  $\delta n / \delta t_{coll}$ .

In order to compare with Wunderer's solutions, the same normalized system of equations must be used. His equation (40) provides the following definitions (with some modifications to described shortly):

$$\begin{aligned}
\rho &= \frac{r}{R} \\
U &= \frac{kT_e}{kT_i} \\
D_{ai} &= D_i(1+U) \\
f(\rho) &= \frac{f_1 R^2}{D_{a1} A} \\
N_{e,i} &= \frac{n_{e,i}}{A} \\
G &= \frac{v_c R^2}{D_{a1}} \\
T &= \frac{\alpha_1}{\alpha_2} \frac{D_{a2}}{D_{a1}} \\
S &= \frac{R^2 A \alpha_2}{D_{a2}} \\
D &= \frac{D_{a1}}{D_{a2}} \\
\frac{\partial}{\partial \rho} &= R \frac{\partial}{\partial r}
\end{aligned} \tag{6-5}$$

where  $R$  = discharge radius (cm)

$D_i$  = diffusion coefficient ( $\text{cm}^2/\text{s}$ )

$f_1$  = external source term ( $\text{cm}^3/\text{s}$ )

$A$  = normalization for the external source ( $\text{cm}^{-3}$ )

$v_c$  = charge transfer collision frequency from species 1 to 2 (Hz)

$\alpha_i$  = recombination coefficient for species  $i$  ( $\text{cm}^3/\text{s}$ )

These definitions correct a minor flaw in Wunderer's definition. His normalizations of  $f_1$  and  $n_{e,i}$  were inconsistent; one or the other was not dimensionless. We chose to correct this by leaving the normalization for  $n_{e,i}$  as Wunderer had it, and correcting that for  $f_1$ . In effect, Wunderer's normalization is equivalent to assuming  $R = 1.0$ .

In addition, we use the following definition for the normalized current density:

$$\gamma = \Gamma_i \frac{R}{D_{ai}A} \quad (6-6)$$

Once more, note that this is not the same normalization used in Chapters III, IV, and V. Instead, this normalization is chosen to be consistent with Wunderer's notation. The confusion is unfortunate, but unavoidable.

These definitions and the new model produce the following system:

$$\begin{aligned} \frac{\partial N_1}{\partial \rho} &= -\gamma_1(1+U) + \frac{N_1}{N_e}U(\gamma_1 + \gamma_2) \\ \frac{\partial N_e}{\partial \rho} &= -(\gamma_1 + \gamma_2) \\ \frac{\partial \gamma_1}{\partial \rho} &= -\frac{\gamma_1}{\rho} + f - TS N_1 N_e - G N_1 \\ \frac{\partial \gamma_2}{\partial \rho} &= -\frac{\gamma_2}{\rho} + G D N_2 - S N_2 N_e \end{aligned} \quad (6-7)$$

The source term is of the form

$$f(\rho) \propto \exp\left(-\left(\frac{\rho}{0.35}\right)^{2.2}\right) \quad (6-8)$$

In this notation, "TS" represents the normalized recombination coefficient and "G" the normalized charge transfer frequency for  $N_1$ , and "S" is the normalized recombination coefficient and "GD" the normalized charge transfer frequency for  $N_2$ . "f" is the external source term. The first two equations are the momentum equations, and the second two the continuity equations.

The solutions were found using the relaxation method algorithm, as described above. All input parameters used were identical to Wunderer's, and are shown below:



**D = 0.9 => The two ions have very similar mobilities and diffusion coefficients.**

**T = 0.2 => Species 2 has approximately five times the recombination rate as species 1.**

**U = 5 => The electron temperature is five times larger than the ion temperature.**

**G = 0.178 => The charge transfer loss frequency for species 1 is about 1/30 the diffusion loss frequency.**

**S = 100 => The recombination loss frequency for species 2 is about 20 times the diffusion loss frequency.**

Here, the diffusion loss frequency is defined as  $D_e/(R/\lambda_0)^2$ , where  $\lambda_0$  is the first zero of the zero-order Bessel function  $J_0$ .

Since no analytic solution was available, even for simplified reactions, a very simplistic initial starting function was used. This starting function was determined by formally integrating the continuity and momentum equations as if the external source had no spatial dependence, but evaluating the densities and fluxes using the actual spatial dependence of the source. This very poor approximation contributed to lengthening the iteration process. Even so, convergence to better than one part in  $10^7$  was achieved in less than 60 iterations. This compares to Wunderer's iteration, which required 100 iterations to achieve convergence to within one part in  $10^5$  (Wunderer, 1978:411). The increased efficiency may be due to a more efficient numerical algorithm. However, it certainly appears that the present model may offer advantages over Wunderer's.

In Figure 6-1 we give our results, comparable to Wunderer's Figure 2. Our results are indistinguishable from Wunderer's Figure 2, within the limits of accuracy of Wunderer's figure (Wunderer, 1978:413).

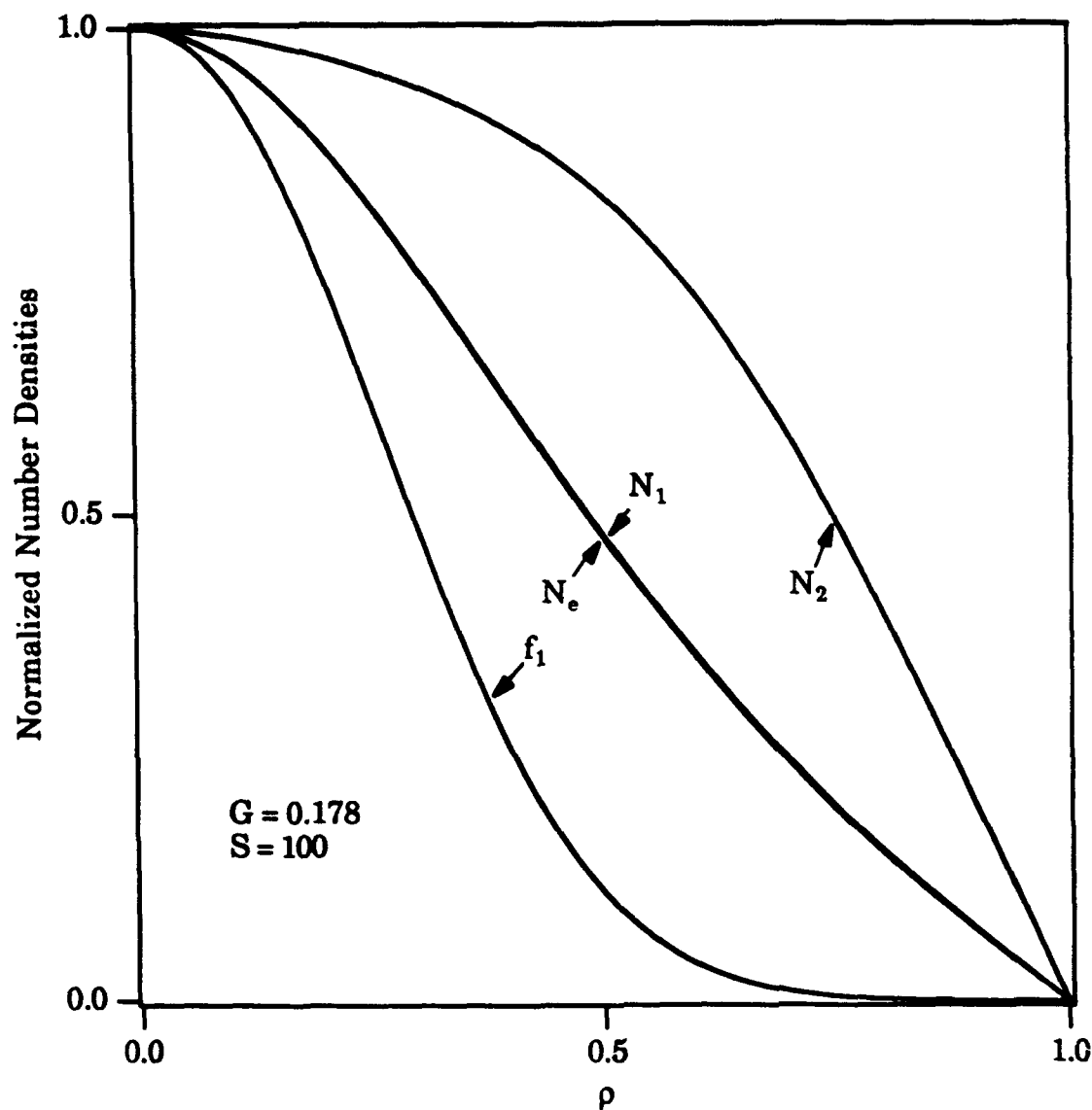


Figure 6-1. Normalized Number Densities and External Source Term For Wunderer's Example System

As in Wunderer, all the densities are normalized by their on-axis values. As a result,  $N_2$  appears to be larger than  $N_e$ .  $N_1$  is proportional to  $N_e$ , within high accuracy. As shown above, the value of  $G$  indicates charge transfer from  $N_1$  to  $N_2$  that is approximately 3% of the diffusion loss for  $N_1$ . In addition,  $S$  indicates recombination for  $N_2$  that is some 20 times the diffusion loss for that species. The overall system is one where  $N_1$ , the species with the largest source term, also has the smallest volume loss

term. As a result, this discharge is dominated by  $N_1$ . For instance, our results indicate that the flux of  $N_1$  at the edge of the plasma is 40 times larger than that of  $N_2$ .

The results shown later in this chapter indicate that the dominant species in a system like this can often be described by a proportional model. This is confirmed by Wunderer's results, which show the same results for  $N_1$  and  $N_e$  with or without assuming proportionality (Wunderer, 1978:412). Later in this chapter we will see other instances of domination by one species leading to proportionality of the dominant species. This proportionality does not imply that solutions for that species can be found by ignoring the nonlinear effects. Instead, it results from one species being such a minority in the discharge that the electron density and other ion density are essentially equal.

Proportionality definitely does not hold for the other species. Clearly,  $N_e$  and  $N_2$  do not have the same spatial profile. In fact, the profile for  $N_2$  is flattened, when compared to  $N_1$ . This is consistent with results to be presented later, which show this effect to a greater extent. Wunderer also presents results which depict the wall flux for species 2 as calculated by a proportional model being in error by 30% (Wunderer, 1978: 412-413).

We should note the implications of the extremely close agreement we found between the results presented above and Wunderer's. The system Wunderer modeled is very complex, with a highly nonuniform external source, charge transfer from one species to another, and recombination for both species. The source term is far from any simple analytic form, and there are linear and nonlinear kinetic reactions occurring. The differential

system we solved bore little resemblance to Wunderer's. Yet, the model produced essentially identical results in fewer calculations. Thus, this case gives very strong evidence to the validity and utility of the new model.

*Temperature As an Eigenvalue.* Next, we wish to evaluate the relationship between the discharge parameters and the electron temperature. As noted in Chapter V, the electron temperature can be considered an eigenvalue of the system for systems driven by volume ionization. In particular, the electron temperature affects the ionization rates of the various species, as well as entering directly into the differential equations. Thus by incorporating the appropriate plasma parameters (ionization thresholds, pressure, dimensions, and so forth), one can calculate the electron temperature for various systems. For this investigation, the electron temperatures determined by the new model were compared to theoretical and experimental results of other researchers.

The investigation serves two useful results. First, it provides verification of the numerical method, including correct solution of the differential equations and proper incorporation of electron temperature into the model. Second, it demonstrates that the proportional analytic solutions described in the last chapter are useful to describe realistic systems.

We compare the results to Young's analysis of electron temperature in helium-neon glow discharges, which was based on an earlier work by Dorgela, Alting, and Boers (Young, 1965. Dorgela *et alia*, 1935). Young used an expression developed by Dorgela, Alting, and Boers that related the mobility, initial slopes of ionization efficiencies, ionization potentials, and gas fraction to the electron temperature in order to calculate electron

temperatures for situations comparable to the experimental conditions of Labuda and Gordon (Young, 1965; Dorgela, *et alia*, 1935; Labuda and Gordon, 1964):

$$\sum_i f_i c_i^2 (pD)^2 \left( \frac{kT_e}{eV_i} \right)^{1/2} \left[ 1 + \frac{eV_i}{2kT_e} \right] \exp \left[ -\frac{eV_i}{kT_e} \right] \quad (6-9)$$

$$= \left( \frac{300\pi}{2} \right)^{1/2} \lambda_0^2 \left( \frac{m}{e} \right)^{1/2} = 1.72 \times 10^{-7} \text{ V}^{1/2} \text{ sec cm}^{-3} \text{ Torr}^{-2}$$

Young showed that the expression gave reasonable agreement to the Labuda and Gordon results. As reported by Young, the Dorgela *et alia* expression is a multi-ion form of von Engel and Steenbeck's earlier work, and states an eigencondition for the electron temperature with a total ionization frequency based on a weighting with the gas fraction  $f$ . If the eigencondition reported in the fifth equation in Equation 5-77 is evaluated using von Engel's Equation 8.36, the results are, with two exceptions, identical to Equation 6-9 (von Engel, 1965:293). First, Equation 6-9 contains an additional  $1/(1+\epsilon)$  term involving the ratio of the ion and electron temperatures appearing on the left hand side of the Equation 6-9. This term accounts for the ion temperature dependence in the differential equations that Young's model did not. Second, the numerical factor of 300 Young uses to correct for inconsistent units does not appear in Equation 5-77. The first difference represents a difference in the physical model. The second difference is inconsequential; Equation 5-77 uses consistent units and does not need the correction factor.

Our intent was to compare our results to Young's. Therefore, we used the same ionization source and diffusion loss term. In addition, we used

Blanc's law and Young's input values for the mobilities, ionization potentials, and ionization efficiencies to calculate the necessary input values of diffusion coefficients and ionization potentials for our calculation.

To perform the calculations, we used a variation of the multi-ion model used for the various volume ionization systems later in the chapter, with the only significant modifications being in the output format. This uses the full formal methodology applicable to nonproportional multi-ion systems. The full nonproportional model was used for several reasons; to verify the accuracy of the program coding, to show that the nonproportional model reduces to proportional solutions for appropriate source terms, and to show that the single-ion solutions are identical to Schottky's well-known solutions.

The numerical method solves for the fluxes, the number densities, and the electron temperature. It begins by assuming the analytic solution from the CV case, Equation 5-13 that for single ions is identical to the Schottky solutions. To determine the values for the analytic solution, it solves the eigencondition of the fifth expression in Equation 5-77 of the last chapter using an ionization frequency  $\nu_i$  based on a Maxwellian distribution for the electrons and a linear dependence of cross-section on energy. The expression for  $\nu_i$  is equivalent to von Engel's (von Engel, 1965:293). This produces an initial value of the temperature that is used to generate the fluxes and number densities. The method then uses the relaxation method to iterate to the actual multi-ion solution that satisfies the momentum and continuity equations, including the electron temperature as one of the variables. The final solution is the set of fluxes, densities, and electron temperature that

meets the multi-ion boundary conditions and satisfied the multi-ion differential equations.

If the two models were equivalent, iteration would not be necessary; the analytic and numerical solutions would be identical. That is exactly the result. The only time that convergence did not occur instantly was when the numerical method used to calculate the temperature for the analytic solution used a larger tolerance than the iteration method used to find the actual multi-ion solution. For instance, if the initial tolerance in finding the analytic solution for  $kT_e$  was  $10^{-3}$ , then the temperature might be off as much as one part in 1000. If the tolerance for solving the differential equation were  $10^{-6}$ , additional iterations might be required to reduce the error in  $kT_e$  from 1 in 1000 to 1 in 1,000,000.

Given the exact match between our results and Young's, we do not present any actual results. Rather, we merely note that in every case the differences were less than 1%, and are attributable to the factor of  $1+\epsilon$  that appears in our model, but not in Young's.

Both Young's results and the present calculations adequately describe experimental results for this rather simple two-ion system. However, the present model can accommodate more accurate descriptions of the reaction kinetics and ion parameters, and can also include the reactions occurring in more complicated discharges that Young would not have been able to describe at all.

In summary, this comparison demonstrates several points:

1. The numerical method properly accommodates electron temperature variation, and correctly solves the differential equations.

2. When using the same expression for ionization frequency and mobilities, the proportional multi-ion solutions of the CV case give the same electron temperatures as previous simpler models do, except for a correction factor of  $1+\epsilon$  that the previous models did not account for.

3. In the single-ion case, the CV case reduces precisely to Schottky's results.

4. Based on the close agreement with Young's results, both models agree well with the experimental results of Labuda and Gordon (Young, 1965. Labuda and Gordon, 1964).

*Comparison to Schmidt.* In the previous discussions we compared our model to other theoretical models, and to experimental measurements of electron temperatures, all in fairly simple systems. Next, we will compare the results of our model to experimental measurements of a more complicated multi-ion system. This comparison does two things. First, it provides a further opportunity to show the applicability of the model to realistic systems. Second, the comparison will demonstrate an effect of introducing an impurity gas of high mobility into a discharge.

We look at a comparison between our model and results obtained by Schmidt for the nitrogen plasma (Schmidt, 1965). Schmidt performed measurements of the positive column of a 40 cm long, 3 cm diameter nitrogen glow discharge at pressures ranging from 0.75 to 3 T, which is high enough to ensure diffusion conditions for both ions and electrons. He measured electron and ion fluxes at the walls, using mass spectrometry to distinguish the various ion species. He also measured longitudinal current and longitudinal field as a function of position. Finally, he reported values for the electron temperature.

Schmidt measured both electron and ion fluxes at the wall of the discharge. His results showed the electron wall flux increasing with



increasing discharge current at a fixed pressure, and with decreasing pressure at a fixed discharge current. His measurements of ion fluxes produced evidence of  $N^+$ ,  $N_2^+$ , and  $N_3^+$  ions at the wall of the discharge. Furthermore, he stated that the measurements of  $N_2^+$  may have included  $N_4^+$  as well. He gave no explanation of this statement. We note that the  $N_4^+$  ion is essentially an  $N_2^+ \cdot N_2$  dimer. Such dimers are often easily dissociated by the high fields used in mass spectrometric measurements, and only the charged constituents detected. Furthermore, for the pressures and number densities of his discharge, we will see that we would expect the flux to be preponderantly  $N_4^+$  in at least some cases. In addition to the various nitrogen ions, he measured  $H^+$  ions, as well as  $NH_4^+$  ions, even though he claimed to have used only pure nitrogen in the discharge. In fact, at the highest pressures and discharge currents,  $H^+$  becomes the dominant ion flux measured (Schmidt, 1965:152-153). No explanation beyond unnamed impurities adsorbed in the apparatus was given for the source of the  $H^+$  ions. Schmidt gave several multi-step processes as the possible sources for the  $NH_4^+$  ions, but did not further discuss the source of the hydrogen (Schmidt, 1965:152-158). His flux results for the individual ion species showed varied dependencies on discharge current; some species increased with discharge current, some decreased, and some attained a maximum and then declined. The data on the individual ion fluxes appear to be so species-dependent that general statements would not be appropriate, except to note the expected result that the fluxes decreased as pressure increased.

He also gives measured values for the electron temperature as a function of discharge current. He shows the electron temperature decreas-

ing as the pressure increases, and as the discharge current increases. The dependence of the electron temperature on discharge current appears to depend on the pressure considered. At 0.75 Torr, there is little dependence; at 1.5 Torr,  $kT_e$  decreases slightly with increasing current, and at 2.0 Torr the decrease is more pronounced (Schmidt, 1965: 155). Either multi-step ionization or ionization from the dissociated state could be an explanation. In either case, the increasing electron number density produces higher densities of the intermediate state with concomitant higher ionization rates. However, there is not enough information in Schmidt's results to clearly determine which is the explanation, or if some other mechanism is present.

Schmidt used probes to measure the longitudinal potential as a function of position, from which he then obtained the longitudinal electric field. His results show the field decreasing as the longitudinal current increases, and as the discharge pressure increases (Schmidt, 1965:155). These agree with the temperature behavior. The ratio of total electric field to background number density is a parameter that can be used to describe the ionization rate much as the electron temperature can be used (von Engel, 1965: 179-185). Therefore, the similarity of the behavior of field to the behavior of the electron temperature is not surprising.

*Basis for Comparison with the New Model.* We will not attempt to accurately simulate all species and all details of this discharge. To do so would require much more information on the gas mixture than is available from Schmidt. Furthermore, although the general theory could certainly be used to develop a model that coupled the longitudinal field into the

discharge, the present version does not do so. Therefore, we will not attempt to model that field. Rather, we used Schmidt's measured values to determine some of the input parameters to our model.

We will select aspects of the discharge, and compare our theoretical results with the experimental results of Schmidt. In particular, we will examine his results for electron temperature in the discharge and for electron fluxes at the wall. The electron temperature comparison is hampered somewhat by the apparent experimental scatter of Schmidt's results and by the impracticality of trying to include all the species in the model.

We will model the discharge in two ways. An  $N_2^+-N_4^+$  system will first be used. This allows clear demonstration of the results of such reactions as charge transfer and dissociative recombination. Experimental examination of such reactions can be complicated by the difficulty of separating the various effects. An  $N_2^+-HN_2^+$  system will be used second. This will highlight the sensitivity of the discharge to trace impurities.

For either case, we must determine various input parameters from Schmidt's data. The physical parameters of the discharge, including pressure, are given directly. However, one of the input parameters needed is the on-axis electron density. Schmidt did not provide values for this. Instead, he presented his results as a function of the longitudinal discharge current. This must be converted into the on-axis electron number density,  $N_{e0}$ . The total longitudinal current is

$$I = ev_d \int_0^R N_e(r) 2\pi r dr \quad (6-10)$$

where  $v_d$  is the electron drift velocity. For the values pertinent to this system  $N_e$  can be written as

$$N_e(r) = N_{e0} J_0\left(\lambda_0 \frac{r}{R}\right) \quad (6-11)$$

Here,  $\lambda_0$  is the first zero of the Bessel function  $J_0$ , and  $R$  is the radius of the discharge. The validity of Equation 6-11 depends on the electron density being well-represented by a Schottky profile. This was the case for all the cases examined. Of course, Equation 6-11 is not necessary to the solution of the problem; it is possible to integrate the actual number density profile and multiply by the drift velocity to get the current. The calculations performed both analytic and numeric integrations. The difference was never as high as 10%, and usually was much less.

Equation 6-11 allows evaluation of the integral in Equation 6-10, expressing  $N_{e0}$  in terms of  $I$ ,  $v_d$ ,  $N_{e0}$ ,  $R$ ,  $e$ , and  $\lambda_0$ .  $N_{e0}$  can then be determined from the data of Schmidt and the drift velocity,  $v_d$ . Fortunately, the information to find a reasonable estimate of the drift velocity is available. Schmidt gave values for the measured longitudinal electric field as a function of the discharge current (Schmidt, 1956). Those values, and the pressure, produce  $E/p$ . The relationship between drift velocity and  $E/p$  has been widely investigated. For convenience, we use results from von Engel (von Engel, 1965:124). Thus, once we determine the pressures and discharge currents we are interested in, we can determine  $N_{e0}$ .

$N_2^+ - N_4^+$  Systems. For the first set of calculations,  $N_2^+$  and  $N_4^+$  were assumed to be the two ionic species in the discharge.  $N_2^+$  is formed by direct electron impact ionization, according to the reaction



$N_4^+$  is formed by three-body collisions, according to the reaction



This reaction, of course, is also a loss for  $N_2^+$ . Finally, the dissociative recombination loss reaction for  $N_4^+$  is



These reactions produce the following set of momentum and continuity equations for the two ions:

$$\begin{aligned} \frac{\partial N_i}{\partial r} &= -\frac{\Gamma_i}{D_i} + \frac{N_i}{N_e} \frac{kT_i \sum_j \frac{\Gamma_j}{D_j}}{(kT_e + kT_i)} \\ \frac{\partial N_e}{\partial r} &= -\frac{kT_i \sum_j \frac{\Gamma_j}{D_j}}{kT_e + kT_i} \\ \frac{\partial \Gamma_1}{\partial r} &= v_i N_e - k N_1 - \frac{\Gamma_1}{r} \\ \frac{\partial \Gamma_2}{\partial r} &= k N_1 - \alpha N_2 N_e - \frac{\Gamma_2}{r} \\ \frac{\partial \Gamma_e}{\partial r} &= v_i N_e - \alpha N_2 N_e - \frac{\Gamma_e}{r} \end{aligned} \quad (6-15)$$

Note the change in the meaning of the subscripts;  $N_1$  refers to ionic species 1, or  $N_2^+$ , while  $N_2$  refers to ionic species 2, or  $N_4^+$ . We obtained the value for  $v_i$  from Von Engel, just as we have in the other numerical calculations. (Von Engel, 1965:293). We obtained the value for  $k$ , the rate coefficient for associative charge transfer, from the Smith and Adams article in Lindinger, Märk, and Howorka (Smith and Adams, 1984: 194 - 217). Finally,

we obtained the value for  $\alpha$ , the recombination coefficient, from Whitaker, Biondi, and Johnsen (Whitaker, Biondi, and Johnsen, 1981). To summarize the values of the various input parameters:

1. Diffusion coefficients were 51.7 and 63.07 cm<sup>2</sup>/s for N<sub>2</sub><sup>+</sup> and N<sub>4</sub><sup>+</sup>, respectively, based on Schmidt's mobility data (Schmidt, 1965:155).
2. Ionization for N<sub>2</sub><sup>+</sup> was based directly on von Engel's formulation, using an ionization potential of 15.8 eV and initial slope of the ionization efficiency of 0.161/cm-Torr-Volt derived from Kieffer (von Engel, 1965: 293. Kieffer). Since N<sub>4</sub><sup>+</sup> is not formed by direct ionization, its ionization rate was set lower than that of N<sub>2</sub><sup>+</sup> by >30 orders of magnitude (the algorithm requires a non-zero value).
3. The rate coefficient for associative charge transfer, from Lindinger, Märk, and Howorka, was 7.5x10<sup>-29</sup> cm<sup>6</sup>/s (Lindinger, Märk, and Howorka, 1984:208).
4. The recombination coefficient was based on Whitaker, Biondi, and Johnsen and was given by  $\alpha = 3.128 \times 10^{-7} (T_e/1\text{eV})^{0.5} \text{cm}^3/\text{s}$  (Whitaker, Biondi, and Johnsen, 1981).

These particular species were chosen for two reasons:

1. They are the dominant species occurring in a pure N<sub>2</sub> discharge for the conditions depicted in Schmidt. This conclusion is supported by Schmidt's results, which show N<sub>2</sub><sup>+</sup> as the dominant nitrogen ion in the discharge and indicate that N<sub>4</sub><sup>+</sup> could have been the species measured instead of N<sub>2</sub><sup>+</sup>. It is also supported by our calculations, which indicate that, if anything, N<sub>4</sub><sup>+</sup> is present in larger quantities than N<sub>2</sub><sup>+</sup>.
2. They allowed us to include a realistic set of reactions that are more complex than the simple systems we have examined so far. Incorporating such complicated processes in the system would test both the numerical correctness of the procedures and the physical validity of the model.

We would be surprised if we were able to match Schmidt's results exactly with this set of ions and reactions. For one thing, Schmidt's system had hydrogen produced from some unknown source. Hydrogen ions (either H<sup>+</sup> or H<sub>2</sub><sup>+</sup>) are extremely mobile compared to the various nitrogen ions. As we will discuss later in more detail, the presence of even small amounts of

hydrogen in the discharge can lead to higher electron fluxes and necessitate higher electron temperatures. In addition, we would expect to see effects due to the presence of the other nitrogen-containing ions in the plasma. However, we feel that testing the ability of the new model to describe discharges accurately using simplified kinetics is important.

We chose to make two comparisons to Schmidt. One was the electron temperatures. The other was the electron fluxes at the wall, determined from the electrical current density due to electrons that Schmidt gives in his Figures 4-6 (Schmidt, 1965:152-153).

Before discussing the two comparisons, some general comments about the results would be appropriate. On axis, the number density for  $N_2^+$  relative to  $N_4^+$  was approximately 2% at 2 T, 5% at 1.5 T, but approximately 35-40% at 0.75 T. The recombination loss was smaller than the charge transfer or ionization rates by factors in the range of 3 to 10, and generally closer to 10. Recombination, though present, is not dominating other source or loss processes. Instead, the discharge is largely governed by volume ionization, charge transfer, and diffusion. The analytic solutions in Chapter V indicate that such discharges are proportional, with Schottky number density profiles (Bessel functions in this geometry). Such a description is consistent with the results for the integral of the electron number density, which showed close agreement between the numerical integration and the analytic integration based on Equations 6-9 and 6-10. This close agreement indicates that the solutions were close to the proportional solutions that charge transfer with no recombination would have produced, and therefore indicates that recombination was a small effect in the overall

system. In fact, given the small contribution of recombination, it would have been possible to model this system analytically with reasonable accuracy, except that determination of the electron temperatures would still require numerical calculations.

We also note that our calculations enable us to distinguish between  $N_2^+$  and  $N_4^+$  and provide predictions of the proportions of each present in the discharge. Schmidt's experiment was unable to do this. Schmidt's only discussion of  $N_4^+$  is a short reference indicating that it may be present in his  $N_2^+$  measurements (Schmidt, 1965:156).

Now, let us examine the results of the comparisons between our model and Schmidt's experiment, starting with the electron temperatures. Figure 6-2 compares the electron temperatures measured by Schmidt and those obtained from the model. There is a clear disagreement in the scaling of the temperatures. Schmidt's values are higher, by as much as 50%. Considering the sensitivity of the ionization rates to electron temperature, this is a significant disparity. For instance, the difference between the value of 1.44 eV that the calculations produced for 70 mA and 1.5 T and Schmidt's measurement of 1.85 eV corresponds to an increase in ionization rate of approximately 12 times. Losses in Schmidt's system that are not included in our system might explain the difference. When we discuss the  $N_2^+$ - $HN_2^+$  system we will examine such a possible loss, and go into more detail on the effects of such losses on  $kT_e$ .

It is difficult to determine if the calculated results and Schmidt's differ in the relationship between current and temperature at each pressure. Schmidt's data gave little definitive correlation about the relationship



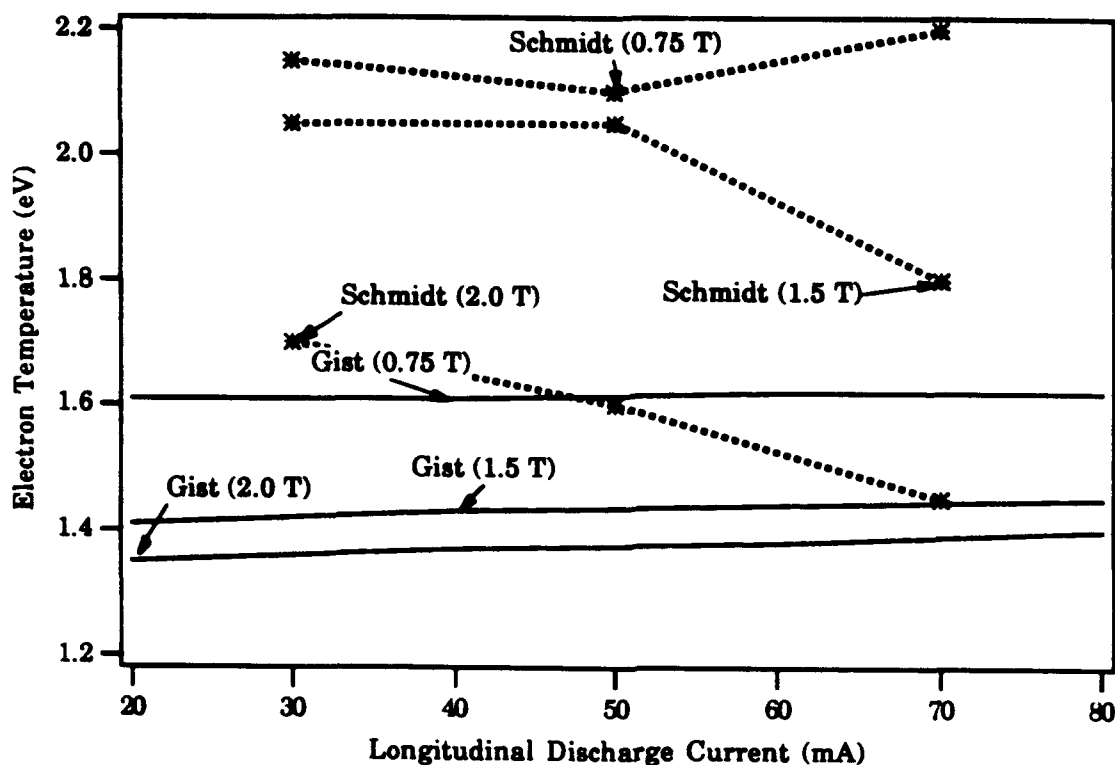


Figure 6-2. Comparison of Calculated and Measured Values of Electron Temperature at Selected Discharge Currents

between current and temperature. Although his data did not include indications of experimental error, this lack of correlation appears to be due primarily to scatter in his data. If any correlation exists, it is in the decreasing temperature with higher current exhibited by the measurements at 1.5 and 2.0 T. Examination of Schmidt's Figures 13, 14, and 15 reveal that the measured  $H^+$  flux as a fraction of the total flux increases with increasing longitudinal current at 0.75 T, but rose to a peak and then declined at 1.5 and 2.0 T (Schmidt, 1965: 156-157). This could provide the explanation; as will be shown in the next section, as hydrogen becomes less of a factor in the discharge, the temperature can decrease.

The calculated temperatures are almost constant with respect to current, exhibiting a slight increase as current increases. This is consis-

tent with a discharge that has recombination present, but for which recombination is not dominant. Higher currents imply higher  $N_{e0}$ . Recombination, as a loss term quadratic in  $N_{e0}$ , will increase more rapidly with increasing  $N_{e0}$  than diffusion or ionization. This increased loss term requires the increased ionization associated with a higher electron temperature.

There is one area of clear agreement between the two sets of data. Even if we take into account the experimental scatter, both our results and Schmidt's show temperature decreasing as pressure increases. This is a direct consequence of the balance between source and loss that determines the electron temperature. Using the example of a proportional volume ionization system, we note that the eigencondition expressed in Equation 5-77 requires  $\epsilon/(1+\epsilon)\sum v_i/D_i$  to be constant. As the pressure increases,  $D_i$  decreases. To maintain the entire expression constant requires a corresponding decrease in  $v_i$  and therefore in  $kT_e$ . Schmidt's system represents a more complicated case, but the general arguments still apply. We still expect to see temperature decreasing as pressure increases.

Results for the fluxes reveal closer agreement. In Figure 6-3 we show the calculated and measured electron fluxes to the wall. Overall, these results show closer agreement to the experimental data. The calculated dependencies of the fluxes on pressure and electron current are very similar to the experimental dependencies. The differences in magnitudes are not disturbing. The calculated results are smaller by factors of at most 2.5. This difference is not surprising, given the generally higher tempera-

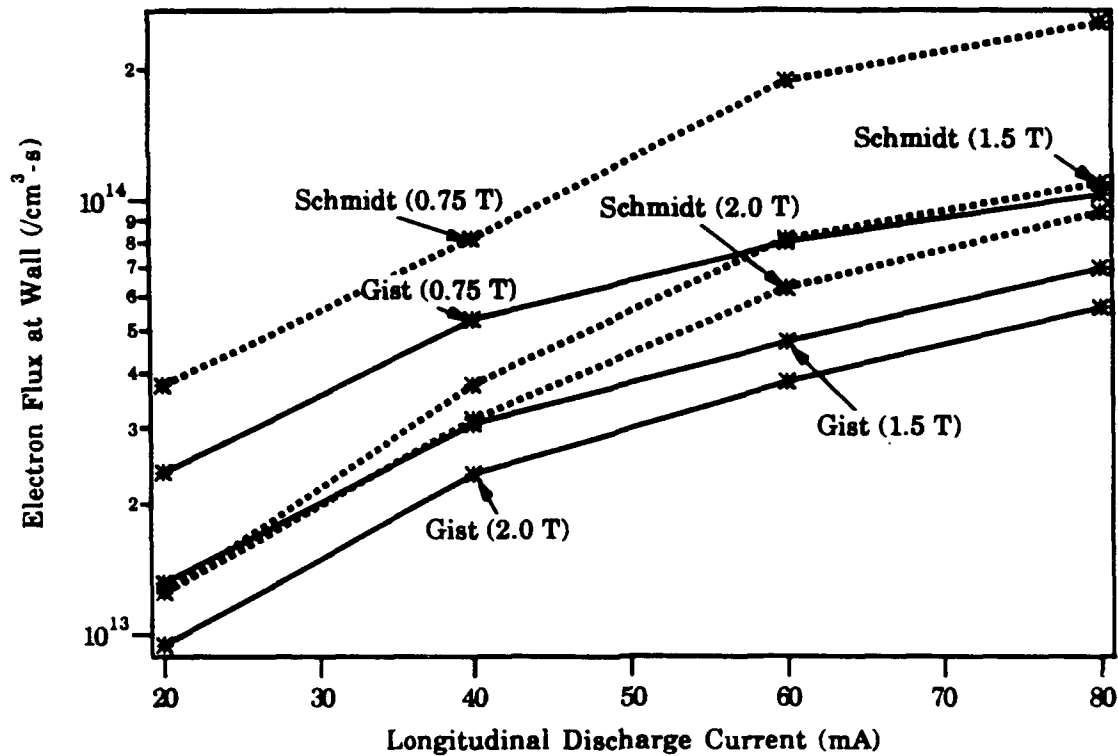


Figure 6-3. Comparison of Calculated and Measured Electron Wall Flux

tures that Schmidt found. In fact, let us demonstrate how those higher temperatures can more than explain the difference.

Consider the effect of higher  $kT_e$  on the fluxes in a recombining plasma. For simplicity, consider a single-ion plasma, with no sources other than volume ionization and recombination. For such a plasma the continuity equation is

$$\frac{\partial \Gamma}{\partial r} = \nu N_e - \alpha N_e^2 - \frac{\Gamma}{r} \quad (6-16)$$

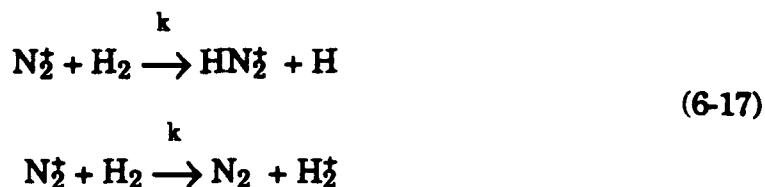
As discussed above, the higher temperatures reported by Schmidt produce an ionization frequency as much as 15 times higher than the calculations. If only volume ionization were present, this would imply fluxes 15 times higher, also. Recombination reduces this somewhat, but not by the factor of

six difference between 2.5 and 15. Experimental error, either on Schmidt's part or in the data used to produce the inputs for the calculation is possible as well. If those effects are not enough to account for the six-fold difference between the ionization rates and the fluxes, then we must assume additional volume losses due to reactions not included in the calculations. Considering the many species Schmidt reported that are not included in the model, such an explanation is reasonable.

For several reasons, we do not compare the calculated results with the experimental ion fluxes. First, our total ion flux, of course, is equal to the electron flux. Schmidt's total ion flux does not equal his total electron flux, implying losses or calibration errors in his measurement equipment. Without more information, it is impossible for us to determine how, or indeed, if his losses varied from ion to ion. Therefore, it is difficult for us to compare relative fluxes. Second, Schmidt does not distinguish between the  $N_2^+$  flux and the  $N_4^+$  flux. This makes comparisons of fluxes of those species in his results impossible. Finally, even if we were modelling species that Schmidt gives distinct results for, the presence of so many other species in Schmidt's experiment distorts the results to the point that comparisons lose much of their meaning.

*$N_2^+$  -  $HN_2^+$  System.* Let us now examine an  $N_2^+$ - $HN_2^+$  system. Our purpose is to demonstrate a mechanism that increases the temperatures and fluxes. The presence of charge transfer from  $N_2^+$  to a more mobile ion would force a higher temperature and also increase ionization. Since charge transfer does not reduce the source for electrons, the higher ionization would also produce higher electron fluxes.

Schmidt reported  $H^+$  in the fluxes at the wall of the discharge (Schmidt, 1965: 152-153). This implies the presence of  $H_2$  as an impurity in his discharge. That being the case, charge transfer will occur according to the following reactions:



This is a near-resonant charge transfer reaction, with a difference in ionization potential of only 0.56 eV for the formation of  $HN_2^+$  and 0.06 eV for the formation of  $H_2^+$ , and with  $N_2^+$  having the higher potential in both cases (McDaniel *et alia*, 1980: 2732). McDaniel *et alia* report that these reactions have a combined reaction rate of  $1.8 \times 10^{-9} \text{ cm}^3/\text{s}$ , with  $HN_2^+$  as the predominant product (McDaniel *et alia*, 1980: 2732), and show other results that  $HN_2^+$  is the only product, with a reaction rate coefficient of  $2 \times 10^{-9} \text{ cm}^3/\text{s}$  (McDaniel *et alia*, 1980: 2345). With only trace amounts of  $H_2$  present, and therefore even less  $H$ , recombination is unlikely for either species. In addition, the intent of the calculation is to examine the effects of hydrogen impurities on the discharge, not the effects of recombination. With no recombination present, this is a three-ion proportional system similar to the CT case of Chapter V. The eigencondition that determines the electron temperature in this system is

$$\left(\frac{\lambda_0}{R}\right)^2 = \frac{\epsilon}{(1+\epsilon)} \left( \frac{v_{t2}(v_{t2} + v_{t3})K_1}{D_1} + \frac{v_{t2}K_1}{D_2} + \frac{v_{t3}K_1}{D_3} \right) \quad (6-18)$$

where  $v_{t2}$  and  $v_{t3}$  are the charge transfer frequencies from  $N_2^+$  to  $N_2H^+$  and  $H_2^+$ , respectively, and  $K_1$  is  $N_1/N_e$ . Equation 6-18 can be expressed as

$$\left(\frac{\lambda_0}{R}\right)^2 = \frac{\epsilon}{(1+\epsilon)} \left( \frac{v_1 - v_t K_1}{D_1} + \frac{v_t K_1}{D_2} - K_1 v_{t3} \frac{(D_3 - D_2)}{D_2 D_3} \right) \quad (6-19)$$

with  $v_t$  defined as ( $v_{t2}$  and  $v_{t3}$ ) . For the values used in these calculations, the third term on the right hand side can be neglected, allowing modelling of the discharge as a two-ion discharge with a charge transfer frequency equal to the total of the two individual charge transfer frequencies.

Although information on the diffusion coefficient for  $\text{HN}_2^+$  ions in  $\text{N}_2$  may exist, we were unable to find any. However,  $\text{HN}_2^+$  has approximately the same mass as  $\text{N}_2^+$  . If both species could undergo resonant charge transfer collisions with the background gas, we would expect them to have similar diffusion coefficients.  $\text{HN}_2^+$  does not undergo any such collisions. Therefore, we estimated its diffusion coefficient as  $200 \text{ cm}^2/\text{s}$ , approximately 4 times larger than that of  $\text{N}_2^+$  . For the range of temperatures we found, large differences in the diffusion coefficient can be accommodated with small differences in  $kT_e$  . The four-to-one difference in diffusion coefficients between  $\text{HN}_2^+$  and  $\text{N}_2^+$  will produce noticeable differences in  $kT_e$ .. However, small errors in  $D_2$  will not lead to large errors in  $kT_e$  .

If we were trying to perform an exact simulation of the discharge, such estimates would be inadequate. However, our purpose is to investigate the effect of the introduction of a small amount of highly mobile ions on  $kT_e$  and the electron flux. For this reason, the exact values of  $kT_e$  and the flux are not as significant as how those values change under  $\text{H}_2$  contamination.

The input values are summarized below, all for 1 Torr pressure and 1 eV electron temperature:

1. Diffusion coefficients were  $51.7$  and  $200 \text{ cm}^2/\text{s}$  for  $\text{N}_2^+$  and  $\text{HN}_2^+$ , respectively.

2. Ionization potential for  $N_2$  was 15.8 V. There is no direct ionization producing  $HN_2^+$ , so its value was irrelevant. An ionization potential of 15.8 V was supplied to the algorithm, simply because the algorithm required a number.

3. Ionization rate for  $N_2^+$  was calculated using a value of the initial slope of the cross-section of  $7.798 \times 10^{-17} \text{ cm}^2/\text{eV}$ , as reported by Kieffer (Kieffer, 1973: 82). With no direct ionization allowed, the ionization cross-section for  $HN_2^+$  is actually zero. However, a nonzero value was required by the algorithm; the value used was some 30 orders of magnitude lower than the  $N_2^+$  value, and therefore effectively zero.

4. The charge transfer rate constant was  $2 \times 10^{-9} \text{ cm}^3/\text{s}$ .

We calculated electron temperatures and wall fluxes for 10%  $H_2$ , 1%  $H_2$ , 0.1%  $H_2$ , 0.01%  $H_2$ , and 0%  $H_2$ , all at 2 T pressure and 80 mA discharge current. There is no special significance to the choice of pressure and discharge current, except that it allows easy comparison to Schmidt and to the previous calculations. In Figure 6-4 we show the results for the electron temperatures.

We see that the admixture of even slight amounts of  $H_2$  can increase the electron temperature. The addition of only 0.1%  $H_2$  produces a value for  $kT_e$  of 1.47 eV. This value is comparable to Schmidt's results, which were in the range of 1.4-1.5 eV. The change from 0 to 0.1% hydrogen represents a 13% increase in  $kT_e$ , corresponding to ionization increasing by over 4 times. This result is readily explainable.  $HN_2^+$  has a larger diffusion coefficient than  $N_2^+$ . As a result, adding hydrogen to the plasma changes the ratio of net source to diffusion. However, as we will discuss in more detail later in this chapter, the boundary conditions fix a particular ratio of net source to diffusion, analogous to the single-ion Schottky condition  $(\lambda_0 R)^2 = \nu/D$ . Since the increase of ionization frequency with electron

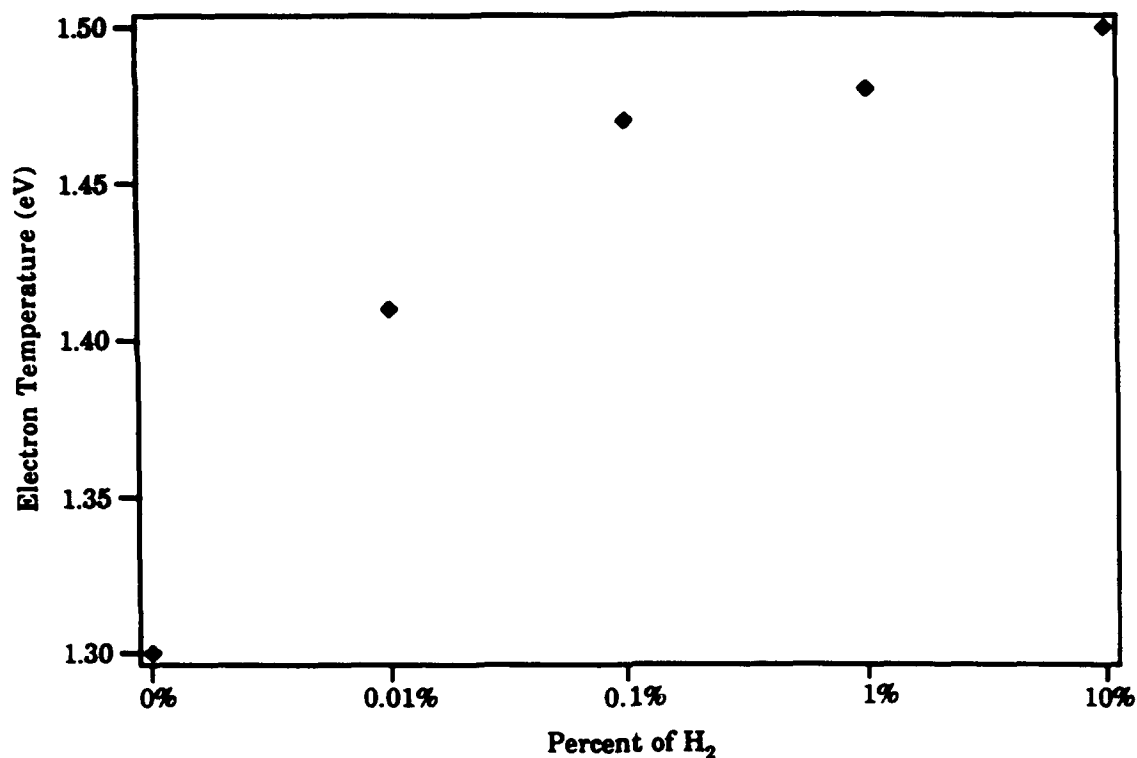


Figure 6-4. Effect on Temperature of Small Amounts of H<sub>2</sub> in N<sub>2</sub>

temperature is stronger than any other  $kT_e$  dependence in the net source or diffusion coefficient, an increase in the electron temperature will increase the ratio of net source to diffusion, counteracting the effect of the increased diffusion losses.

We note a clear saturation effect on the temperatures. The temperature is approaching the value that would result if the only ions present were  $\text{HN}_2^+$ . This value is slightly above 1.5 eV. Similar effects were seen in the helium-neon temperature calculations presented earlier. There is a significant difference. In the helium-neon example, the presence of one gas had no effect on the net source of the ions of the other gas. Here, charge transfer not only provides a source  $\text{HN}_2^+$ , but also is a loss for  $\text{N}_2^+$ . This causes a much quicker change in the amount of each ion species as



the gas mixture changes. The result is that at only a 1% hydrogen gas fraction,  $\text{HN}_2^+$  represents almost 99% of the ions in the discharge. As a result, the transition from a temperature characteristic of  $\text{N}_2^+$  to a temperature characteristic of  $\text{HN}_2^+$  is more abrupt.

Our results show that admixtures of even small amounts of  $\text{H}_2$  can have a significant effect on the electron temperatures and partially explain disparities in  $kT_e$  between the original calculations in pure  $\text{N}_2$  and Schmidt's results. The presence of  $\text{NH}_2^+$  in the discharge has a significant effect on the wall fluxes as well. Figure 6-5 shows the particle fluxes to the wall, again for increasing percentages of  $\text{H}_2$ . These are complementary results from the same series of calculations that produced Figure 6-4.

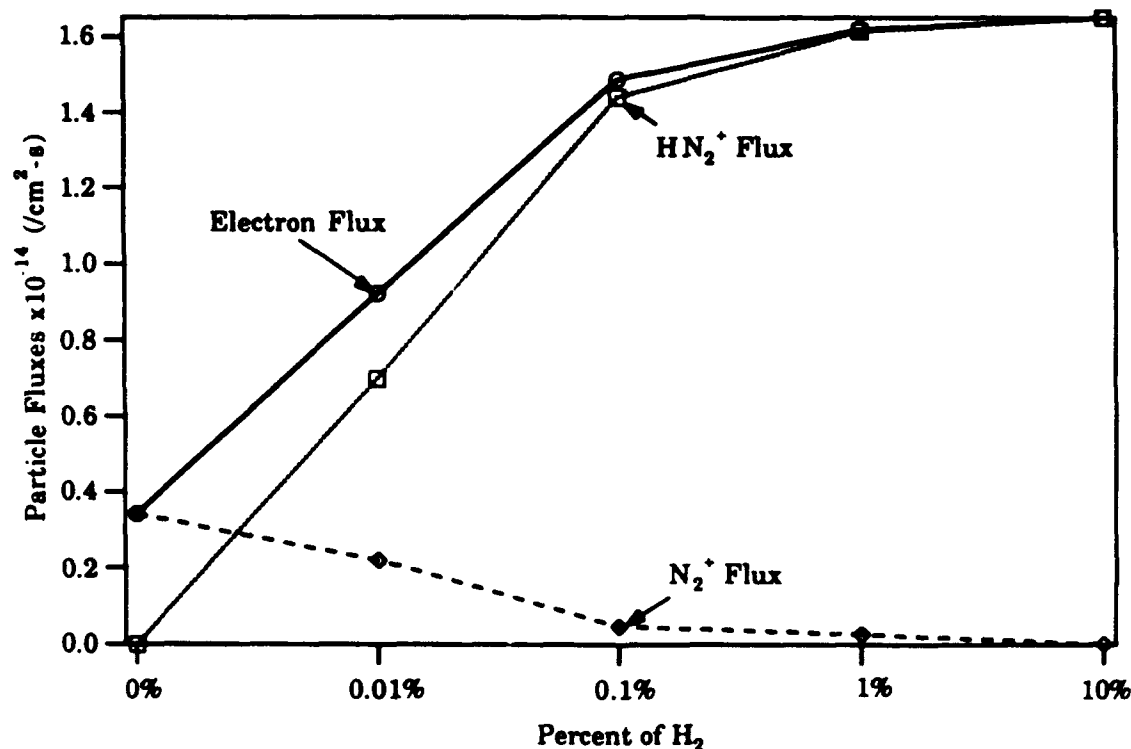


Figure 6-5. Influence of Hydrogen on Particle Fluxes

Once more, we see a dramatic rise with the inclusion of even small amounts of  $H_2$ . This time, a 0.1% addition of  $H_2$  increases the flux by a factor of 4.35, equal to the change in ionization. As point of reference, Schmidt's result was approximately  $9 \times 10^{13}/\text{cm}^2\text{-s}$ , which is achieved by addition of less than 0.01% hydrogen gas. Again, the importance of these results lies not in the exact values, but in the fact that small admixtures of  $H_2$  can produce significant increases.

As did the temperature, the dependence of the flux on  $H_2$  percentage shows a clear saturation effect. Figure 6-6 shows how the particle fluxes at the wall shift from  $N_2^+$  to  $HN_2^+$  by depicting the ratio of each flux to the electron flux.

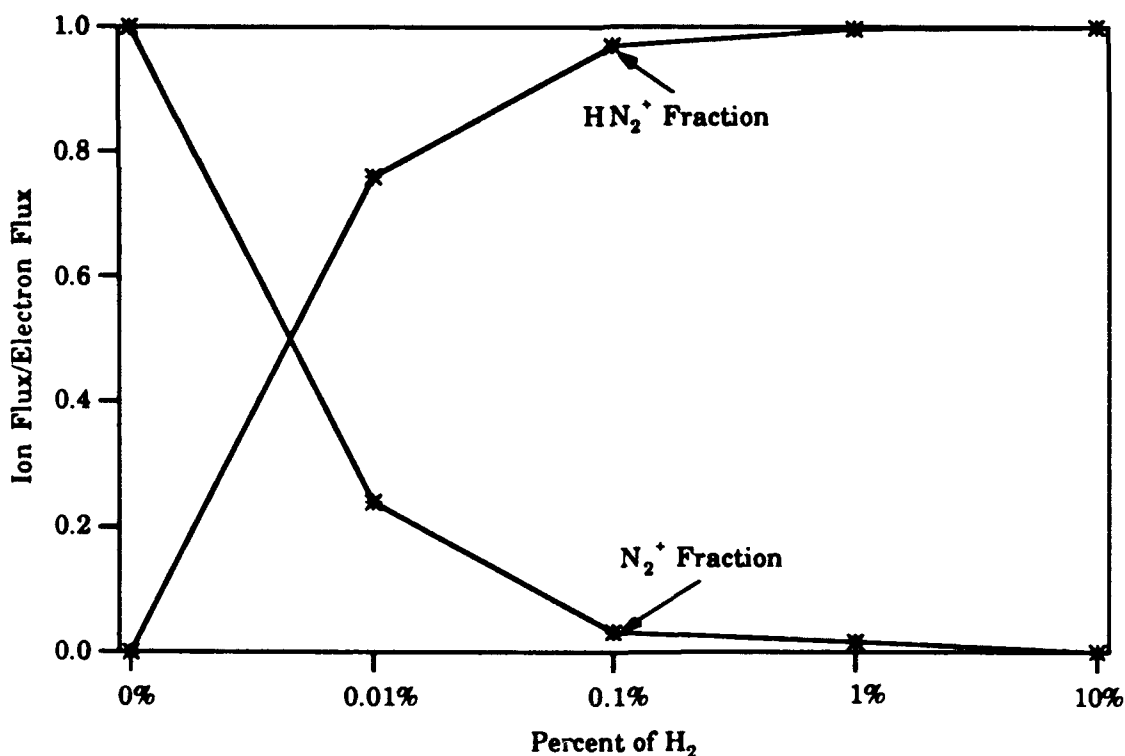


Figure 6-6. Comparison of  $H_2^+$  and  $N_2^+$  Fluxes with Changing Gas Mix

For our estimated values, it appears that saturation occurred for a less than 10%  $H_2$  fraction. In fact, for a 10%  $H_2$  mixture, the discharge is completely dominated by  $HN_2^+$ . The  $HN_2^+$  number density is 750 times that of  $N_2^+$ , and the  $H_2^+$  flux is 3000 times larger than the  $N_2^+$  flux.

This dominance is the result of charge transfer. At these fractions of  $H_2$ , the charge transfer rate from  $N_2^+$  to  $HN_2^+$  is so high that the nitrogen ions essentially disappear from the discharge. For instance, at 1%  $H_2$  present in the discharge, we found that the charge transfer rate was  $5.152 \times 10^{14}/\text{cm}^3\text{-s}$ , while the  $N_2^+$  source term was  $5.154 \times 10^{14}/\text{cm}^3\text{-s}$ . In effect, all the ionization that occurs produces  $HN_2^+$ .

We should not place too much reliance on the exact point where this domination occurs, nor on the values we calculated, because of the estimates of the kinetic and plasma parameters we had to use. The significance of this analysis is that it clearly shows that the presence of a minority species can cause significant changes in the nature of the discharge, far out of proportion to the percentage of the minority ion's parent gas.

In summary, we compared calculated results from two very simple models to Schmidt's experimental results. The  $N_2^+ - N_4^+$  model was substantially in agreement with Schmidt's results for the pressure and current dependence of the electron fluxes at the walls. It also agreed with Schmidt's results for the pressure dependence of the electron temperature. Schmidt's temperature data had too much scatter to compare the dependence between temperature and longitudinal current for the two models. A possible discrepancy between the calculations and the measurements can

be ascribed to varying amounts of hydrogen ions in the plasma. The only significant disagreement between the two sets of results was in the overall magnitudes of the electron temperatures and fluxes. However, the second of the two models, which used charge transfer from  $N_2^+$  to  $HN_2^+$  clearly demonstrated that the presence of minority gases can cause changes sufficient to resolve the differences between the first model and the experimental results. In addition, the simulation was able to provide information about the relative values for the  $N_2^+$  and  $N_4^+$  fluxes and densities that Schmidt was unable to produce.

*Summary of Verification Results.* We have compared the results of this new ambipolar diffusion model to a number of experimental and theoretical findings. We found exact agreement with the results that Wunderer obtained for a very complex system, even though the two models were based on substantially different assumptions. We verified Young's analytic model of electron temperature for the restricted regime where that model were valid, producing results consistent with Labuda and Gordon's experimental results in that regime. Finally, we found reasonable agreement between our simple simulations of Schmidt's very complicated discharge, and were able to use the capabilities of model to demonstrate plausible explanations for those discrepancies that did exist.

### *Investigation of Generic Plasma Systems*

Having established the validity of the new model, we now turn to using it to explore physical systems. The systems we will examine can be divided into two regimes; those driven by external sources, which are not affected

by the plasma itself, and those driven by volume ionization caused by the electrons in the plasma. For simplicity, we use cylindrical geometry in all cases; adding planar geometry would have given different spatial profiles for the densities and fluxes, but would have added no significant new physical insight. All the systems involved electrons plus two ion species.

We chose several different phenomena to include in the simulations:

1. We included recombination of the second species. Recombination is an important process in many gases. In principle, it can occur in any discharge, if the charged particle number densities are high enough. In practice, it is one of the more common nonlinear processes. It is also easier to describe than other nonlinear processes such as multi-step ionization, since it does not require keeping track of any neutral species.
2. We also included nonresonant charge transfer. Unlike recombination, it is not a possibility in every discharge. However, as we saw in the comparison with Schmidt using the  $N_2^+-N_4^+$  system, there are situations in some discharges where it can become significant.

We deliberately chose to neglect some phenomena that might be significant in a real plasma. In the two examples involving external sources volume ionization was neglected, and the electron temperature was assumed fixed, independent of the external source conditions. In the charge transfer example, recombination was neglected. In a real discharge, these assumptions might not be valid. However, including them in these investigations would have obscured the effects of the processes being investigated. This neglect does not mean that the model could not have included these effects. It only means that in the present examples the choice was made not to do so.

*External Sources.* First, we examine the cases that rely on an external source of ionization. We discussed plausible mechanisms for external

ionization in Chapter V. Those same mechanisms are applicable here: photo-ionization, electron beam, and so forth. For these studies, we assumed uniform ionization of levels appropriate to intense electron beams. These source terms correspond to the ionization produced by kilovolt-range electrons at current densities ranging from microamps to a few tens of milliamps per square centimeter, with ionization efficiencies per electron on the order of 1 ionization/cm-T (von Engel, 1965:63). For example, a  $10 \text{ mA/cm}^2$  beam corresponds to  $6.25 \times 10^{16}$  electrons/cm<sup>2</sup>/s. At 1 ionization per cm of flight, this produces a source of  $6.25 \times 10^{16}$  electrons/cm<sup>3</sup>-s. We included recombination as one example, and charge transfer as another example.

With no volume ionization sources, the eigencondition involving the electron temperature is no longer appropriate. In an actual plasma, the temperature would be determined by the energy balance between the energy input into the system and the energy losses. Describing that process correctly involves the third moment of the Boltzmann equation. Since this investigation only includes the first two moments of the Boltzmann equation, energy balance cannot be addressed. Instead,  $kT_e$  becomes an input parameter, instead of being a result of the calculation as it was in the comparisons to Young and to Schmidt. A value of 1.0 eV was used for all the calculations. The on-axis electron number density  $N_{e0}$  is now determined from the calculations.

*External Source plus Recombination.* We examined at a system that involved recombination for the second ionic species,  $N_2$ . The diffusion and continuity equations for the system are

$$\begin{aligned}
\frac{\partial N_i}{\partial r} &= -\frac{\Gamma_i}{D_i} + \frac{N_i}{N_e} \frac{kT_i \sum_j \frac{\Gamma_j}{D_j}}{(kT_e + kT_i)} \\
\frac{\partial N_e}{\partial r} &= -\frac{kT_i \sum_j \frac{\Gamma_j}{D_j}}{kT_e + kT_i} \\
\frac{\partial \Gamma_1}{\partial r} &= S_1(r) - \frac{\Gamma_1}{r} \\
\frac{\partial \Gamma_2}{\partial r} &= S_2(r) - \alpha N_2 N_e - \frac{\Gamma_2}{r} \\
\frac{\partial \Gamma_e}{\partial r} &= S_e(r) - \alpha N_2 N_e - \frac{\Gamma_e}{r}
\end{aligned} \tag{6-20}$$

The pressure was varied between 0.1 and 2.0 T, a range which gives a reasonable variation and still guarantees that the plasmas investigated satisfied the basic assumptions of ambipolar diffusion. Electron temperature  $kT_e$  was 1.0 eV, and  $kT_i$  was 0.02585 eV. The tube radius was chosen to be 5.0 cm; there was no significance to the value, except to insure that the diameter of the discharge was more than large enough to ensure that the model remained valid.

The primary parameter of interest was the recombination rate coefficient  $\alpha$ , which ranged between 0 and  $10^{-5} \text{ cm}^3/\text{s}$ . The upper limit is somewhat higher than what we would expect in real gases (*e. g.*, von Engel, 1965:158, 160). However, such high values allowed examination of extremes of recombination which emphasized effects that otherwise might not be as readily observable. The external source term for both species ranged from  $10^{14}$  to  $10^{17}/\text{cm}^3\text{-s}$  at a pressure of 1 T, varying linearly

with pressure. The variation in external source term was used to keep the number density of the two species roughly comparable as recombination varied. Although this variation would not occur in a realistic gas, it was useful in that it reduced the tendency that would otherwise occur for one species to completely dominate the discharge at high recombination strengths. Calculations were also performed with the sources fixed but with recombination varying in order to verify the effects of only recombination changing.

Parameters for the individual species (source terms,  $D$ ,  $T_e$ , and  $T_i$ ) were chosen to approximate a 10/90% helium-neon mixture. However, there was no attempt to match that system exactly. The diffusion coefficient for species 1, which approximated helium, was chosen to be  $300 \text{ cm}^2/\text{s}$ , with species 2, which approximated neon, at  $100 \text{ cm}^2/\text{s}$ . In all cases the diffusion coefficients were to assumed to be constant with respect to changes in recombination rate.

For that assumption to be valid, the momentum transfer collision frequency  $\nu_c$  must be greater than the recombination frequency for each affected species. For ions, the recombination frequency is given by  $\alpha N_e$ ; the corresponding electron recombination frequency is  $\alpha N_2$ . The diffusion coefficient and average particle energy determine  $\nu_c$ . For the ions, the pressure range, diffusion coefficients, and ion temperature given above produced a value in excess of  $10^8 \text{ Hz}$  for  $\nu_c$ , while the recombination frequency was less than  $10^7 \text{ Hz}$ . The electron collision frequency can be estimated using a value for the diffusion coefficient  $D_e$  of  $10^6 \text{ cm}^2/\text{s}$  at one



Torr (von Engel, 1965: 141). This produces a value for  $v_c$  greater than  $10^9$  Hz, while  $\alpha N_2$  was less than  $3 \times 10^6$  Hz in the worst case. Even if  $D_e$  is two orders of magnitude higher,  $v_c$  is still greater than  $\alpha N_2$ . Therefore, we conclude that we are justified in ignoring the effects of the varying recombination on the diffusion coefficients.

*High-Recombination Example.* Figures 6-7 through 6-9 show the results of one calculation. The input values and pertinent parameters were:

1.  $D_1 = 150$  and  $D_2 = 50 \text{ cm}^2/\text{s}$ , adjusted for pressure.
2.  $S_1 = 2 \times 10^{15}$  and  $S_2 = 2 \times 10^{19} /(\text{cm}^3\text{-s})$ , also adjusted for pressure.
3.  $\alpha = 10^{-6} \text{ cm}^3/\text{s}$ .
4. Pressure = 2.0 Torr.
5. Debye length on axis  $\approx 2.5 \times 10^{-4} \text{ cm}$ .
6. Deviation from proportionality:  $\beta_1 = 0.0102$  and  $\beta_2 = 1.0099$ .

The value for  $\beta_1$  was the smallest of any of the cases examined, and therefore represents the largest deviation of species 1 from proportionality of any case examined. On the other hand, the value for  $\beta_2$  represents a value very close to what one would expect for a proportional discharge, even though the spatial dependence of  $N_2$  is indeed far from proportional. We will discuss this point shortly.

Figure 6-7 shows the particle densities:

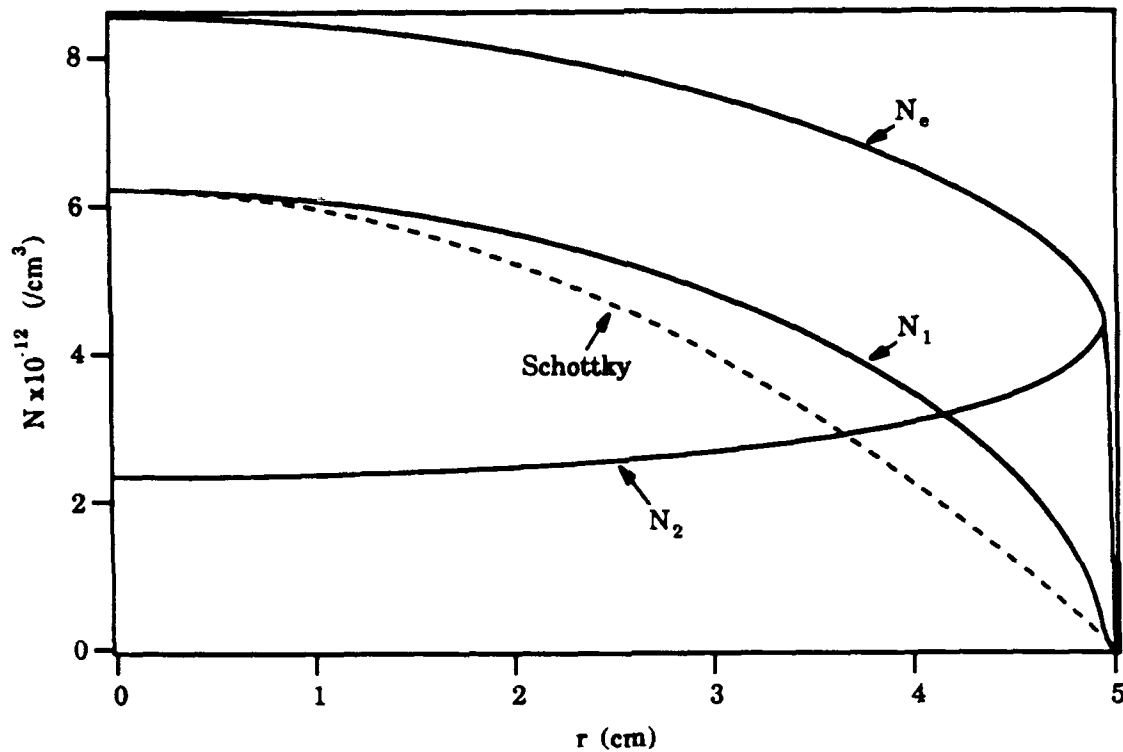


Figure 6-7. Particle Densities for High Recombination

The "Schottky" profile, included for reference in Figure 6-7, is the parabolic distribution that would result if only external sources were present, with those sources adjusted to cause the two curves to match at  $r = 0$ . This highlights the spatial profile difference between the "Schottky" profile and the profile that  $N_1$  assumes with recombination present for  $N_2$ . In addition to the change in spatial profile,  $N_1$  actually has a higher overall density than it would have with no recombination. For the external source terms listed on the previous page, but with no recombination, the on-axis value for  $N_1$  would have been approximately 3 times smaller than that shown in Figure 6-7. At first, this seems contradictory. However, recall the momentum equation for  $N_1$ :  $\partial N_1 / \partial r = -\Gamma_1 / D_1 + \epsilon N_1 / N_e (\Gamma_1 / D_1 + \Gamma_2 / D_2) / (1 + \epsilon)$ . The presence of recombination reduces  $\Gamma_2$ . This allows the gradient of  $N_1$

to be more negative. As a result,  $N_1$  increases more rapidly as  $r$  decreases from the edge of the plasma. As a result, its on-axis value is higher. At the same time,  $N_e$  is getting smaller as well. Eventually, the effect of  $N_e$ 's decrease overcomes the effect of  $\Gamma_2$ 's decrease, and the on-axis value of  $N_1$  starts to decrease again.

It is possible to form an estimate of the on-axis ratio  $N_2/N_e$  by noting that the losses for  $N_2$  are dominated by volume processes. In that case, the divergence of  $\Gamma_2$  is zero, producing  $S_2 = \alpha N_e N_2$ . The value of  $N_2$  produced from this express is exactly the same as that volume calculations.

The solutions presented in Figures 6-6 are obviously not equivalent to the proportional solutions obtained previously for the CX case (which had no recombination but which was otherwise analogous). We note significant changes in the functional dependence of the number densities. In particular, the spatial dependence of  $N_2$  is clearly not the same as that of  $N_e$ . The number density for species 2 is no longer monotonically decreasing, but increases throughout most of the discharge, then decreases near the edge.

Let us consider why the recombination-less CX case had the behavior it did. In the CX case, the source term is external. In the steady state there must be a sufficient loss to offset that source. If we examine the steady-state continuity equation for electrons we find that the loss associated with the divergence of the flux had two contributions: the diffusive fluxes, defined by  $\Gamma = -D\nabla N$ , and the field-driven fluxes, defined by the expression  $\Gamma = \mu N E$ . Electrons respond much more readily to the field than the ions. Therefore, the equality of electron loss and ion loss that is implicit in the

ambipolar assumption is achieved by reducing electron flux much more than by increasing ion flux. Thus, the ambipolar electric field is determined by the need to reduce the electron flux enough to match the overall ion flux. However, there must still be a net flow of electrons outward at every point. Since the electric field is driving electrons inward, diffusion must drive them outward. Therefore, the slope of the electron density is negative. Since we had proportional source terms and solutions for the CX case, the ion densities also have a negative slope.

A different condition pertains for the present case. The electric field is still reducing the electron flux and increasing the ion flux. But here, recombination is so large (essentially equal to the source) for species 2 that the field-induced drift of species 2 from the center of the discharge to the edge causes larger losses than the external source term can compensate for. As a result, the diffusion-induced current must oppose the field-induced drift current for that species. The result is  $N_2$  increasing towards the edge of the plasma. In fact, if recombination increases while all other parameters remain constant, the on-axis losses can become so large as to force flow radially inward instead of outward. Such a flow requires an increasing particle density, not decreasing. It is this effect that we are starting to see here.

We can also show the requirement for increasing  $N_2$  from the diffusion equation for  $N_2$ .  $N_2$  increasing at  $r = 0$  requires  $\partial^2 N_2 / \partial r^2 \geq 0$ . The continuity and momentum equations for  $N_2$  can be combined to form an expression for  $\partial^2 N_2 / \partial r^2$ . Evaluating that expression with the small-e-flux approximation at the origin and taking advantage of both  $\Gamma(0) = 0$  and  $\partial N(0) / \partial r = 0$

produces an expression involving the gas parameters and number densities, all evaluated at  $r = 0$  :

$$\frac{\epsilon N_e + N_1}{N_2} < \frac{\frac{S_1}{D_1}}{\frac{S_2}{D_2} - \frac{\alpha}{D_2} N_2 N_e} \quad (6-21)$$

This form can be used to draw some immediate conclusions. First, note that the right hand side is the ratio of the dimensionless net source terms for the two ion species. In the limit as  $\alpha$  goes to zero, this approaches  $(S_1/D_2)/(S_2/D_2)$ , which equals  $N_1/N_2$  for the nonrecombining CV case. However, the left hand side is always greater than  $N_1/N_2$  , implying that Equation 6-21 cannot be satisfied for  $\alpha = 0$ . Indeed, the analytic solutions in the CV case showed  $N_2$  decreasing near the axis. Second, allowing  $\alpha$  to increase causes the right hand side to increase. At the same time,  $N_2$  and  $N_e$  decrease, changing the left hand side as well. The calculations indicate that for large enough values of  $\alpha$  it is possible for the inequality to be satisfied, thus producing an increasing  $N_2$  .

It would be useful to simplify Equation 6-21. From Chapter V, for a discharge with no recombination (which is proportional) the conditions for proportionality can be used to find the ratio  $N_2/N_e$  at any point in the discharge:

$$\frac{N_2}{N_e} = \frac{\frac{S_2}{D_2}}{\left(\frac{S_1}{D_1} + \frac{S_2}{D_2}\right)} \quad (6-22)$$

Since adding recombination to species 2 can only reduce  $N_2/N_e$ , this value is an upper bound on  $N_2/N_e$ . This allows us to determine a necessary condition for  $N_2$  to have a positive curvature at  $r = 0$ :

$$\frac{S_2 \epsilon}{\alpha N_2 (N_1(1+\epsilon) - N_2)} < 1 \quad (6-21)$$

In Figure 6-8 we show the ratio  $S_2 \epsilon / \alpha N_2 (N_1(1+\epsilon) - N_2)$  resulting from a series of solutions over a range of recombination coefficients.

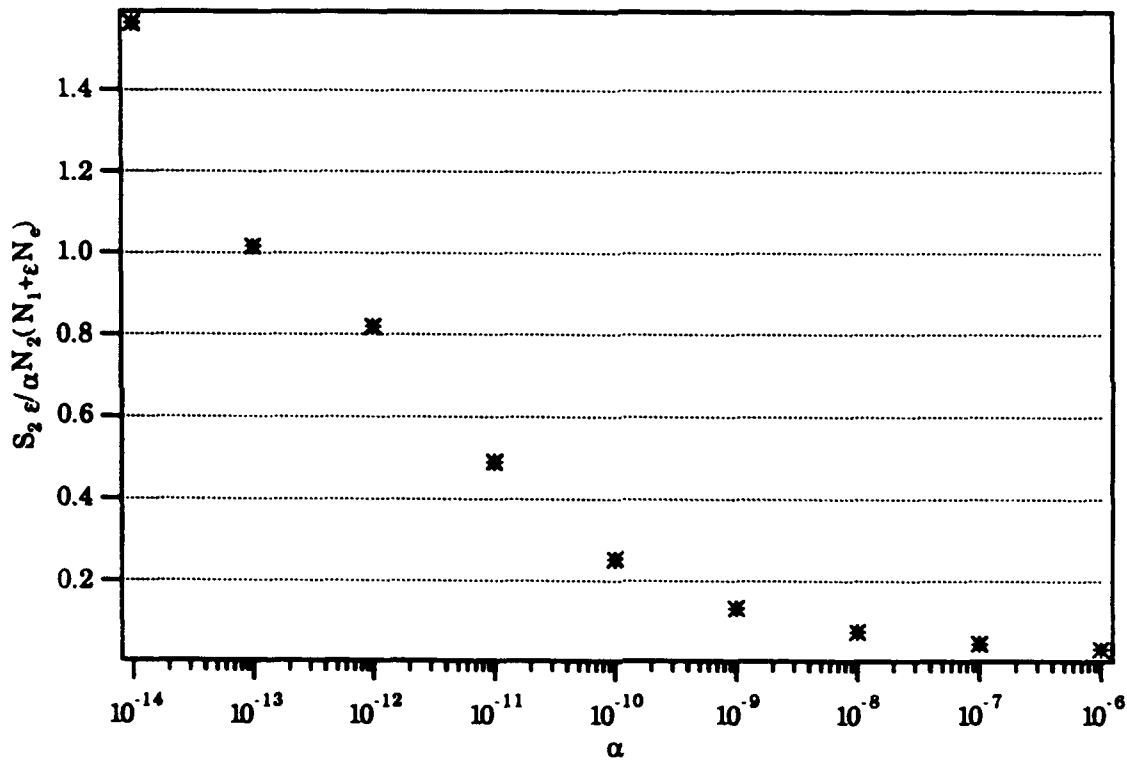


Figure 6-8. Effect of Increasing Recombination on On-Axis Curvature

As predicted in Equation 6-23, only the first two solutions shown ( $\alpha = 10^{-14}$  and  $10^{-13}$  cm<sup>3</sup>/s, respectively) demonstrated a negative curvature for  $N_2(0)$ . (We show the particle density profiles for these systems in Figure 6-10. Although that figure has relevance to our discussion here, some of its

features are more readily explained after we have examined the fluxes. Therefore, we will not introduce it here.)

Let us now return to a discussion of other features of Figure 6-7. Note that the dominant ion species in the discharge changes, from  $N_1$ , on axis, to  $N_2$ , near the edge of the plasma. This is a direct consequence of the strongly rising  $N_2$  and the steadily decreasing  $N_1$  and is the result of a loss term that does not have the same spatial dependence as the source terms. In this case the loss is proportional to  $N^2$  with the sources proportional to  $N^0$ .

This change in the dominant species can appear in many situations. In order for it to occur, the two ion species must have net source terms that differ qualitatively in their spatial dependence. A typical example is where other than linear source dependencies on number density (that is, none and quadratic dependence) give rise to differing spatial profiles. The latter situation can occur if two conditions hold:

1. One species must have a loss that is a function of number density, while the other has a gain of some kind (or at least much less corresponding loss). In the examples above, recombination or charge transfer served this function.
2. There must be other source terms which do not counteract effects of the loss term above. They could be independent of the electron number density, as in external ionization, or at least depend differently on  $N$  than the loss term. An external source term or volume ionization term can serve this function.

Let us now examine in detail how this switch in species dominance can occur. Recall the general continuity and momentum equations for the ions:

$$\frac{\partial \Gamma_i}{\partial r} = S_i - \frac{\Gamma_i}{r}$$

(6-24)

$$\frac{\partial N_i}{\partial r} = -\frac{\Gamma_i}{D_i} + \frac{N_i}{N_e} \frac{kT_i \sum_j \frac{\Gamma_j}{D_j}}{(kT_e + kT_i)}$$

Assume that the plasma conditions are such that the net source for species 1 is positive and slowly varying at the center of the plasma while the source for species 2 is approximately zero (including the  $\Gamma/r$  term). As a result species 1 has a flux that increases from zero while the flux for species 2 remains at or near zero. Now consider the form the momentum equation takes for species 2 for those regions where  $\Gamma_2 \approx 0$ :

$$\frac{\partial N_2}{\partial r} = \frac{N_2}{N_e} \frac{kT_i \Gamma_1}{D_1} \quad (6-25)$$

Every term in the right hand side of Equation 6-25 is positive, implying  $\partial N_2 / \partial r$  is also greater than zero. Therefore,  $N_2$  increases from the center of the plasma toward the edge. However, due to the boundary condition, it must eventually reverse and drop to zero near the boundary. This implies that  $\partial N_2 / \partial r$  will eventually become negative. The only possible negative term in the complete momentum equation is a non-zero  $\Gamma_2$ . Therefore,  $\Gamma_2$  cannot remain near zero. At some point it must rise. Furthermore, the closer to the edge of the discharge that point is, the more quickly  $N_2$  must drop, and the larger  $\Gamma_2$  must be. This sudden rise in  $\Gamma_2$  will be shown shortly.



In contrast to the changes of  $N_2$ ,  $N_1$  will decrease smoothly to zero. If  $N_2(0)$  is close to the value of  $N_1$ , but lower, and if the changes in  $N_2$  are large enough, the result can be the change of the dominant ion species shown in Figure 6-7.

Next, let us look at the fluxes, shown in Figure 6-9, for the same case for which we depicted the particle densities in Figure 6-7. A limited vertical axis allows clear depiction of the details away from the edge. At the edge, we have values of  $5.0 \times 10^{15}$ ,  $5.04 \times 10^{17}$ , and  $5.09 \times 10^{17}$  /cm<sup>2</sup>-s for  $\Gamma_1$ ,  $\Gamma_2$ , and  $\Gamma_e$ , respectively.

We see differences from the proportional cases discussed in Chapter V. There, we had fluxes that were linear functions of  $r$ ; here,  $\Gamma_e$  and  $\Gamma_2$  are decidedly nonlinear in their overall behavior. In addition, the recombination-less CX case gives values at the edge of the discharge of  $5 \times 10^{15}$  and  $5 \times 10^{19}$  cm<sup>2</sup>/s for  $\Gamma_1$  and  $\Gamma_2$ , respectively. The present calculation gives the same value for  $\Gamma_1$ ; from Equation 6-20, it is unaffected by the recombination. However,  $\Gamma_2$  at the edge of the plasma is approximately 1% of the value for the same source terms without recombination, and is even less within the discharge. This is not surprising; for this example, the losses due to recombination (calculated on axis) are equal to  $S_2$  (within 4 significant digits). Recall the continuity equation for species 2:

$$\nabla \cdot \Gamma_2 = S_2 - \alpha N_e N_2 \quad (6-26)$$

If  $S_2 = \alpha N_1 N_2$ , then  $\nabla \cdot \Gamma_2 = 0$ . If we evaluate  $\nabla \cdot \Gamma$  at  $r = 0$  using L'Hospitale's rule, we find that  $\Gamma$  is given by  $\Gamma = (S_2 - \alpha N_1 N_2)r/2$ . With no

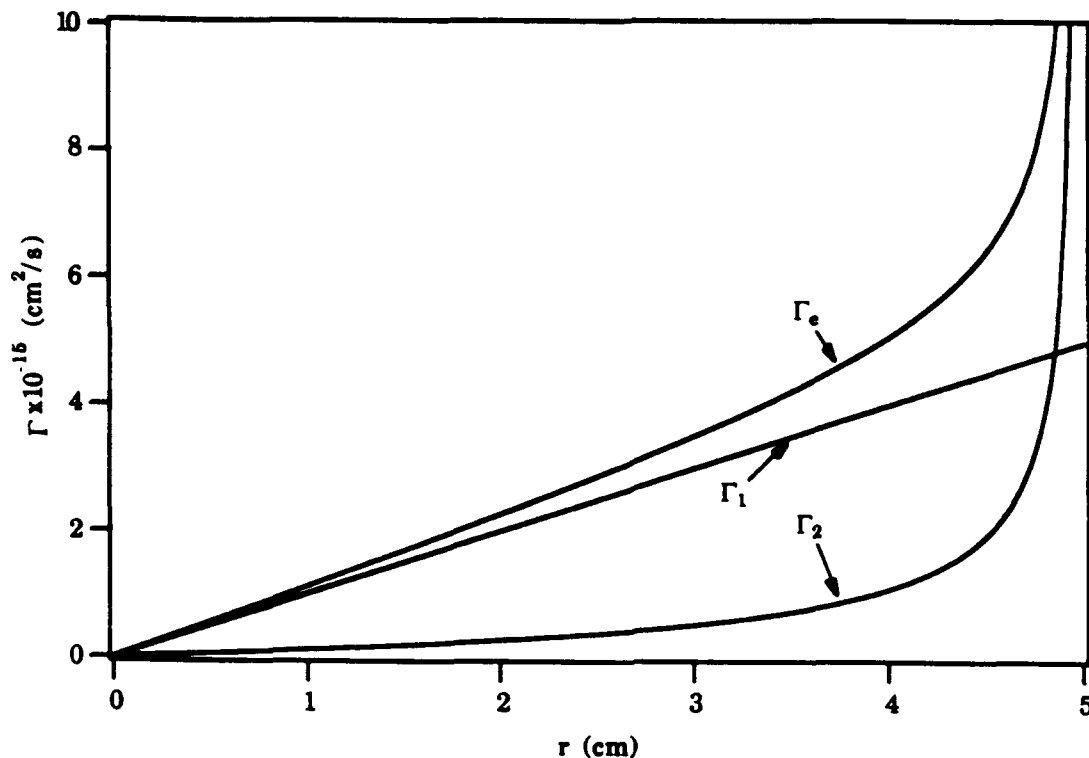


Figure 6-9. Fluxes with External Sources and High Recombination

recombination, we have  $\Gamma \approx S_2 r/2$ , which is a much larger value. Both approximations are valid only in the immediate vicinity of the axis, but the behavior they exhibit continues throughout the region where  $S_2 \approx \alpha N_1 N_2$ . At the edge of the discharge, the rapid drop in  $N_2$  reduces the recombination which no longer offsets  $S_2$  and thereby produces a very large increase in  $\Gamma_2$ . Even so,  $\Gamma_2$  is still much less than it would have been without recombination.

In Figure 6-10 we show the effect of increasing recombination clearly by presenting a series of solutions with increasing recombination rates. These are exactly the same solutions presented in Figure 6-8. We should point out that the negative curvature of  $N_2$  discussed in conjunction with

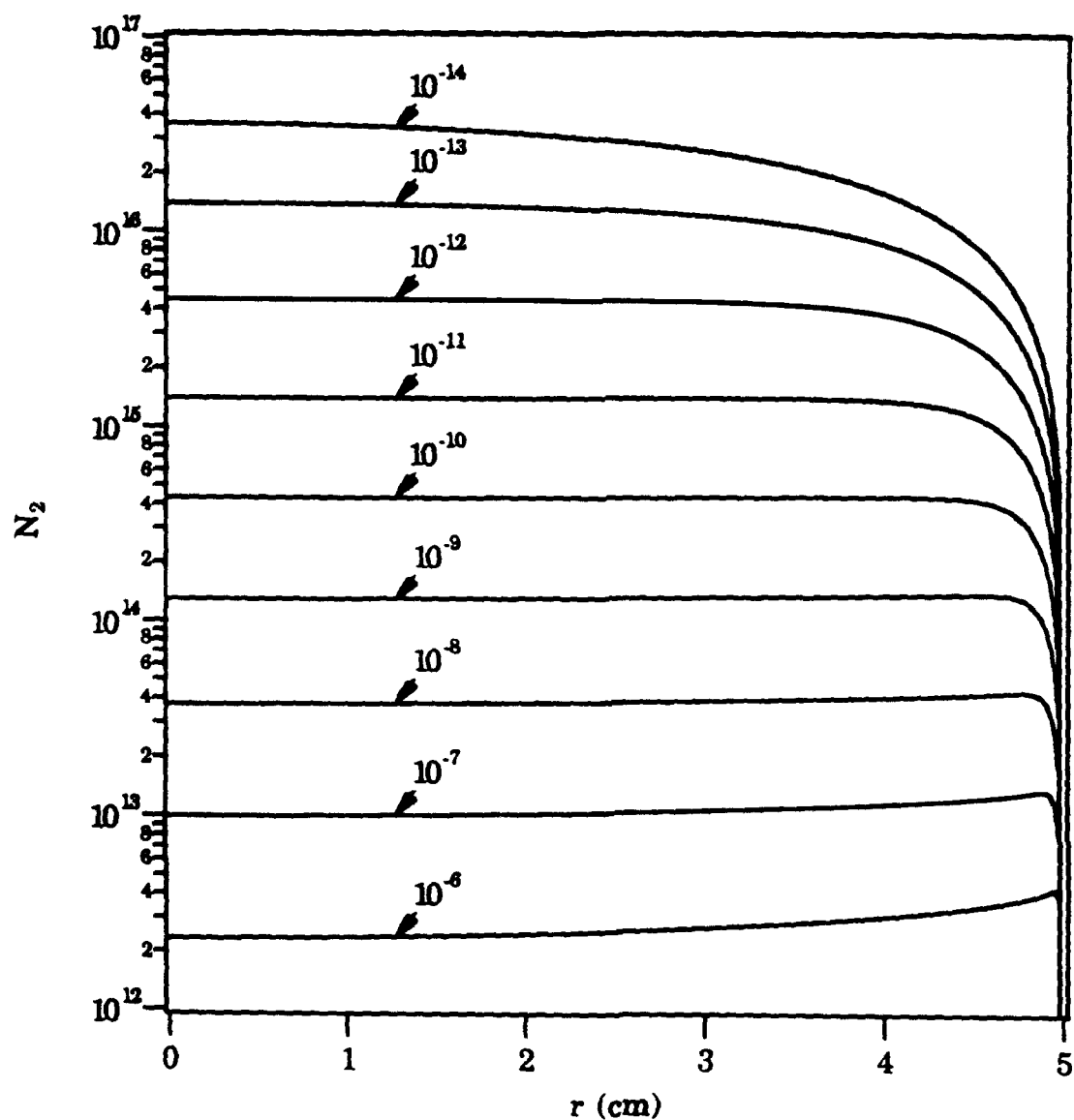


Figure 6-10. Radial Profiles of Recombining Ions for Recombination Rates Ranging from  $10^{-6}$  to  $10^{-14}$   $\text{cm}^3/\text{s}$  in a 2-Torr Discharge

Figure 6-8 is difficult to distinguish in Figure 6-10. However, careful examination of the data reveals that the results are indeed consistent with Equation 6-23.

All the curves differ only in their recombination rate, which is one order of magnitude smaller for each curve up the graph. The lowest curve,

which has the largest recombination rate, is the same system as that presented in Figure 6-7.

Here we can clearly see the effect of the recombination; as the recombination increases, the overall density drops, the profile becomes flatter, and eventually the curvature in the center reverses. Note that the reduction in  $N_2$  varies as  $\alpha^{1/2}$ : as  $\alpha$  changes by 100,  $N_2$  changes by approximately 10. A simple explanation is that recombination goes as  $N^2$ ; a 10-fold change in the number densities compensates for a 100-fold change in  $\alpha$ .

In Figure 6-11 we show the ratio of the field with no recombination ( $E_0$ ) to the calculated electric field ( $E$ ) for the case just examined. In both cases we evaluate the field from Equation 6-1.

Note that there is a sizeable difference between the two fields, with  $E_0$  greater than  $E$  throughout the discharge. This is to be expected. As we discussed on several occasions, both in this chapter and previously, the main effect of the ambipolar field is to counteract the diffusion term in the electron flux, not the ion flux. With heavy recombination, the interior of the discharge is dominated by volume losses, not diffusion. With electron diffusion less important, the need for a field to counteract the diffusive flux of the electrons is lessened. Near the edge of the discharge, where recombination is becoming less of a factor, this situation changes. The discharge is no longer dominated by recombination, and the field must increase to reduce the electron flux. Indeed, this behavior is exactly what the graph above depicts. At the edge, both fields approach infinity, but their ratio approaches one. However, at the edge of the discharge, the ambipolar model is no longer valid, and so the value of the field has little meaning.

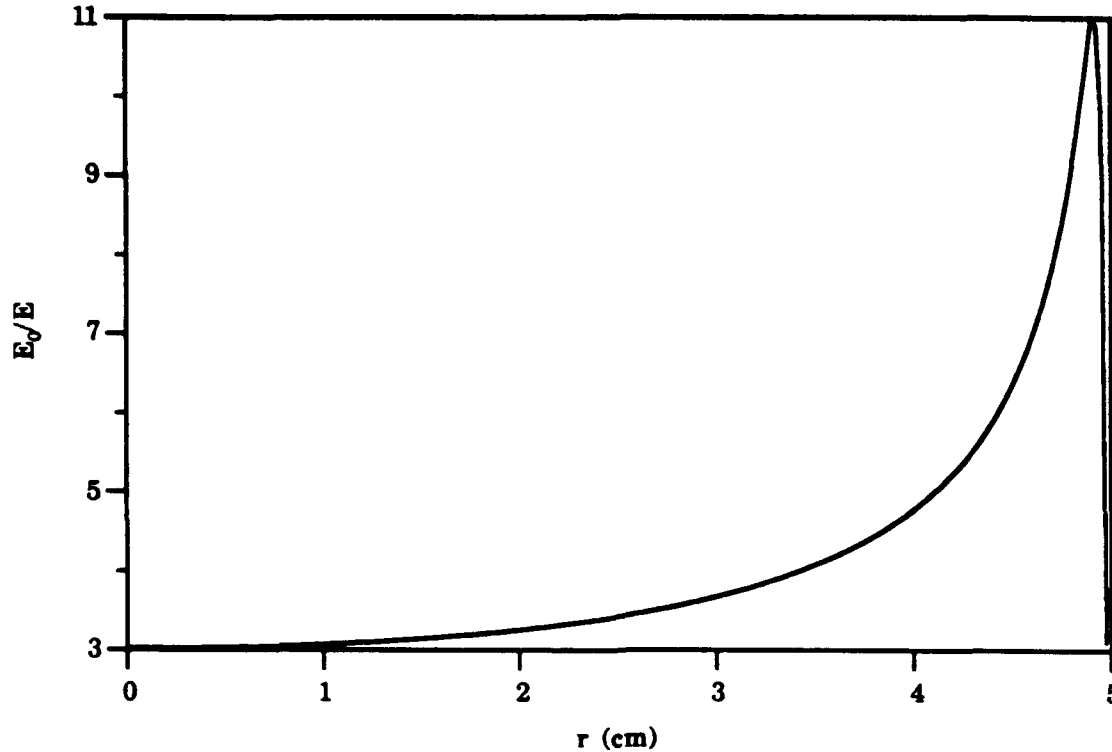


Figure 6-11. Ratio of Non-recombining to Recombining Field

The reduction of the field due to recombination can also be seen from the general expression for the field, given in Equation 6-1, and repeated here:

$$E = \frac{kT_e}{e} \frac{kT_i \left( \frac{\Gamma_1}{D_1} + \frac{\Gamma_2}{D_2} \right)}{N_e (kT_e + kT_i)} \quad (6-27)$$

By using the Einstein relation to express  $q/kT$  in terms of  $\mu/D$ , and noting the expression for  $\partial N_e / \partial r$  from Equation 6-1, we can rewrite this as

$$E = - \frac{D_e}{\mu_e} \frac{\nabla N_e}{N_e} \quad (6-28)$$

This expression describes the electric field as proportional to the normalized gradient of the electron number density  $\nabla N_e / N_e$ . Note that as we add recombination, we increase the volume loss per electron. Therefore, to keep the total losses in the plasma equal to the total source term, we must decrease the diffusion loss per electron. But the diffusion losses per

electron are proportional to  $\sqrt{N_e}/N_e$ . Therefore, from Equation 6-28, adding recombination reduces the electric field.

Some of the features depicted in Figures 6-7 through 6-11 are related to the somewhat artificial uniform external source term, not to the discrete numerical method. In particular, note the sudden drop in  $N_2$  at the edge of the plasma. This drop occurs over the last two calculation points in the grid, and is just an extreme example of what occurs in systems with less recombination. The constant source term is almost exactly matched by the recombination term. If there were no boundary at all, the match would be exact and the solution would be a spatially uniform value for  $N_2$ . However, this solution does not satisfy the boundary conditions. Eventually, the presence of the boundary forces  $N_2$  to zero, with a transition from a recombination-dominated to a diffusion-dominated discharge. The larger the recombination rate, the closer to the boundary this transition occurs. An estimate of the transition point can be made by equating the recombination frequency  $\alpha N_e$  to the effective diffusion loss frequency defined by  $D_a/(\Delta x)^2$ , where  $\Delta x$  is the distance from the transition point to the edge of the discharge. For the example given in Figure 6-7, the data reveals that the transition occurs at  $\Delta x$  on the order of 0.025 cm, or equivalently,  $r=4.975$  cm. At that point,  $\alpha N_e$  is  $3.8 \times 10^6$  Hz, and  $D_a/(\Delta x)^2$  is  $3.2 \times 10^6$  Hz. This is acceptable agreement.

*Nonproportionality.* We wish to discuss the implications these results have for the onset of nonproportionality. We will first discuss the example described in Figures 6-7 through 6-11, concentrating on conclu-

sions we can draw from that single case that are valid for a wide variety of cases. We will then compare results from a number of different cases, with the intent of drawing conclusions about the general relationship between recombination and nonproportionality.

Let us quickly review proportionality. Proportionality is the property of some multi-ion discharges that  $N_i = K_i N_e$ , for every ion species  $i$ . The results of Chapter IV included the following necessary condition for proportionality to hold:

$$\frac{\nabla \cdot \vec{\gamma}_i}{\sum_j \nabla \cdot \vec{\gamma}_j} = K_i \quad (4-13)$$

We defined a measure  $\beta_i = (S_i/S_e)/(\Gamma_i/\Gamma_e)$  which describes how far each species deviates from proportionality. A value of 1.0 indicates that the ion flux fraction at the edge of the discharge is precisely what would occur in a proportional discharge with the same values for the proportional source terms. Other values indicate that the flux is different from the proportional result by a ratio  $\beta_i$ . Although  $\beta_i$  is not an ideal measure, it does provide a consistent means of describing a variety of discharges.

Note the anomalies between our measures of nonproportionality and the results of Figures 6-7 and 6-8. Recombination affects  $N_2$  much more strongly than it does  $N_1$ . Yet,  $\beta_2$  had a value very near to 1.0, indicating a proportional system, and  $\beta_1$  was far from 1.0, indicating nonproportionality. The reason is the extremely high recombination rate in this discharge, coupled with the large difference in source terms. Since  $S_2$  is  $10^4$  larger than  $S_1$ ,  $S_e$  is essentially equal to  $S_2$ . Recombination reduces the

net source for  $\Gamma_2$  and therefore  $\Gamma_2$  itself to essentially zero throughout most of the discharge. However,  $N_2$  and  $N_e$  fall precipitously near the edge of the discharge, reducing recombination and increasing the net source for  $\Gamma_2$ . As a result,  $\Gamma_2$  rises rapidly until  $\Gamma_2$  and  $\Gamma_e$  are almost equal at the edge of the plasma. Since  $\beta_2$  compares  $S_2$  and  $S_e$  on axis to  $\Gamma_2$  and  $\Gamma_e$  at the edge we are left with  $\beta_2$  remaining close to 1.0. Effectively, we compare a ratio that ignores recombination ( $S_2/S_e$ ) to one that is evaluated where recombination affects both factors equally ( $\Gamma_2/\Gamma_e$ ). The situation is different for  $\Gamma_1$ .  $\Gamma_1$  is not directly affected by recombination anywhere; its continuity equation contains only the uniform source term. (Note that the same cannot be said for  $N_1$ ; the momentum equation for each species contains the fluxes for all the ion species.)  $\Gamma_e$  is affected by recombination everywhere. Thus,  $\beta_1$  is comparing a ratio that is independent of recombination ( $S_1/S_e$ ) to a ratio where the two factors are affected differently by recombination ( $\Gamma_1/\Gamma_e$ ). Therefore,  $\beta_1$  is markedly changed as recombination losses competitive to the diffusion losses are added.

This should not be construed as a failing in our measure of nonproportionality. Rather, it should alert us to the fact that "nonproportionality" is a highly mutable concept. From Chapter IV, we note that proportionality fails when we have source or loss terms that affect the different species by different amounts. In Figures 6-7 and 6-8, we depict a system where species 2 and the electrons have similar source terms, and therefore



similar spatial dependence. Species 1, with its different source term, has a different spatial dependence, and therefore demonstrates "nonproportionality". A single evaluation of  $\beta$  is not sufficient to demonstrate proportionality. Rather, both of the  $\beta$  parameters must be examined.

In spite of these considerations, note that in some sense a system such as that described in Figures 6-7 through 6-11 can be said to approach a limit of proportionality at both very high and very low recombination rates. For no recombination, the system corresponds to the proportional solutions we obtained as the CX case in Chapter IV, earlier. But consider the opposite extreme, where recombination for  $N_2$  is extremely high. There are two contrasting possibilities.

First, we could have a source term for the recombining species large enough to prevent it from vanishing from the discharge. This was the case for Figures 6-7 through 6-11. Even though  $N_2$  undergoes an extremely high recombination rate, its source is so high that its contribution dominates the total electron source  $S_e$ . The result, as we saw, is a value for  $\beta_2$  indicating a proportional discharge, and one for  $\beta_1$  indicating a non-proportional discharge.

For comparable source terms and high recombination of  $N_2$ , we find that  $N_2$  will essentially vanish from most of the discharge. We then are left with a single-ion plasma, which is trivially proportional if we consider only the dominant non-recombining species  $N_1$ . However, in such a case the recombining species  $N_2$  would have a nonproportional profile.

From such considerations we can see that a universal measure of proportionality is difficult to define. As discussed above,  $\beta_1$  actually gave a stronger indication of nonproportionality than  $\beta_2$  in a system where species 2 had a source so high that  $S_2$  and  $S_0$  were essentially equal, but species 2 was also much more strongly affected by recombination. In that system the sources and fluxes were both dominated by species 1. As a result, even though recombination reduced  $\Gamma_1$ , it was still so much larger than  $\Gamma_2$  at the wall that it dominated, and  $\beta_2$  was close to 1. In a system where the source terms are more closely equal, the reductions in  $\Gamma_2$  produced by recombination are more discernible, and  $\beta_2$  can give stronger indications of nonproportionality than  $\beta_1$ .

Because of situations such as this, it is important to define the proportionality or nonproportionality of a system in terms of both species, not just one.

Next, we wish to examine the correlation between the ratio of external sources to on-axis recombination loss on the one hand, and the deviation from proportionality on the other. Because of the widespread use of proportionality to describe systems which are not strictly proportional, it is worthwhile to examine this in more detail, by investigating a number of systems where the only change is the amount of recombination. All the systems investigated were at a pressure of 1.0 T, with a radius of 5.0 cm. All parameters not mentioned specifically below were identical to the system in Figure 6-7.

In Figure 6-12 we show  $1/\beta_1$  and  $\beta_2$  as functions of  $\alpha N_2 N_e / S_2$ , which measures the importance of the recombination term versus the external source term for species 2. The source terms for both species were equal to  $10^{17} / \text{cm}^3 \cdot \text{s}$ . We show  $1/\beta_1$  instead of  $\beta_1$  strictly for convenience; nonproportionality is indicated by deviation either above or below 1.0. Our choice of  $1/\beta_1$  causes both measures to deviate in the same direction.

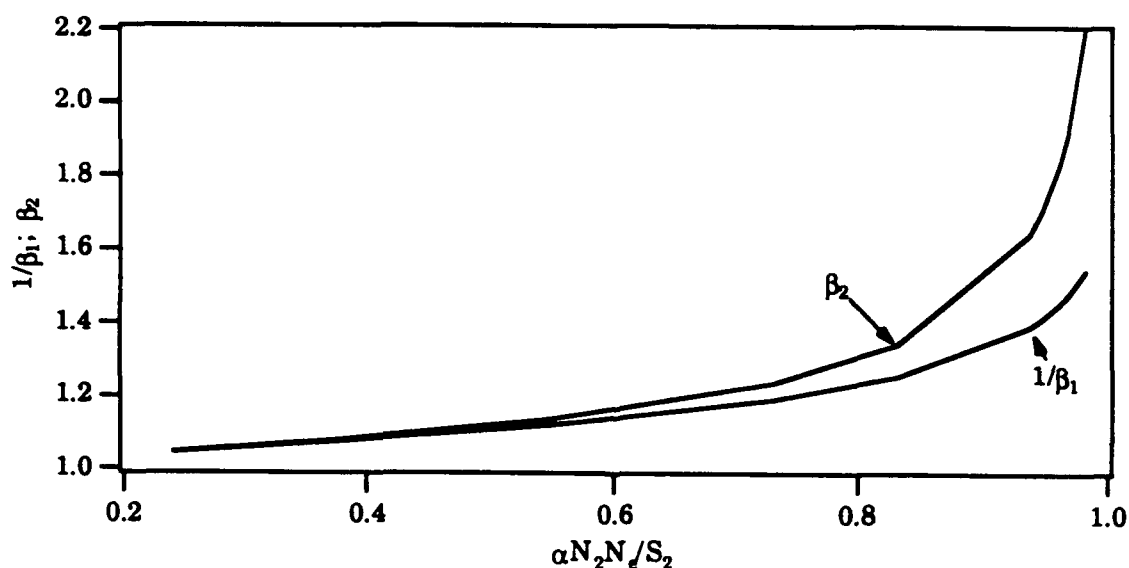


Figure 6-12. Deviation from Proportionality As Recombination Increases, Equal Sources

Figure 6-12 presents a system where  $\beta_1$  and  $\beta_2$  give consistent measures of nonproportionality. As the ratio  $\alpha N_2 N_e / S_2$  increases so do both  $1/\beta_1$  and  $\beta_2$ , indicating increasing nonproportionality. Note that  $\beta_2$  is always slightly greater than  $1/\beta_1$ . Without the perturbing effect of differing source terms, the species that is directly involved in the recombination is the one showing the greatest deviation from proportionality.

In Figure 6-13 we show similar results for a case where the sources terms differ. The "Nonequal Sources" cases had  $S_1$  equal to  $10^{16}$  and  $S_2$  equal to  $10^{17}/\text{cm}^{-3}\cdot\text{s}$ . All other parameters were identical to the previous cases.

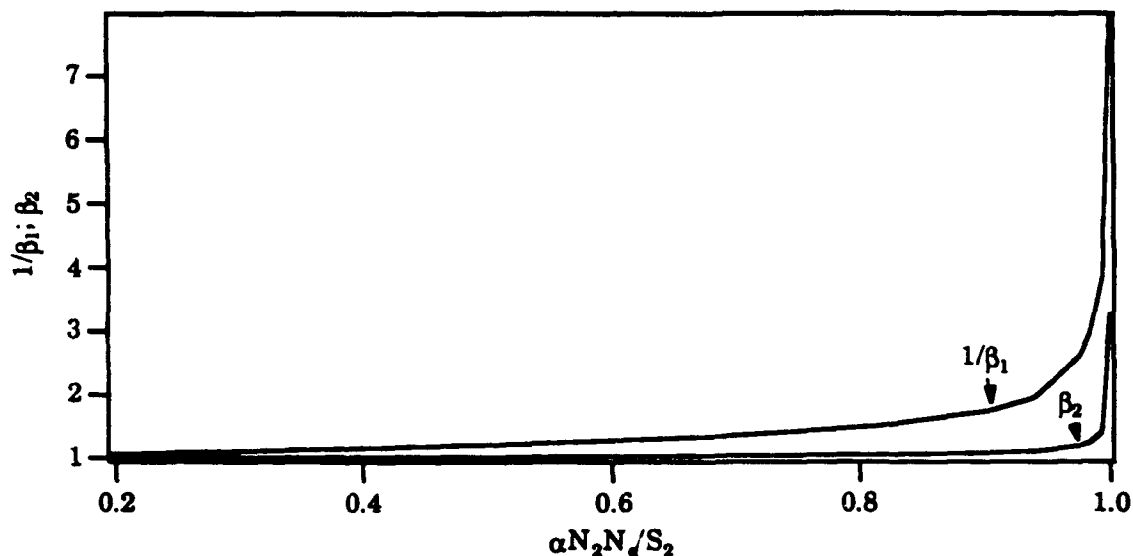


Figure 6-13. Deviation from Proportionality As Recombination Increases, Nonequal Sources

Again, as recombination increases, so does nonproportionality. However, now  $1/\beta_1$  is larger than  $\beta_2$ . The effect of the nonequal sources is changing the relative importance of the two measures. This is a milder case of what we saw in Figures 6-7 to 6-11; even though species 2 is more strongly affected by recombination, the difference in source terms masks the effects on species 2, so that species 1 shows the most nonproportionality.

As we saw from the system shown in Figures 6-7 through 6-11, it is possible for a system with widely differing sources to have at least one of the  $\beta$ 's nearly 1, even with recombination losses approximately equal to the sources. Such cases arise when the recombining species ( $N_2$ , in this case)

has a large enough source term that it would dominate the system, were it not for the presence of the recombination. We are beginning to see that effect here, for a system with sources more nearly equal.

*Conclusions.* Several conclusions can be drawn for recombining plasmas maintained by external ionization sources:

1. In a multi-ion plasma with significant recombination present, if the recombining species is not negligible, none of the densities will have spatial profiles the same as those in a recombination-free discharge.
2. If the ratio  $S_2/\alpha$  is small enough the particle density for the recombining species will have a minimum at the center of the discharge. Equation 6-23 gives a sufficient condition for this to occur:

$$\frac{S_2\epsilon}{\alpha N_2(N_1(1+\epsilon) - N_2)} < 1 \quad (6-23)$$

This can occur for fairly small values of  $\alpha$ , as shown in Figure 6-8.

3. Measures of the deviation from proportionality give results that are inherently dependent on the definition of the measurement parameter. Therefore, it is imprudent to claim that a system deviates little from proportionality unless the measurement is defined.

*External Sources plus Charge Transfer.* For the case just finished, we examined nonproportional systems arising from source terms that were independent of charged species number density and loss terms that were quadratic in number density. Now we will examine the nonproportional systems that arise from the same source terms combined with a non-resonant charge transfer term that is linear in charged species number density. We saw an example of nonresonant charge transfer in the comparisons to Wunderer, who used an external source and included recombination, and to Schmidt, which used volume sources and included recombination in one of the two sets of calculations. Here, we use a simpler

uniform external source term than Wunderer's, and include no recombination. The choice of a simpler system enables us to distinguish the charge transfer effects from effects such as recombination.

Under such conditions, the diffusion and continuity equations are

$$\begin{aligned}\frac{\partial N_i}{\partial r} &= -\frac{\Gamma_i}{D_i} + \frac{N_i}{N_e} \frac{kT_i \sum_j \frac{\Gamma_j}{D_j}}{(kT_e + kT_i)} \\ \frac{\partial N_e}{\partial r} &= -\frac{kT_i \sum_j \frac{\Gamma_j}{D_j}}{kT_e + kT_i} \\ \frac{\partial \Gamma_1}{\partial r} &= S_1 - v_t N_1 - \frac{\Gamma_1}{r} \\ \frac{\partial \Gamma_2}{\partial r} &= S_2 + v_t N_1 - \frac{\Gamma_2}{r} \\ \frac{\partial \Gamma_e}{\partial r} &= S_2 + S_1 - \frac{\Gamma_e}{r}\end{aligned}\tag{6-29}$$

where  $v_t$  is the charge transfer frequency, and where the other quantities retain the same definitions as in the recombination case.

The algorithm used to perform the calculations was the same that was used to perform the recombination calculations; the input parameters were changed to reflect no recombination, and to add charge transfer. The actual charge transfer mechanism was based on associative charge transfer, which requires a mediating background particle. This reaction was chosen because it was appropriate for the  $N_2^+-N_4^+$  system used for the comparison with Schmidt's experiments.

For these calculations,  $\nu_t$  ranged from 0 to  $7 \times 10^7$  Hz. We have assumed the diffusion coefficient to be constant as  $\nu_t$  changes. For this to be a valid assumption, we must have  $\nu_t$  much less than the momentum transfer collision frequency for ions. For the diffusion coefficients ( $\sim 100$  cm<sup>2</sup>/s), ion temperatures (0.02585 eV), and hypothetical ion masses ( $\sim 10$  amu), the momentum transfer collision frequency is on the order of several times  $10^8$  Hz or higher. Therefore, even at the highest values of  $\nu_t$ , it is reasonable to assume that the diffusion coefficient is independent of  $\nu_t$ .

As was discussed in the introduction to the investigations of generic plasmas, no claim is made that this system completely models a realistic discharge. Nonetheless, the simplifications (constant  $kT_e$ , constant  $kT_i$ , and so forth) allow concentration on the effects of charge transfer *per se*.

*High Charge Transfer Example.* In Figure 6-14 we show the number densities for one particular case. This case was chosen because it illustrated high nonproportionality. The input parameters for this case were

1.  $D_1 = 3000$  and  $D_2 = 1000$  cm<sup>2</sup>/s.
2. Pressure was 0.1 Torr.
3. The external sources were  $10^{16}$  /cm<sup>3</sup>-s for each species.
4. The charge transfer frequency was given by  $\nu_t = 7 \times 10^7$  Hz.
5. The Debye length was  $\sim 4 \times 10^{-4}$  cm.
6. The deviations from proportionality were given by  $\beta_1 = 49.94$  and  $\beta_2 = 0.50505$ .

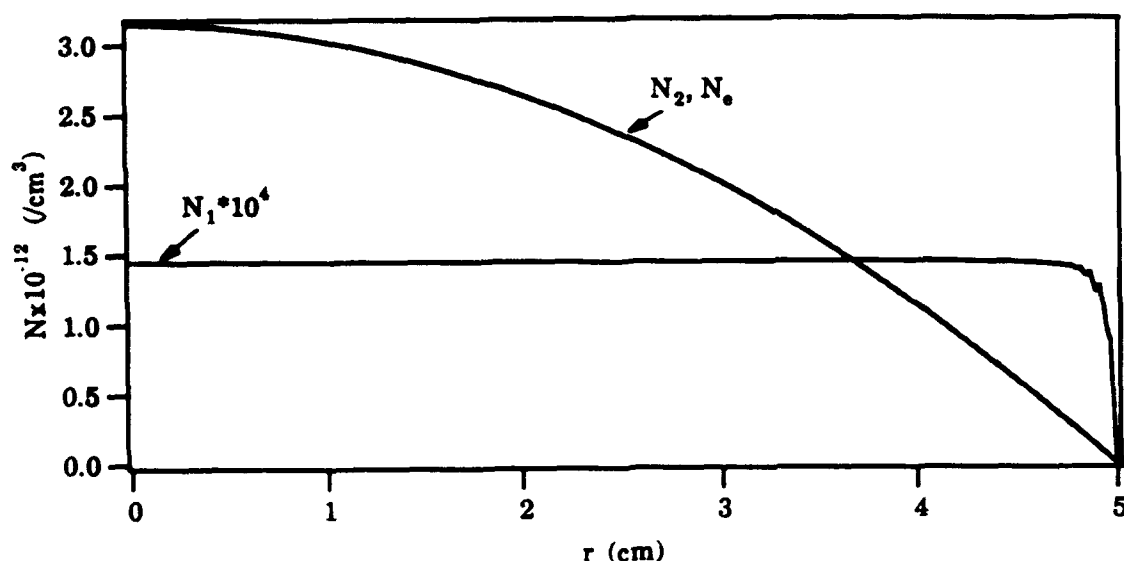


Figure 6-14 Number Densities with High Charge Transfer Present

The charge transfer term is so large as to be essentially equal to the external source term. In fact, the charge transfer term on axis is .9997 of the external source term for this case, and approaches 1.0 in the limit of increasing charge transfer. This is not coincidence. Charge transfer for  $N_1$  is much larger than diffusion, except near the edge. With the dominant loss mechanism not being diffusion, there is no need for a density gradient. Instead, the number density is controlled by the balance between source and loss:

$$S_1 = v_t N_1 \quad (6-30)$$

This produces a value for  $N_1$  of  $1.44 \times 10^{12}/\text{cm}^3$ , exactly the value shown above. The only significant departure from the flat profile is near the edge, at approximately 4.7 cm. As before, the presence of the boundary of the plasma starts to affect the plasma, allowing diffusion to become significant again.



$N_1$  is reduced almost to the point of extinction, compared to  $N_2$ . As a result,  $N_2$  and  $N_e$  are identical to within less than one part in  $10^3$ , except at the very edge of the discharge. In fact, except near the edge,  $N_2$  and  $N_e$  have a functional dependence as if there were only one species in the plasma, whose source was  $S_1 + S_2$ . The profiles for species 2 and the electrons agree with the Schottky profiles for such a source within an error of considerably less than 1%. This contrasts with the recombination case, where the effect of recombination on the electron source term affected  $N_e$  and kept any of the particle densities from attaining Bessel function Schottky profiles. However, the very large charge transfer rates do not affect the electrons, and thus produce a Schottky-like profile both for the electrons and the dominant ion.

We did not find a spatial profile for any species that increased from the center to the edge, for any of the charge transfer cases examined. This is somewhat in contrast to the previous recombination case, where one species ( $N_2$ ) rose on axis. Let us examine why. If we take the divergence of the momentum equation for  $N_1$ , and then use the continuity equations to evaluate the results, we can determine an expression for the curvature of  $N_1$  and evaluate it on axis. For  $N_1$  to rise from on axis, that expression must be greater than zero. From that condition, we derive the following equivalent expressions:

$$\frac{(N_e (1 + \epsilon) - N_1)}{N_1} \leq \frac{\left(\frac{S_2 + v_t N_1}{D_2}\right)}{\left(\frac{S_1 - v_t N_1}{D_1}\right)} \quad (6-31)$$

$$\frac{(\epsilon N_e + N_2)}{N_1} \leq \frac{\left(\frac{S_2 + v_t N_1}{D_2}\right)}{\left(\frac{S_1 - v_t N_1}{D_1}\right)}$$

These are analogous to the relations expressed in Equations 6-21 through 6-23. The related structure is clear. Just as in the Equation 6-21, we have an inequality relating the ratio of the source terms to a quantity that is nearly the ratio of the ion number densities. In the limit as  $v_t$  goes to zero, the right hand side of Equation 6-31 becomes the ratio  $N_2/N_1$  for a proportional system with uniform external sources. This ratio was discussed for any proportional system in Chapter IV, and for the CX case in Chapter V. The left hand side is always greater than  $N_2/N_1$ . Therefore, our conclusion is that  $N_1$  does not increase at  $r = 0$  for such proportional cases. This is in agreement with the analytic solution we found for the CX case in Chapter V.

We see no general conclusions that can be drawn at this time from Equation 6-31, except to note that the spatial profile of  $N_1$  will rise if the inequality is true when evaluated on axis. For the example depicted in Figure 6-14, Equation 6-31 would require  $2.24 \times 10^4 \leq 2.22 \times 10^4$ . This, of course, is not a valid relationship, and is consistent with our results, that showed no rise in  $N_1$  as a function of increasing  $r$ .

Figure 6-15 shows the fluxes for the same case. Note that  $\Gamma_1$  demonstrates the same nonproportionality (as defined in Chapters III and IV)

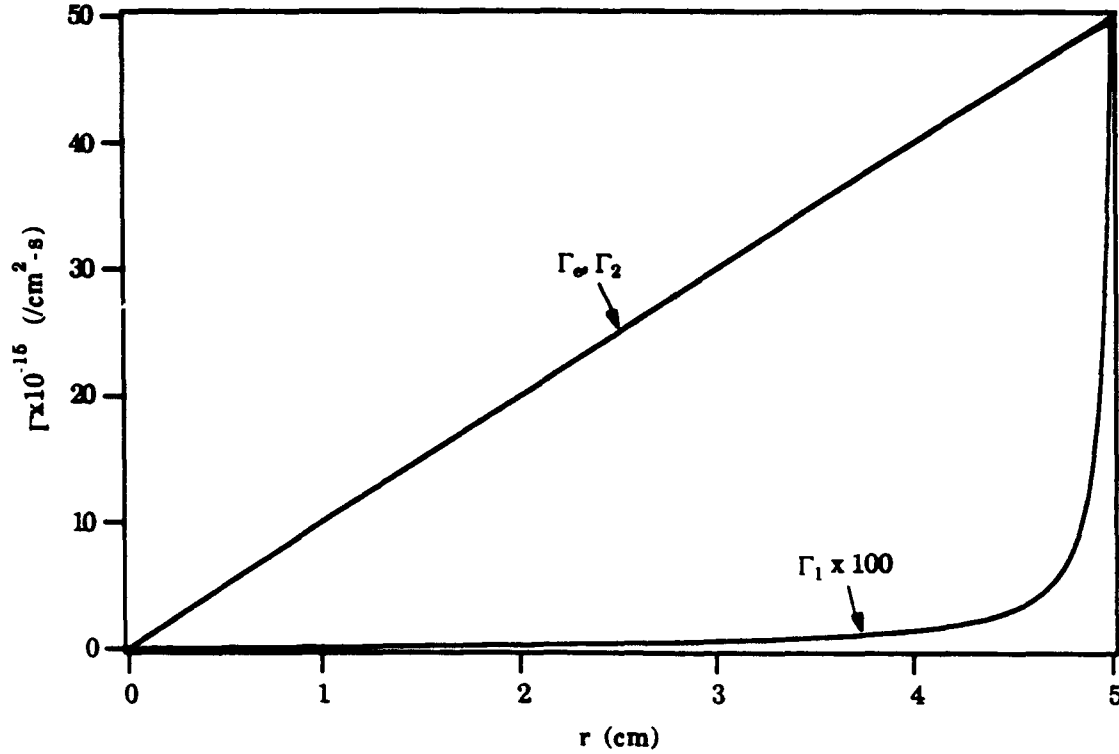


Figure 6-15. Particle Fluxes with High Charge Transfer

that  $N_1$  demonstrated in Figure 6-14, and for much the same reasons.

Recall the continuity equation for  $\Gamma_1$  :

$$\frac{\partial \Gamma_1}{\partial r} = S_1 - v_t N_1 - \frac{\Gamma_1}{r} \quad (6-32)$$

For this example,  $S_1$  and  $v_t N_1$  were almost equal through most of the discharge. Therefore,  $\Gamma_1$  remained very small. Only at the edge, where  $N_1$  starts to decrease, does the net source become appreciable, allowing  $\Gamma_1$  to rise.

This near-equality of  $S_1$  and  $v_t N_1$  also explains the nearly flat spatial dependence we saw for  $N_1$  . Consider the momentum equation for  $N_1$  :

$$\frac{\partial N_1}{\partial r} = -\frac{\Gamma_1}{D_1} + \frac{N_1}{N_e} \frac{kT_1 \sum_j \frac{\Gamma_j}{D_j}}{(kT_e + kT_1)} \quad (6-33)$$

The last term on the right hand side varies as  $\sum \Gamma/D$ , scaled roughly by  $kT_1/kT_e$  and  $N_1/N_e$ . Both these scaling factors are less than one. This reduces the effect of this term and increases the relative effect of the first term on the right hand side. In addition, as charge transfer reduces  $N_1$ ,  $N_1/N_e$  reduces the second term even more. Therefore, the  $-\Gamma_1/D_1$  term has the largest effect on  $N_1$ . In this particular case,  $\Gamma_1/D_1$  is reduced almost to zero, producing the flat density profile. Only at the edge where  $\Gamma_1/D_1$  becomes much larger do we see significant changes in  $N_1$ .

We do not show the electric field. The reason we do not is that our results show that it differed by less than 0.2% from the field produced with no charge transfer at all. There is a simple explanation for this. This discharge is so dominated by charge transfer as to appear as a simple single ion, uniform external source system. Let us recall the electric field for such a case from the CX case of Chapter V. The field in the small-e-flux approximation is

$$E = \frac{kT_e 2r}{e(R^2 - r^2)} \quad (6-34)$$

This is a field that depends only on position and the electron temperature. (If we did not use the small-e-flux approximation, we would see a small additional dependence on the ion temperature.) For the same electron temperature, all such systems have the same electric field. Thus, the field for the present case is essentially identical to the field in the CX case and

independent of all ion properties (to the extent that the small-e-flux approximation is valid).

Finally, before we leave this example, we should note that we also made calculations where we used a zero source term for  $N_2$ , but with all other parameters the same. The only significant difference was that  $N_2$  and  $N_e$ , along with their corresponding current densities, were reduced by a factor of 2. This is not unexpected; the charge transfer rate is so high that any ions of species 1 that are created are immediately lost to produce ions of species 2. Therefore, the total source for species 2 is  $S_1 + S_2$ . If we eliminate  $S_2$ , we reduce the species 2 source by the appropriate amount; one half, in this particular case.

*Nonproportionality.* Finally, we wish to discuss the onset of proportionality, much as we did for the recombination case. In Figures 6-16 and 6-17 we show  $\beta_1$  and  $1/\beta_2$  as a function of the normalized charge transfer term. As before, we show the reciprocal of one measure so that both measures will vary in the same direction. The last point on the right in each figure corresponds to the high charge transfer case just presented.

Nonproportionality steadily increases as the term producing the nonproportionality increases. Initially  $\beta_1$  increases much more slowly than  $1/\beta_2$ , but eventually reaches much higher values. Note that, for a system with an infinite charge transfer rate from species 1 to species 2 (impossible, except as a limiting case),  $\Gamma_1$  at the edge of the discharge goes to zero and  $\Gamma_2$  goes to twice the value it would have with no charge transfer

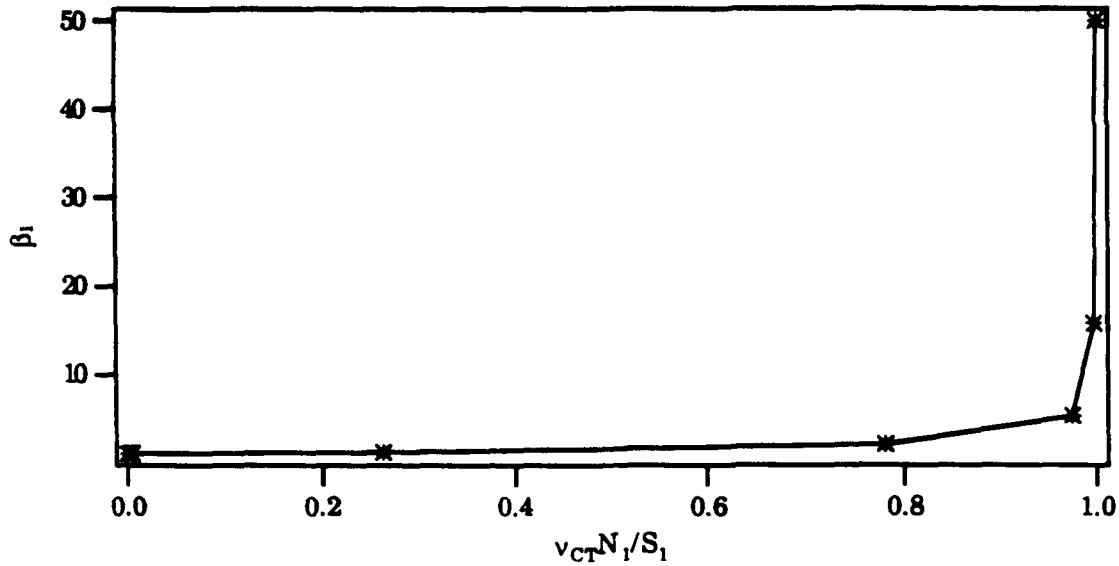


Figure 6-16. Deviation from Proportionality As Charge Transfer Increases, Species 1

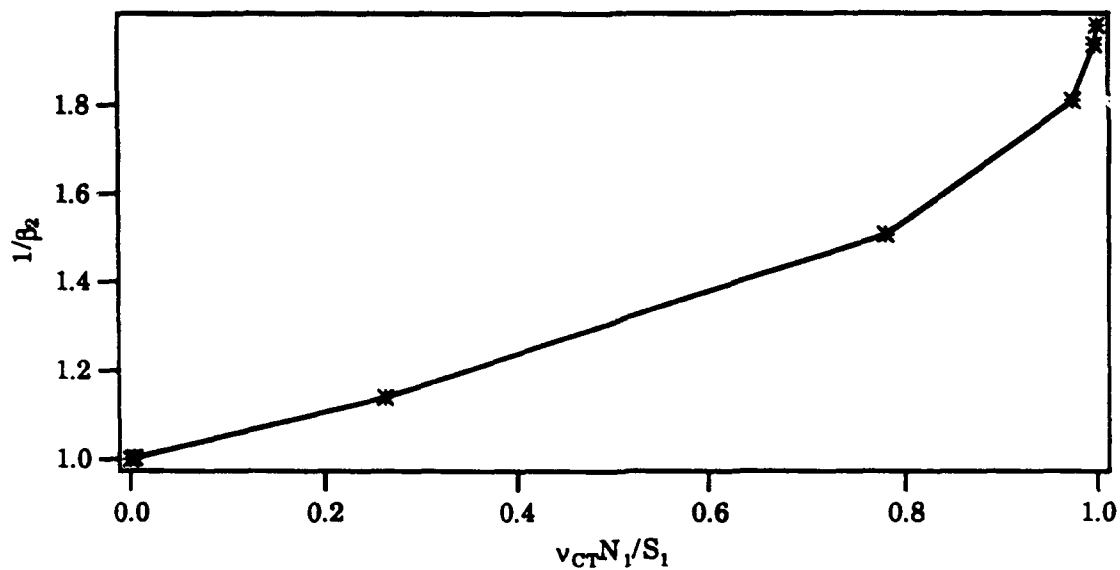


Figure 6-17. Deviation from Proportionality As Charge Transfer Increases, Species 2

(for equal sources). Under those circumstances,  $1/\beta_2$  would be limited to a value of 2 and  $\beta_1$  would become infinite.

*Similarity Parameters.* There is one last observation to make about charge transfer. For certain combinations of plasma parameters,

two different discharges could have the same values for their spatial profiles and for the quantities related to those profiles. As an example, we will compare two discharges, one at 0.1 T, and the other at 1 T. The following values, which determine plasma conditions, were the same for both discharges:

1.  $S_k/p$ , where  $k$  represents either ion species, or the electrons and  $p$  is the pressure.
2.  $v_t N_1/S_1$ .

With these inputs to the model, we found the following output parameters to be the same for both discharges:

1.  $\beta_1$ .
2.  $\beta_2$ .
3.  $E/E_0$ .
4. Spatial dependence of the various fluxes.

Although the particle fluxes had the same position dependence for both species, they differed by a factor of 10 in magnitude (*i. e.*,  $\Gamma/p$  was invariant). This is in accordance with the model, which predicts that the fluxes should scale linearly with net source (see Equation 6-1); the source terms for the two discharges also differed by a factor of 10. (This was due to the 10:1 pressure ratio of the two discharges.) The number densities also had the same position dependence, but differed by a factor of 100. Equation 6-1 indicates that the number densities scale by  $\Gamma/D$ . For these discharges, the pressure difference caused the diffusion coefficients to differ by a factor of

10. In conjunction with the scaling of the fluxes, the model predicts a change by a total factor of 100.

We can draw the following conclusions from these observations:

1. Discharges at different pressures, whose external sources are proportional to the pressure, and whose ratios of charge transfer to external source for the losing species are identical, will have the same spatial dependence, with all that implies for nonproportionality, field, and so forth.
2. Discharges that are driven by external sources, and undergo charge transfer as their only volume kinetic reaction, scale the same as discharges with the same sources, but no charge transfer. That is to say, the flux densities will scale as the external source, and the particle densities will scale as the source divided by the diffusion coefficients.

In practice, of course, it would be very difficult to find discharges satisfying these constraints. However, the existence of these relationships forms a useful validation for theoretical analyses. For instance, any numerical model would have to satisfy these constraints. This provides a useful tool for verification of the numerical method.

*Summary of Charge Transfer Results.* To summarize the results for the charge transfer case:

1. As the level of charge transfer is increased, some parameters of the system becomes more non-proportional, either in the absolute sense or in the sense of deviating more from the values found with no charge transfer. In particular, those parameters which depend on a single ion species, such as the spatial profiles of the individual fluxes, are more likely to display these effects than parameters that depend on more than one species, such as the field.
2. At extreme levels of charge transfer, some parameters of the discharge act as if it were a single-ion discharge, whose source is equal to the total source for both ions. In particular, those parameters that depend on the electrons, as opposed to the individual ion species, are more likely to take the values appropriate for single ion Schottky cases. The electric field in particular displays such behavior.



3. The parameters  $S_k/p$  and  $v_r N_1/S_1$  serve somewhat as similarity parameters; any two discharges for which these are equal will have similar spatial dependencies.

4. At no time did we find cases where any of the particle densities increased from the center of the discharge. It is possible to determine tests to see if such increases will occur, but we drew no conclusions about whether such conditions could hold.

*Volume Sources.* Next, we will investigate one example of a volume sources of ionization, in addition to the various examples addressed while verifying the model. This example examines the effects of recombination in volume source discharges. The discharge chosen has volume sources proportional to  $N_e$ . We will not examine charge transfer. Since both charge transfer and the volume source term depend linearly on the number densities, the results for that system in cylindrical geometry are proportional analytic solutions analogous to those discussed in Chapter V as the PT case.

*Volume Source plus Recombination.* For this case, the momentum and continuity equations become:

$$\begin{aligned}
\frac{\partial N_i}{\partial r} &= -\frac{\Gamma_i}{D_i} + \frac{N_i}{N_e} \frac{kT_e \sum_j \frac{\Gamma_j}{D_j}}{(kT_e + kT_i)} \\
\frac{\partial N_e}{\partial r} &= -\frac{kT_i \sum_j \frac{\Gamma_j}{D_j}}{kT_e + kT_i} \\
\frac{\partial \Gamma_1}{\partial r} &= v_1 N_e - \frac{\Gamma_1}{r} \\
\frac{\partial \Gamma_2}{\partial r} &= v_2 N_e - \alpha N_2 N_e - \frac{\Gamma_2}{r} \\
\frac{\partial \Gamma_e}{\partial r} &= (v_1 + v_2) N_e - \alpha N_2 N_e - \frac{\Gamma_e}{r}
\end{aligned} \tag{6-35}$$

We chose parameters that correspond roughly to a 10/90 mixture of helium ( $N_1$ ) and neon ( $N_2$ ), although with no pretense that we are modeling that system. With the predominance of the background gas being the species with the higher ionization frequency ( $N_2$  in this case), we could thus ensure that only one species would undergo significant recombination. We chose  $D_1$  and  $D_2$  as 100 and 400 cm<sup>2</sup>/s, and determined  $v_1$  and  $v_2$  partly by the relative fraction of each gas, and partly by the characteristics of the gas species itself, to be  $10^{-20}$  and  $10^{-18}$  times the total background gas number density. All four parameters were input with values appropriate for  $p = 1$  T and  $kT_e = 1$  eV. These values are of the same order as the values for unmixed helium or neon discharges, but are otherwise chosen purely for convenience. We chose values of  $\alpha$  between 0 and  $10^{-5}$  cm<sup>3</sup>/s. Although the latter value was considerably more recombination than typical in a real gas, the range was chosen to demonstrate the effects of the recombination.

Pressures ranged from 1.0 to 5.0 T. As before, the radius of the discharge was chosen as 5.0 cm.

In the external ionization case, the presence of a source term that was independent of the conditions in the plasma determined a particular value for the on-axis number densities. The lack of an external ionization source changed the nature of the problem significantly. As was discussed in the comparable PS and CS analytic cases in the previous chapter, the removal of the external source, combined with boundary conditions of the fluxes being zero on axis and the densities being zero at the discharge edge, allows only trivial solutions unless the electron temperature is fixed at a particular value. For the PS and CS cases, an explicit analytic eigencondition fixed  $kT_e$ . This eigencondition was based on the additional constraint that  $N_e$  be non-zero at at least one point, with that point being chosen  $r = 0$  for convenience. A similar constraint leads to eigenvalues for the volume source with recombination case, as well. We established that constraint by normalizing all the densities and current densities in the system by dividing by the electron density on axis,  $N_{e0}$ . This normalization produced an additional constraint on the normalized  $N_e$ , which acted as an additional boundary condition:

$$\frac{N_e(0)}{N_{e0}} = 1.0 \quad (6-36)$$

Algorithmically, the additional boundary condition requires an additional differential equation and dependent variable in the numerical system.  $kT_e$  became the additional dependent variable, with a derivative identically zero.

The result was a system of five differential equations: the momentum equations for  $N_2$  and  $N_e$  and continuity equations for the ions, as described

in Equation 6-35, plus the trivial equation  $\partial kT_e / \partial r = 0$ . The five boundary conditions were  $N(R) = 0$  and  $\Gamma(0) = 0$  for the appropriate species, plus Equation 6-36.

In such a system, it is necessary to have some mechanism to allow the system to respond to changes in the eigenvalue. Otherwise, there is no coupling between the plasma conditions and the eigenvalue. In this calculation there were several such mechanisms. First,  $kT_e$  enters directly into the momentum equations. Second, the ionization frequencies and recombination rate were realistic functions of  $kT_e$ . Details of this modelling will be left to Appendices C and D, which document all the numerical algorithms used.

The normalization produced an additional input parameter, the actual on-axis electron number density,  $N_{e0}$ . In a real discharge,  $N_{e0}$  would be fixed by the energy balance in the system. For instance, in a glow discharge, the external circuit parameters fix the longitudinal current. That current, along with the diffusion losses, then fixes  $N_{e0}$ . Energy balance is not included in this model. Therefore,  $N_{e0}$  becomes a free parameter and was allowed this to range from  $10^{10}$  to  $10^{12} \text{ cm}^{-3}$ . This range was chosen in conjunction with the pressures mentioned earlier. The upper value was chosen somewhat arbitrarily; we feel that  $10^{12}$  was high enough to demonstrate the effects we wished to examine, and was at the upper end of densities that can be realistically considered as weakly ionized. At higher densities, Coulomb collisions start to become significant, and the weakly ionized nature of the discharge is lost. For instance, from Mitchner and Kruger, we calculate that a 1 T, 1 eV hydrogen plasma can no longer be

considered weakly ionized for electron densities greater than  $10^{14}/\text{cm}^3$  (Mitchner and Kruger, 1973:60). Since we wished to stay well into the weakly ionized regime, we used  $10^{12}/\text{cm}^3$ . The lower limit of  $N_{e0}$  was chosen because, even at the maximum pressure and  $\alpha$  used, any lower  $N_{e0}$  would have produced no discernible recombination. Such cases can be modelled by the solutions of the previous chapter, and need not be examined here.

*High-Recombination Example.* At this point, we shall present an example, with the parameters shown:

1.  $D_1$  and  $D_2$  were 100 and  $400 \text{ cm}^2/\text{s}$ .
2. Pressure was 1.0 T.
3.  $N_e(0)$  was  $10^{12} \text{ cm}^{-3}$ .
4.  $\alpha$  was  $10^{-5} N_{bg} \text{ cm}^3/\text{s}$ , with  $N_{bg}$  the number density of the background gas.
5. The ionization frequencies  $\nu_1$  and  $\nu_2$  were given by  $10^{-20} N_{bg}$  and  $10^{-18} N_{bg} \text{ Hz}$ , at an electron temperature of 1 eV. The program adjusted the frequencies to account for the actual value of  $kT_e$ .
6. The program calculated a value of  $kT_e = 2.66 \text{ eV}$ .
7. The value calculated for  $\beta_1$  was 0.0939, and for  $\beta_1$ , 2.68.
8. The Debye length was  $1.2 \times 10^{-3} \text{ cm}$ .

The densities are shown in Figure 6-18. Note that  $N_2$  has an almost flat density profile. The reason is that the recombination term is so large as to dominate the diffusion term. In other words, there is enough recombination to eliminate most of the ions produced in the volume of the plasma. Note also that  $N_2$  does not rise toward the edge of the discharge. This is

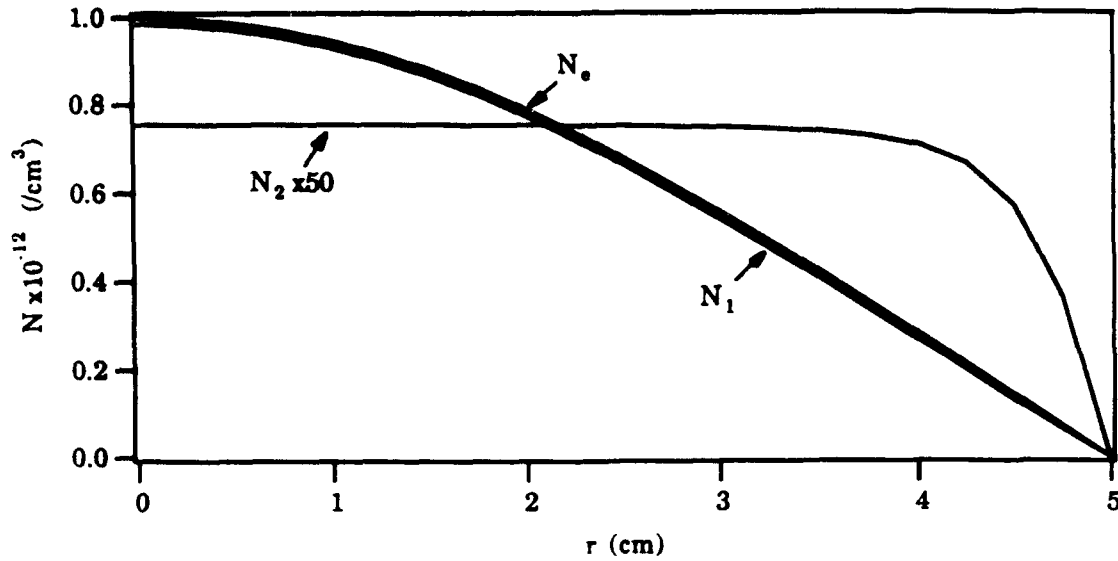


Figure 6-18.  $N$  versus  $r$ , Maximum Recombination

contrary to the results we found for the external source term, but consistent with the results we saw for the external source-charge transfer case.

Recall Equation 6-21, which gave a condition for  $N_2$  increasing on axis for the external source-recombination case:

$$\frac{\epsilon N_e + N_1}{N_2} < \frac{\frac{S_1}{D_1}}{\frac{S_2}{D_2} - \frac{\alpha}{D_2} N_2 N_e} \quad (6-21)$$

A similar derivation can be used to find the condition for  $N_2$  increasing on axis for the volume source-recombination case:

$$\frac{\epsilon N_e + N_1}{N_2} < \frac{\frac{v_1}{D_1}}{\frac{v_2}{D_2} - \frac{\alpha}{D_2} N_2} \quad (6-37)$$

For the parameters of our example, the left hand side of Equation 6-37 yields 65.8, whereas the right hand side yields 64.97. Thus, the condition is not satisfied. This is in agreement with our observation that  $N_1$  steadily

decreased from the center to the edge of the discharge, and is similar to the results of the external source-charge transfer case. There appears to be no reason why rising profiles could occur for sufficiently high  $\alpha$ 's. However, in the present investigation this effect only appeared in the external source-recombination cases. Shortly, we will discuss this effect in the context of all three cases presented.

Finally, we note that  $N_1$  and  $N_e$  have profiles within 1-2% of the Schottky Bessel function profile. This is caused by the extremely high recombination eliminating one species from the discharge. This is not to say, however, that the entire discharge can be modeled by the Schottky profiles.  $N_2$  is so reduced that it might be thought that one could approximate this discharge as having only one ion species. However, the various fluxes shown in Figure 6-19 negate any such claim, and show the importance of a complete analysis to compare with wall sampling measurements.

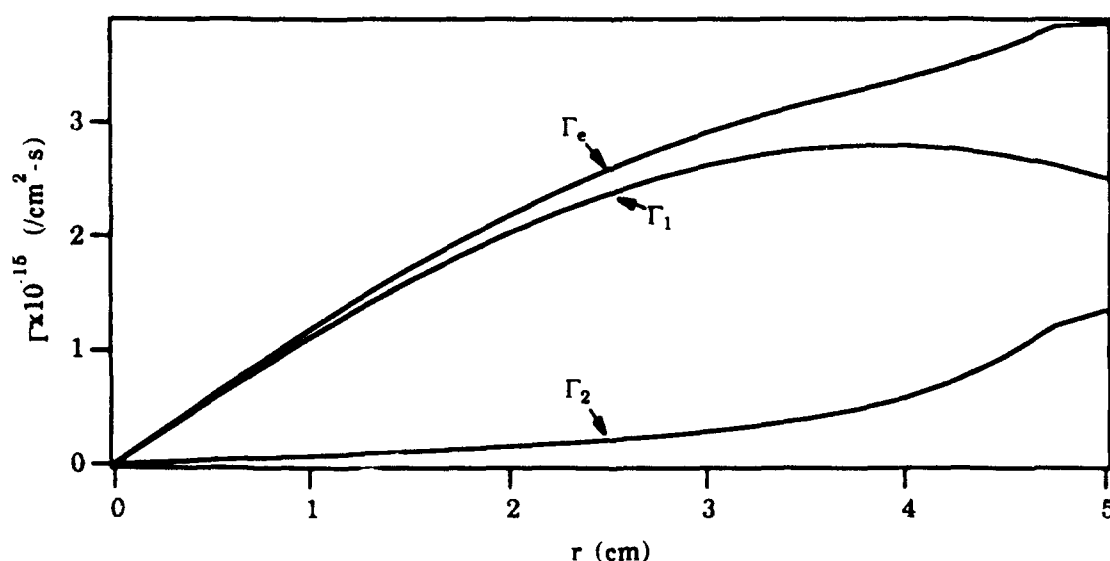


Figure 6-19. Particle Fluxes for High Recombination and Volume Sources

Note that  $\Gamma_2$  at the edge of the discharge is approximately  $1/2 \Gamma_1$ . The implication is that both species are playing a significant role in discharge, and must be taken into account. This is in dramatic contrast to Figure 6-18. For instance, even though the number densities would imply that this might be approximated as a single ion discharge, measurements of the fluxes at the wall would clearly show two ionic species.

Figure 6-18 indicates that  $N_2$  can be neglected in describing the discharge, while Figure 6-19 indicates that it clearly plays a significant role. This dichotomy is explainable by the present model. Note that  $N_2$  is approximately  $N_1/50$ . In the central region of the plasma,  $\partial N_2/\partial r$  is approximately zero. In that case, the momentum equation for  $N_2$  produces

$$\frac{\Gamma_2}{D_2} = \frac{N_2}{N_e} \frac{\left( \frac{\Gamma_1}{D_1} + \frac{\Gamma_2}{D_2} \right)}{(1 + \epsilon)} \quad (6-38)$$

If we solve this equation for  $\Gamma_2$ , we find

$$\Gamma_2 = \frac{N_2}{N_1 + \epsilon N_e} \frac{D_2 \Gamma_1}{D_1} \quad (6-39)$$

If we evaluate this for the values of the example, we find  $\Gamma_1/\Gamma_2 \approx 11.2$ . In comparison, the value of  $\Gamma_1/\Gamma_2$  calculated directly from the fluxes produced by the numerical solution at  $r = 2.5$  cm was 12.1.

*Electron Temperature versus Recombination.* Finally, let us examine the parameterization of electron temperature as a function of the strength of the recombination losses, based on data extracted from the full range of cases examined, not just the extreme example presented in Figures 6-18 and 6-19. We chose to examine the electron temperature



because it depends on the overall response of the plasma to changing conditions, not just on the response of a single species.

We compared the multi-ion temperatures with results from a Galerkin approximation from Belousova (Belousova, 1968). Belousova examined cylindrical single-ion plasmas with single-step volume ionization, recombination, and stepwise ionization. The following diffusion equation results:

$$\frac{d}{dx} \left( x \frac{dy}{dx} \right) + \frac{\nu R^2}{D_a} xy + \frac{(\beta - \alpha) N_0 R^2}{D_a} xy^2 = 0 \quad (6-40)$$

where  $y = N/N_0$ ,  $N$  is the electron density,  $x = r/R$ ,  $R$  is the discharge radius,  $\nu$  is the ionization frequency,  $\beta$  is the coefficient for stepwise ionization,  $\alpha$  is the recombination coefficient, and  $D_a$  is the ambipolar diffusion coefficient. Belousova used a form of the Galerkin method equivalent to assuming that the solution to this equation could be approximated in terms of a series of orthogonal functions, the first of which was  $\phi = \cos(\pi x/2)$ . The next function in the series must be orthogonal to  $\phi$ , which implies that the left hand side of Equation 6-40 with  $y$  replaced by  $\phi$  must be orthogonal to  $\phi$  as well (Belousova, 1968: 337). From this Belousova developed the following relationship:

$$\frac{\nu R^2}{D_a} = 5.830 - 0.734 \frac{(\beta - \alpha) N_0 R^2}{D_a} \quad (6-41)$$

We used this relationship to calculate the temperature of the system, with the stepwise ionization coefficient  $\beta$  set to zero.

Before we compare Belousova's results to our multi-ion calculations, we should note the limitations of Equation 6-41. That equation is derived in

part from an assumption that the form of the solutions is expressed accurately by trigonometric functions, needing only a first-order correction to produce valid results. As we have already seen, this is a poor assumption for high recombination rates. As a result, we view with reservations the exact values of the electron temperature that Equation 6-41 produces for large values of  $\alpha N_0$ . Rather, we use the comparison to indicate the trend as  $\alpha N_0$  increases.

We compared Belousova's results to calculations for systems identical with those presented in Figures 6-18 and 6-19, but with  $\alpha$  changed to vary  $\alpha N_0$ . We used the values appropriate to the recombining gas to perform the single-ion calculations. This is equivalent to assuming that the recombining ion was the only species present. As was true in the case displayed in Figures 6-18 and 6-19, the ionization frequency and recombination rate for both calculations were functions of  $kT_e$ , with the ionization frequency given by von Engel's Equation 11-9, and with the recombination rate having the  $kT_e^{-1.5}$  dependence appropriate to radiative recombination (von Engel, 1965: 164, 293). We included recombination ranging from  $\alpha N_{e0} = 0$  to  $\alpha N_{e0} = 10^7$  Hz, even though this is beyond the range of validity for Belousova's model. This was done to demonstrate the behavior of the temperature in a multi-ion discharge in the limit of high recombination, and to depict the nature of the errors that Belousova's model gives when applied outside its region of validity. We should note that many gases have radiative recombination rate coefficients on the order of  $10^{-7}$  to  $10^{-6}$  cm<sup>3</sup>-s or

slightly higher (von Engel, 1965: 166). Under those circumstances, a value for  $\alpha N_{e0}$  of  $10^5$  is a conservative estimate of the value achievable in real systems. The higher values of this investigation allowed us to look at limiting cases.

Figure 6-20 compares the electron temperatures calculated from Belousova's model to those calculated using a full multi-ion calculation. In both cases, the temperatures are normalized by the values calculated for no recombination. These values were 2.275 and 2.23 eV for the single-ion and multi-ion calculations, respectively. We attribute the small difference to the approximate nature of Belousova's model; it reproduces the Schottky eigencondition within only 0.5% of the Schottky results for the recombination-free case (Belousova, 1968:337). We used normalized values to minimize the effects of these differences. We also include the result of an exact single-ion calculation using the only the first ion species, which does not undergo recombination. The electron temperature produced, 2.67 eV, was normalized by the multi-ion value of 2.23 eV to indicate the limit as the recombining species is eliminated from the discharge.

Figure 6-20 demonstrates the overall behavior expected in any recombining discharge. Increasing recombination implies higher losses, which implies a higher electron temperature to produce more ionization. However, the presence of the second ion changes the limiting behavior of the system. In contrast to the single-ion model, which increases steadily as the recombination rate increases, the multi-ion model saturates at a limit of 2.67 eV, which is the value that would result if the second ion were not present at all.

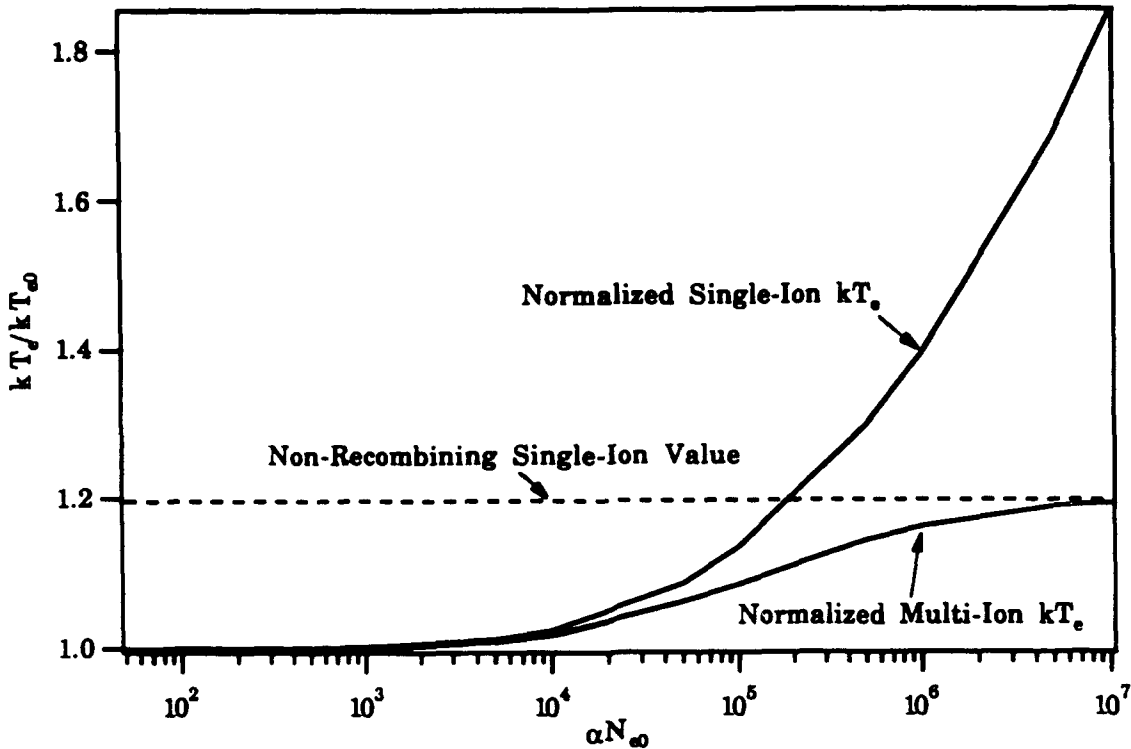


Figure 6-20. Effect of Increasing Recombination on Electron Temperature for Single and Multi-Ion Models

Let us examine the approach to that limit. With no recombination present, the single-ion model produces a temperature within 2% of that of the multi-ion model. The ratio of ionization frequency to diffusion coefficient  $\nu/D$  for the second species is larger by a factor of 25 than that of the first species. Thus, the second species controls the discharge, producing temperatures very close to what Belousova's single-ion expression gives. For small amounts of recombination, the two calculations remain in reasonably close agreement. Even at  $\alpha N_{e0} = 10^4$  Hz, the two are in fairly close agreement, with Belousova's value being 2.33 eV *versus* 2.27 eV. For this level of recombination, the ratio of the net source to diffusion coefficient for the second species is still over three times  $\nu/D$  for the first species.

Therefore, the second species still has the largest influence on the electron temperature. By the time we reach  $\alpha N_{e0} = 10^5$  Hz, the situation has changed. Now, the net source to diffusion ratio for the second species is less than the corresponding ratio  $v/D$  for the first species. As a result, the temperature is controlled more by the first species than the second, and the single-ion and multi-ion values diverge. At this point, the value for  $\alpha N_{e0}$  is still achievable in realistic discharges. Belousova's model may or may not be valid, due to the approximations discussed above. Belousova's model produces a temperature of 2.58 eV in contrast with the multi-ion value of 2.42 eV. As recombination in the multi-ion system increases, species 2 plays even less of a part in the determination of the electron temperature, and the temperature is now controlled by species 1, which undergoes no recombination. Eventually, the temperature saturates at 2.67 eV. For the single-ion case, it is no longer clear that Belousova's model is still valid. In any case, since species 2 is the only ion in the system, the temperature must rise dramatically to compensate for the increased recombination losses of species 2.

From this investigation, we conclude that a single-ion model such as Belousova's can give reasonably accurate values for the electron temperature, as long as the recombining ion species is the dominant species in the plasma.

*Deviations from Proportionality.* In Figure 6-21 we show  $1/\beta_1$  as a function of  $\alpha N_{e0}$ , at a pressure of 1 T. We show  $1/\beta_1$  instead of  $\beta_1$  in order to maintain a consistent standard of higher values implying more nonpropor-

tionality. The results are consistent with our results for other cases; as the nonlinear term increases, so does nonproportionality. Similar results are obtained at other pressures.

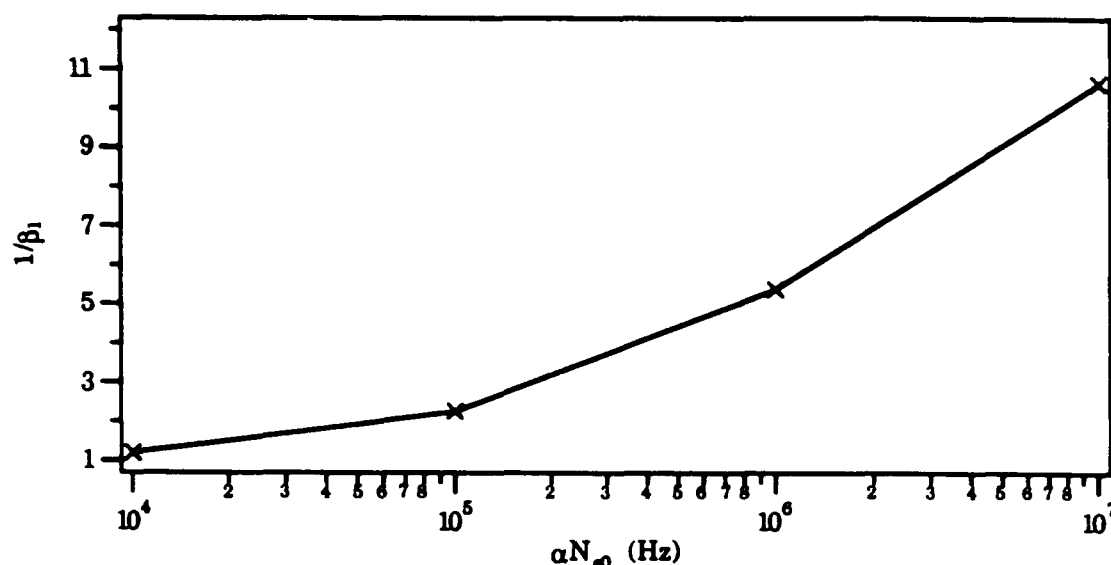


Figure 6-21. Deviation From Proportionality *versus* Recombination; 1 T

In Figure 6-22 we show  $\beta_2$  as a function of  $\alpha N_{e0}$ , at a pressure of 1 T. These results are also completely consistent with what we observed in the external source cases. Again, similar results obtain at other pressures.

*Conclusions.* Let us now restate the conclusions we reached for the case of volume sources with recombination.

1. Although sufficient recombination can cause the number densities to appear as if the discharge contained only a single species, it is still possible for the fluxes of both species to be significant.
2. As in the external source cases, the ion species with a volume loss term assumes a relatively flat profile if the losses are high enough. However, unlike the external source-recombination case, we never saw the densities increasing from the center to the edge of the discharge. We were able to determine a condition to indicate when (if ever) such a rise would occur, but were unable to determine if it could be satisfied.

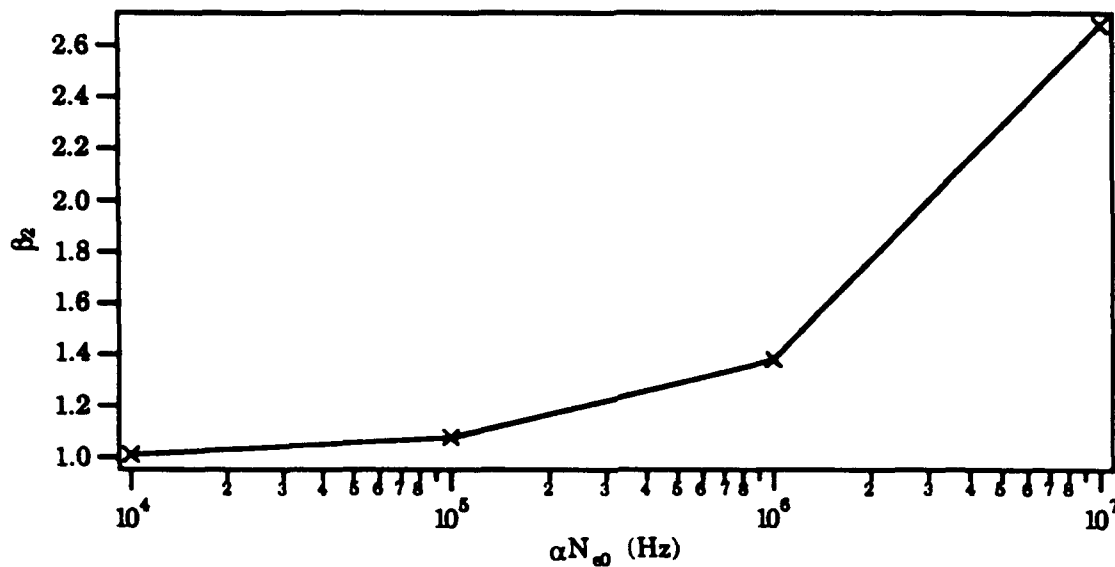


Figure 6-22. Deviation From Proportionality *versus* Recombination; 1T

3. As is the case for single ion diffusion with recombination, the electron temperature scaled in a manner reflecting the changes in the losses as recombination or pressure changed. As recombination increased or pressure decreased, the losses to recombination or diffusion, respectively, increased. These increased losses required increased ionization, implying higher electron temperatures.

*General Result.* All three of the investigations of generic plasmas presented criteria for existence of an off-axis maximum in ion density. Those criteria can be generalized to a form that is applicable for the cylindrical geometries examined here and planar and spherical geometries in addition. In fact, the derivation is geometry-independent, except that the geometry chosen must lead to  $\gamma$  and  $\nabla n$  being zero at the center of the discharge. The dimensionless form of the system will be used, to simplify the derivation.

The dimensionless momentum and continuity equations for some ionic species  $i$  are

$$\nabla n_i = -\vec{\gamma}_i + \frac{n_i}{n_e} \frac{\sum_j \vec{\gamma}_j \cdot \vec{\gamma}_e}{1 + \epsilon}$$

$$\nabla \cdot \vec{\gamma}_i = s_i \quad (6-40)$$

Here,  $s_i$  is the most general form of the dimensionless source term, including both external and volume sources. Taking the divergence of the momentum equation:

$$\begin{aligned} \nabla^2 n_i = & -\nabla \cdot \vec{\gamma}_i + \frac{\nabla n_i}{n_e} \frac{\sum_j \vec{\gamma}_j \cdot \vec{\gamma}_e}{1 + \epsilon} \\ & - \frac{\nabla n_e n_i}{(n_e)^2} \frac{\sum_j \vec{\gamma}_j \cdot \vec{\gamma}_e}{1 + \epsilon} \\ & + \frac{n_i}{n_e} \frac{\sum_j \nabla \cdot \vec{\gamma}_j - \nabla \cdot \vec{\gamma}_e}{1 + \epsilon} \end{aligned} \quad (6-41)$$

At the center of the discharge,  $\nabla n$  and  $\gamma$  are both zero. Evaluating Equation 6-41 on axis, and replacing  $\nabla \cdot \vec{\gamma}_k$  with  $s_k$ , produces the following expression for  $\nabla^2 n$ :

$$\nabla^2 n_i = -s_i + \frac{n_i}{n_e} \frac{\sum_j s_j - s_e}{1 + \epsilon} \quad (6-42)$$

Since  $\nabla n_i$  is zero at the axis,  $\partial^2 n_i / \partial \rho^2$  can be expressed in terms of  $\nabla^2 n_i$  at  $\rho = 0$  for planar, cylindrical, or spherical geometries:

$$\frac{\nabla^2 n_i}{(1+m)} = \frac{\partial^2 n_i}{\partial \rho^2} \quad (6-43)$$

The index  $m$  is 0, 1, or 2 in planar, cylindrical, or spherical geometries. Since  $1+m > 0$ , for  $n_i$  to have a positive curvature and thus be increasing at



0,  $\nabla^2 n_i$  must be greater than zero. Setting  $\nabla^2 n_i = 0$  and rearranging Equation 6-42 produces

$$\frac{\epsilon n_e + \sum_{j \neq i} n_j}{n_i} < \frac{\sum_{j \neq i} s_j - s_e}{s_i} \quad (6-44)$$

Or, for two ion species:

$$\frac{\epsilon n_e + n_j}{n_i} \leq \frac{s_j - s_e}{s_i} \quad (6-45)$$

Finally, invoking the small-e-flux approximation produces a condition that, if met, implies that  $n_i$  will rise to an off-axis maximum:

$$\frac{(1+\epsilon)n_e - n_i}{n_i} \leq \frac{s_j}{s_i} \quad (6-46)$$

This is the form that led to Equations 6-21, 6-31, and 6-38. We should note the differences in the form of the right hand side of Equation 6-21 *versus* Equations 6-31 and 5-38. Equivalent to Equation 6-21, which dealt with recombination and external sources, we have

$$\frac{(1+\epsilon)n_e - n_2}{n_2} < \frac{s_1}{s_2 - a_2 n_2 n_e} \quad (6-47)$$

For Equation 6-31, which dealt with external sources and charge transfer, we find the equivalent dimensionless form is

$$\frac{(1+\epsilon)n_e - n_1}{n_1} < \frac{s_2 + f_{c2} n_1}{s_1 - f_{c1} n_1} \quad (6-48)$$

Here,  $f_{ci}$  represents the dimensionless charge transfer frequency for the source term for species  $i$ . Finally, for Equation 6-38, which dealt with volume sources and recombination, we find

$$\frac{(1+\epsilon)n_e - n_2}{n_2} < \frac{f_1}{f_2 - a_2 n_2} \quad (6-49)$$

Equations 6-47, 6-48, and 6-49 differ only in their right hand sides. The left hand sides are identical except for a trivial reindexing of species. In Equation 6-47, which describes the only case where we saw positive curvature, all terms are either independent of number density or have a quadratic dependence on the number density. In Equations 6-48 and 6-49, the terms that depend on number density vary linearly, not quadratically.

We were unable to determine if the conditions of Equation 6-46 could be achieved in real discharges. The value of  $\alpha N_{e0}$  required to produce the effect shown in Figure 6-7 is  $8.6 \times 10^6$  Hz, and corresponds to a recombination rate coefficient of the order of  $10^{-5}$  cm<sup>3</sup>/s, even at an electron number density of  $10^{12}$ /cm<sup>3</sup>-s. Such high values are difficult to achieve simultaneously in a discharge. In addition, if the effect could be achieved, it might be difficult to detect. At present, we can but point out the possibility of an off-axis maximum being observed in real discharges.

### *Summary of Results*

At this time we will summarize the results of this chapter. We will do so in the same order as the material was presented in the chapter itself; first the results of the verifications, then new results from our investigation of quasi-realistic gases. In most cases this summary will be an abbreviated version of what was presented in the chapter. However, there will be occasions where we will collect results of several investigations and form a more general conclusion.

*Comparisons.* In general, we found that the results our new model produced were consistent with previous experimental and theoretical

investigations. In all cases the differences, if any, either could be ascribed to features of the system we chose not to model, or to experimental error.

Our model produced extremely close agreement with Wunderer's results, and in considerably fewer calculations. Wunderer used an ambipolar model based on Schottky's assumptions of quasi-neutrality and congruence. That is a different starting point than the present model, and leads to significantly different differential equations. In addition, the geometry and kinetics of the calculation were fairly complicated. Under those circumstances, it is unlikely that two different calculations could fortuitously produce the same results. Therefore, we conclude that both models correctly describe the physical situation, within the constraints imposed by the assumptions implicit in the models.

Our model also produces exact agreement with Young's electron temperature calculations and with the experimental measurements of Labuda and Gordon, for He-Ne mixtures ranging from pure helium to pure neon. Although the results of the two calculations are the same, the process used to arrive at them is different. It appears that the model Young used was based on assuming proportionality in the discharge. In the present case the assumption of proportionality was not required. In fact, the same algorithm that was used for the Young comparisons was also used throughout the numerical research to calculate complete solutions to highly nonproportional systems, including calculations of the electron temperature.

Finally, we were able to use our model to develop a simplified description of Schmidt's contaminated nitrogen discharge. We were able to predict the

overall behavior of Schmidt's discharge with a very simple  $N_2^+-N_4^+$  model. The results of that model revealed discrepancies between the model's description of the relationship between electron fluxes and temperature and Schmidt's measurements of the same quantities. We were able to provide a reasonable explanation of the discrepancies by showing that even small amounts of  $H_2$  led to a system that was dominated by  $HN_2^+$  produced by charge transfer from  $N_2^+$ .

*General Plasma Systems.* Next we wish to summarize the results that our investigations of three quasi-realistic plasmas produced. We will first discuss general conclusions that can be drawn for all three investigations, and then summarize individual results.

We found a general relationship that established conditions for the occurrence of off-axis maxima in an ion density:

$$\frac{\epsilon n_e + \sum_{j \neq i} n_j}{n_i} < \frac{\sum_{j \neq i} s_j - s_e}{s_i} \quad (6-44)$$

We found this relationship satisfied for one system, that of external ionization with extreme recombination. In this system we observed off-axis maxima for conditions consistent with Equation 6-44. In no other systems was Equation 6-44 satisfied, nor were off-axis maxima observed in any other systems. We were unable to determine if Equation 6-44 could be satisfied for a realistic discharge, or if any maximum that resulted would be detectable.

The relationship between nonproportionality and magnitude of the "nonproportional" source terms was similar for all three cases; the more the nonproportional source term, the more nonproportional the system was by at least one measure. There were cases where one ion density was

proportional, but the fluxes and the system as a whole were not. This illustrates the difficulties in determining a consistent, all-encompassing measure of proportionality. Quantitative measures of nonproportionality are very situation-specific. We used a single set of measures for all three cases, to provide a common ground for comparison. In practice, it would be more beneficial to tailor measures to the specific system being examined.

For the external source-charge transfer example, we found that the parameters  $S_k/p$  and  $vN_1/S_1$  serve somewhat as similarity parameters; any two discharges for which these are equal will have the same spatial dependencies. For sufficient charge transfer, the discharge acts as a single ion discharge, in that the electron and dominant ion parameters were the same as those of a single ion discharge whose ion source term was equal to the total ion source term of the actual system, and in that the second ion was almost completely eliminated from the discharge. However, the spatial dependencies of the particle density and flux of the minority ion could not be described by the Schottky solutions.

For the system involving volume source terms and recombination we saw a significant difference in the behavior of the fluxes from the charge transfer case; even if the particle densities were dominated by a single ion, the fluxes for both species could still be significant. The fluxes could decrease near the edge of the plasma, confirming the similar result that the  $J_1$  Schottky solutions produce. Finally, the electron temperature behaved predictably and in accordance with single-ion diffusion theory; as pressure decreased or recombination increased, the electron temperature

increased so that higher ionization rates could offset the increased diffusion or recombination losses.

## *VII. Conclusions and Recommendations*

### *Introduction*

This research has presented a new approach and model for multi-ion ambipolar diffusion. The model provided a number of individual results, including analytic solutions for some systems, numerical solutions that expanded on previous experimental or numerical results, information about scaling in multi-ion systems, and the effects of minority gases in a discharge. Those individual results allow the synthesis of an important result; criteria now exist for determining when multi-ion ambipolar diffusion discharges may be adequately described using single-ion models, when proportional multi-ion models may be used, and when full nonproportional multi-ion models must be used.

This chapter provides those criteria in the form of decision trees that guide the process of determining the level of detail required to describe multi-ion ambipolar diffusion discharges. It also summarizes the contributions to research in multi-ion discharges made by this investigation and provides recommendations for future research in multi-ion discharges. It emphasizes the new results, and only discusses previous research in the context of comparison to the new results. The discussion of the criteria is presented and then followed by a discussion of the resolution of the problems initially identified in Chapter II. Suggestions for future directions of research come last.

### *Regime of Validity of Ambipolar Diffusion*

Forrest and Franklin addressed the topic of the validity of various plasma models, including ambipolar diffusion, in great detail (Forrest and Franklin, 1968). They described cylindrical plasma discharges in terms of two dimensionless parameters, which they used to identify the transitions between the various regimes pertinent to plasma discharges.

Because of their need to describe a wide variety of discharges, Forrest and Franklin's two parameters are functions of a number of characteristic plasma values, including ion mass, electron temperature, ionization frequency, ion mean free path for collision, electron Debye length, and ion mobility. However, for our purposes the important points are the physical transitions: from free-fall to collisional plasmas, and from free diffusion to ambipolar diffusion. Forrest and Franklin point out that the transition between free-fall and collision-dominated plasmas starts when the discharge radius is equal to the mean free path for collision (Forrest and Franklin, 1968: 1362). They also imply that the corresponding transition from ambipolar to free diffusion has occurred when the Debye length is comparable to the discharge radius (Forrest and Franklin, 1968: 1361-1362). In both cases, they note that the boundaries "cannot be defined uniquely and with precision" (Forrest and Franklin, 1968: 1361).

If we generalize Forrest and Franklin's results to arbitrary geometries by defining a characteristic physical scale length  $\Lambda$ , we obtain two conditions:

1. The mean free path for collision for each species must be considerably smaller than the smallest characteristic dimension of the plasma:



$$\lambda_{mfp} \ll \Lambda \quad (7-1)$$

2. The Debye length must also be considerably smaller than the smallest characteristic dimension of the plasma:

$$\lambda_D \ll \Lambda \quad (7-2)$$

where  $\Lambda$  can be expressed in terms of a physical length in the discharge.

The first constraint ensures that diffusion is valid to describe the plasma. It is necessary whether or not an ambipolar model is used. The second constraint ensures that the charged particle number density is high enough that the fields produced by the plasma itself are strong enough to affect the motion of the particles. At low charged particle densities, the diffusion is a free diffusion process. If the second constraint is met, the diffusion process is ambipolar diffusion.

A further condition used in this research is that the change in species temperature across the discharge must be small. This condition is the result of neglecting the  $N\nabla kT$  term that arises from expressing the gradient of the charged particle species pressure in terms of  $\nabla(kTN)$  when developing the momentum equation. The question of spatial temperature variation has been addressed by previous authors. Cohen and Whitman, who address volume ionization, recombination, and thermal energy balance in the positive column of a single-ion plasma, also give a review of previous efforts in this area (Cohen and Whitman, 1973). Rather than completely investigate the effects of thermal gradients in this work, we point out that for any species (charged or neutral) the neglect of  $N\nabla kT$  is valid if  $(kT(0) - kT(1))/\langle kT \rangle$  is much less than one, where  $\langle kT \rangle$  is the

average value of  $kT(r)$ . The validity of this assumption depends very strongly on the details of the gas species kinetics and boundary conditions, since the gas kinetics affect the transfer of energy from the electrons to the neutrals and the boundary conditions describe the influence of the discharge walls on the temperature of the discharge. Thus, it is impractical to draw conclusions about the validity of this neglect without addressing a specific system. However, we can point out that the temperature gradient is controlled by the ratio of two quantities:

$$\nabla T \propto \frac{j \cdot E}{\kappa} \quad (7-3)$$

where  $j \cdot E$  is the total thermal energy deposited into the plasma, and  $\kappa$  is the thermal conductivity. For convenience, we can consider  $j$  to be fixed (as it often is in glow discharges). In that case, the magnitude of the electric field is determined by how much of the energy the electrons gain from the field is applied to ionization. For instance, consider a species with large cross-sections for excitation. The excitation extracts a significant fraction of the total discharge energy to populate the corresponding excited states. This energy is not available to produce ionization, and the ionization is less efficient. Examples include molecular gases, with low-lying vibrational and rotational states. Such gases typically require higher fields, and therefore have higher Joule heating, than atomic gases. The rate at which energy is removed from the plasma is controlled by the thermal conductivity of the gas, with boundary condition effects as well. As an example, a discharge in a molecular gas of low thermal conductivity, with walls maintained at a fixed temperature by a cooling water jacket, is a good

candidate for significant temperature gradients. On the other hand, a discharge in an atomic gas of high thermal conductivity, in a vessel with insulated walls, is less likely to have significant temperature gradients.

No further conditions are necessary for the model developed in this research to be valid; in the general form presented in Equation 3-7 the present model holds wherever any other single-ion or multi-ion ambipolar diffusion model of a uniform-temperature plasma is valid. Examples can be drawn from laboratory plasmas, lighting discharges, plasma processing reactors, and electric discharge lasers.

To determine whether a particular system can be described by an ambipolar diffusion model requires evaluation of the Equations 7-1 and 7-2 in terms of quantities that are experimentally accessible. In general, Equation 7-1 can be evaluated by considering the product  $pL$  of the pressure and plasma physical size. The mean free path for collision is given by  $\lambda = 1/\sigma N_{bg}$ , where  $\sigma$  is the total cross-section for collision, and  $N_{bg}$  is the background gas pressure. The pressure is given by  $p = N_{bg}kT_{bg}$ , producing the following relationship equivalent to Equation 7-1:

$$pL \gg \frac{kT}{\sigma} \quad (7-4)$$

For typical gases,  $\sigma$  is on the order of  $10^{-15} \text{ cm}^2$  for both ions and electrons (Mitchner and Kruger, 1973:102-110). Using a value on the order of  $300^\circ\text{K}$  for the background gas temperature allows evaluation of Equation 7-4:

$$pL \gg 0.3T\text{-mm} \quad (7-5)$$

Equation 7-2 can also be evaluated. The electron Debye length is

$$\lambda_D = \sqrt{\frac{\epsilon_0 k T}{N e^2}} \quad (7-6)$$

With this definition, Equation 7-2 can be re-written:

$$NL^2 \gg \frac{\epsilon_0 k T_e}{e^2} \quad (7-7)$$

Using a value of  $kT_e = 1$  eV, which was shown in this research to be a typical measure of the electron temperature for many plasmas, produces the following constraint:

$$NL^2 \gg 5.5 \times 10^5 / \text{cm} \quad (7-8)$$

Equations 7-5 and 7-8 can be met for a variety of systems. For instance, consider a one cm diameter discharge plasma. Evaluation of Equation 7-5 indicates that the two sides of the expression are equal at a pressure of 0.06 Torr, implying the validity of a collisional description in this geometry for pressures much greater. For the same discharge, expressing Equation 7-8 as an equality produces a lower bound at an electron density of  $2.2 \times 10^6 / \text{cm}^3$ . This implies ambipolarity for fractional ionizations  $N_e/N_{bg}$  down to a lower limit of  $10^{-9}$ , for the lower bound pressure of 0.06 Torr. Both Equations 7-5 and 7-8 are easily met in typical laboratory plasmas, as well in other systems (Mitchner and Kruger, 1973: 56. Chen, 1984: 12-14. von Engel, 1965:241).

#### *Criteria for Determining an Appropriate Multi-Ion Model*

Having established the conditions under which ambipolar diffusion is valid, it remains to determine how complex a model must be used for an adequate description of a particular system. The results of this research provide the criteria necessary to make such a determination. Evaluation of

the criteria requires knowledge of the specific system being investigated. Such knowledge might be available from experimental results or from previous calculations. In the absence of the information necessary to evaluate a particular effect, it would be necessary to assume the effect to be significant.

Figures 7-1, 7-2, and 7-3 provide a recursive decision tree that selects the proper method to describe an ambipolar discharge containing electrons and positive ions. In general, there are four methods. From most general to least general, they are

1. A full multi-ion ambipolar model, as defined by the continuity equations in Equation 3-8 and the momentum equations of Equation 3-10. This model usually requires numerical solution of the differential equation system. This was the model used for the numerical solutions of Chapter VI.
2. A proportional multi-ion model. Such models take advantage of any proportionality present in the discharge, but still use a set of continuity and momentum equations that couple the various species. For most geometries this model can be solved analytically with the possible exception of the determination of the electron temperature. An example of this model would be the PT case of Chapter V, where charge transfer coupled the various species together and required solution of all the equations to produce an answer. Other examples would be the electron temperature comparisons Chapter VI, where determination of the electron temperature required incorporation of information on all the species into the numerical solution.
3. Use of the multi-ion ambipolar diffusion coefficients defined by  $D_a = D_i(1 + T_e/T_i)$ , with each ion species modelled independently of the others. The difference between this method and the previous method is that the momentum and continuity equations for the each ion only include transport coefficients for and functional dependencies on that ion. As a result, only those species for which information is required need be modelled.
4. Single-ion ambipolar diffusion, as first developed by Schottky for simple volume ionization only (Schottky, 1924). In the form presented by Schottky, this method produces closed form analytic solutions for most systems. Numerical methods may be needed if the system contains both external and volume sources, if recombination is significant, or to calculate  $kT_e$ .

Multi-step ionization was not discussed in detail in this research. Therefore, it is not addressed in the decision tree, either. Multi-step ionization can be approximated by a source term quadratic in the number densities, as will be discussed later. In that formulation it can be treated in the decision tree exactly the same as recombination, since it is the quadratic number density dependence of recombination on the number densities that affects which decision to make.

*Basis for Evaluating Decisions.* The basic question in each step of the decision tree involves the significance of some effect in the plasma. Generally, the significance involves comparing two source or loss terms, either for two different species, or for the same species. In all cases, the actual comparison is the source or loss term divided by the corresponding diffusion coefficient.

The tree depicts each decision as a binary choice, when it actually involves a range of significance. As the tree is described, criteria for determining how to make the decision will be discussed. In general, the criteria were developed by a comparison of the ratios of the on-axis number densities in the numerical solutions. If the effect in question changed any of the ratios  $N_i/N_e$ , by 10% or more it was considered significant. In some cases there is no decisive theoretical guidance available to determine the significance of an effect. In such cases it is often possible to at least describe the type of information that would be needed to make the determination.

In general, the comparisons involve the relative strengths of ionization, recombination (or other non-linear effects such as multi-step ionization),

and charge transfer. All of these can be expressed in terms of equivalent collision frequencies per electron. For volume sources, the Schottky eigencondition  $(\lambda_0/L)^2 = \nu_i/D_a$  or a multi-ion form as expressed in Equation 5-59 can be used to relate the ionization frequencies to the geometry of the discharge. Here  $\lambda_0$ , appropriate for cylindrical geometries, is the first zero of the Bessel function  $J_0$ ; other values are appropriate for other geometries. For external sources, the ionization frequency can be approximated by  $S_i/N_e$ , where  $S_i$  is the external source for species  $i$ , and where  $N_e$  is determined from the analytic solutions for external sources. The charge transfer frequency is given by  $\nu_{ct}N_i/N_e$ . The normalization by the number densities is needed to compare all frequencies to the standard of charge transfer collision frequency per electron. The equivalent recombination frequency is given by  $\nu_r = \alpha N_i$ , again producing a value for recombining collision frequency per electron. Finally, multi-step ionization can often be described as a quadratic source term  $\alpha_i N_x N_e$ , where  $\alpha_i$  is the collision rate coefficient for ionization of the excited species by electron impact and  $N_x$  is the excited species number density. This produces an equivalent ionization frequency per electron of  $\nu_{xi} = \alpha_i N_x$ . An estimate for  $N_x$  can be made by assuming that volume processes dominate the excited species behavior. If we assume that the dominant processes are excitation, given by  $\nu_x N_e$ ; quenching, given by  $\nu_q N_x$ ; and ionization, we find  $N_x$  can be expressed in terms of the other parameters as  $N_x = \nu_x N_e / (\nu_q + \alpha_i N_e)$ . This produces a

value of  $v_{xi} = \alpha_i v_x N_e / (v_q + \alpha_i N_e)$  . Multi-step ionization will be discussed in more detail later.

We note that knowledge of the electron and ion number densities is required for some of these comparisons. The analysis of proportionality in Chapter IV produced an expression for  $N_i/N_e$  that we will discuss later in this chapter as Equation 7-12. This can be used to determine  $N_i$  exactly for some systems, and to estimate it for others, from the value of  $N_e$ .  $N_e$  can be determined in several ways. One obvious method is experimental measurement, either directly by such means as measurement of the plasma frequency, or indirectly from parameters such as total discharge current. For a proportional externally driven system, analytic solutions similar to those developed in Chapter V as the PX, CX, and PE cases can be used. In addition, there are occasions where the electron temperature is required. This can be determined in one of three ways. First, experimental results can be used. Second, the Schottky eigencondition or a multi-ion equivalent, both of which are plasma-balance equations, can be used to determine the electron temperature. Examples of the multi-ion plasma balance equation are Equation 5-49, which is the most general form, or Equations 5-59, 5-61, 5-69, 5-76, or 5-77, which give examples for particular systems. Finally, there are some circumstances where the plasma-balance equation is satisfied independently of the electron temperature. The simplest example would be a plasma sustained entirely by external sources. In these cases energy balance must be used to determine  $kT_e$ . Because of the repetition that would result, we will not discuss the means of making the compari-



sons in the detailed discussion below. Rather, the methods of this paragraph are implied.

In many cases a decision cannot be made the first time through the tree. In such cases, the correct procedure is to assume the effect is significant. As the tree is traversed recursively, such decisions will be corrected.

Each decision point in the three figures is numbered to reference the discussion following.

*Implementation of the Decision Tree.* Figure 7-1 gives the first part of the tree. The first decision is whether multiple ions produce significant effects in the system. There can be systems where there is truly only a single species present. In other cases, the analytic solutions available from this model can be used to show that only one species is significant, even though others are possible. The pertinent analytic result is that, for proportional systems, the ion number densities are proportional to  $S_i/D_i$ . If that ratio for a particular species is much greater than for any other species, and if there are no other effects that invalidate proportionality, then the other species can be neglected. In most cases, however, the initial answer will be that the multiple ions are significant. As the tree is traversed, it is possible to arrive at points where one species is neglected and the tree re-entered. Eventually, all species but one may be eliminated. This would lead to a decision at step 1 that multiple ions are not significant.

If multiple ions are not significant, the next decision at step 2 involves the significance of non-linear effects, in particular recombination. The effects of recombination in single-ion discharges have been addressed by other authors. In general, the significance of recombination can be

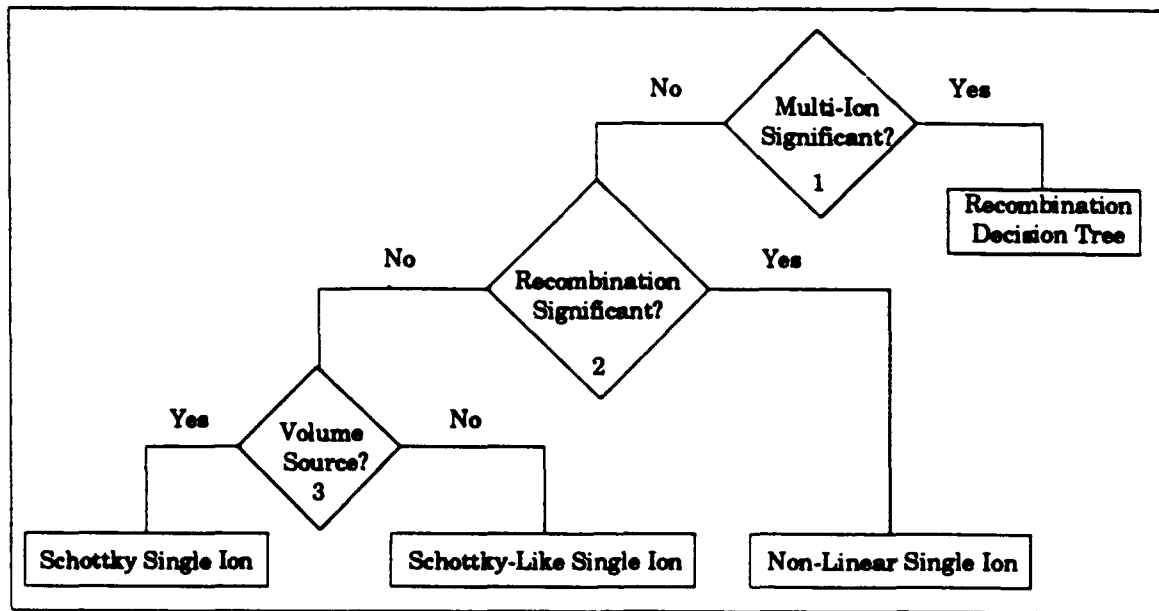


Figure 7-1. Initial Decision Tree for Multi-Ion Models

expressed in terms of a comparison of the strength of the source term *versus* the recombination term. This leads to results such as that of Solunskii and Timan, who used a series expansion to address recombination in single-ion volume source discharges (Solunskii and Timan, 1964). They produced a expression giving the relative importance of diffusion versus recombination:

$$\frac{N_{\beta}}{N_D} = 0.11 \frac{\beta R^2}{D_a} N_{e0} \quad (7-9)$$

where  $N_{\beta}$  is the loss rate due to recombination,  $N_D$  the loss rate due to diffusion,  $N_{e0}$  the on-axis number density, and  $\beta$  the recombination rate coefficient (Solunskii and Timan, 1964: 209). Solunskii and Timan's results indicate that electron losses to recombination are on the order of 10% of the diffusion losses when the on-axis ratio of recombination frequency to effective diffusion loss frequency  $\beta N_{e0}/(\lambda_0^2 D_a/R^2)$  is 15%. The numeric

calculations from this research are consistent with Solunskii and Timan in that they indicate recombination to be significant when the recombination frequency is 10% or more of the ionization frequency for a particular species.

For sources other than simple volume ionization, such as external sources, the Schottky eigencondition may not hold. In those cases, a direct estimate must be made of the strength of the recombination loss term. In many cases, the analytic solutions available for recombination-less discharges can be used. For instance, for a uniform external source in cylindrical geometry, the single-ion equivalent of the solutions from the CX case in Chapter V can be used to determine the on-axis values for the electron number density  $N_e$  and ion number density  $N_i$  (which will, of course, be equal for the single-ion case). The source term  $S_i$  can then be compared to the recombination loss term  $\alpha N_i N_e$ . Since the values of  $N_i$  and  $N_e$  will both be lower with recombination present than the CX case would produce, this comparison provides a conservative evaluation of the significance of recombination.

If effects such as recombination, multi-step ionization, or a combination of external and volume sources are determined to be significant, then Schottky's original model is inappropriate. Using Schottky's model under such circumstances can produce inaccurate values for measurable parameters such as the total discharge current, electron temperature, and electric field. The ionization frequency depends exponentially on the field or temperature. As a result, small changes in the field or temperature can accommodate required changes in the ionization frequency. Therefore, the

field and temperature will be fairly insensitive to departures from a pure volume source. Calculations of the total discharge current depend on correct values of the drift velocity of the electrons and correct integration of the number density as a function of position. The drift velocity is often a monotonic increasing function of the longitudinal field. Incorrect spatial profiles cause errors in the integration of the number density. The combination of the drift velocity dependence and errors in the number density can cause the current to be more sensitive than the field or temperature.

If none of these effects are significant, then the discharge can be modelled by Schottky's original ambipolar diffusion model, using volume sources, external sources, or both, as appropriate (Step 3). Neglect of external sources for simple volume sources produces the same solutions Schottky found. Neglect of volume sources for proportional external sources produces the single-ion equivalents to the various external cases PX, CX, and PE discussed in Chapter V. If both types of sources are present, the results will correspond to none of the solutions presented here. This research did not investigate systems with combined external and volume sources. Therefore, no firm conclusions can be drawn with regard to when one type of source term can be neglected, relative to another. In general, however, it is necessary to compare the strength of the two source terms. The simplest such comparison is to compare the ionization frequencies, not the overall source terms. The volume ionization frequencies are determined from the plasma balance equation, assuming no external sources. The external ionization frequency is written as  $S_i/N_e$ , where  $S_i$  is

the external source term, and  $N_e$  is the electron number density determined from the analytic solutions assuming no volume sources. This formulation is advantageous because it avoids the necessity of determining the electron number density for volume ionization.

Figure 7-2 describes the necessary actions if the answer in step 1 was that multiple ion effects were significant. The first decision to make, in step 4, is to determine whether recombination is significant. The numerical results of the volume source and external source recombination cases indicated that recombination can still affect the discharge if the on-axis ratio of the total recombination loss  $\alpha_i N_i N_e$  to source for some species  $i$  is as low as 15%. Once the number densities have been estimated, the decision in step 4 can be made.

If the decision in step 4 is that recombination can be neglected, then Figure 7-3, the charge transfer decision tree, describes the decision process. Otherwise, the algorithm moves to step 5, which addresses the presence of a dominant source for some species  $k$ .

If one species has a source considerably larger than all the others, by one or more orders of magnitude, then the possibility exists that one or more of the minority species can be neglected. Note that the question to be addressed in step 5 is not just the magnitude of the various sources, but the ratio of their magnitudes to their free diffusion coefficients. As was stated at the beginning of the discussion of the decision tree, it is this ratio which is the significant parameter. Up to this point, we have been comparing source and loss terms within a single species, so the diffusion coefficient did not enter into the results. Now, however, we are comparing among

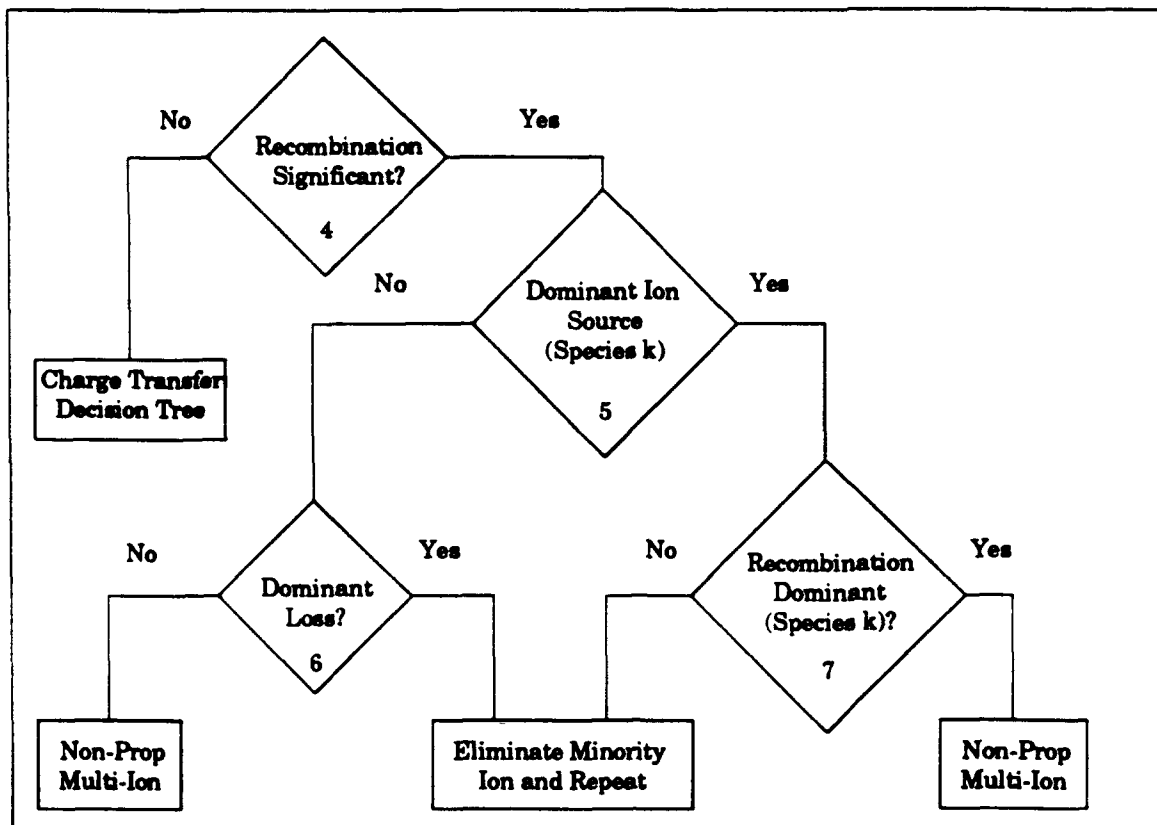


Figure 7-2. Decision Tree for Multi-Ion Recombining Systems

different species, and the distinction among the various diffusion coefficients must be made.

Step 6 addresses the case where no species has a dominant source. The possibility still exists that one or more species have such high recombination rates that they can be neglected. If the recombination of any species is sufficient to reduce its net source to the point that the net source divided by the diffusion coefficient is at least an order of magnitude less than that of the other ions, then the species can generally be neglected. In such cases the decision tree is re-entered at step 1 in Figure 7-1, but with one fewer species. Otherwise, a nonproportional multi-ion model must be used.

Step 7 deals with whether the species with the dominant source also undergoes significant recombination. For this case, the significance of the recombination for the dominant species is determined by the net source, that is, ionization minus recombination, for that species. If the net source including recombination losses divided by the diffusion coefficient is still high enough to dominate the other species, then the dominant species is considered not to have significant recombination for this decision point.

If the result of step 7 is "No", then at least one species has a very small source compared to the dominant species. The minority species can be neglected, and the decision tree re-entered from the beginning with one less species. Otherwise, a non-proportional multi-ion model must be used.

Figure 7-3 is the decision tree for discharges with non-resonant charge transfer possible. The tree starts at step 8, as the result of a "No" decision at step 4 in Figure 7-2. The decision in step 8 is whether charge transfer is significant. Generally, the numerical results indicate that the errors in the number densities or fluxes induced by neglecting small amounts of charge transfer are proportional to the ratio of the charge transfer term to the source term, with a ratio of 10% giving errors of 10%.

This ratio can be estimated using the analytic solutions for either volume or external sources. Since both volume ionization and charge transfer are linear processes with respect to the number densities, the actual number densities are not needed to evaluate the ratio for volume sources. The analytic solutions for external sources provide the number densities, which can then be used to estimate the ratio.

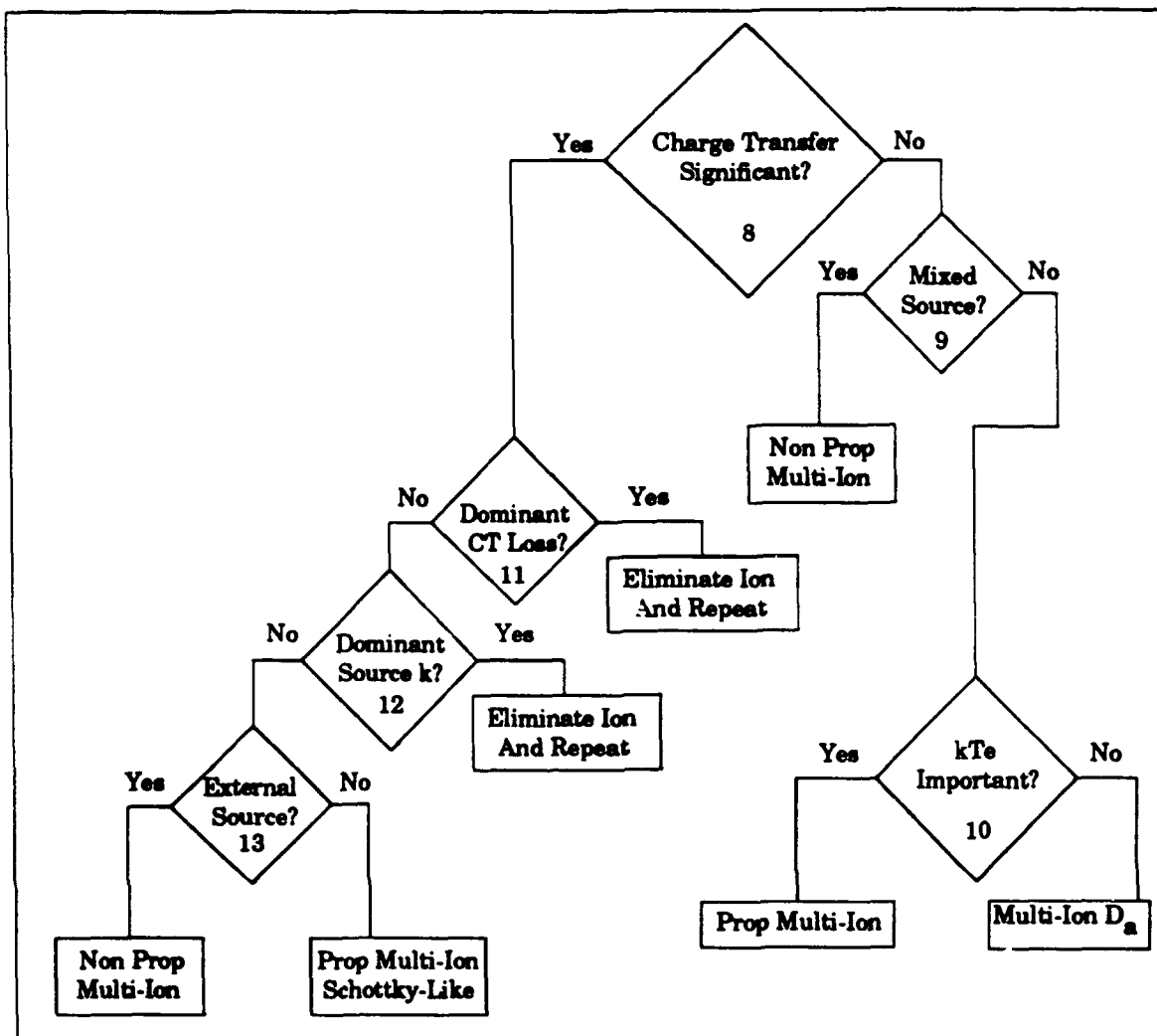


Figure 7-3. Decision Tree for Multi-Ion Charge Transfer Systems

If the answer to step 8 is "No", indicating that no significant charge transfer can occur for the discharge, then the nature of the source terms must be addressed, as in step 9. The question in step 9 can be resolved by calculating the ratio of the source to diffusion coefficient for each process.

This research did not specifically address the question of mixed sources. However, based on the results of the analytic investigations in Chapter V, it is reasonable to neglect a process if its source/diffusion coefficient ratio is an order of magnitude less than that of some other process. If the process-



es left have differing spatial dependencies, then the solutions will be non-proportional, and a full multi-ion non-proportional model must be used. The most common example of this would be a combination of external and volume ionization sources.

Step 10 addresses the case of volume sources only, where calculation of  $kT_e$  must be addressed. Calculation of  $kT_e$  is not always pertinent. An example would be in an experimental discharge, where  $kT_e$  could be measured. If the answer in step 10 is "No", indicating calculation of  $kT_e$  is unnecessary, then the problem resolves into a set of independent Schottky solutions, one for each ion, and with no coupling from species to species. However, if exact determination of the electron temperature is required, then a proportional multi-ion model must be used. In either case the multi-ion ambipolar diffusion coefficient  $D_a = D_i(1+T_e/T_i)$  can be used.

An answer of "Yes" in step 8 indicates that significant charge transfer can occur in the discharge. The question then to be resolved in step 11 is whether the charge transfer rate for any species is high enough that the species can be neglected. Our numerical results indicate that it is reasonable to neglect a species if its estimated charge transfer loss  $v_i N_i$  is at least equal to its source, where  $N_i$  is calculated by assuming no charge transfer. Note that both  $N_i$  and the estimated loss will be higher than the actual values. If the species can be neglected, then the decision tree is re-entered with that species eliminated. Note, however, that there must be adjustments to the total source for the recipient of the charge transfer. The effective source for the gaining species is its original source, plus the source for the species that is being eliminated. If several species gain in

the charge transfer process, then the sources for those species are adjusted proportionally.

In step 12 we address the question of whether any species  $k$  has a source to diffusion coefficient ratio at least an order of magnitude greater than that of the other species. If the total source for species  $k$  (ionization and charge transfer) divided by its diffusion coefficient is at least an order of magnitude larger than the net source (ionization and charge transfer) divided by diffusion coefficient for some minority species, then that minority species can be neglected. In that case, the decision tree is re-entered at step 1 in Figure 7-1, with any charge transfer losses of the neglected species being allocated as sources for the gaining species.

If no species can be neglected as the result of step 12, then in step 13 it is necessary to determine if any species has a significant external source term. If the only source terms are external, then the system will be non-proportional, and a non-proportional multi-ion model must be used. The present research did not investigate combined external and volume sources with charge transfer present, and so no firm conclusions are available about the criterion for significance of the external source compared to any possible volume sources. However, the external source term is independent of number density while charge transfer and volume ionization are both linear in the number densities. Therefore, it is reasonable to compare the external source to the combination of volume source and charge transfer source (or loss, as appropriate). If that combination divided by the appropriate diffusion coefficient is much greater than the external source divided by the diffusion coefficient, then the external source may be neglected, and

a proportional multi-ion model may be used. In this case the solutions will resemble the single-ion Schottky solutions. If the external source cannot be neglected, a non-proportional multi-ion model must be used.

### *Results of the Investigation*

A new approach to ambipolar diffusion has been developed, that involves a slightly different set of assumptions from more traditional models. In its most general form, this new model can describe any temperature gradient-free quasi-neutral collisional plasma. In particular, the most general form of the new model includes positive or negative ions of any state of charge, arbitrary species temperature, and arbitrary source terms. The model was used to examine systems containing electrons and positive ions, with all the ions at the same temperature. We analyzed the implications that this model has for the concept of proportionality, and developed a number of solutions, both analytic and numerical. The model gave good agreement with previous theoretical and experimental investigations.

*Summary of Results.* The research produced a consistent description of the behavior of quasi-neutral multi-ion plasmas:

1. It is possible to exert some control of the discharge temperature by introducing a minority species that has a higher diffusion coefficient than the background species and a source that includes charge transfer from the dominant species. This is a consequence of the multi-ion version of a plasma-balance condition that requires a balance between the ionization source and the total losses. The present model duplicates the single-ion version of the plasma-balance equation, which is Schottky's eigencondition (Schottky, 1924). The model also presents a multi-ion version in Equations 5-59 and 5-76 that reduces to Young's plasma-balance expression for cold ions and explains portions of Schmidt's experimental results (Young, 1965. Schmidt, 1965).

2. Knowledge of the spatial behavior of the source terms is sufficient to determine whether a system is proportional. If the system is proportional, then the relative magnitudes of the various particle densities, and of the various fluxes, can be determined from Equations 4-11 and 4-13 without determining the complete solutions.

3. As expected, the model predicts that systems whose number densities are proportional will have fluxes and net source terms that are proportional as well.

4. The spatial dependence of the ambipolar electric field is insensitive to the multi-ion nature of the discharge. In fact, for the proportional discharges of Chapter V, the spatial dependence of the field is identical for both single and multiple ions. However, as in single-ion ambipolar diffusion, the field is still sensitive to such effects as recombination, and to the electron temperature.

5. A number of scaling relationships were demonstrated. In several cases, these relationships duplicated or were straightforward extensions of the corresponding relationships for single-ion diffusion; any other result would have been suspect. However, new expressions giving the ratio of the number densities and fluxes for proportional discharges were developed as Equations 4-11 and 4-13.

*Proportionality.* We briefly restate the conditions under which the species density profiles will have the same spatial dependence, and then discuss the implications that those conditions have for the scaling of discharge parameters.

*Requirements for Proportionality.* There are a number of equivalent statements of proportionality, starting with the definition:

$$N_i = K_i N_e \quad (7-10)$$

Here,  $K_i$  is the constant of proportionality.

For those systems which contain only electrons and positive ions with the same ion temperature for all species, and for which the Schottky boundary conditions are a reasonable choice, sufficient conditions for proportionality are

$$\frac{\frac{\nabla \cdot \Gamma_i}{D_i}}{\sum_j \frac{\nabla \cdot \Gamma_j}{D_j}} = K_i \quad (7-11)$$

$$\frac{\frac{\Gamma_i}{D_i}}{\sum_j \frac{\Gamma_j}{D_j}} = K_i$$

Equation 7-11 is the most significant result of the analysis of proportionality. It provides a criterion to eliminate the possibility of a system being proportional, as well as stating that the flux or source for each proportional species has the same spatial dependence as the sum of the fluxes or sources for all species. In practice, a very large number of situations of practical interest satisfy Equation 7-11, or come very close. Many of these systems have been shown to be proportional, and we expect them all to be. Mathematically, except for pathological cases with no practical application, all these situations of practical interest are equivalent to one of two cases:

1. The only sources or losses for any species are external sources, and those sources are proportional in the sense that all the sources have the same spatial dependence. Examples include all the external source cases of Chapter V.
2. The only sources or losses are generalized volume sources, with all net sources having the same dependence on the number densities. Examples include the volume source cases of Chapter V, as well as the volume source-charge transfer case. A less common example would be a discharge with sources dominated by multi-step ionization, and the only volume losses being recombination. In such cases, the volume sources and losses would all be quadratic in the number densities, that is, with  $N_e^2$  or  $N_e N_i$  dependence, and proportional solutions would be possible.

Equation 7-11 can also be used to show that analytic solutions for multi-ion diffusion can be obtained through two different procedures:

1. The analytic solution can be found without assuming proportionality, as in the PX, CX, and PE examples of Chapter V.
2. The form of the source term can be used to show that proportionality is allowed and what the constant of proportionality must be, as in the PT example of Chapter V.

*Applications of the Proportionality Conditions.* Having restated the conclusions from Chapter IV, let us discuss how those conclusions addressed the problems of Chapter II.

Equation 7-11 provide a concise statement of when proportionality is possible. In particular, the first expression in Equation 7-11 provides a means of ruling out proportionality prior to attempting to describe a physical situation. In fact, much of the structure of the decision trees is based on applying Equation 7-11 to the various combinations of external and volume sources, charge transfer, and recombination examined in this research.

Now, consider the information that proportionality provides in determining solutions. Prior to the present effort, the assumption of proportionality was sufficient by definition to guarantee that the number densities would have the same spatial dependence, but provided no more information about the solutions. However, the relationships in Equation 7-11 change that. Even before solutions are known, the ratios of the various number densities to the electron density and of the various fluxes to the electron flux can be determined. An example is the analysis of the volume source plus charge transfer PT system in Chapter V. The equivalent of Equation 7-11 was used to show that the ratios of the number densities were constant prior to determining the solutions. The value for  $K_i$  determined from

Equation 7-11 was then used as part of the process of solving the system of differential equations.

In addition to using proportionality to determine solutions of the differential equations, it is possible to use proportionality to simplify the system of differential equations. Recall the discussion in Chapter IV of the definition of ambipolar diffusion coefficients for the not uncommon case of proportional systems of positive ions at the same temperature where the electron mobility is much higher than the ion mobility. Summarizing the results of Equations 4-28 through 4-32, the momentum equations become

$$\Gamma_i = -D_i \left( 1 + \frac{T_e}{T_+} \right) \nabla N_i \quad (7-12)$$

$$\Gamma_e = \sum_i^M \Gamma_i = - \sum_i^M \frac{S_i}{\sum_j^M \frac{S_j}{D_j}} \left( 1 + \frac{T_e}{T_+} \right) \nabla N_e$$

where  $S_j$  represents the ion source term; *e. g.*, ionization frequency, external source, or so forth. These expressions were well-known in the field prior to this research, and are in textbooks such as Brown (Brown, 1966: 67-68). However, until now there was no analysis that explicitly stated the limitations of this simplification. For example, Brown's unstated assumptions placed his discussion in the context of simple volume ionization only, for which his conclusions are valid.

There are many cases where simple volume ionization is the only significant volume process. In those cases the use of Equation 7-12 can completely uncouple the solutions for the various ion species from each other. As a result, the problem of finding solutions is vastly simplified; in general, each species can be treated completely independently, turning a

system of  $2M + 2$  coupled differential equations in  $M + 1$  systems of two equations each. Not only can the equations for one species be solved independently of those of another species, it is unnecessary to solve the equations for a species at all if the a description of that species' behavior is not needed. We make this statement while recognizing that the effort of including additional species may be very small. However, it is conceivable that only some of the species in the system would be of interest. For instance, experimental determination of ionization frequency for a particular species could be made by measuring the ion wall flux of that species for a known external source. Such determinations would require knowledge only of the transport properties of that species, and the electron temperature.

There are proportional cases where the use of Equation 7-12, although perfectly correct, is not as useful. For instance, charge transfer changes one ion species to another. In that case, the species involved are coupled through their respective continuity equations. Although the formal solution itself may be no more difficult than a case without charge transfer, the requirement to include more than one species in the solution makes it no longer possible to consider each ion species separately. Instead, describing either of the species involved in the charged transfer requires accurate input values for both species.

*Analytic Solutions.* The results above are complementary to the analytic solutions developed in this research. This investigation identified a broad range of systems for which proportional analytic solutions exist and can be found without the restrictive *a priori* assumption of proportionality. To the



best of our knowledge, no other model has produced analytic solutions for multi-ion ambipolar diffusion without assuming proportionality, or some equally restrictive constraint. Much of the information in the solutions, such as relative scaling of the fluxes and densities, was available from the proportionality results, without actually producing the solutions. For the simple geometries chosen here, the ability to gain information without producing the full solutions was not significant. However, in more complicated geometries, such as multi-dimensional systems with non-trivial boundaries, producing full solutions might be very difficult. In such cases knowledge of the relative scaling might be sufficient. The ability of this model to produce useful information in such circumstances is a significant improvement over previous models.

The solutions can be divided into two types. For a large number of cases (PX, CX, PV, CV, and PE), including Schottky-like volume sources proportional to electron number density and external sources with the same spatial dependence for all species, it was possible to solve the system while making no assumptions about proportionality at all. Once the solutions were obtained, they were shown to be proportional, as the results of Chapter IV had indicated. One other case involving the same volume source plus charge transfer served as an example of using the knowledge about proportionality to guide the solution process (PT). From Equation 7-11, it was possible to determine the form that the proportionality constants had to take. This knowledge was used to determine those constants. Once that was done, it was possible to find the solutions, and then verify the proportionality. Without Equation 7-11, finding solutions would have been very

difficult, if not impossible. Although this technique was only used once, it would generally be applicable to a large number of systems.

*Influence of Charge Transfer on Plasma Balance.* The effect of the discharge conditions, such as pressure, tube radius, and volume losses, on the electron temperature was investigated. The electron temperature is governed by plasma balance: in the steady state the net source of each type of charged particle, integrated over the volume of the discharge, is equal to the flux of that particle at the edge of the plasma, integrated over the area of the walls. As a result, a self-consistent solution is produced where  $kT_e$  is determined by the need for the ionization to be appropriate for the losses in the volume and at the walls. Any process that increases losses requires a higher electron temperature to offset the higher losses.

The investigations pertinent to demonstration of this effect included only systems with volume sources, where the ionization source is an explicit function of  $kT_e$ . The quantitative results were numerical only, since accurate solutions of the eigencondition relating the discharge parameters to the temperature can only be found numerically. However, there were also qualitative results based on the various numerical solutions. The most significant of these was the effect of charge transfer on the electron temperature.

In a plasma containing multiple ion species, any process that increases the number of ions of one species will cause the electron temperature to rise or drop, depending on whether the species has a diffusion coefficient higher or lower than those of the other species. For instance, adding a minority gas of higher diffusion coefficient to a single-ion plasma will raise the

temperature due to the increased overall losses. With no charge transfer, the relative fraction  $N_i/N_j$  of the each ion species  $i$  scales linearly with its relative gas fraction. Charge transfer represents a loss to the dominant species but a gain to the minority species. Therefore, for small amounts of the minority gas, charge transfer causes the relative fraction of the minority species to increase faster with gas fraction than in the charge-transfer-free case. As a result, it is possible to raise the temperature of the discharge by an amount incommensurate with the gas fraction of the contaminant species.

Figure 7-4 shows the temperature and ionization frequency variation produced by small admixtures of a charge transferring gas, with the ratio of the diffusion coefficient as the parameter of interest. The gas parameters were chosen to emphasize the changes, and therefore are not completely realistic. They correspond to a background gas whose ionization potential is 15 V, comparable to  $N_2$ , A, or  $H_2$ . The background gas ions have a diffusion coefficient of  $10 \text{ cm}^2/\text{s}$ , comparable to Xe. The overall charge transfer rate is equivalent to 0.1% of an impurity that has a charge transfer rate coefficient of  $10^{-9} \text{ cm}^3/\text{s}$ . The data are depicted as a function of  $D_i/D_b$ , the ratio of the diffusion coefficient of the gaining species to that of the background species. The temperature is 1.15 eV with the impurity and the background gas ions having the same diffusion coefficient, and rises to a value in excess of 1.6 eV for a value for  $D_2/D_1$  of 200. The ionization frequency for the same range of diffusion coefficients rose from 455 Hz to 24,820 Hz.

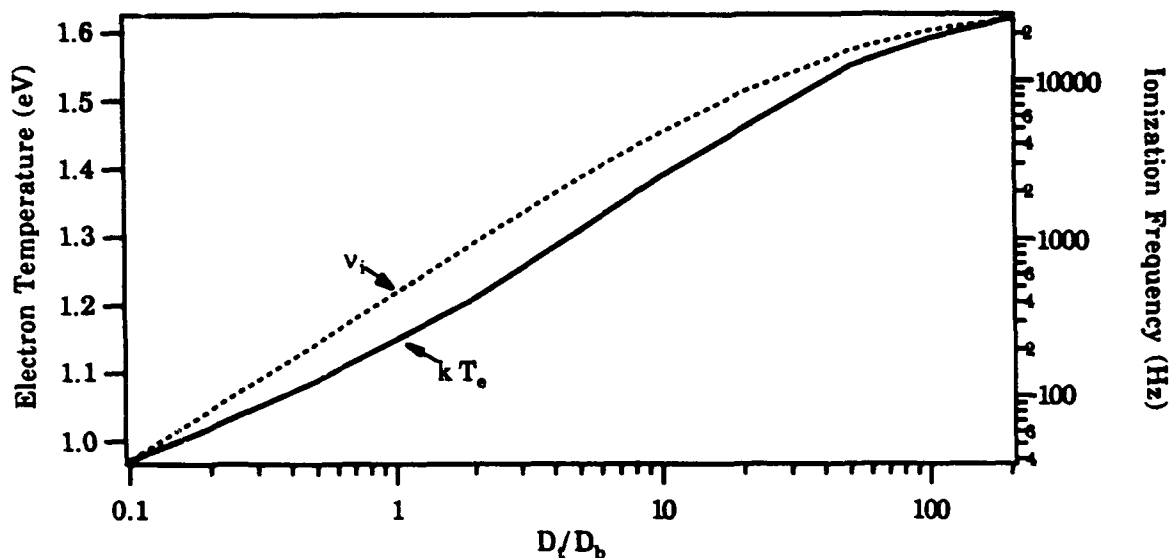


Figure 7-4. Effect of Changing Diffusion Coefficient on Electron Temperature and Ionization Frequency

These results arise directly from the multi-ion nature of the discharge. Charge transfer produces one species at the expense of another. If the diffusion coefficients of the two species are similar, the losses are unaffected by the transfer, and the temperature does not change. As the diffusion coefficient of the contaminant ion increases, its losses increase. These losses must be made up by increased ionization, and therefore a higher electron temperature. On the other hand, as the diffusion coefficient drops, the contaminant ion is retained in the discharge, allowing the ionization frequency and temperature to drop.

Given an appropriate choice of gases, this phenomenon allows adjustment of the temperature of the plasma, while still retaining the background gas as a significant, or even dominant, ion. In fact, as the contaminant ion achieves a higher and higher loss rate, the discharge becomes more and more dominated by the background gas ion. For instance, in Figure 7-4, the

charge transfer rate is so high that the discharge is dominated by the gaining ion as long as the diffusion coefficients are at all comparable. The mixture ratio for equal diffusion coefficients was only 1.5% of the background gas ion to 98.5% for the contaminant ion. With the contaminant ion having 10 times the diffusion coefficient of the background ion, the ratio increased to 15:85. For a 50-to-1 diffusion coefficient ratio, the mixture was 50/50. Finally, for the extreme diffusion coefficient ratio of 100:1, the mixture reached 68:32.

This example emphasizes the temperature variation by its choice of the range of  $D_v/D_b$ . The more realistic example of the Schmidt comparison in Chapter VI shows a similar effect. At 2.0 Torr, 80 mA current, no  $H_2$ , and only a single ion species, the electron temperature was 1.30 eV, and the discharge contained 100%  $N_2^+$  ions. With 0.01%  $H_2$  added, the temperature rose to 1.41 eV, but the discharge still contained 55%  $N_2^+$  ions. Even at 0.1%  $H_2$ , with the temperature up to 1.47 eV, the discharge contained 11%  $N_2^+$  ions. In other systems, with a larger difference in diffusion coefficients, the effect would be more pronounced.

### *Recommendations for Future Research*

*New Investigations Suggested by the Present Model.* There are two areas in particular where the new model brought out the need for further investigations. One was an experimental investigation, backed up by further calculations using extensions of the present model. The other is primarily theoretical, and represents an area which the present model is ill-suited to address.

*N<sub>2</sub>-H<sub>2</sub> Investigations.* We saw, in the comparison to Schmidt, the ability of the new model to describe experimental discharges. As we noted at the time, Schmidt's results were not an ideal subject for comparison. It would be useful to perform an experiment analogous to Schmidt's, but with the better control that the improvements in experimental apparatus and techniques have made possible. We suggest the following experimental conditions:

1. Use of hard seal high vacuum equipment for the discharge vessel, to allow bake-out of impurities.
2. Use of high-purity gases, with controlled admixtures of H<sub>2</sub> in an N<sub>2</sub> carrier gas.
3. Direct measurement of electron number density.
4. Use of mass spectrometers of sufficient resolution and sensitivity to resolve all the various nitrogen ions, as well as to distinguish the possible hydrogen ions.

Such an experiment would allow a comparison similar to the comparison made to Schmidt, but with the higher precision made possible by modern equipment.

There must be a more precise theoretical calculation to go with the more precise experiment. Some processes would need to be modelled with more precision than was possible in the initial Schmidt comparison. Other processes be neglected in that comparison need to be added. In particular,

1. The calculation of the ionization frequencies as a function of the electron energy distribution would have to be more precise. The assumption of a Maxwellian energy distribution used in the Schmidt comparison is not completely accurate for N<sub>2</sub>, which has low-lying vibrational and rotational levels that alter the distribution function. Numerical algorithms are widely available to perform such calculations; they need to be incorporated.
2. The existence of excited levels below ionization allows for the possibility of multi-step ionization. As the number density increases,

the importance of multi-step ionization increases, until it can no longer be neglected. Estimates of the relative significance of multi-step ionization were discussed at the beginning of the decision tree section. We will shortly discuss multi-step ionization in a broader context. At that point we will address this in greater detail.

3.  $N_2$  and  $H_2$  are subject to electron impact dissociation. This leads to the formation of ionic species such as  $N_3^+$ ,  $H^+$ , and  $H_3^+$ . This dissociation, and the accompanying additional species, would need to be included.

4. Recombination was ignored for  $N_2^+$ . In practice, it will occur, although in many cases at insignificant levels. The possibility of such recombination, as well as for species such as  $N_3^+$ ,  $N_4^+$ , and  $H_3^+$ , needs to be addressed.

All the effects above can be included in the present model, although not without considerable revision of the numerical algorithm. Those revisions will be discussed later.

*Multi-ion Effects on Sheaths.* There are a number of questions that arise when addressing the plasma sheath in any plasma, whether multiple ions are present or not. Riemann has presented a very thorough review of the field, with primary emphasis on single ions, but with some mention made of multi-ion effects as well (Riemann, 1991). He pointed out the importance of the well-known Bohm criterion (Riemann, 1991: 496):

$$v_i > \left( \frac{kT_e}{M} \right)^{1/2} \quad (7-13)$$

where  $v_i$  is the directed ion speed entering the sheath, and  $M$  is the ion mass. This criterion is appropriate for a collisionless sheath in the limit where the Debye length goes to zero (Riemann, 1991: 493, 495). Since the ion velocity represents an energy greater than the ion thermal energy, the Bohm criterion requires the presence of a field penetrating slightly into the plasma, in what is referred to commonly as the "presheath" region (Riemann, 1991: 493). Riemann also showed that a generalized form of

Bohm's criterion is related to a singularity in describing the plasma-sheath transition region (Riemann, 1991: 493). The presence of the singularity requires addressing the problem in at least three regions: the presheath, where quasi-neutrality still holds; the sheath, where Poisson's equation must be used; and a transition region between the two (Riemann, 1991: 498-499).

From Riemann's article, we can see that many of the phenomena in the sheath involve such parameters as the ion mass, the ion energy distribution, and the fraction of ions absorbed, reflected, or emitted at the wall, (Riemann, 1991: 496, 502-506, 503-504). Clearly, the presence of multiple ions complicates this already complex situation.

Some of these difficulties have been addressed. For instance, Riemann presented a form of the Bohm criterion for multiple positive ions, but neither pursues it nor explains its development (Riemann, 1991: 506). Braithwaite and Allen discussed a constraint on the positive ion directed velocity at the sheath for a discharge containing positive ions, negative ions, and electrons (Braithwaite and Allen, 1988). They assumed that both the electron and the negative ion densities were related to the species temperatures by the Boltzmann relation, which implied negative ion densities lower than the electron densities (Braithwaite and Allen, 1988: 1733). They found that the positive ion velocity depended upon both the electron and negative ion temperatures and upon the negative species densities (Braithwaite and Allen, 1988: 1733).

A related question to the proper formulation of a multi-ion Bohm criterion is the choice of boundary conditions for the description of the quasi-



neutral plasma. The Schottky boundary conditions were used in this research:  $N(L) = 0$  . More accurate boundary conditions would allow a better depiction of the transition from the plasma to the sheath. Since the nature of the sheath depends in part on the particles entering from the plasma, modelling the sheath accurately requires a good description of the interior of the plasma, with boundary conditions that accurately depict the number densities and fluxes at the beginning of the sheath.

We also point out that sheaths can be addressed in two extremes. One is the collisional sheath, where the mean free path for collision is much less than the sheath thickness. In such sheaths the particles are in a field-driven diffusion condition. The other extreme is the collisionless sheath, where the particles are in a field-driven free fall. Regardless of which extreme is chosen, the sheath description is simplified compared to an intermediate regime. The presence of multiple ions can prevent such a description, since the different mean free paths for collision can cause a sheath to be collisional for one species but collisionless for another.

Charge transfer in the sheath can further complicate this situation. In a single-ion plasma, the identity of the ion species does not change in the sheath. In a multi-ion plasma, non-resonant charge transfer can cause the identity of the ion species to change. This alone can require more sophisticated models than a simple single-ion sheath model. The losing species must be in a collisional regime, or charge transfer cannot be a significant process. If the other species is in a collisionless regime, the situation is complicated still further.

*Extensions of the Present Model.* We have discussed further research into areas the present model may not be able to fully address. There are also areas of fruitful research that the present model can address quite well.

*Additional Ion Species.* The simplest would be to include more ion species than the two addressed here. This requires changes in neither the formalism of the differential equations, nor in the nature of the processes included in the numerical algorithm. The only changes would be those due directly to the larger number of equations included in the numerical system.

*More Accurate Kinetic Coefficients.* In addition, it would be straightforward but more complex to include more accurate values for the kinetic coefficients. As discussed earlier in the context of applying modern experimental techniques to an equivalent of Schmidt's experiment, the model used in this research assumed Maxwellian electron energy distributions. This was appropriate for the purposes of the research and the experimental data available. However, such an assumption is often not appropriate. It is relatively straightforward to include calculations of the ionization frequencies and other kinetic coefficients that are based on calculations of the electron energy distributions. Inclusion of such calculations would allow accurate modelling of laboratory discharges such as Schmidt's.

*Expansion of Sources.* Adding more complicated kinetic reactions than the single step ionization, recombination, and charge transfer already included would be conceptually simple, but more complex to put into

practice. However, there are reactions where the work would be justified. The most obvious would be multi-step ionization, which occurs in a number of discharges. Multi-step ionization could be included in two ways. First, it could be approximated by a source term quadratic in number density, instead of linear. Such a method has already been applied to single-ion systems by, for example, Spenke (Spenke, 1950).

The difficulty with such a simplistic approach is that multi-step ionization is not always accurately modelled by a quadratic dependence. If we assume that the behavior of the excited species is dominated by volume processes and neglect diffusion, we can write the continuity equation for that species as

$$\frac{\partial N_x}{\partial t} = v_x N_e - \alpha_i N_x N_e - v_q N_x \quad (7-14)$$

where  $v_x$  is the excitation frequency,  $\alpha_i$  the ionization rate coefficient from the excited state,  $v_q$  the quenching frequency due to any of a number of possible mechanisms,  $N_x$  is the number density of excited species, and  $N_e$  is the electron density. In the steady state the time derivative is zero. This allows us to find  $N_x$  in terms of the other quantities in Equation 7-14. We can then use this information to express the ionization rate:

$$\alpha_i N_x N_e = \frac{\alpha_i v_x N_e^2}{v_q + \alpha_i N_e} \quad (7-15)$$

Equation 7-15 allows us to determine the number density dependence of the multi-step ionization. If the dominant loss from the excited species is quenching, then the ionization rate is quadratic in  $N_e$ . On the other hand, if the dominant loss is the ionization itself, then the ionization rate is linear

in  $N_0$ . If we were include diffusion as an effective loss rate, we would find that it would have the same effect on the ionization rate dependence as quenching.

The most accurate method would be to accurately include diffusion by using a continuity and momentum equation for the excited species  $N_x$ , as was done in simplified form by Ingold for a single-ion plasma (Ingold, 1970). To paraphrase Ingold's results, both continuity and momentum equations would have to be included, since the excited species would undergo losses at the wall due to collisional quenching. The momentum equation would be considerably simpler than those for the charged species, since there would be no electric field term. However, the boundary conditions could be more complex, depending on the efficiency of wall quenching. If the quenching is 100% effective, then the boundary condition would be  $N_x(L) = 0$ , comparable to the charged particle boundary conditions. On the other hand, if there is no wall quenching, the gradient of the excited species is zero. In that case the momentum equation is eliminated from the differential equation system, producing a form equivalent to Spence solution or to Ingold's final solution. For intermediate values of the quenching efficiency, a boundary condition can be established in terms of the ratio of the outgoing and reflected flux (Ingold, 1970).

The resulting system could be solved by the same numerical methods used in the present research. For a system equivalent to Ingold's, which assumed no diffusion for the excited species, the numerical system is very straightforward, producing additional volume terms in the continuity equations for the charged species (Ingold, 1970:91). In any case, inclusion

of such reactions would allow accurate modelling of systems for which multi-step ionization is important, and would be a worthwhile extension of the present research.

*Magnetic Fields.* Using previous ambipolar models to describe diffusion in the presence of a magnetic field was difficult, due to the possible failure of congruence in multi-dimensional systems. This failure is a consequence of the possibility of diffusion occurring in different directions for the different species. As Boeschoten points out (including the trivial limit of no collisions, where diffusion is no longer valid at all)

In a strong magnetic field the rate of diffusion of a plasma becomes anisotropic; in the direction parallel to the field the diffusion rate is almost unaffected, while normal to the field the diffusion may be greatly reduced, and on the simplest theories would vanish completely in the limit where interparticle collisions are neglected. (Boeschoten, 1964: 341)

An effective ambipolar diffusion coefficient in this situation is given by

$$D_{\perp} = \frac{D}{(1 + (\omega_c/v)^2)} \quad (7-16)$$

where  $D_{\perp}$  is the diffusion coefficient perpendicular to the field,  $D$  is the diffusion coefficient in the absence of the magnetic field,  $\omega_c$  is the cyclotron frequency, and  $v$  the collision frequency between the charged species and the background gas (Boeschoten, 1964:342). If the field is sufficiently large,  $D_{\perp}$  for the electrons will be greatly reduced compared to  $D_e$ . Simon was the first to point out that this produces a two-dimensional diffusion, with the primary direction of electron diffusion being along the field, and that for the ions being perpendicular to the field (Simon, 1955).

Consider what this two-dimensional flux does to the assumption of congruence. For convenience, we treat a single-ion case. Under those circumstances, charge conservation in a steady-state situation implies

$$\nabla \cdot \vec{\Gamma}_e = \nabla \cdot \vec{\Gamma}_i \quad (7-17)$$

If we are treating a one-dimensional case, the divergences in Equation 7-17 reduce to an ordinary derivative. In addition, many systems have a point or axis of symmetry where any vector quantity, even a one-dimensional one, must be zero. An example would be at  $r = 0$  in cylindrical geometry. The existence of such symmetry implies that the fluxes are both zero at  $r = 0$ . Equation 7-17 then describes two quantities that are equal at one point, and whose ordinary derivatives are equal. The conclusion is that the two quantities are equal everywhere, which implies congruence. Congruence is then used to derive the ambipolar electric field, making the use of Poisson's equation unnecessary.

Now consider the situation in Simon diffusion. We still have Equation 7-17. However, it is no longer sufficient to guarantee congruence. Consider a single-ion discharge in cylindrical geometry where the two fluxes are given by

$$\begin{aligned} \vec{\Gamma}_i &= \frac{v_i}{\lambda} \cos\left(\frac{\pi}{2} z\right) J_1(\lambda \rho) \hat{\rho} \\ \vec{\Gamma}_e &= \frac{2v_i}{\pi} \sin\left(\frac{\pi}{2} z\right) J_0(\lambda \rho) \hat{z} \end{aligned} \quad (7-18)$$

In this example the fluxes are obviously not equal. Yet, they each meet a boundary condition of zero radial flux along the line where  $\rho$  is zero, and the divergence of each is  $v_i J_0(\lambda \rho)$ . Although we make no claim that this

describes a real discharge, it does have some of the features expected for diffusion in a cylindrical discharge with a longitudinal magnetic field and a volume source term. The electron diffusion is in the longitudinal direction; the ion flux is purely radial. The spatial dependence in each direction is appropriate to a one-dimensional system diffusing in that direction. Clearly, this is a situation that is achievable in concept, or even in practice, and yet congruence does not hold.

Previous ambipolar diffusion models could not fully describe discharges such as that depicted in Equation 7-18. Limited attempts have been made. For instance, Ecker outlined a treatment of ambipolar diffusion that replaced congruence with a condition that the radial ion flux was equal to an unspecified fraction of the electron flux. He addressed the case for one-dimensional diffusion, but did not develop Simon diffusion further (Ecker, 1967).

The present ambipolar model can address this problem, since it does not rely upon congruence as the ambipolar condition used to replace Poisson's equation. Instead, the ambipolar condition that the present model uses is that the gradient of the net charge density is zero. This assumption is as valid in multiple dimensions as it is in a single dimension. Therefore, the present model could be used to address Simon diffusion.

To clarify the ability of the model to address these conditions, it is appropriate to offer a schematic development of the appropriate version of the model. Consider a discharge where the mobilities and diffusion coefficients are anisotropic. We can designate  $D_{i\alpha}$  as the coefficient for the diffusion of positive species  $i$  in the direction of the coordinate  $\alpha$ , and

similarly for  $\mu_{i\alpha}$ . The corresponding expressions for the negative species are identical, but will use the index "k" instead of "i". The momentum equations for the positive and negative species then become

$$\begin{aligned} (\nabla N_i)_\alpha &= -\frac{\Gamma_{i\alpha}}{D_{i\alpha}} + \frac{\mu_{i\alpha}}{D_{i\alpha}} N_i E_\alpha \\ (\nabla N_k)_\alpha &= -\frac{\Gamma_{k\alpha}}{D_{k\alpha}} - \frac{\mu_{k\alpha}}{D_{k\alpha}} N_k E_\alpha \end{aligned} \quad (7-19)$$

Similar to the development in Chapter III, we set the sums of the gradients of the positive and negative species equal, and solve the resulting equation for the electric field. The expression produced for the field is then used in Equation 7-19. The result is

$$\begin{aligned} (\nabla N_i)_\alpha &= -\frac{\Gamma_{i\alpha}}{D_{i\alpha}} + \frac{\mu_{i\alpha}}{D_{i\alpha}} N_i \frac{\sum_i \frac{\Gamma_{i\alpha}}{D_{i\alpha}} - \sum_k \frac{\Gamma_{k\alpha}}{D_{k\alpha}}}{\sum_i \frac{\mu_{i\alpha}}{D_{i\alpha}} N_i + \sum_k \frac{\mu_{k\alpha}}{D_{k\alpha}} N_k} \\ (\nabla N_k)_\alpha &= -\frac{\Gamma_{k\alpha}}{D_{k\alpha}} - \frac{\mu_{k\alpha}}{D_{k\alpha}} N_k \frac{\sum_i \frac{\Gamma_{i\alpha}}{D_{i\alpha}} - \sum_k \frac{\Gamma_{k\alpha}}{D_{k\alpha}}}{\sum_i \frac{\mu_{i\alpha}}{D_{i\alpha}} N_i + \sum_k \frac{\mu_{k\alpha}}{D_{k\alpha}} N_k} \end{aligned} \quad (7-20)$$

Except for the additional coordinate dependence of the diffusion coefficients and mobilities, this is equivalent to a singly-charged-particle version of the momentum equations in Equation 3-7, which is the most general form of the model presented in this research. The only difference is in the transport coefficients. With no magnetic field, the transport coefficients are isotropic, and Equation 7-20 is exactly equivalent to Equation 3-7. With a magnetic field present, the transport coefficients are no longer isotropic.



The addition of anisotropy is not necessarily as complex as it might appear. Some of the momentum component equations may reduce to simpler cases. The electron diffusion can be dominated by motion parallel to the magnetic field, while the ion motion can be dominated by ion diffusion perpendicular to the magnetic field (Boeschoten, 1964: 343). Each flux is predominantly in one direction, with the two one-dimensional fluxes perpendicular to each other. Thus, the individual continuity equations involve only one component each, and are therefore ordinary differential equations, while the system as a whole is multi-dimensional.

*Spatial Temperature Variations.* One circumstance where the a modification of the model would be worthwhile would be situations where the temperatures of the charged particle species are spatially varying. As it was used in this research, the model was valid only for uniform temperatures. This limited the applicability to situations where the combination of gas heating rates, heat capacity, diffusion of thermal energy, and thermal boundary conditions was such that the temperature was fairly uniform across the discharge. However, there are discharges where such uniformity does not hold, especially at higher discharge currents.

The situation where spatial temperature variations arise is in a positive column with Joule heating by the electrons heating the background gas, producing a higher temperature on axis. This produces several effects:

1. Since in most cases the ions are in thermal equilibrium with the background gas, the ions also have a higher temperature on axis.
2. In steady state the background gas pressure is constant across the diameter of the discharge. Since  $p = NkT$ , the background gas density is lower on axis. This causes changes in the diffusion coefficient for all species.

3. In addition, since the electrons have a longer mean free path on axis, the electrons acquire a higher speed between collisions from the acceleration due to the electric field. This latter effect can be considered to be equivalent to a higher on-axis electron temperature, with corresponding higher ionization frequencies.

We will consider the changes this produces in the momentum equation for the various charged particles:

$$\begin{aligned}\vec{\Gamma} &= -\frac{\nabla p}{mv} \pm \frac{\mu N \vec{E}}{mv} \\ &= -\frac{NkT}{mv} \frac{\nabla kT}{kT} - \frac{kT}{mv} \nabla N \pm \frac{\mu N \vec{E}}{mv}\end{aligned}\quad (7-21)$$

If we note the definition of  $D = kT/mv$ , we see that Equation 7-21 can be expressed as

$$\vec{\Gamma} = -DN \left( \frac{\nabla kT}{kT} + \frac{\nabla N}{N} \right) \pm \frac{\mu N \vec{E}}{mv} \quad (7-22)$$

This differs from the form used in this research in two ways. First,  $D$  is no longer a constant, but varies spatially. Second, there is an additional gradient  $kT$  term. To estimate the contribution of that term, we can approximate the gradient terms as

$$\begin{aligned}\frac{\nabla N}{N} &\approx \frac{N(R)-N(0)}{RN(0)} = -\frac{1}{R} \\ \frac{\nabla kT}{kT} &\approx \frac{kT(R)-kT(0)}{RkT(0)} = \frac{C-1}{CR}\end{aligned}\quad (7-23)$$

where  $C$  is the ratio of the on-axis temperature to the wall temperature. Regardless of the value of  $C$ , we find that the density gradient term is never smaller than the temperature gradient term, and is generally larger. The conclusion we draw is that the thermal gradient term has an effect on the momentum, but will never dominate the pressure gradient term.

Now let us consider the continuity equation. Typically, the longitudinal electric field is fixed by external conditions. Under such circumstances, a decrease in background number density will allow the electrons to accelerate longer, and therefore achieve high energies, between each collision. The result is an increase in ionization frequency. Von Engel gives a basic treatment of this in the context of uniform number density (von Engel, 1965): 172-180). In that context, pressure and background number density are inversely proportional. Taking that into effect, we see that his results imply an exponential dependence of ionization frequency on number density. This is a much stronger dependence than we saw for the momentum equation.

Under such conditions, it is reasonable to model the spatial dependence of the diffusion coefficients and the changes in source terms accurately, but to approximate the changed momentum equation by increasing the diffusion coefficients rather than by inclusion of the temperature gradient. The present model can, with at most slight modifications, be used for such a model. However, the model does not address how to determine the temperature gradients.

In general, determining the temperature gradients would require including energy balance in the system. This is most appropriately done by inclusion of the energy equation, which is an energy moment of the Boltzmann equation (Mitchner and Kruger, 1973: 183). With such an addition, a considerably more complicated version of the model developed here should be able to treat ambipolar diffusion including spatial temperature variations.

## *Conclusions*

This research has produced a useful description of multi-ion ambipolar diffusion. The model provides guidance on the level of detail needed to describe the various types of multi-ion discharges containing positive ions and electrons. The model duplicated the results of previous theoretical models, but with a description that was valid in regimes where the previous descriptions were not. A condition for proportionality was established that can be used to determine whether a proportional model can adequately describe a plasma. For proportional systems the model can provide the relative scaling of the ion species without the necessity for finding complete solutions of the differential equations. Numerical results demonstrated the possibility of controlling the temperature of a discharge by the admixture of small amounts of a rapidly diffusing contaminant species. In addition, the numerical solutions were used to develop a number of results describing the scaling of discharge parameters with changing recombination or charge transfer. The model brought out the need for future investigations, both experimental and theoretical. Finally, further developments of the model were suggested.

### *Appendix A. Derivation of the Dimensionless Equations*

In this appendix we will explain the details of going from the definitions of the dimensionless quantities to the dimensionless form of the continuity and diffusion equations.

Expressing the physical quantities in terms of the dimensionless quantities produces

$$\begin{aligned}\vec{r} &= \vec{\rho} \cdot L \\ N &= \frac{n}{L^3} \\ S &= \frac{sD}{L^5} \\ \vec{\Gamma} &= \frac{\vec{\gamma}D}{L^4} \\ v &= \frac{vD}{L^2} \\ \vec{E} &= \frac{\vec{\mathcal{E}}D_+}{L \mu_+}\end{aligned}\tag{A-1}$$

Notice that the form for  $S$  is extremely non-specific and much more general we used in Chapter III. We will perform the derivation for this more general case, which is the one that leads to Equation 3-22.

Now, let us consider the  $\nabla$  operator. Without loss of generality, we can express this operator in Cartesian coordinates. If we do so, and use the definition of  $\vec{\rho}$  above, the del operator becomes

$$\begin{aligned}
\nabla &= \frac{\partial}{\partial \vec{r}} \\
&= \frac{\partial}{\partial \vec{\rho} L} \\
&= \frac{\nabla_{\rho}}{L}
\end{aligned}
\tag{A-2}$$

With this definition, and the definitions of  $\vec{\Gamma}$ ,  $S$ , and  $n$ , the continuity equation (for any particle) becomes

$$\frac{\nabla_{\rho}}{L} \cdot \frac{\vec{\gamma} D}{L^4} = \frac{s D}{L^5} + \frac{n D}{L^2 L^3} \tag{A-3}$$

Eliminating the common factors of  $L^5$  and  $D$  produces the continuity equations given in Equation 3-22.

Now, let us consider the diffusion equation for electrons. Starting from Equation 3-11, we redefine the physical quantities as above, to arrive at

$$\frac{\nabla_{\rho} n_e}{L L^3} = - \frac{\vec{\gamma}_e D_e}{D_e L^4} + \frac{\mu_e}{D_e} \frac{\sum_j \frac{\vec{\gamma}_j D_j}{D_j L^4} \cdot \frac{\vec{\gamma}_e D_e}{D_e L^4}}{\frac{\mu_+}{D_+} + \frac{\mu_e}{D_e}} \tag{A-4}$$

Elimination of the common factors of  $L^4$  from every term, and elimination of the  $D/D$  factors, gives us

$$\nabla_{\rho} n_e = -\vec{\gamma}_e + \frac{\mu_e}{D_e} \frac{\sum_j \vec{\gamma}_j \cdot \vec{\gamma}_e}{\frac{\mu_+}{D_+} + \frac{\mu_e}{D_e}} \tag{A-5}$$

Next, we factor out  $\mu_+/D_+$  from both of the terms in the denominator of the second term in the right hand side. That, plus the definition of  $\epsilon$  in terms of the mobilities and diffusion coefficients, makes the entire denom-

inator equal to  $\mu_+/D_+(1+\epsilon)$ . The  $\mu_+/D_+$ , combined with the  $\mu_e/D_e$  term in the numerator, produces  $\epsilon$ . The result is the form given in Equation 3-22.

The derivation of the diffusion equation for  $n_i$  follows the same pattern, except for some minor changes. First, we note the presence of  $N_1/N_e$ . From the definition of  $n$ , we see that  $N_1/N_e = n_1/n_e$ , as in the dimensionless form of the equation. Second, we change indices from  $e$  to  $i$ , as appropriate. Third, we change the "+" in the middle of the right-hand-side to a "-". Fourth, we note that factoring out the  $\mu_+/D_+$  in the denominator, instead of producing  $\epsilon$ , cancels out the  $\mu_+/D_+$  in the numerator entirely.

Finally, consider the definition of  $\vec{E}$ . Recall Equation 3-12. If we consider the case of singly-charged positive ions, this equation becomes

$$\vec{E} = \frac{\sum_j \frac{\vec{\Gamma}_j}{D_j} - \frac{\vec{\Gamma}_e}{D_e}}{N_e \left( \frac{\mu_+}{D_+} + \frac{\mu_e}{D_e} \right)} \quad (\text{A-6})$$

If we now replace the physical quantities with their definitions in terms of the dimensionless quantities, we come to

$$\frac{\vec{E} D_+}{L \mu_+} = \frac{\sum_j \frac{\vec{\gamma}_j D_j}{D_j L^4} - \frac{\vec{\gamma}_e D_e}{D_e L^4}}{\frac{n_e}{L^3} \left( \frac{\mu_+}{D_+} + \frac{\mu_e}{D_e} \right)} \quad (\text{A-7})$$

Again, we eliminate common terms and factors and use the definition of  $\epsilon$ . The result is the form in Equation 3-22.

**Appendix B. Integration of the Equation for N**

Recall Equation IV-18:

$$n_i = - \int_1^p \int_0^{p'} s_i(p'') dp'' \quad (A-1)$$

$$\times \exp \left( \frac{\int_0^{p''} \left( \sum_j s_j(p''') - s_e(p''') \right) dp'''}{\int_1^{p''} \int_0^{p'''} \left( \epsilon \sum_j s_j(p'''' ) + s_e(p'''' ) \right) dp'''' dp'''} \right) dp'' dp'$$

If we consider only proportional sources of the type described in Equation IV-19, we get the following:

$$n_i = - s_i \int_1^p \int_0^{p'} g(p'') dp'' \quad (A-2)$$

$$\times \exp \left( \frac{\left( \sum_j s_j - s_e \right) \int_0^{p''} g(p''') dp'''}{\left( \epsilon \sum_j s_j + s_e \right) \int_1^{p''} \int_0^{p'''} g(p'''' ) dp'''' dp'''} \right) dp'' dp'$$

Next, we make the following definitions:



$$G(\rho) = \int_0^{\rho} g(\rho') d\rho'$$

$$F(\rho) = \int_1^{\rho} G(\rho') d\rho' = \int_1^{\rho} \int_0^{\rho'} g(\rho'') d\rho'' d\rho' \quad (A-3)$$

$$K = \frac{\left( \sum_j s_j - s_e \right)}{\left( \epsilon \sum_j s_j + s_e \right)}$$

$$Y = \frac{n_i}{s_i}$$

With those definitions, Equation A-2 becomes:

$$Y = - \int_1^{\rho} G(\rho') \exp \left( K \int_{\rho}^{\rho'} \frac{G(\rho'')}{F(\rho'')} d\rho'' \right) d\rho' \quad (A-4)$$

Now, note that  $dF/d\rho = G$ . Therefore, we get

$$Y = - \int_1^{\rho} G(\rho') \exp \left( K \int_{\rho}^{\rho'} \frac{F'(\rho'')}{F(\rho'')} d\rho'' \right) d\rho' \quad (A-5)$$

Next, we note that

$$\int_{\rho}^{\rho'} \frac{F'(\rho'')}{F(\rho'')} d\rho'' = \ln(F) \quad (A-6)$$

This gives us

$$Y = - \int_1^{\rho} G(\rho') \exp \left( K [\ln(F(\rho''))]_{\rho}^{\rho'} \right) d\rho' \quad (A-7)$$

Evaluating the limits, we find that

$$\begin{aligned}
Y &= - \int_1^{\rho} G(\rho') \exp(K \ln(F(\rho'))) \exp(-K \ln(F(\rho))) d\rho' \\
&= - \int_1^{\rho} G(\rho') (\exp(\ln(F(\rho'))))^K (\exp(-\ln(F(\rho))))^K d\rho'
\end{aligned}
\tag{A-8}$$

Taking advantage of the fact that the  $\ln$  and  $\exp$  functions are inverses of each other, we find

$$Y = - \int_1^{\rho} G(\rho') \frac{F(\rho')^K}{F(\rho)^K} d\rho' \tag{A-9}$$

From the definitions of  $G$  and  $F$ , we see that

$$G(\rho) = F'(\rho) \tag{A-10}$$

This implies

$$Y = - \frac{1}{F(\rho)^K} \int_1^{\rho} F'(\rho') F(\rho')^K d\rho' \tag{A-11}$$

Evaluating the integral is now straightforward. Upon so doing, we obtain the following result:

$$Y = - \left( \frac{F(\rho)^{K+1} - F(1)^{K+1}}{F(\rho)^K (K+1)} \right) \tag{A-12}$$

From the definition of  $F$ , we note that  $F(1) = 0$ . Therefore, we find that

$$Y = - \left( \frac{F(\rho)}{K+1} \right) \tag{A-13}$$

Finally, we use the definitions of  $Y$ ,  $K$ , and  $F$  to find the expression for the ion number density. Note that we have also simplified the expression  $K+1$ :

$$n_i = - \frac{s_i \left( \epsilon \sum_j s_j + s_e \right)}{\sum_j s_j (1 + \epsilon)} \int_1^p \int_0^{p'} g(p'') dp'' dp' \quad (\text{A-14})$$

## *Appendix C. Numerical Algorithms*

### *Introduction*

In this appendix we discuss the details of the numerical algorithms used to find the numerical solutions in this investigation. Note that we are not concerned in this appendix with the physics embodied in the programs; that is explained in Appendix D. Rather, we involve ourselves with the numerical methods themselves.

We will describe two algorithms. The first we describe will be the relaxation method, which was used to solve all the differential equation systems in the investigation. This algorithm was the most intensively used in the investigation, and will require the longest explanation. The other is the Brent algorithm, used to find zeros of several functions where roots could not be found analytically.

The implementations of these algorithms were those of *Numerical Recipes: The Art of Scientific Computing (FORTRAN)*, by Press, Flannery, Teukolsky, and Vetterling (Press, *et alia*, 1989). The only modifications made to the algorithms as published were to define all reals REAL\*8, and to change the error-handling procedures to be more useful in the present investigation. We heartily recommend this volume to anyone interested in numerical methods. It is by far the best we have seen at providing both practical solutions for and mathematical insight into the problems that arise in numerical physics.

## *Relaxation Method*

*Previous Methods.* The relaxation method is a method of solving two point boundary value problems. Traditionally, these problems have been attacked using some variation of the shooting method; an initial value is assumed at one boundary, the equation system is integrated to the other boundary, and the results are used to choose a new initial value, until the condition at the second boundary is met. (See, for instance, Edgley and von Engel, 1980.) In principal, such methods can solve any problem, as long as the boundary conditions at the final boundary are continuous functions of the initial values.

In practice, however, severe problems can result. The most common is the failure of the numerical method to successfully traverse from one end of the region to the other. This is not due to deficiencies in the method, but due to the nature of the mathematical system. As an example, consider a system where the general solution to the differential equations includes a function of the following form:

$$f(x) = c_1 e^{+ax} + c_2 e^{-bx} \quad (B-1)$$

Let us assume that the decreasing exponential represents the actual solution, so that  $c_1 = 0$ . If our shooting algorithm chooses an initial value equivalent to  $c_1 \neq 0$ , it will include an exponentially increasing term as well as the decreasing one. In order to successfully integrate the equation, that increasing term must stay bounded in the interval of interest. Quite often, it grows beyond the machine limits and the method fails.

This failure can show up in many ways, depending on the algorithm. In some cases, a true floating point overflow occurs. In others, the matri-

ces the algorithm is manipulating become ill-conditioned to the point that the integration cannot continue. In any event, no solution is possible under these circumstances.

*Relaxation Method Overall Methodology.* The relaxation method overcomes this problem by always using solutions that meet the boundary condition. This is a significant difference from the shooting method. In both cases, we can consider that the methods are choosing the correct solution from a set of possible solutions. With the shooting method, the possible solutions are those that satisfy the differential equation system, but may not satisfy the boundary conditions. The exact opposite is true for the relaxation method; the possible solutions satisfy all boundary conditions, but may not satisfy the differential equations (Press *et alia*, 1989:579). The intersection of these two sets, of course, is the actual solution.

We can best see how this is done by examining the example that Press *et alia* use (Press *et alia*, 1989:588-600)

*Explanation of the Relaxation Method.* Let us consider a simple first order differential equation:

$$\frac{\partial y}{\partial x} = g(x, y) \quad (B-2)$$

We transform this into a system of finite difference equations over a grid of points  $k$ . At interior points on the grid, we define

$$E_k = y_k - y_{k-1} - (x_k - x_{k-1}) g_k(x_k, x_{k-1}, y_k, y_{k-1}) \quad (B-3)$$

Now we come to the crucial point in the concept: if the  $y_k$ 's were the actual solutions, then the  $E_k$ 's would be zero (within the limits of the approximation in replacing the differential equation with a difference equation).

Initially, the  $y$ 's are not solutions. Instead, we start with some initial values for the  $y_k$ 's, which may or may not be close to the final solution, but which do meet the boundary conditions. We then allow the algorithm to find the values of all the  $y_k$ 's which reduces the total error (represented by the  $E_k$ 's) to a minimum. At that point, we have the solution (within the limits of numerical approximation).

To do this, we treat each  $E_k$  as a function of the  $y_k$ 's, and expand in a Taylor's series in  $\Delta y_k$ . We can write this as

$$E_k(y_k + \Delta y_k, y_{k-1} + \Delta y_{k-1}) = E_k(y_k, y_{k-1}) + \frac{\partial E_k}{\partial y_{k-1}} \Delta y_{k-1} + \frac{\partial E_k}{\partial y_k} \Delta y_k \quad (\text{B-4})$$

(Note the notation change between this equation and Press *et alia*'s 16.3.6; we treat a single differential equation for simplicity, where they treat the more general system of differential equations.)

Note that, to first order, we have found the correct solution when we have

$$E_k(y_k + \Delta y_k, y_{k-1} + \Delta y_{k-1}) = 0 \quad (\text{B-5})$$

The remainder of the algorithm consists in finding the proper  $y_k$ 's to bring this about. We note that the boundary conditions give rise to similar, but not identical, equations at the first and last points.

The algorithm uses five subroutines to do this: SOLVDE, BKSUB, PINVS, RED, and DIFEQ. SOLVDE is the driver routine. It iteratively finds the solution to Equation B-4 by using a modified form of Gaussian elimination. For the general case, the system represented by Equations B-4 and B-5 can be described by a block diagonal matrix. SOLVDE calls DIFEQ

(a user-supplied routine to calculate the derivatives in Equation B-4) to provide the current values of the derivatives, RED to eliminate leading columns of each block in the matrix, PINVS to diagonalize the matrix, and BKSUB to perform the back substitution and solve the system.

Note that Equation B-5 is based on a Taylor's series expansion that retains only first order terms. Equation B-2 will generally have terms of higher order than first. Therefore, the method generally requires repeated iterations. SOLVDE keeps track of the total error and number of iterations. It returns successfully if the total error is less than the supplied tolerance. It returns unsuccessfully if the number of iterations exceeds the supplied maximum.

The implementation in Press *et alia* has a number of sophisticated features not discussed in detail here. For further details, we refer you to that text ( Press *et alia*, 1989:588-611).

*Strengths and Weaknesses of Relaxation.* The greatest strength is its ability to always satisfy the boundary conditions. It is especially good at finding the correct solution when extraneous solutions exist which satisfy the differential equations but not the boundary conditions (Press *et alia*, 1989:580-581). Since it chooses solutions only from those that meet the boundary conditions, such extraneous solutions are excluded.

It is also very good for systems where the boundary conditions are in some fashion difficult to handle. In such cases it can be more efficient than shooting methods, even considering the complexity of solving a very large linear system (Press *et alia*, 1989:580).



The method is also quite flexible. Press *et alia* give examples of how to use it to calculate not only the solutions to the differential equation, but also to adapt the grid it is using at the same time (Press *et alia*, 1989:608-611). They also discuss how it can be used to handle singularities (Press *et alia*, 1989:611-614).

The method is not a panacea. It is essentially minimizing a multi-variate function using first order methods. These methods are quite adequate if the initial values of the function are "reasonably" close to the final solution. However, if they are not, convergence can become quite slow or even impossible. Because of this, it may not be the best choice for systems which require repeated solution, but where the solutions have little relationship to each other. However, as Press *et alia* point out, it can be extremely powerful when the repeated solutions are closely related. In those cases, the results of one calculation can be used as the initial values for the next (Press *et alia*, 1989:581). In fact, that is exactly the situation we saw in the present investigations.

In addition, relaxation does not handle non-smooth or oscillatory solutions as well as shooting methods. Such problems generally require adaptive grids for efficient solution. Relaxation can utilize adaptive grids. However, it does not do so as well as shooting methods (Press *et alia*, 1989:580).

### *Brent Algorithm*

The Brent algorithm (or more precisely, the Van Wijngaarden-Dekker-Brent algorithm) is a general purpose root finder for certain types of one-

dimensional problems. In particular, it solves problems with the following characteristics:

1. The function depends on a single variable.
2. The derivatives of the function are unknown in closed form, or are impractical to determine.
3. It is known that the solution lies between two values; that is, the root has been bracketed.

For such problems, it is considered to be the best algorithm available (Press *et alia*, 1989:252).

The algorithm is based on a combination of inverse quadratic interpolation and bisection. It assumes the independent variable  $x$  to be a quadratic function of  $y$ , and then uses that quadratic form to estimate the root of the function. It keeps repeating this process as long as it is successful. The process basically can fail for one of two reasons. Either the next value for  $x$  is beyond the brackets for the root, or the solutions are converging too slowly. If either of these occurs, the algorithm performs a bisection step by dividing the bracketing region in half and starting over again in whichever half is the new bracket for the root (Press *et alia*, 1989:251-254). It continues until convergence is achieved, or the number of iterations is exceeded.

## *Appendix D. Source Codes and Documentation*

### *Introduction*

This appendix contains a short description of the general layout of the programs and the actual source code for each of the programs used in the research. The only changes in the code are cosmetic ones, and additional comments. There are no changes to the executable code itself. A short discussion of each routine is included, as well.

*General Discussion.* The overall program flow for all the programs is the same. The main program (dissoc, ext, wunderer, etc) is very short, and serves mainly to call subroutines.

The first subroutine called is *getparms*. It reads in the input data from the file "infile". The data includes housekeeping information about the numerics, such as total number of grid points to use, number of output points, convergence limits, output flags, and name of the output files. It also includes data that establishes the overall discharge parameters: radius, pressure, on-axis number density, and temperature profiles. The gas parameters are defined in terms of the ionization potentials, diffusion coefficients, the ionization frequencies and reaction rates, and the external source rates.

The next subroutine called is "defprms". All the input values were defined for a pressure of 1 Torr and an electron temperature of 1 eV. The main purpose of *defprms* is to correct the input values of the various gas parameters to be consistent with the actual values of pressure and

temperature. It also initializes various arrays, including the variables themselves.

The next significant call is to "solvde". This is the *Numerical Recipes* routine that actually performs the iteration. It makes calls to several routines, including the user-supplied routine "difeq" that evaluates the Jacobian of the differential equation system.

Once solvde has successfully solved the system, "outparms", "outhead", and "output" are called to output input parameters, headers, and the actual output data.

Note that not all the various versions of the programs perform all these functions. The differences are primarily in the output routines. Dissoc, ext, and wunderer generate complete density and flux information. However, hene, yng, and von are used only to calculate electron temperatures. For this reason, the exact program flow in hene changes slightly to accommodate looping through changing gas mixes. In addition, yng and von simply evaluate closed form expressions.

### DISSOC

First we discuss the program dissoci. This is the code that was used for the volume recombination and  $N_2^+-N_4^+$  cases. The minor differences between the code for the first two cases and the last case are discussed as they appear, below.

This code solves a system of five differential equations: the continuity equations for the two ion fluxes, the momentum equations for  $N_2$  and  $N_e$ , and the trivial equation  $\partial kT_e / \partial r = 0$ . It normalizes the equations by the on-axis electron number density, so that the value of  $N_e(0)$  is identically 1.

That relationship constitutes one of the four boundary conditions; the other four are zero values for the two ion fluxes on axis, and for the two number densities at the edge of the discharge.

Most of the kinetics are straightforward. The only point to notice is that the recombination rate has two different versions; one appropriate for dissociative recombination which varies as  $kT_e = 0.5$ , and one appropriate for radiative recombination, which varies as  $kT_e = 1.5$ . This causes differences in `defprms.f` and `difeq.f`; the differences are noted in both places.

*DISSOC.F.* `Dissoc.f` is the source code for the main program itself. It was identical for all the cases mentioned above.

```

program dissoc
c* Comments beginning "c*" are those added for this appendix. They are
  added as free-form text, not as individually commented lines. The end of
  each added comment is denoted by a line containing only "c**". The only
  other changes were to some comment lines that were a single line in the
  original source, but were too long to fit on a single line for this appendix.
  These lines were broken into two separate comment lines.
c**
c* The next line ensures that any typographical errors that produce new
  variables are caught. With the unix f77 compiler, a runtime flag of "-u"
  accomplishes the same thing. NKR's ftn compiler does not support that
  flag.
c**
  implicit undefined (a-z,A-Z)
  integer m,ndy,ndx,ne,nb,itmax,nsi,nsj,nci,ncj,nck,errflag
c* Parameters are exactly as defined in Numerical Recipes. The values
  chosen allow for 201 points in the physical mesh (m), a maximum of 5
  dependent variables (ndy), 3 boundary conditions at  $x = 0$  (nb), and a
  maximum of 201 points in the physical mesh (ndx). The other parameters
  are for various algorithmic limits.
c**
  parameter(m=201,ndy=5,ne=5,nb=3,nsi=ne,ndx=m,nsj=2*ne+1
    $,nci=ne,ncj=ne-nb+1,nck=m+1)
  real*8 x(ndx),y(ndy,ndx),s(nsi,nsj)
c* p is pressure, deltap and oldp are to allow for a changing pressure (not
  implemented in the final code, but never removed).
c**
  real*8 p,deltap,oldp,c(nci,ncj,nck),slowc,scalv(ne)

```

c\* tival and tislope allow for changing temperatures in the plasma. xs is the external source input parameter, and vi is the array of ionization potentials.

```
c**
      real*8 tival(ndx),tislope(ndx),xs(ndy),vi(ndy)
      common /ionparm/xs,vi
      common /ticomm/ tival,tislope
      common /fnparms/ss,dc,conv,ne0,l,h5,x,nbg
```

c\* errflag is used to tell the calling routines that an error occurred. Used primarily in debugging.

```
c**
      common /errblock/errflag
```

c\* ss is the array of the various collision frequencies. dc is the diffusion coefficients. l is the cavity size (radius or half-width; radius here). h5 is one half of the delta in x. ne0 is the on-axis electron density. nbg is the background number density.

```
c**
      real*8 ss(ndy),dc(ndy),conv,l,h5,ne0,nbg
```

c\* numout is the number of output points. numseg is the number of points used in the mesh. pcount and pcountmax were used to implement changing pressures. totit is used to keep track of how many iterations have occurred. anflag is used to toggle output of the analytic solution used as the starting point of the iterations. It is primarily used in debugging.

```
c**
      integer indexv(ndy),numout,numseg,i,pcount,pcountmax,totit,anflag
c* outfile1 and outfile2 are the text and plot output files
```

```
c**
      character*20 outfile1,outfile2
c* getparms uses the file "infile" to get the initial data.
```

```
c**
      call getparms (numseg,itmax,outfile1,outfile2,p,anflag,
&numout,slowc)
```

c\* defprms adjusts the initial values of the parameters to the actual plasma conditions specified, initializes a number of variables, and defines several subroutines.

```
c**
      call defprms(numseg,p,indexv,scalv,y)
c* If anflag = 0, the analytic initial solution is not output.
```

```
c**
      if (anflag.ne.0)then
          call outheadr(outfile1,outfile2,conv)
          call output(numseg,y,numout,ne0)
          call outparms(numseg,p)
```

```
      endif
```

c\* The next line is used for debugging. It allows the entire iteration to be skipped, with only (at most) the analytic solution output.

```
c**
c      goto30
      totit=0
20  errflag = 0
```

```

    call solvde(itmax,conv,slowc,scalv,indexv,ne,nb,numseg
    * ,y,ndy,ndx,c,nci,ncj,nck,s,nsi,nsj)
c* If solvde exceeds the maximum number of iterations, it calls errout to set
errflag=1. The code allows the user to interactively determine whether to
continue the iteration (itmax <>0), end and output (itmax=0), or interrupt
(^C). It is often desirable to interrupt the program, so that the file nextit.for
is not updated with bad data.
c**
    if (errflag.ne.0)then
        totit=totit+itmax
        write(*,*)'Total iterations so far = ',totit
        write(*,*)'How many more to try?'
        read(*,*)itmax
        if (itmax.gt.0)goto20
    endif
c* outheader outputs header information.
c**
    call outheader(outfile1,outfile2,conv)
c* output outputs the data itself.
c**
    call output(numseg,y,numout,ne0)
c* outparms echoes some of the input parameters.
c**
    call outparms(numseg,p)
30 continue
c* The endfile statements terminate the files after the last statement.
Otherwise, data from previous runs with longer output lengths will still
appear in the files. The close statements close the files.
c**
    endfile (7)
    endfile (8)
    endfile (9)
    close(7)
    close(8)
    close(9)
    end

c* This routine is called by the Numerical Recipes codes. It is very simple,
but provides a hook for more complicated error routines.
c**
    SUBROUTINE ERROUT
    COMMON/ERRBLOCK/ERRFLAG
    INTEGER ERRFLAG
    ERRFLAG=1
    RETURN
    END

```

*GETPARMS.F.* Getparms does very little more than get input data.

```

subroutine getparms(numseg,itmax,outfile1,outfile2,p,anflag,
$numout,slowc)
implicit undefined (a-z,A-Z)
integer ndx,itmax,ndy,anflag
parameter(ndy=5,ndx=201)
real*8 conv,slowc,p,tival(ndx),tislope(ndx)
common/ticomm/tival,tislope
common/fnparms/ss,dc,conv,ne0,l,h5,x,nbg
real*8 ss(ndy),dc(ndy),ne0,l,deltap,h5,x(ndx),nbg
real*8 xs(ndy),vi(ndy)
common /ionparm/xs,vi
integer numseg,numout,i
character*20 outfile1,outfile2
open(7,FILE='infile',STATUS='OLD')
rewind(7)
read(7,*)numseg
read(7,*)numout
read(7,*)itmax
read(7,*)conv
read(7,*)slowc
read(7,*)l
read(7,*)ne0
read(7,*)ss(1)
read(7,*)ss(2)
read(7,*)ss(3)
read(7,*)ss(4)
read(7,*)xs(1)
read(7,*)xs(2)
read(7,*)vi(1)
read(7,*)vi(2)
read(7,*)dc(1)
read(7,*)dc(2)
read(7,*)dc(3)
read(7,*)tislope(1)
read(7,*)tislope(2)
read(7,*)p
read(7,*)anflag
read(7,*)outfile1
read(7,*)outfile2
close(7)
return
end

```

**DEFPRMS.F.** Defprms initializes variables, and recalculates parameters to match the input values of pressure, size, and so forth.

c\* The first two lines contain information for the Source Code Control System, a unix utility to manage large programs.



```

c**
c SCCS Release %I%
c SCCS Delta created %G%
c This is defprms.f for the N2-N4 system. Volume ionization, associative
c charge transfer, and dissociative recombination.
  subroutine defprms(numseg,p,indexv,scalv,y)
  implicit undefined (A-Z,a-z)
  integer ndy,ndx,numseg,i,ns,j
  parameter (ndy = 5, ndx = 201, ns = 3)
  integer indexv(ndy)
c* lambdj0 is the first zero of the Bessel function  $J_0$ . The other variables
  will be explained where they are used.
c**
  real*8 conv,nbg,p,scalv(*),h,y(ndy,ndx),lmbdj0,xfunc
  integer errflag
  real*8 ss(ndy),dc(ndy),ne0,l,h5,x(ndx),k1,ti,xs,epsdiv
  real*8 func,zbrent,bessj0,bessj1,kTe,s1kTe,s2kTe,rho,vi
  real*8 kTeup
  external func,s1kTe,s2kTe,zbrent,ti
  parameter (lmbdj0 = 2.4048255576958)
  common/fnparms/ss,dc,conv,ne0,l,h5,x,nbg
  common /ionparm/ xs(ndy),vi(ndy)
  common /errblock/errflag
c* This initialization is based on Numerical Recipes. The first three must
  include 2, 3, and 4, and the last two must be 1 and 5. For some reason, the
  order within each group seems to have significant effects on stability,
  presumably because of the direction in which roundoff and truncation
  errors are propagated.
c**
  indexv(1) = 4
  indexv(2) = 2
  indexv(3) = 3
  indexv(4) = 1
  indexv(5) = 5
c First, we calculate the background number density from the pressure
c 3.1219E16 is N for 1 Torr, 300K
  nbg = 3.2191E16*p
c Next, we adjust the diffusion coefficients for the density;
c they are entered normalized to 1 T. We assume kTe=1.0ev.
c If we were to choose a different kTe, we would have to scale
c D sub e linearly with sqrt(kTe) to keep it accurate. However, notice
c that the calculations do not actually involve D sub e. It is not used
c in the normalization of ne, and we calculate Ge from G1 and G2 directly.
c We include D sub e only for completeness sake.
  do 10 i = 1,ns
10  dc(i)=dc(i)/p
c S's also have to be adjusted for nbg.
c* Originally, ss was used for both external and N-dependent source terms.
  Therefore, the comment below. Later, xs was added to separate the two
  types of sources.

```

```

c**
c ***** In this case, we will look at N-dependent source terms only*****
c Therefore, ss(i) really represents various collision frequencies.
c We have [ss(1)*ne*nbg] = 1/(cm*cm*cm*s), which implies
c [ss(1)*nbg] = 1/(s). We adjust for the various dependencies to get
  ss(1)= ss(1)*nbg*exp(vi(1))/vi(1)*0.02585
c ss(2) would work exactly the same way for the second species.
  ss(2)= ss(2)*nbg*exp(vi(2))/vi(2)*0.02585
c* ss(3) also describes ordinary charge transfer. The reactions described
are, of course, different, but the dependences on external parameters are
the same.
c**
c ss(3) is the "charge transfer" frequency that describes the production
c of the second ion species from the first by associative charge transfer.
c The reaction is N2+ + N2 + N2 -> N4+ + N2. We have
c [ss(3)*nbg*nbg*n1] = 1/(cm*cm*cm*s) again, which is not equivalent to
c to ss(1) and ss(2). In fact, we get ss prop to (nbg/kTi)**2 to get
  ss(3)= ss(3)*p*p
c In this case, p == nbg/nb0; nb0=3.21926E16. ss(3) as input already
c includes nb0*nbg in it. We divide by (Ti(rho)*Ti(rho)) in difeq to account
c for temperature-induced changes in number density..
c* ss(4) is also used for radiative recombination in the VR case. The only
differences are different forms for the reactions (which change the
comments below) and a kTe**(-1.5) dependence for ss(4). Rather than
reproduce the entire source code, we merely note the difference. As
explained below, for an input kTe of 1.0 eV, the exact exponent on kTe does
not matter. The codes actually differ in difeq, however. The unix file
s.defprms.f contains both versions of defprms.f. Since only the comments
differ, the second version is not presented here.
c**
c Finally, we have ss(4), which describes the dissociative recombination
c loss
c term for species 2. The appropriate reaction is
c      N4+ + e- -> N2 + N2.
c We have [ss(4)*n2*ne]=1/(cm*cm*cm*s), which depends
c on none of the temperatures or pressures. Therefore, we need only adjust
c for the dependence of ss(4) itself, which depends on kTe**(-0.5). Since
c we input values for kTe=1.0, no adjustment is required. We put in a
c commented line anyway, just to help keep track.
c
c      ss(4) = ss(4)
c Last thing we do is generate xs(3), the source term for electrons
  xs(3) = xs(1)+xs(2)
  do 5 i = 1,3
5    xs(i) = xs(i)/ne0
c This corrects for the normalized electron density we're using.
c
c Now we check to see if we want analytic initial solutions, or to read
c in from the last time we ran the program. numseg = 1 => read'em in.
  if (numseg.ne.1) then

```

```

c *****THIS PART GENERATES THE INITIAL SOLUTIONS
c ANALYTICALLY*****
c First, we generate h and h/2.
  h = 1/(numseg-1)
  h5 = h/2.0
c Next, we initialize the constants for the initial solutions. We use
c the value of kTe at the edge of the discharge, even though our initial
c value for k1 is really from the center values. We do this because we
c want to make sure that we use the room temperature value for kTi.

c Here's the analytic solution for self-ionization
c* The next section of code uses the zbrent algorith from Numerical
Recipes to find the initial value of the electron temperature. kTeup is the
upper value that zbrent searches over. The code allows repeated searches,
with different values of kTeup, until the solution is bracketed. The correct
value of kTe can vary so widely that some interactive control was necessary.
c**
  kTeup = 5.0D0
80  errflag = 0
  kTe = zbrent(func,1.0D-5,kTeup,1.D-9)
  if(errflag.eq.1)then
    write(*,*)'kTe in defprms = ',kTe,' enter new kteup'
    read(*,*)kteup
    if(kteup.ne.0.0D0)then
      goto 80
    else
      stop
    endif
  endif
c* k1 is  $N_1/N_e$  for the proportional analytic solutions. s1kTe and s2kTe are
functions that return  $v_i$  for each of the two species, for a given temperature
and value of  $\rho/l$ .
c**
  k1 = s1kTe(kTe,1.0)*dc(2)/(s1kTe(kTe,1.0)*dc(2)
    $ +s2kTe(kTe,1.0)*dc(1))
c Next, we generate x(i). It is not vital to the relaxation process; we
c are using constant grid size. However, this way we only calculate it once.
c Note also that this version does not use any analytic current densities.
c Therefore, we do not calculate ge(i).
c* The calculation of x(i) is slightly contrived, to make sure that x(1) is
exactly 0.0, and x(numseg) is exactly 1.0. Simpler methods allow round-off
error at one end or the other.
c**
  x(numseg) = 1
  do 20 i=numseg-1,2,-1
    x(i) = x(i+1)-h
20  continue
  x(1) = 0.0D0

```

c\* The next do loop calculates the initial values for Y(i,j)

c\*\*

do 30 i=1,numseg

y(1,i) = k1\*bessj0(x(i)/l\*lmbdj0)

y(2,i) = bessj0(x(i)/l\*lmbdj0)

y(3,i) = slkTe(kTe,x(i)/l\*lmbdj0\*bessj1(x(i)/l\*lmbdj0)

y(4,i) = s2kTe(kTe,x(i)/l\*lmbdj0\*bessj1(x(i)/l\*lmbdj0)

y(5,i) = kTe

30 continue

else

c \*\*\*\*\*THIS PART IS FOR READING IN THE SOLUTIONS

c \*\*\*\*\*

c\* nextit.for stored the previous run's results. Often it was necessary to approach the final solution gradually, by starting with plasma conditions close to those for the analytic solutions, and gradually adding the terms that produced the non-analytic solutions. nextit.for stored the results from one run to the next. It contained numseg on the first line, and then x(i) and y(j,i) on each succeeding line.

c\*\*

open(9, STATUS='UNKNOWN',FILE='nextit.for')

read(9,\*)numseg

do 60 i=1,numseg

read(9,\*)x(i),(y(j,i))j=1,ndy)

60 continue

h5 = (x(2)-x(1))\*0.5

close(9)

endif

c \*\*\*\*\*NOW WE'RE BACK TO THE OVERALL INITIALIZATION

c \*\*\*\*\*

c Finally, we initialize scalv, and indexv

c\* Actually, indexv is initialized at the beginning. The comment never got changed.

c\*\*

scalv(1) = y(1,1)

scalv(2) = y(2,1)

scalv(3) = y(3,numseg)

scalv(4) = y(4,numseg)

scalv(5) = y(5,1)

return

c\* Format 9999 was used for debugging.

c\*\*

9999 format (1g10.4)

end

c\* slkTe gives the external source as a function of kTe and rho=r/l. ti(rho) is a function that give the position dependence (if any) of the ion and gas temperature. kTi is the value of the ion temperature at the boundary, and ti

is normalized such that  $ti(1.0)=1.0$ . Therefore,  $ti(1.0)*kTi$  is the value at the edge, and it varies from there on. Variations in  $Te$  are handled by the calling routine. The calculation is consistent with Von Engel's Appendix 3.

c\*\*

```
function s1kTe(Te,rho)
implicit undefined (A-Z,a-z)
integer ndy,ndx
real*8 s1kTe,Te,eps,ti,rho,xs,vi,kTi
parameter(ndy=5,ndx=201,kTi=0.02585)
real*8 ss(ndy),dc(ndy),l,h5,conv,x(ndx),nbg,ne0
common/fnparms/ss,dc,conv,ne0,l,h5,x,nbg
common /ionparm/xs(ndy),vi(ndy)
s1kTe=ss(1)*sqrt(Te)*exp(-vi(1)/Te)*vi(1)/(ti(rho)*kTi)
return
end
```

c\* s2kTe does exactly the same thing for species 2.

c\*\*

```
function s2kTe(Te,rho)
implicit undefined (A-Z,a-z)
integer ndy,ndx
real*8 s2kTe,Te,eps,rho,ti,xs,vi,kTi
c external ti
parameter(ndy=5,ndx=201,kTi=0.02585)
real*8 ss(ndy),dc(ndy),l,ne0,h5,conv,x(ndx),nbg
common/fnparms/ss,dc,conv,ne0,l,h5,x,nbg
common /ionparm/xs(ndy),vi(ndy)
s2kTe=ss(2)*sqrt(Te)*exp(-vi(2)/Te)*vi(2)/(ti(rho)*kTi)
return
end
```

c\* func is the eigencondition given in Equation IV-49:

$$\lambda^2 = \frac{\epsilon \sum_j f_j + f_e}{1 + \epsilon} \quad (IV-49)$$

We evaluate it at the edge of the discharge, and in terms of the physical quantities, as opposed to the non-dimensionalized ones used in Chapter IV.

c\*\*

```
function func(kTe)
implicit undefined (A-Z,a-z)
real*8 kTe,func,s1kTe,s2kTe
integer ndy,ndx
real*8 kTi
parameter (ndy=5,ndx=201,kTi=0.02585)
real*8 ss(ndy),dc(ndy),l,ne0,h5,conv,x(ndx),nbg
common/fnparms/ss,dc,conv,ne0,l,h5,x,nbg
func=5.7831859629468-kTi
$ *(s1kTe(kTe,1.0D0)*dc(2)+s2kTe(kTe,1.0D0)*dc(1))/
```

```

$(dc(1)*dc(2)*(kTi+kTe))*1*1
return
end

```

**DIFEQ.F.** Difeq is where the bulk of the physics is contained. The subroutine has three sections. The first two handle the boundary conditions at the center and edge of the discharge, and the third section handles the rest of the discharge.

c\* Again, the first two lines contain SCCS data.

c\*\*

c SCCS id %I%

c SCCS release %G%

```

subroutine difeq(k,k1,k2,jsf,is1,isf,indexv,ne,s,nsi,nsj
1,y,nyj,nyk)

```

```

implicit undefined (a-z,A-Z)

```

c\* We will explain the variables as they are used.

c\*\*

```

integer k,k1,k2,jsf,is1,isf,indexv(*),ne,nsi,nsj,nyj,nyk

```

```

integer ndx,ndy,i,j

```

```

parameter (ndx=201,ndy=5)

```

```

real*8 s(nsi,nsj),y(ndy,ndx),n1,n3,g1,g2,divisor,n2,d1,d2

```

```

real*8 s1,s2,s4,ds1,ds2,ds4,s1kTe,s2kTe,xinv,tix,ti,rho,s3

```

```

real*8 ss(ndy),dc(ndy),ne0,conv,l,h5,x(ndx),nbg,kTe,kTi,xfunc

```

```

real*8 xs(ndy),vi(ndy),te

```

```

common /ionparm/xs,vi

```

```

common /fnparms/ ss,dc,conv,ne0,l,h5,x,nbg

```

c Y(1,k) is ion one. Y(2,k) is electrons. Y(3,k) is ion current 1.

c Y(4,k) is ion current 2. Y(5,k) is kTe(l)

```

if (k.eq.k1)then

```

c\* We are at the center of the plasma. y(2,1) is the electron density on axis, which is normalized to 1.0. y(3,1) and y(4,1) are the particle fluxes, which are identically zero. See *Numerical Recipes* for a detailed explanation of s(i,j); at present, it is sufficient to note that s(i,j,sf) is the expression that equals 0 when the boundary condition is satisfied, and s(i,5+indexv(j)) is the derivative of s(i,j,sf) with respect to variable j.

c\*\*

```

s(3,5+indexv(1))=0.0

```

```

s(3,5+indexv(2))=1.0

```

```

s(3,5+indexv(3))=0.0

```

```

s(3,5+indexv(4))=0.0

```

```

s(3,5+indexv(5))=0.0

```

```

s(3,jsf) = y(2,1)-1.0

```

```

s(4,5+indexv(1))=0.0

```

```

s(4,5+indexv(2))=0.0

```

```

s(4,5+indexv(3))=1.0

```

```

s(4,5+indexv(4))=0.0
s(4,5+indexv(5))=0.0
s(4,jsf) = y(3,1)
s(5,5+indexv(1))=0.0
s(5,5+indexv(2))=0.0
s(5,5+indexv(3))=0.0
s(5,5+indexv(4))=1.0
s(5,5+indexv(5))=0.0
s(5,jsf) = y(4,1)

```

c\* We are now at the edge of the plasma. The two number densities are identically 0 at that point.

c\*\*

```

else if (k.gt.k2)then

```

```

s(1,5+indexv(1))=1.0
s(1,5+indexv(2))=0.0
s(1,5+indexv(3))=0.0
s(1,5+indexv(4))=0.0
s(1,5+indexv(5))=0.0
s(1,jsf) = y(1,k2)
s(2,5+indexv(1))=0.0
s(2,5+indexv(2))=1.0
s(2,5+indexv(3))=0.0
s(2,5+indexv(4))=0.0
s(2,5+indexv(5))=0.0
s(2,jsf) = y(2,k2)

```

else

c\* Now we are in the interior of the plasma. rho is r/l. tix is used to keep from having to repeatedly evaluate ti(rho). kTe is the electron temperature, including any positional variation. Note that the differential equations assume that y(5,j) does not depend on position. The positional dependence is accommodated here.

c\*\*

```

rho = (x(k)+x(k-1))*0.5/l
tix = ti(rho)
kTe = 0.5*(y(5,k)+y(5,k-1))*te(rho)
kTi = tix*0.02585

```

c\* s1, s2, s3, and s4 are the collision frequencies for ionization of species 1, ionization of species 2, charge transfer from 1 to 2, and recombination of 2. ds1, ds2, and ds4 are the derivatives of s1, s2, and s4, respectively, with respect to kTe.

c\*\*

```

s1 = s1kTe(kTe,rho)
ds1 = s1/kTe*(0.5+vi(1)/kTe)
s2 = s2kTe(kTe,rho)
ds2 = s2/kTe*(0.5+vi(2)/kTe)
s3 = ss(3)/(tix*tix)

```

c\* The next two lines are where the differences between the two different systems arise. The radiative recombination version, used for the VR case, has the following lines:

```

s4 = ss(4)/(kTe*sqrt(kTe))*ne0

```

$ds4 = -s4 * 1.5 / kTe$   
 instead of the ones below. s.difeq.f can be used to produce either version.  
 Given the slight difference, the entire second version will not be reproduced.  
 c\*\*

$s4 = ss(4) / \sqrt{kTe} * ne0$   
 $ds4 = -s4 * 0.5 / kTe$

c\* Next, we define the physical variables, using centered differencing. g2  
 and g2 are the particle fluxes for species 1 and 2. n1, n2, and n3 are the  
 species 1, species 2, and electron particle densities, respectively. We could  
 not use ne for n3, since it represents the number of equations. We left ne  
 defined as it is in *Numerical Recipes*, to reduce confusion.  
 c\*\*

$n1 = (y(1,k) + y(1,k-1)) * 0.5$   
 $n3 = (y(2,k) + y(2,k-1)) * 0.5$   
 $n2 = n3 - n1$   
 $g1 = (y(3,k) + y(3,k-1)) * 0.5$   
 $g2 = (y(4,k) + y(4,k-1)) * 0.5$

c\* xinv and divisor are defined for convenience, and to speed up the code.  
 c\*\*

$xinv = 2.0 / (x(k) + x(k-1))$   
 $divisor = 1.0 / (n3 * n3 * (kTe + tix))$

c\* d1 and d2 are  $D_1$  and  $D_2$ , respectively.  
 c\*\*

$d1 = tix * tix * \sqrt{tix}$

c I'm using d1 temporarily to store  $tix^{2.5}$   
 $d2 = d1 * dc(2)$   
 $d1 = d1 * dc(1)$

c\* The s(ijsf) lines represent the differential equations. The other lines  
 represent the derivatives of the equations with respect to  $Y_k$  and  $Y_{k+1}$ .  
 Please see *Numerical Recipes* for details.  
 c\*\*

$s(1, indexv(1)) = -1.0 - h5 * kTe * (g1/d1 + g2/d2) / (n3 * (kTe + kTi))$   
 $s(1, indexv(2)) = h5 * n1 * kTe * (g1/d1 + g2/d2) * divisor$   
 $s(1, indexv(3)) = -h5 * (n1 * kTe / (n3 * (kTe + kTi)) - 1.0) / d1$   
 $s(1, indexv(4)) = -h5 * n1 * kTe / (n3 * (kTe + kTi)) / d2$   
 $s(1, indexv(5)) = -h5 * n1 / n3 * tix * (g1/d1 + g2/d2) /$   
 $\$((kTe + kTi) * (kTe + kTi))$   
 $s(1, 5 + indexv(1)) = s(1, indexv(1)) + 2.0$   
 $s(1, 5 + indexv(2)) = s(1, indexv(2))$   
 $s(1, 5 + indexv(3)) = s(1, indexv(3))$   
 $s(1, 5 + indexv(4)) = s(1, indexv(4))$   
 $s(1, 5 + indexv(5)) = s(1, indexv(5))$   
 $s(1, jsf) = y(1,k) - y(1,k-1) - 2.0 * h5 * (n1 * kTe /$   
 $\$ (n3 * (kTe + kTi)) * (g1/d1 + g2/d2) - g1/d1)$   
 $s(2, indexv(1)) = 0.0$   
 $s(2, indexv(2)) = -1.0$   
 $s(2, indexv(3)) = h5 * kTi / ((kTe + kTi) * d1)$   
 $s(2, indexv(4)) = s(2, indexv(3)) * d1 / d2$   
 $s(2, indexv(5)) = -h5 * (g1/d1 + g2/d2) * kTi / ((kTe + kTi) * (kTe + kTi))$



```

s(2,5+indexv(1)) = 0.0
s(2,5+indexv(2)) = 1.0
s(2,5+indexv(3)) = s(2,indexv(3))
s(2,5+indexv(4)) = s(2,indexv(4))
s(2,5+indexv(5)) = s(2,indexv(5))
s(2,jsf)=y(2,k)-y(2,k-1)+2.0*h5*kTi/(kTe+kTi)*(g1/d1+g2/d2)
s(3,indexv(1)) = h5*s3
s(3,indexv(2)) = -h5*s1
s(3,indexv(3)) = -1.0+h5*xinv
s(3,indexv(4)) = 0.0
s(3,indexv(5)) = -h5*n3*ds1
s(3,5+indexv(1)) = s(3,indexv(1))
s(3,5+indexv(2)) = s(3,indexv(2))
s(3,5+indexv(3)) = 1.0+h5*xinv
s(3,5+indexv(4)) = 0.0
s(3,5+indexv(5)) = s(3,indexv(5))
s(3,jsf) = y(3,k)-y(3,k-1)-2.0*h5*(s1*n3
$ -s3*n1-g1*xinv+xfunc(1,rho))
s(4,indexv(1)) = -h5*(s3+s4*n3)
s(4,indexv(2)) = -h5*(s2+s4*(n1-2.0*n3))
s(4,indexv(3)) = 0.0
s(4,indexv(4)) = -1.0+h5*xinv
s(4,indexv(5)) = -h5*(n3*ds2+ds4*n3*(n1-n3))
s(4,5+indexv(1)) = s(4,indexv(1))
s(4,5+indexv(2)) = s(4,indexv(2))
s(4,5+indexv(3)) = 0.0
s(4,5+indexv(4)) = 1.0+h5*xinv
s(4,5+indexv(5)) = s(4,indexv(5))
s(4,jsf) = y(4,k)-y(4,k-1)-2.0*h5*(s2*n3+
$ s3*n1-s4*n3*n3+s4*n1*n3-g2*xinv+xfunc(2,rho))
s(5,indexv(1)) = 0.0
s(5,indexv(2)) = 0.0
s(5,indexv(3)) = 0.0
s(5,indexv(4)) = 0.0
s(5,indexv(5)) = -1.0
s(5,5+indexv(1)) = 0.0
s(5,5+indexv(2)) = 0.0
s(5,5+indexv(3)) = 0.0
s(5,5+indexv(4)) = 0.0
s(5,5+indexv(5)) = 1.0
s(5,jsf) = y(5,k)-y(5,k-1)
endif
return
end

```

**TIFUNC.F.** Tifunc provides for position-dependent values for  $kTe$ ,  $kTi$ , and the external source term.

function ti(x)

```

implicit undefined (a-z,A-Z)
integer ndx
parameter (ndx = 201)
real*8 x,ti,tival(ndx),tislope(ndx)
common /ticomm/tival,tislope
c  ti = 1.0
  ti = tislope(1)*(1.-x)*(1.-x)+1.0
  return
end

```

```

function te(x)
implicit undefined (a-z,A-Z)
integer ndx
parameter (ndx = 201)
real*8 x,te,tival(ndx),tislope(ndx)
common /ticomm/tival,tislope
te = tislope(2)*(1.-x)*(1.-x)+1.0
return
end

```

c\* xfunc(i,rho) returns the positional dependenced of the i-th source function. In these investigations, it returned a constant value. It was included to allow for future positional variation, but the positional variation was never included in dissoc.

```

c**
function xfunc(i,rho)
implicit undefined (a-z,A-Z)
integer i,ndy
parameter (ndy=5)
real*8 rho,xs(ndy),xfunc,ti,vi(ndy)
external ti
common /ionparm/xs,vi
xfunc=xs(i)
return
end

```

*OUTHEADER.F.* Outheader prints out column headings and the value

of conv. It also opens the outputfiles.

```

subroutine outheader(outfile1,outfile2,conv)
implicit undefined (a-z,A-Z)
character outfile1*20,outfile2*20
real*8 conv
open(7,STATUS='UNKNOWN',FILE=outfile1)
open(8,STATUS='UNKNOWN',FILE=outfile2)
open(9,STATUS='UNKNOWN',FILE='nextit.for')
write(7,2000)conv
write(7,2001)
2000  format('Tolerance on relaxation is ',1pg10.3)
2001  format('x',10x,'n1',10x,'n2',10x,'ne',10x,'g1',10x,'g2',10x,'ge')

```

end

**OUTPARMS.F.** Outparms prints out the values of some of the input parameters.

```
subroutine outparms (numseg,p)
implicit undefined (a-z,A-Z)
integer ndy,ndx,ns
parameter(ndy=5,ndx=201,ns=3)
integer numseg,i
real*8 p,nbg
common/fnparms/ss,dc,conv,ne0,l,h5,x,nbg
real*8 ss(ndy),dc(ndy),ne0,l,h5,x(ndx),conv
write(7,*)'dc, conv, p, ne0'
write(7,1000)(dc(i),i=1,ns)
write(7,1000)conv,p,ne0
1000 format(8(1pg10.3,:','))
return
end
```

**OUTPUT.F.** Output prints out the data into outfile1 and outfile2.

c SCCS SID %I%

```
subroutine output(numseg,y,numout)
implicit undefined (a-h,o-z,A-H,O-Z)
integer ndy,ndx,numout,numseg,i,counter,j
parameter(ndy=5,ndx=201)
real*8 y(ndy,ndx),l3,l4,ne0,s1kTe,s2kTe,s4,kTe,xfunc
common/fnparms/ss,dc,conv,ne0,l,h5,x,nbg
real*8 ss(ndy),dc(ndy),conv,l,h5,x(ndx),nbg,func,ti
real*8 nratio,n1src,n2src,srcrat,te,netot
external s1kTe,s2kTe,ti,xfunc,func,te
write(9,*)numseg
kTe = y(5,1)*te(0.0D0)
s4 = ss(4)/(sqrt(kTe)*kTe)
counter = max((numseg-1)/numout,1)
c* The first do loop prints the densities and fluxes to outfill1 and outfile2.
  Outfile1 also includes additional information, printed out later in the
  subroutine. Outfile2, which is intended for plotting results, does not.
c**
  do 10 i=1,numseg,counter
    write(7,1000)x(i),y(1,i)*ne0,(y(2,i)-y(1,i))*ne0,y(2,i)*ne0,
    1 y(3,i)*ne0,y(4,i)*ne0,(y(3,i)+y(4,i))*ne0
    write(8,1000)x(i),y(1,i)*ne0,(y(2,i)-y(1,i))*ne0,y(2,i)*ne0,
    1 y(3,i)*ne0,y(4,i)*ne0,(y(3,i)+y(4,i))*ne0
  10 continue
c* netot is used in calculating the actual integrated current. The next loop
  performs a simple-minded integration of  $2\pi n(r)rdr$  over the area of the
```

discharge, to obtain the value of netot, and prints out all the variables to nextit.for for the next run of the program.

```

c**
  netot=0.0
  do 20 i=1,numseg
20  write(9,3000)x(i),(y(j,i),j=1,ndy)
    do 30 i=1,numseg-1
      netot = netot + x(i)*6.2832*y(2,i)*(x(i+1)-x(i))
30  continue
    write(7,2000)'Recombination coefficient at center = ',s4
    write(7,2000)'Recombination term at center = ',s4*y(2,1)*ne0
    $(y(2,1)-y(1,1))*ne0
    write(7,2000)'CT term at center = ',ss(3)*y(1,1)*ne0
    $(ti(0.0)*ti(0.0D0))
    write(7,2000)'kTi(rho) at center = ',300.0*ti(0.0D0)
    write(7,2000)'s1kTe at center = ',s1kTe(kTe,0.0D0)
    n1src = s1kTe(kTe,0.0D0)*y(2,1)*ne0
    n2src = s2kTe(kTe,0.0D0)*y(2,1)*ne0
    write(7,2000)'n1,n2 source at center = ',n1src,n2src
    write(7,2000)'external sources = ',xfunc(1,0.0)*ne0
    $,xfunc(2,0.0D0)*ne0
c* We print out the eigencondition to help determine how well the solutions
  match the Schottky solutions.
c**
  write(7,2000)'electron temperature at edge,eigencondition = '
  $,y(5,numseg),func(y(5,numseg))
c* nratio was a measure of nonproportionality, later discarded. The code
  was not changed, since the runs were not repeated.
c**
  i=int(0.6*numseg+.5)
  nratio = y(2,1)/y(2,i)*(y(2,i)-y(1,i))/(y(2,1)-y(1,1))
  write(7,2000)'nratio = ',nratio
  write(7,2000)'src ratio = ',s4*y(2,1)*(y(2,1)-y(1,1))
  $*ne0*ne0/n2src
c Actual Ne tot is from numerical integration. Bessel is from assuming a
c Bessel (ie, Schottky) form for the solutions. This was added for
c Release 1.1.1.1, for Schmidt comparisons
  write(7,2000)'Ne total (actual) = ',netot*ne0
  write(7,2000)'Ne total (Bessel) = ',1.356*ne0*1*1
  return
3000  format(f6.3,x,5(pg19.9,x))
2000  format((a:),2(1pg10.3))
1000  format(f7.3,x,8(1pg10.3,x))
  end

```

**MAKEFILE.** Makefile is the file used by unix to generate the various object files and executables. Little attempt will be made to explain this file;

to those persons familiar with the make utility in unix, no documentation should be necessary.

```
recipepath = $(HOME)/recipes/
dissoc: dissoc.o getparms.o defprms.o outheader.o \
    outparms.o output.o difeq.o $(recipepath)solvde.o \
    $(recipepath)red.o $(recipepath)pinvs.o $(recipepath)bksub.o \
    $(recipepath)zbrent.o tfunc.o $(recipepath)bessj1.o \
    $(recipepath)bessj0.o
ftn -o dissoc dissoc.o difeq.o getparms.o \
    defprms.o outheader.o outparms.o output.o \
    $(recipepath)solvde.o $(recipepath)red.o $(recipepath)pinvs.o \
    $(recipepath)bksub.o $(recipepath)zbrent.o tfunc.o \
    $(recipepath)bessj0.o $(recipepath)bessj1.o
dissoc.o: dissoc.f
ftn -c -f -O2 dissoc.f
difeq.o: difeq.f
ftn -c -f -O2 difeq.f
tfunc.o: tfunc.f
ftn -c -f -O2 tfunc.f
$(recipepath)solvde.o: $(recipepath)solvde.f
ftn -c -f -O2 $(recipepath)solvde.f
$(recipepath)pinvs.o: $(recipepath)pinvs.f
ftn -c -f -O2 $(recipepath)pinvs.f
$(recipepath)red.o: $(recipepath)red.f
ftn -c -f -O2 $(recipepath)red.f
$(recipepath)bksub.o: $(recipepath)bksub.f
ftn -c -f -O2 $(recipepath)bksub.f
$(recipepath)zbrent.o: $(recipepath)zbrent.f
ftn -c -f -O2 $(recipepath)zbrent.f
getparms.o: getparms.f
ftn -c -f -O2 getparms.f
defprms.o: defprms.f
ftn -c -f -O2 defprms.f
newparams.o: newparams.f
ftn -c -f -O2 newparams.f
outheader.o: outheader.f
ftn -c -f -O2 outheader.f
output.o: output.f
ftn -c -f -O2 output.f
outparms.o: outparms.f
ftn -c -f -O2 outparms.f
$(recipepath)bessj0.o: $(recipepath)bessj0.f
ftn -c -f -O2 $(recipepath)bessj0.f
$(recipepath)bessj1.o: $(recipepath)bessj1.f
ftn -c -f -O2 $(recipepath)bessj1.f
```

## EXT

Next, we examine ext, which was the code used to examine systems depending on external sources only. In particular, it was used for the XR and XT cases. Much of the code is identical to the dissoci program, discussed above. The most significant change is that we no longer have  $kT_e$  as an eigenvalue. Rather, it is a fixed input value. This reduces the number of variables, differential equations, and boundary conditions from five to four. The discussion below will only add comments to the original source code that explain differences from dissoci.

*EXT.F.* Ext is the main routine for the program.

```
program ext
  integer m,ndy,ndx,ne,nb,itmax,nsi,nsj,nci,ncj,nck,errflag
c* Note that we have only four variables (ne=4), not 5. For this system, kTe
is not an eigenvalue, and so is not included as a variable.
c**
  parameter(m=201,ndy=4,ne=4,nb=2,nsi=ne,ndx=m,nsj=2*ne+1
$,nci=ne,ncj=ne-nb+1,nck=m+1)
  real*8 x(ndx),y(ndy,ndx),s(nsi,nsj)
  real*8 p,deltap,oldp,c(nci,ncj,nck),slowc,scalv(ne)
  real*8 tival(ndx),tislope(ndx),xs(ndy),conv
  common /extsrce/xs
  common /ticomm/ tival,tislope
  common /fnparms/ss,dc,kTe,ne0,l,h5,x,nbg
  common /errblock/errflag
  real*8 ss(ndy),dc(ndy),kTe,l,h5,ne0,nbg
  integer indexv(ndy),numout,numseg,i,pcount,pcountmax,totit,anflag
  character*20 outfile1,outfile2
  call getparms (numseg,itmax,outfile1,outfile2,p,anflag,
$numout,slowc,conv)
  call defprms(numseg,p,indexv,scalv,y)
  if (anflag.ne.0)then
    call outparms(numseg,p,conv)
    call outheader(outfile1,outfile2,conv)
    call output(numseg,y,numout,ne0)
  endif
c  goto30
  totit=0
20  errflag = 0
  call solvde(itmax,conv,slowc,scalv,indexv,ne,nb,numseg
* ,y,ndy,ndx,c,nci,ncj,nck,s,nsi,nsj)
```

```

if (errflag.ne.0)then
    totit=totit+itmax
    write(*,*)'Total iterations so far = ',totit
    write(*,*)'How many more to try?'
    read(*,*)itmax
    if (itmax.gt.0)goto20
endif
call outparms(numseg,p,conv)
call outheader(outfile1,outfile2,conv)
call output(numseg,y,numout,ne0)
30 continue
endfile (7)
endfile (8)
endfile (9)
close(7)
close(8)
close(9)
end

```

```

SUBROUTINE ERROUT
COMMON/ERRBLOCK/ERRFLAG
INTEGER ERRFLAG
ERRFLAG=1
RETURN
END

```

*GETPARMS.F.* Again, getparms gets the initial input parameters.

```

subroutine getparms(numseg,itmax,outfile1,outfile2,p,anflag,
$numout,slowc,conv)
integer ndx,itmax,ndy,anflag
parameter(ndy=4,ndx=201)
real*8 kTe,slowc,p,tival(ndx),tislope(ndx)
common/ticomm/tival,tislope
common/fnparms/ss,dc,kTe,ne0,l,h5,x,nbg
real*8 ss(ndy),dc(ndy),ne0,l,deltap,h5,x(ndx),nbg
real*8 xs(ndy),conv
common /extsrce/xs
integer numseg,numout,i
character*20 outfile1,outfile2
open(7,FILE='infile',STATUS='OLD')
rewind(7)
read(7,*)numseg
read(7,*)numout
read(7,*)itmax
read(7,*)conv
read(7,*)slowc
read(7,*)l
read(7,*)ne0
read(7,*)kTe

```

```

read(7,*)ss(1)
read(7,*)ss(2)
read(7,*)ss(3)
read(7,*)ss(4)
read(7,*)xs(1)
read(7,*)xs(2)
read(7,*)dc(1)
read(7,*)dc(2)
read(7,*)dc(3)
read(7,*)tislope(1)
read(7,*)p
read(7,*)anflag
read(7,*)outfile1
read(7,*)outfile2
close(7)
return
end

```

*DEFPRMS.F.* As before, defprms initializes the system.

```

subroutine defprms(numseg,p,indexv,scalv,y)
integer ndy,ndx,numseg,i,ns,j
parameter (ndy = 4, ndx = 201, ns = 3)
integer indexv(ndy)
real*8 nbgp,p,scalv(*),h,y(ndy,ndx),lmbdj0,xfunc
common/fnparms/ss,dc,kTe,ne0,l,h5,x,nbg
common / extsrce/ xs(ndy)
real*8 ss(ndy),dc(ndy),ne0,l,h5,x(ndx),k1,ti,xs,epsdiv
real*8 zbrent,dbesj0,dbesj1,kTe,s1kTe,s2kTe,rho
external s1kTe,s2kTe,zbrent,ti
parameter (lmbdj0 = 2.4048255576958)
indexv(1) = 3
indexv(2) = 4
indexv(3) = 1
indexv(4) = 2

```

c First, we calculate the background number density from the pressure  
c 3.1219E16 is N for 1 Torr, 300K

nbgp = 3.2191E16\*p

c Next, we adjust the diffusion coefficients for the density;

c they are entered normalized to 1 T. We assume kTe=1.0ev.

c If we were to choose a different kTe, we would have to scale

c D sub e linearly with sqrt(kTe) to keep it accurate. However, notice

c that the calculations do not actually involve D sub e. It is not used

c in the normalization of ne, and we calculate Ge from G1 and G2 directly.

c We include D sub e only for completeness sake.

do 10 i = 1,ns

10 dc(i)=dc(i)/p

c\* Note an important distinction between ext and dissoc. Since ext does not  
need the eigencondition that dissoc does, it does not have to adjust the  
temperature in defprms to get the analytic initial values.



There is another important distinction as well. ext assumed a value of 15.5 eV for the ionization potential of all species. This simplified the code in what was, after all, a model of idealized gases. dissoci needed to treat physically realistic gases, and so it included  $vi(i)$  as an input. The normalization constant below for  $ss(1)$  and  $ss(2)$  includes the ionization potential, where the equivalent normalization for dissoci uses  $vi(i)$  explicitly.

c\*\*

c S's also have to be adjusted for nbg.

c \*\*\*\*\* In this case, we will look at N-dependent source terms only\*\*\*\*\*

c Therefore,  $ss(i)$  really represents various collision frequencies.

c We have  $[ss(1)*ne*nbg] = 1/(cm*cm*cm*s)$ , which implies

c  $[ss(1)*nbg] = 1/(s)$ . We adjust for the various dependencies to get

$ss(1) = ss(1)*nbg*5.389698476E6$

c  $ss(2)$  would work exactly the same way for the second species.

$ss(2) = ss(2)*nbg*5.389698476E6$

c  $ss(3)$  is the "charge transfer" frequency that describes the production

c of the second ion species from the first. We have

c  $[ss(3)*nbg*nbg*n1] = 1/(cm*cm*cm*s)$  again, which is not equivalent to

c to  $ss(1)$  and  $ss(2)$ . In fact, we get  $ss$  prop to  $(nbg/kTi)**2$  to get

$ss(3) = ss(3)*6.9246E29$

c 6.9246E29 is  $nb0*nb0*kt0*kt0$ ; we divide by  $(kTi*kTi)$  in difeq

c\* This normalization is actually mistaken; it does not account for pressure differences. We should multiply by  $N_b^2$ , not by  $nb0*nb0$ . This was not discovered until after all calculations were finished and analyzed. Since the analysis was based on the calculated value of the charge transfer rate, not the input one, the error had no effect, and therefore was not corrected here. It was corrected in the version of defprms.f used with dissoci; otherwise, the calculations for Schmidt would have been incorrect.

c\*\*

c Note that we have to carefully define what we mean by this; the value of

c  $ss(3)$  will depend heavily on the partial pressures of the various gases.

c Finally, we have  $ss(4)$ , which describes the dissociative attachment loss

c term for species 2. We have  $[ss(4)*n2*ne] = 1/(cm*cm*cm*s)$ , which

c depends

c on none of the temperatures or pressures. Therefore, we need only adjust

c for the dependence of  $ss(4)$  itself, which depends on  $kTe**(-0.75)$ . Since

c we input values for  $kTe=1.0$ , no adjustment it required. We put in a

c commented line anyway, just to help keep track.

c

c  $ss(4) = ss(4)$

c Last thing we do is generate  $xs(3)$ , the source term for electrons

$xs(3) = xs(1)+xs(2)$

do 5 i = 1,3

5  $xs(i) = xs(i)/ne0*p$

c This corrects for the normalized electron density and the actual pressure;

c we input  $xs$  for  $p = 1.0$  Torr.

c

c Now we check to see if we want analytic initial solutions, or to read

c in from the last time we ran the program.  $numseg = 1 \Rightarrow$  read'em in.

if (numseg.ne.1) then

c \*\*\*\*\*THIS PART GENERATES THE INITIAL SOLUTIONS

c ANALYTICALLY\*\*\*\*\*

c First, we generate h and h/2.

h = l/(numseg-1)

h5 = h/2.0

c Next, we initialize the constants for the initial solutions. We use

c the value of kTe at the edge of the discharge, even though our initial

c value for k1 is really from the center values. We do this because we

c want to make sure that we use the room temperature value for kTi.

c This is the volume solution for external uniform sources

x(numseg) = 1

do 40 i = numseg-1, 2, -1

x(i) = x(i+1)-h

40 continue

x(1) = 0.0D0

do 50 i = 1, numseg

rho = x(i)/l

epsdiv = 0.02585\*ti(rho)/(1.0+0.02585\*ti(rho))

y(1,i) = epsdiv\*xfunc(1,rho)/dc(1)\*(1-x(i)\*x(i))/4.0

y(2,i) = y(1,i)/xfunc(1,rho)\*dc(1)\*(xfunc(1,rho)/dc(1)

\$+xfunc(2,rho)/dc(2))

y(3,i) = xfunc(1,rho)\*x(i)/2.0

y(4,i) = xfunc(2,rho)\*x(i)/2.0

50 continue

c Now we exit the analytic solutions loop

else

c \*\*\*\*\*THIS PART IS FOR READING IN THE SOLUTIONS

\*\*\*\*\*

open(9, STATUS='UNKNOWN',FILE='nextit.for')

read(9,\*)numseg

do 60 i=1,numseg

read(9,\*)x(i),(y(j,i))j=1,ndy)

60 continue

h5 = (x(2)-x(1))\*0.5

close(9)

endif

c \*\*\*\*\*NOW WE'RE BACK TO THE OVERALL INITIALIZATION

\*\*\*\*\*

c Finally, we initialize scalv

scalv(1) = y(1,1)

scalv(2) = y(2,1)

scalv(3) = y(3,numseg)

scalv(4) = y(4,numseg)

do 70 i=1,4

70 if (scalv(i).eq.0.0) write(\*,\*)'scalv = 0; i= ',i

```

    return
9999    format(1g10.4)
    end

    function s1kTe(Te,rho)
    integer ndy,ndx
    real*8 s1kTe,Te,eps,ti,rho,kTi
c* external statement was used for debugging. It turned out to be
unnecessary, so it was commented out. It is much easier to uncomment a
line than to rewrite it.
c**
c    external ti
    parameter(ndy=4,ndx=201,kTi=0.02585)
    common/fnparms/ss,dc,kTe,ne0,l,h5,x,nbg
    real*8 ss(ndy),dc(ndy),l,h5,kTe,x(ndx),nbg,ne0
c* Note that the  $V_1$  dependence is already included in the normalization.
c**
    s1kTe=ss(1)*sqrt(Te)/(ti(rho)*kTi)*exp(-15.5/Te)
    return
    end

    function s2kTe(Te,rho)
    integer ndy,ndx
    real*8 s2kTe,Te,eps,rho,ti,kTi
c    external ti
    parameter(ndy=4,ndx=201,kTi=0.02585)
    common/fnparms/ss,dc,kTe,ne0,l,h5,x,nbg
    real*8 ss(ndy),dc(ndy),l,ne0,h5,kTe,x(ndx),nbg
    s2kTe=ss(2)*sqrt(Te)/(ti(rho)*kTi)*exp(-15.5/Te)
    return
    end

```

*DIFEQ.F.* This version of difeq is essentially the same as dissoc's version, except for the differences noted. The primary difference is the reduction from five variables to four.

```

    subroutine difeq(k,k1,k2,jsf,is1,isf,indexv,ne,s,nsi,nsj
    1,y,nyj,nyk)
    integer k,k1,k2,jsf,is1,isf,indexv(*),ne,nsi,nsj,nyj,nyk
    integer ndx,ndy,i,j
c* Note; 4 variables instead of 5.
c**
    parameter (ndx=201,ndy=4)
    real*8 s(nsi,nsj),y(ndy,ndx),n1,n3,g1,g2,divisor,n2,d1,d2
    real*8 s1,s2,s4,ds1,ds2,ds4,s1kTe,s2kTe,xinv,tix,ti,rho,s3
    common /fnparms/ ss,dc,kTe,ne0,l,h5,x,nbg
    real*8 ss(ndy),dc(ndy),ne0,l,h5,x(ndx),nbg,kTe,kTi,xfunc
c Y(1,k) is ion one. Y(2,k) is electrons. Y(3,k) is ion current 1.

```

c Y(4,k) is ion current 2.  
c\* Boundary conditions: densities = 0 at the edge, fluxes = 0 at the center.  
c\*\*

```

if (k.eq.k1)then
  s(3,4+indexv(1))=0.0
  s(3,4+indexv(2))=0.0
  s(3,4+indexv(3))=1.0
  s(3,4+indexv(4))=0.0
  s(3,jsf) = y(3,1)
  s(4,4+indexv(1))=0.0
  s(4,4+indexv(2))=0.0
  s(4,4+indexv(3))=0.0
  s(4,4+indexv(4))=1.0
  s(4,jsf) = y(4,1)
else if (k.gt.k2)then
  s(1,4+indexv(1))=1.0
  s(1,4+indexv(2))=0.0
  s(1,4+indexv(3))=0.0
  s(1,4+indexv(4))=0.0
  s(1,jsf) = y(1,k2)
  s(2,4+indexv(1))=0.0
  s(2,4+indexv(2))=1.0
  s(2,4+indexv(3))=0.0
  s(2,4+indexv(4))=0.0
  s(2,jsf) = y(2,k2)
else
  rho = (x(k)+x(k-1))*0.5/1
  tix = ti(rho)
  kTi = tix*0.02585
  s1 = s1kTe(kTe,rho)
  ds1 = s1/kTe*(0.4+15.5/kTe)
  s2 = s2kTe(kTe,rho)
  ds2 = s2/kTe*(0.4+15.5/kTe)
  s3 = ss(3)/(tix*tix)
  s4 = ss(4)/(sqrt(kTe)*kTe)*ne0
  ds4 = -s4*1.5/kTe
  n1=(y(1,k)+y(1,k-1))*0.5
  n3=(y(2,k)+y(2,k-1))*0.5
  n2=n3-n1
  g1=(y(3,k)+y(3,k-1))*0.5
  g2=(y(4,k)+y(4,k-1))*0.5
  xinv=2.0/(x(k)+x(k-1))
  divisor = 1.0/(n3*n3*(kTe+tix))
  d1 = tix*tix*sqrt(tix)

```

c I'm using d1 temporarily to store tix\*\*2.5

```

d2 = d1*dc(2)
d1 = d1*dc(1)
s(1,indexv(1)) = -1.0-h5*kTe*(g1/d1+g2/d2)/(n3*(kTe+kTi))
s(1,indexv(2)) = h5*n1*kTe*(g1/d1+g2/d2)*divisor
s(1,indexv(3)) = -h5*(n1*kTe/(n3*(kTe+kTi))-1.0)/d1

```

```

s(1,indexv(4)) = -h5*n1*kTe/(n3*(kTe+kTi))/d2
s(1,4+indexv(1)) = s(1,indexv(1))+2.0
s(1,4+indexv(2)) = s(1,indexv(2))
s(1,4+indexv(3)) = s(1,indexv(3))
s(1,4+indexv(4)) = s(1,indexv(4))
s(1,jst) = y(1,k)-y(1,k-1)-2.0*h5*(n1*kTe/
$ (n3*(kTe+kTi))*(g1/d1+g2/d2)-g1/d1)
s(2,indexv(1)) = 0.0
s(2,indexv(2)) = -1.0
s(2,indexv(3)) = h5*kTi/((kTe+kTi)*d1)
s(2,indexv(4)) = s(2,indexv(3))*d1/d2
s(2,4+indexv(1)) = 0.0
s(2,4+indexv(2)) = 1.0
s(2,4+indexv(3)) = s(2,indexv(3))
s(2,4+indexv(4)) = s(2,indexv(4))
s(2,jst)=y(2,k)-y(2,k-1)+2.0*h5*kTi/(kTe+kTi)*(g1/d1+g2/d2)
s(3,indexv(1)) = h5*s3
s(3,indexv(2)) = -h5*s1
s(3,indexv(3)) = -1.0+h5*xinv
s(3,indexv(4)) = 0.0
s(3,4+indexv(1)) = s(3,indexv(1))
s(3,4+indexv(2)) = s(3,indexv(2))
s(3,4+indexv(3)) = 1.0+h5*xinv
s(3,4+indexv(4)) = 0.0
s(3,jst) = y(3,k)-y(3,k-1)-2.0*h5*(s1*n3
$ -s3*n1-g1*xinv+xfunc(1,rho))
s(4,indexv(1)) = -h5*(s3+s4*n3)
s(4,indexv(2)) = -h5*(s2+s4*(n1-2.0*n3))
s(4,indexv(3)) = 0.0
s(4,indexv(4)) = -1.0+h5*xinv
s(4,4+indexv(1)) = s(4,indexv(1))
s(4,4+indexv(2)) = s(4,indexv(2))
s(4,4+indexv(3)) = 0.0
s(4,4+indexv(4)) = 1.0+h5*xinv
s(4,jst) = y(4,k)-y(4,k-1)-2.0*h5*(s2*n3+
$ s3*n1-s4*n3*n3+s4*n1*n3-g2*xinv+xfunc(2,rho))
endif
return
end

```

**OUTHEADER.F.** This is very similar to the dissoc version.

```

subroutine outheader(outfile1,outfile2,conv)
character outfile1*20,outfile2*20
real*8 conv
open(7,STATUS='UNKNOWN',FILE=outfile1)
open(8,STATUS='UNKNOWN',FILE=outfile2)
open(9,STATUS='UNKNOWN',FILE='nextit.for')
write(7,2000)conv
write(7,2001)

```

```

2000      format('Tolerance on relaxation is ',1pg10.3)
2001      format('x',10x,'n1',10x,'n2',10x,'ne',10x,'g1',10x,'g2',10x,'ge')
end

```

*OUTPARMS.F.* This is also simliar to the dissoc version.

```

subroutine outparms (numseg,p,conv)
integer ndy,ndx,ns
parameter(ndy=4,ndx=201,ns=3)
integer numseg,i
real*8 p,nbg
common/fnparms/ss,dc,kTe,ne0,l,h5,x,nbg
real*8 ss(ndy),dc(ndy),ne0,l,h5,x(ndx),conv,kTe
write(7,*)'dc, conv, p, ne0'
write(7,1000)(dc(i),i=1,ns)
write(7,1000)conv,p,ne0
1000      format(8(1pg10.3,.,'))
return
end

```

*OUTPUT.F.* Again, similar to the dissoc version.

```

subroutine output(numseg,y,numout)
integer ndy,ndx,numout,numseg,i,counter,j
parameter(ndy=4,ndx=201)
real*8 y(ndy,ndx),l3,l4,ne0,s1kTe,s2kTe,s4,xfunc
common/fnparms/ss,dc,kTe,ne0,l,h5,x,nbg
real*8 ss(ndy),dc(ndy),kTe,l,h5,x(ndx),nbg,func,ti
real*8 efield,kTi
external s1kTe,s2kTe,ti,xfunc
write(9,*)numseg
s4 = ss(4)/(sqrt(kTe)*kTe)
counter = max((numseg-1)/numout,1)
do 10 i=1,numseg-1,counter
kTi = ti(x(i))*0.02584

```

c\* ext included the electric field in the output. It turned out it was easier to calculate it in the plotting package, since it is a simple function of the other variables. Therefore, this term was dropped from dissoc and the other programs.

```

c**
      efield = (y(3,i)/dc(1)+y(4,i)/dc(2))*kTi/y(2,i)/(1.+kTi/kTe)
      write(7,1000)x(i),y(1,i)*ne0,(y(2,i)-y(1,i))*ne0,y(2,i)*ne0,
1 y(3,i)*ne0,y(4,i)*ne0,(y(3,i)+y(4,i))*ne0
      write(8,1000)x(i),y(1,i)*ne0,(y(2,i)-y(1,i))*ne0,y(2,i)*ne0,
1 y(3,i)*ne0,y(4,i)*ne0,(y(3,i)+y(4,i))*ne0,efield
10 continue
      write(7,1000)x(numseg),y(1,numseg)*ne0,(y(2,numseg)-y(1,numseg)
1 )*ne0,y(2,numseg)*ne0,y(3,i)*ne0,y(4,i)*ne0,(y(3,i)+y(4,i))*ne0
      write(8,1000)x(numseg),y(1,numseg)*ne0,(y(2,numseg)-
y(1,numseg))*ne0

```

```

1 ,y(2,numseg)*ne0,y(3,i)*ne0,y(4,i)*ne0,(y(3,i)+y(4,i))*ne0,efield
do 20 i=1,numseg
20 write(9,3000)x(i),(y(j,i),j=1,ndy)
   write(7,2000)'Recombination term at center = ',s4*y(2,1)
   $*ne0*(y(2,1)-y(1,1))*ne0
   write(7,2000)'CT term at center = ',ss(3)*y(1,1)*ne0
   write(7,2000)'kTi(rho) at center = ',300.0*ti(0.0)
   write(7,2000)'n1 volume source at center = ',s1kTe(kTe,0.0)*y(2,1)*ne0
   write(7,2000)'n2 volume source at center = ',s2kTe(kTe,0.0)*y(2,1)*ne0
   write(7,2000)'electron temperature = ',kTe
   write(7,2000)'n1 external source at center = ',xfunc(1,0.0)*ne0
   write(7,2000)'n2 external source at center = ',xfunc(2,0.0)*ne0
c* Again, this measure of non-proportionality was eventually not used.
c**
   i = int(0.6*numseg)+1
c   write(*,*)
c   write(*,*)i,x(i)
   write(7,*)'non-proportionality ratio ',
   $y(1,1)/y(2,1)*y(2,i)/y(1,i)
   return
3000   format(f6.3,x,5(1pg16.9,x))
2000   format((a:),1pg10.3)
1000   format(f6.2,x,8(1pg10.3,x))
end

```

*TIFUNC.F.* Note that the program allows for temperature variation, although it was not used.

```

function ti(x)
integer ndx
parameter (ndx = 201)
real*8 x,ti,tival(ndx),tislope(ndx)
common /ticomm/tival,tislope
c   ti = 1.0
   ti = tislope(1)*(1.-x)*(1.-x)+1.0
   return
end

function xfunc(i,rho)
integer i,ndy
parameter (ndy=4)
real*8 rho,xs(ndy),xfunc
common /extsrce/xs
xfunc=xs(i)
return
end

```

**MAKEFILE.** We do not include the makefile, as it has not significant differences from dissociation's.

## **HENE**

Hene was the program used to calculate the electron temperatures for neon-helium mixes. It is similar to dissociation, but with some significant changes, as discussed below. In addition, the programs yng and von are used to duplicate published results from Von Engel and from Young. This allowed an accurate comparison of the new model's results to previous results, without trying to extract data from published graphs.

**HENE.F.** The biggest difference between hene and the previous codes is that hene allows the gas mix to change. Much of the initialization that dissociation did via defprms.f involved gas mixture-dependent values. This part of the initialization was moved to a module called newparms.f so that it could be conveniently repeated for each new gas mix.

Hene produces the solution for the original gas, calls newparams to change the mix, and then repeats until it has produced a solution for the opposite extreme of pure gas again.

```
program hene
implicit undefined (a-z,A-Z)
integer m,ndy,ndx,ne,nb,itmax,nsi,nsj,nci,ncj,nck,errflag
parameter(m=201,ndy=5,ne=5,nb=3,nsi=ne,ndx=m,nsj=2*ne+1
$,nci=ne,ncj=ne-nb+1,nck=m+1)
real*8 x(ndx),y(ndy,ndx),s(nsi,nsj),frac
real*8 p,deltap,oldp,c(nci,ncj,nck),slowc,scalv(ne)
real*8 tival(ndx),tislope(ndx),xs(ndy),vi(ndy)
common /ionparm/xs,vi
common /ticomm/ tival,tislope
common /fnparms/ss,dc,conv,ne0,l,h5,x,nbg
common /errblock/errflag
real*8 ss(ndy),dc(ndy),conv,l,h5,ne0,nbg
integer indexv(ndy),numout,numseg,i,pcount,pcountmax,totit,anflag
```



```

character*20 outfile1,outfile2
c* numout is now the number of different gas mixes to include, not the
number of points in the x mesh to use.
c**
  call getparms (numseg,itmax,outfile1,outfile2,p,anflag,
$numout,slowc)
  call defprms(numseg,p,indexv,scalv,y)
c* defprms does only those initializations that do not depend on gas mix.
outheader and outparms are called at the beginning, before the mix
changes.
c**
  call outheader(outfile1,outfile2,conv)
  call outparms(numseg,p)
  do 40 i=0,numout
c* frac is the  $N_{bg1}/N_{bgT}$ .
c**
    frac =1.0-float(i)/numout
c* newparams adjusts for the current fraction of species one.
c**
    call newparams(y,scalv,frac,numseg)
    totit=0
20  errflag = 0
    call solvde(itmax,conv,slowc,scalv,indexv,ne,nb,numseg
    * ,y,ndy,ndx,c,nci,ncj,nck,s,nsi,nsj)
    if (errflag.ne.0)then
      totit=totit+itmax
      write(*,*)'Total iterations so far = ',totit
      write(*,*)'How many more to try?'
      read(*,*)itmax
      if (itmax.gt.0)goto20
    endif
c* Note that, instead of passing numout to output, we call output numout
times from here.
c**
  call output(frac,y)
40  continue
  endfile (7)
  endfile (8)
  endfile (9)
  close(7)
  close(8)
  close(9)
end

SUBROUTINE ERROUT
COMMON/ERRBLOCK/ERRFLAG
INTEGER ERRFLAG
ERRFLAG=1
RETURN
END

```

**GETPARMS.F.** Getparms changes to add more diffusion coefficients.

Not only do we need the diffusion coefficient for  $\text{He}^+$  in He and  $\text{Ne}^+$  in Ne, we need the coefficients for  $\text{He}^+$  in Ne and  $\text{Ne}^+$  in He. getparms was changed to accommodate.

```
subroutine getparms(numseg,itmax,outfile1,outfile2,p,anflag,
$numout,slowc)
implicit undefined (a-z,A-Z)
integer ndx,itmax,ndy,anflag
parameter(ndy=5,ndx=201)
real*8 conv,slowc,p,tival(ndx),tislope(ndx)
common/ticomm/tival,tislope
common/fnparms/ss,dc,conv,ne0,l,h5,x,nbg
real*8 ss(ndy),dc(ndy),ne0,l,deltap,h5,x(ndx),nbg
real*8 xs(ndy),vi(ndy)
common /ionparm/xs,vi
integer numseg,numout,i
character*20 outfile1,outfile2
open(7,FILE='infile',STATUS='OLD')
rewind(7)
read(7,*)numseg
read(7,*)numout
read(7,*)itmax
read(7,*)conv
read(7,*)slowc
read(7,*)l
read(7,*)ne0
read(7,*)ss(1)
read(7,*)ss(2)
read(7,*)ss(3)
read(7,*)ss(4)
read(7,*)xs(1)
read(7,*)xs(2)
read(7,*)vi(1)
read(7,*)vi(2)
read(7,*)dc(1)
read(7,*)dc(2)
```

c\* We will explain the meaning of dc(3) and dc(4) in newparams.f  
c\*\*

```
read(7,*)dc(3)
read(7,*)dc(4)
read(7,*)tislope(1)
read(7,*)tislope(2)
read(7,*)p
read(7,*)anflag
read(7,*)outfile1
```

```

read(7,*)outfile2
close(7)
return
end

```

**FREQCOMPLEX.F.** We had originally used Von Engel's approximate form, as in his Appendix 3. However, this form is only appropriate for cases where the  $kTe/e$  is small compared to  $V_i$ . This condition did not hold for this system. Therefore, we pulled the `s1kTe`, `s2kTe`, and `func` routines out of `defprms.f` and placed them in a separate file, `freq.f`. We had two versions of `freq.f`. One, called `freqsimple.f`, used the original functions, so we could match Von Engel's results for pure helium and pure neon. The other version, called `freqcomplex.f`, had the physically more accurate version.

```

function s1kTe(Te,rho)
implicit undefined (A-Z,a-z)
integer ndy,ndx
real*8 s1kTe,Te,eps,ti,rho,xs,vi,kTi
parameter(ndy=5,ndx=201,kTi=0.02585)
real*8 ss(ndy),dc(ndy),l,h5,conv,x(ndx),nbg,ne0
common/fnparms/ss,dc,conv,ne0,l,h5,x,nbg
common /ionparm/xs(ndy),vi(ndy)
c* Note the difference; in dissociation, we had vi(1), where here we have
(2.0*Te+vi(1)). defprms.f is changed also, to accommodate the changed
normalization.
c**
  s1kTe=ss(1)*(2.0*Te+vi(1))*sqrt(Te)*exp(-vi(1)/Te)/(ti(rho)*kTi)
  return
end

function s2kTe(Te,rho)
implicit undefined (A-Z,a-z)
integer ndy,ndx
real*8 s2kTe,Te,eps,rho,ti,xs,vi,kTi
c  external ti
  parameter(ndy=5,ndx=201,kTi=0.02585)
  real*8 ss(ndy),dc(ndy),l,ne0,h5,conv,x(ndx),nbg
  common/fnparms/ss,dc,conv,ne0,l,h5,x,nbg
  common /ionparm/xs(ndy),vi(ndy)
c* We have the same change here.
c**

```

```

s2kTe=ss(2)*(2.0*Te+vi(2))*sqrt(Te)*exp(-vi(2)/Te)/(ti(rho)*kTi)
return
end

```

c\* func is identical to the dissoc version.

c\*\*

```

function func(kTe)
implicit undefined (A-Z,a-z)
real*8 kTe,func,s1kTe,s2kTe
integer ndy,ndx
real*8 kTi
parameter (ndy=5,ndx=201,kTi=0.02585)
real*8 ss(ndy),dc(ndy),l,ne0,h5,conv,x(ndx),nbg
common/fnparms/ss,dc,conv,ne0,l,h5,x,nbg
func=5.7831859629468-kTi
$ *(s1kTe(kTe,1.0D0)*dc(2)+s2kTe(kTe,1.0D0)*dc(1))/
$(dc(1)*dc(2)*(kTi+kTe))*l*1
return
end

```

*DEFPRMSN.F.* As noted above, we placed three functions in a separate source file. We also moved several operations from *defprms* to *newparams*. Finally, we changed the normalizations of *ss(1)* and *ss(2)*. The source with the new normalizations (corresponding to *freqcomplex.f*) is called *defprmsn.f*, for "new". With the old normalizations, the source is called "defprms0.f".

```

subroutine defprms(numseg,p,indexv,scalv,y)
implicit undefined (A-Z,a-z)
integer ndy,ndx,numseg,i,ns,j
parameter (ndy = 5, ndx = 201, ns = 4)
integer indexv(ndy)
real*8 conv,nbg,p,scalv(*),h,y(ndy,ndx),lmbdj0,xfunc
integer errflag
real*8 ss(ndy),dc(ndy),ne0,l,h5,x(ndx),k1,ti,xs,epsdiv
real*8 func,zbrent,bessj0,bessj1,kTe,s1kTe,s2kTe,rho,vi
real*8 kTeup
external func,s1kTe,s2kTe,zbrent,ti
parameter (lmbdj0 = 2.4048255576958)
common/fnparms/ss,dc,conv,ne0,l,h5,x,nbg
common /ionparm/ xs(ndy),vi(ndy)
common /errblock/errflag
indexv(1) = 4
indexv(2) = 2

```

```

indexv(3) = 3
indexv(4) = 1
indexv(5) = 5
c First, we calculate the background number density from the pressure
c 3.1219E16 is N for 1 Torr, 300K
  nbg = 3.2191E16*p
c Next, we adjust the diffusion coefficients for the density;
c they are entered normalized to 1 T. We assume kTe=1.0ev.
  do 10 i = 1,ns
10  dc(i)=dc(i)/p
c S's also have to be adjusted for nbg.
c ***** In this case, we will look at N-dependent source terms only*****
c Therefore, ss(i) really represents various collision frequencies.
c We have [ss(1)*ne*nbg] = 1/(cm*cm*cm*s), which implies
c [ss(1)*nbg] = 1/(s). We adjust for the various dependencies to get
c* In dissoc, we have a term "v(1)", where here we have (2.0*Te+vi(1)).
  That is the normalization difference.
c**
  ss(1)= ss(1)*nbg*exp(vi(1))/(2.0+vi(1))*0.02585
c ss(2) would work exactly the same way for the second species.
c* The same change occurs for ss(2).
c**
  ss(2)= ss(2)*nbg*exp(vi(2))/(2.0+vi(2))*0.02585
c ss(3) is the "charge transfer" frequency that describes the production
c of the second ion species from the first. We have
c [ss(3)*nbg*nbg*n1] = 1/(cm*cm*cm*s) again, which is not equivalent to
c to ss(1) and ss(2). In fact, we get ss prop to (nbg/kTi)**2 to get
  ss(3)= ss(3)*6.9246E29
c 6.9246E29 is nb0*nb0*kt0*kt0; we divide by (kTi*kTi) in difeq
c Note that we have to carefully define what we mean by this; the value of
c ss(3) will depend heavily on the partial pressures of the various gases.
c Finally, we have ss(4), which describes the dissociative attachment loss
c term for species 2. We have [ss(4)*n2*ne]=1/(cm*cm*cm*s), which
c depends
c on none of the temperatures or pressures. Therefore, we need only adjust
c for the dependence of ss(4) itself, which depends on kTe**(-1.5). Since
c we input values for kTe=1.0, no adjustment it required. We put in a
c commented line anyway, just to help keep track.
c
c  ss(4) = ss(4)
c Last thing we do is generate xs(3), the source term for electrons
  xs(3) = xs(1)+xs(2)
  do 5 i = 1,3
5  xs(i) = xs(i)/ne0
c This corrects for the normalized electron density we're using.
c
c *****THIS PART GENERATES VARIOUS FIXED
PARAMETERS*****
c First, we generate h and h/2.
  h = 1/(numseg-1)

```

h5 = h/2.0

c Next, we generate x(i). It is not vital to the relaxation process; we  
c are using constant grid size. However, this way we only calculate it once.  
c Note also that this version does not use any analytic current densities.  
c Therefore, we do not calculate ge(i).

```
x(numseg) = 1
do 20 i=numseg-1,2,-1
  x(i) = x(i+1)-h
20 continue
x(1) = 0.0D0
return
end
```

*NEWPARAMS.F.* Newparams replaces some of the operations of the  
former defprms.f. We use only a single version for either version of freq.f.

```
subroutine newparams(y,scalv,f1,numseg)
implicit undefined (a-z,A-Z)
integer ndy,ndx,errflag,flag
parameter(ndy=5,ndx=201)
integer numseg,i
c* f1 and f2 are the fractions of species 1 and 2.
c**
  real*8 scalv(*),f1,f2,s1,s2,s1kte,s2kte,bessj0,bessj1
c* dij is the diffusion coefficient for species i in background gas j.
c**
  real*8 y(ndy,ndx),kTeup,zbrent,func,d11,d12,d21,d22
  real*8 kte,lmbdj0,conv,nbg
  real*8 ss(ndy),dc(ndy),ne0,l,h5,x(ndx),k1
  common/fnparms/ss,dc,conv,ne0,l,h5,x,nbg
  common/errblock/ errflag
  parameter(lmbdj0 = 2.4048255576958)
c* This code ensures that the variables are retained from one call to the
next
c**
  save d11,d12,d21,d22,s1,s2,flag
c* For the first call, flag is 0.
c**
  data flag /0/
  external func
c* We want to save the original values of dc(i) and ss(i), so we can
recalculate dc(1), dc(2), ss(1), and ss(2) for later calls. So, the first time, we
save them, and then set flag to 1 so we know we've done so.
c**
  if (flag.eq.0)then
    flag=1
    d11 = dc(1)
```

c\* We actually don't need to save dc(3) and dc(4), since we never change them. However, doing so makes the code clearer.

c\*\*

d12 = dc(3)

d22 = dc(2)

d21 = dc(4)

s1 = ss(1)

s2 = ss(2)

endif

c\* Recall that f1 is different for each call to newparams.

c\*\*

f2 = 1.0-f1

c\* This is Blanc's law.

c\*\*

dc(1)=d11\*d12/(f1\*d12+f2\*d11)

dc(2)=d21\*d22/(f2\*d21+f1\*d22)

ss(1)=max(1.0D-40,s1\*f1)

ss(2)=max(1.0D-40,s2\*f2)

c\* The write statement is debugging code. As noted before, it's much easier to uncomment than to rewrite.

c\*\*

c write(\*,\*)'dc',dc(1),dc(2)

kTeup = 40.0D0

80 errflag = 0

kTe = zbrent(func,1.0D-5,kTeup,1.D-9)

if(errflag.eq.1)then

write(\*,\*)'kTe in defprms = 'kTe,' enter new kteup'

read(\*,\*)kteup

if(kteup.ne.0.0D0)then

goto 80

else

stop

endif

endif

k1 = s1kTe(kTe,1.0)\*dc(2)/(s1kTe(kTe,1.0)\*dc(2)

\$ +s2kTe(kTe,1.0)\*dc(1))

do 30 i=1,numseg

y(1,i) = k1\*bessj0(x(i)/l\*lmbdj0)

y(2,i) = bessj0(x(i)/l\*lmbdj0)

y(3,i) = s1kTe(kTe,x(i)/l)\*lmbdj0\*bessj1(x(i)/l\*lmbdj0)

y(4,i) = s2kTe(kTe,x(i)/l)\*lmbdj0\*bessj1(x(i)/l\*lmbdj0)

y(5,i) = kTe

30 continue

scalv(1) = y(1,1)

scalv(2) = y(2,1)

scalv(3) = y(3,numseg)

scalv(4) = y(4,numseg)

scalv(5) = y(5,1)

return

end

**OUTHEADER.F.** This prints our header information.

```

subroutine outheader(outfile1,outfile2,conv)
implicit undefined (a-z,A-Z)
character outfile1*20,outfile2*20
real*8 conv
open(7,STATUS='UNKNOWN',FILE=outfile1)
open(8,STATUS='UNKNOWN',FILE=outfile2)
open(9,STATUS='UNKNOWN',FILE='nextit.for')
write(7,2000)conv
2000    format('Tolerance on relaxation is ',1pg10.3)
end

```

**OUTPARMS.F.** This prints our the parameters.

```

subroutine outparms (numseg,p)
implicit undefined (a-z,A-Z)
integer ndy,ndx,ns
parameter(ndy=5,ndx=201,ns=3)
integer numseg,i
real*8 p,nbg
common/fnparms/ss,dc,conv,ne0,l,h5,x,nbg
real*8 ss(ndy),dc(ndy),ne0,l,h5,x(ndx),conv
write(7,*)'l, conv, p, ne0'
write(7,1000)l,conv,p,ne0
write(7,*)
1000    format(8(1pg10.3,:','))
return
end

```

**OUTPUT.F.** This prints out the data we need for the comparisons.

```

subroutine output(frac,y)
implicit undefined (a-h,o-z,A-H,O-Z)
integer ndy,ndx
parameter(ndy=5,ndx=201)
real*8 y(ndy,ndx),frac
write(7,*)'Percentage of species 2; kTe(degrees K) '
c numerical constant is conversion from eV to Te; =e/k
c* outfile1 gets percentages; outfile2, the actual fraction.
c**
write(7,2000) 100.0*(1.0-frac),y(5,1)*11604.9
write(8,1000)(1.0-frac),y(5,1)*11604.9
return
2000    format (f8.3,x,f9.0)
1000    format(f7.3,x,8(1pg10.3,x))
end

```



**TIFUNC.F.** This is the same as in **dissoc**. Therefore, we do not list it here.

**VON.F.** This program duplicates Von Engel's calculations of electron temperature versus gas, pressure, and radius ("cpR").

```
program von
real*8 cpR, Vi, Te, vonfunc
common Vi,cpR
external vonfunc
write(*,*)'input cpR, Vi'
read(*,*)cpR,Vi
Te = zbrent(vonfunc,1.D-2, 200.0D0, 1.0D-6)
write(*,*)'kTe in eV; kTe/Vi in K =',Te, Te/Vi*11694.8
end

function vonfunc(Te)
real*8 Te,Vi,cpR,vonfunc,xx
common Vi,cpR
c* Debugging code.
c**
c  write(*,*)'in vonfunc;Vi,Te ',Vi,Te
  x=Vi/Te
  xx=exp(x)/sqrt(x)-(1.2D7)*cpR*cpR
c  write(*,*)'out vonfunc'
  vonfunc=xx
  return
end

SUBROUTINE ERROUT
COMMON/ERRBLOCK/ERRFLAG
INTEGER ERRFLAG
ERRFLAG=1
RETURN
END
```

**YNG.F.** This program duplicates Young's calculations, using DAB's expression.

```
program yng
implicit undefined (a-h,o-z,A-H,O-Z)
real*8 pD,f1,f2,Te,zbrent,yngfunc
common f1,f2,pD
external yngfunc
write(*,*)'Input pD'
read(*,*)pD
```

```

do 10 i=1,7
f2 = (i-1)/6.0
f1=1.0-f2
Te=zbrent(yngfunc, 1.D-1, 10.0, 1.D-6)
c  write(*,1000)'f1, Te ',f1,Te*1.6D-19/1.38D-23
  write(*,1000)'f1, Te ',f1,Te*11604.8
10  continue
1000  format((a:),f7.4,x,f10.0)
  end

function yngfunc(Te)
implicit undefined (a-h,o-z,A-H,O-Z)
real*8 b1,b2,u11,u12,u22,u21,a1,a2,v1,v2,c1,c2,f1,f2
real*8 x1,x2,ans,Te,pD,yngfunc
common f1,f2,pD
parameter(u11=10.5,u12=16.0, u21=12.5,u22=4.0,a1=4.6D-2)
parameter(a2=5.6D-2,v1=24.5,v2=21.5)
b1=760.0/(f1/u11+f2/u12)
b2=760.0/(f1/u21+f2/u22)
c1=a1*sqrt(v1)/b1
c2=a2*sqrt(v2)/b2
x1=v1/Te
x2=v2/Te
ans=f1*c1*pD*pD/sqrt(x1)*(1.0+0.5*x1)*exp(-x1)
ans=ans+f2*c2*pD*pD/sqrt(x2)*(1.0+0.5*x2)*exp(-x2)
yngfunc=ans-1.72D-7
c  if(f1.lt.1.0)then
c      write(*,*)'b1,b2,c1,c2',b1,b2,c1,c2
c      write(*,*)'f1,ans ',f1,ans
c      stop
c  endif
  return
  end

SUBROUTINE ERROUT
COMMON/ERRBLOCK/ERRFLAG
INTEGER ERRFLAG
ERRFLAG=1
RETURN
END

```

**MAKEFILE.** The makefile has some significant differences from the previous ones, so we list it.

```

recipepath = $(HOME)/recipes/
hene: heneobs
    ftm -o hene hene.o newparams.o difeq.o getparms.o \
    defprms.o outheader.o outparms.o output.o \

```

```

$(recipepath)solvde.o $(recipepath)red.o $(recipepath)pinvs.o \
$(recipepath)bksub.o $(recipepath)zbrent.o tfunc.o \
$(recipepath)bessj0.o $(recipepath)bessj1.o freq.o
heneobs: hene.o newparams.o getparms.o defprms.o outheader.o \
outparms.o output.o difeq.o $(recipepath)solvde.o \
$(recipepath)red.o $(recipepath)pinvs.o $(recipepath)bksub.o \
$(recipepath)zbrent.o tfunc.o $(recipepath)bessj1.o \
$(recipepath)bessj0.o freq.o
hene.o: hene.f
ftn -c -f -O2 hene.f
newparams.o: newparams.f
ftn -c -f -O2 newparams.f
difeq.o: difeq.f
ftn -c -f -O2 difeq.f
freq.o: freq.f
ftn -c -F -O2 freq.f
tfunc.o: tfunc.f
ftn -c -f -O2 tfunc.f
$(recipepath)solvde.o: $(recipepath)solvde.f
ftn -c -f -O2 $(recipepath)solvde.f
$(recipepath)pinvs.o: $(recipepath)pinvs.f
ftn -c -f -O2 $(recipepath)pinvs.f
$(recipepath)red.o: $(recipepath)red.f
ftn -c -f -O2 $(recipepath)red.f
$(recipepath)bksub.o: $(recipepath)bksub.f
ftn -c -f -O2 $(recipepath)bksub.f
$(recipepath)zbrent.o: $(recipepath)zbrent.f
ftn -c -f -O2 $(recipepath)zbrent.f
getparms.o: getparms.f
ftn -c -f -O2 getparms.f
defprms.o: defprms.f
ftn -c -f -O2 defprms.f
outheader.o: outheader.f
ftn -c -f -O2 outheader.f
output.o: output.f
ftn -c -f -O2 output.f
outparms.o: outparms.f
ftn -c -f -O2 outparms.f
$(recipepath)bessj0.o: $(recipepath)bessj0.f
ftn -c -f -O2 $(recipepath)bessj0.f
$(recipepath)bessj1.o: $(recipepath)bessj1.f
ftn -c -f -O2 $(recipepath)bessj1.f
testfre: testfre.o newparams.o getparms.o defprms.o outheader.o \
outparms.o output.o \
$(recipepath)zbrent.o tfunc.o $(recipepath)bessj1.o \
$(recipepath)bessj0.o freq.o
ftn -o testfre testfre.o newparams.o getparms.o \
defprms.o outheader.o outparms.o output.o \
$(recipepath)zbrent.o tfunc.o \
$(recipepath)bessj0.o $(recipepath)bessj1.o freq.o

```

```

testfre.o: testfre.f
    ftm -c -f -O2 testfre.f
von: von.o $(recipepath)zbrent.o
    ftm -o von von.o $(recipepath)zbrent.o
von.o: von.f
    ftm -c -f -O2 von.f
yng: yng.o $(recipepath)zbrent.o
    ftm -o yng yng.o $(recipepath)zbrent.o
yng.o: yng.f
    ftm -c -f -O2 yng.f
henec: freqcomplex.o defprmsn.o heneobs
    cp freqcomplex.o freq.o
    cp defprmsn.o defprms.o
    make hene
    mv hene henec
henes: freqsimple.o defprmso.o heneobs
    cp freqsimple.o freq.o
    cp defprmso.o defprms.o
    make hene
    mv hene henes
freqsimple.o:freqsimple.f
    ftm -c -f -O2 freqsimple.f
freqcomplex.o:freqcomplex.f
    ftm -c -f -O2 freqcomplex.f
defprmso.o:defprmso.f
    ftm -c -f -O2 defprmso.f
defprmsn.o:defprmsn.f
    ftm -c -f -O2 defprmsn.f
testfrec:freqcomplex.o defprmsn.o testfre
    cp freqcomplex.o freq.o
    cp defprmsn.o defprms.o
    make testfre
    mv testfre testfrec
testfres:freqsimple.o defprmso.o testfre
    cp freqsimple.o freq.o
    cp defprmso.o defprms.o
    make testfre
    mv testfre testfres

```

The primary differences are at the end, where we establish targets for henes and henec. These are formed by copying the appropriate versions of freq.f and defprms.f, making hene, and then copying hene to henec or henes. We also add targets for von and yng.

**WUNDERER**

The last program is the one used to duplicate Wunderer's results (Wunderer, 1978). The program has similarities in broad form to ext, but has considerable differences in detail, due to the desire to match Wunderer's system as closely as possible.

*EXT.F.* The main program was still called ext. The most significant changes were to remove the descriptions of the common blocks and variables into include files, and the recasting of variable names to match Wunderer.

```

program ext
include 'comparm.f'
include 'common.f'
integer itmax,errflag
real*8 y(ndy,ndx),s(nsi,nsj)
real*8 c(nci,ncj,nck),slowc,scalv(ne)
real*8 conv,rhob
common /extsrce/ rhob
common /errblock/errflag
integer indexv(ndy),numout,numseg,i,totit,anflag
character*20 outfile1,outfile2
call getparms (numseg,itmax,outfile1,outfile2,anflag,
$numout,slowc,conv,rhob)
call defprms(numseg,indexv,scalv,y)
if (anflag.ne.0)then
    call outheadr(outfile1,outfile2,conv)
    call output(numseg,y,numout)
endif
totit=0
20  errflag = 0
    call solvde(itmax,conv,slowc,scalv,indexv,ne,nb,numseg
    * ,y,ndy,ndx,c,nci,ncj,nck,s,nsi,nsj)
    if (errflag.ne.0)then
        totit=totit+itmax
        write(*,*)'Total iterations so far = ',totit
        write(*,*)'How many more to try?'
        read(*,*)itmax
        if (itmax.gt.0)goto20
    endif
    call outheadr(outfile1,outfile2,conv)
    call output(numseg,y,numout)
30  continue
    endfile(7)
    endfile(8)

```

```

endfile(9)
close(7)
close(8)
close(9)
end

```

```

SUBROUTINE ERROUT
COMMON/ERRBLOCK/ERRFLAG
INTEGER ERRFLAG
ERRFLAG=1
RETURN
END

```

*COMMONS.F* and *COMPARM.F*. These two files contain the definitions of the most widely used common blocks.

```

implicit none
integer ndx, ndy
parameter (ndx= 201, ndy=8)
real*8 ss,t,g,d,u,l,h5,x
common/fnparms/ss,t,g,d,u,l,h5,x(ndx)

```

```

integer m,ne,nb,nsi,nsj,nci,ncj,nck
parameter(m=201,ne=4,nb=2,nsi=ne,nsj=2*ne+1
$,nci=ne,ncj=ne-nb+1,nck=m+1)

```

*GETPARMS.F*. This routine gets the input parameters.

```

subroutine getparms(numseg,itmax,outfile1,outfile2,anflag,
$numout,slowc,conv,rhob)
include 'comparm.f'
include 'common.f'
integer itmax,anflag
real*8 conv,rhob,slowc
integer numseg,numout
character*20 outfile1,outfile2
open(7,FILE='infile',STATUS='OLD')
rewind(7)
read(7,*)numseg
read(7,*)numout
read(7,*)itmax
read(7,*)conv
read(7,*)slowc
read(7,*)l

```

c\* The next 6 lines read in variables we did not use before except ss, and that is used in a different meaning. These correspond to normalized variables defined by Wunderer.

```

c**
    read(7,*)rhob

```

```

read(7,*)ss
read(7,*)t
read(7,*)g
read(7,*)d
read(7,*)u
read(7,*)anflag
read(7,*)outfile1
read(7,*)outfile2
close(7)
return
end

```

**DEFPRMS.F.** This initializes the variables.

```

subroutine defprms(numseg,indexv,scalv,y)
include 'comparm.f'
include 'common.f'
integer numseg,ij
integer indexv(ndy)
real*8 scalv(*),h,y(ndy,ndx),xfunc
indexv(1) = 3
indexv(2) = 4
indexv(3) = 1
indexv(4) = 2

```

c We have eliminated a LOT of stuff from the other implementations  
c of the code. This is because Wunderer deals with a single case,  
c not a range of paramaters. So, we change nothing.  
c Now we check to see if we want analytic initial solutions, or to read  
c in from the last time we ran the program. numseg = 1 => read'em in.  
if (numseg.ne.1) then

c \*\*\*\*\*THIS PART GENERATES THE INITIAL SOLUTIONS  
ANALYTICALLY\*\*\*\*\*

c First, we generate h and h/2.

```

h = 1.0/(numseg-1)
h5 = h/2.0
x(numseg) = 1.0
do 40 i = numseg-1, 2, -1
x(i) = x(i+1)-h

```

```

40 continue
x(1) = 0.0D0

```

c Next, we initialize the dependent variables with a pseudo-solution  
c\* The pseudo-solution is not even a solution recombination or charge  
transfer ignored, since no analytic solution exists, even in that case.  
c\*\*

```

do 50, i=1,numseg
y(1,i) = u*xfunc(x(i))*(1.0+u)/(1*1*4.0)*(1.0-x(i)*x(i))
y(2,i) = y(1,i)*2.0
y(3,i) = xfunc(x(i))*x(i)*1*0.5
y(4,i) = xfunc(x(i))*x(i)*1*0.5

```

```

50 continue
c Now we exit the analytic solutions loop

    else

c *****THIS PART IS FOR READING IN THE SOLUTIONS
*****
    open(9, STATUS='UNKNOWN',FILE='nextit.for')
    read(9,*)numseg
    do 60 i=1,numseg
    read(9,*)x(i),(y(j,i))j=1,ne)
60 continue
    h5 = (x(2)-x(1))*0.5
    close(9)
    endif

c *****NOW WE'RE BACK TO THE OVERALL INITIALIZATION
*****
c Finally, we initialize scalv
    scalv(1) = y(1,1)
    scalv(2) = y(2,1)
    scalv(3) = y(3,numseg)
    scalv(4) = y(4,numseg)
    do 70 i=1,4
70 if (scalv(i).eq.0.0) write(*,*)'scalv = 0; i= ',i
    return
9999 format (1g10.4)
    end

```

*DIFEQ.F.* This is changed to reflect the different physics of Wunderer's system.

```

subroutine difeq(k,k1,k2,jsf,is1,isf,indexv,ne,s,nsi,nsj
1,y,nyj,nyk)
include 'common.f'
integer k,k1,k2,jsf,is1,isf,indexv(*),ne,nsi,nsj,nyj,nyk
integer ij
real*8 s(nsi,nsj),y(ndy,ndx),n1,n3,g1,g2,divisor,n2,d1,d2
real*8 xfunc,rho
c Y(1,k) is ion one. Y(2,k) is electrons. Y(3,k) is ion current 1.
c Y(4,k) is ion current 2.
if (k.eq.k1)then
    s(3,4+indexv(1))=0.0
    s(3,4+indexv(2))=0.0
    s(3,4+indexv(3))=1.0
    s(3,4+indexv(4))=0.0
    s(3,jsf) = y(3,1)
    s(4,4+indexv(1))=0.0

```



```

s(4,4+indexv(2))=0.0
s(4,4+indexv(3))=0.0
s(4,4+indexv(4))=1.0
s(4,jsf) = y(4,1)

```

```

else if (k.gt.k2)then
s(1,4+indexv(1))=1.0
s(1,4+indexv(2))=0.0
s(1,4+indexv(3))=0.0
s(1,4+indexv(4))=0.0
s(1,jsf) = y(1,k2)
s(2,4+indexv(1))=0.0
s(2,4+indexv(2))=1.0
s(2,4+indexv(3))=0.0
s(2,4+indexv(4))=0.0
s(2,jsf) = y(2,k2)

```

else

c\* rho is the dimensionless distance.

c\*\*

```

rho = (x(k)+x(k-1))*0.5
n1=(y(1,k)+y(1,k-1))*0.5
n3=(y(2,k)+y(2,k-1))*0.5
n2=n3-n1
g1=(y(3,k)+y(3,k-1))*0.5
g2=(y(4,k)+y(4,k-1))*0.5
s(1,jsf)=y(1,k)-y(1,k-1)-2.0*h5*1*1*(n1/n3*u
$(g1+g2)-g1*(1+u))
s(1,indexv(1))=-1.0-h5*1*1*u*(g1+g2)/n3
s(1,indexv(2))=h5*1*1*n1*(g1+g2)*u/(n3*n3)
s(1,indexv(3))=-h5*1*1*(n1/n3*u-(1+u))
s(1,indexv(4))=-h5*1*1*n1/n3*u
s(1,indexv(1)+4)=s(1,indexv(1))+2.0
s(1,indexv(2)+4)=s(1,indexv(2))
s(1,indexv(3)+4)=s(1,indexv(3))
s(1,indexv(4)+4)=s(1,indexv(4))
s(2,jsf)=y(2,k)-y(2,k-1)+2.0*h5*1*1*(g1+g2)
s(2,indexv(1))=0.0
s(2,indexv(2))=-1.0
s(2,indexv(3))=h5*1*1
s(2,indexv(4))=h5*1*1
s(2,indexv(1)+4)=0.0
s(2,indexv(2)+4)=+1.0
s(2,indexv(3)+4)=h5*1*1
s(2,indexv(4)+4)=h5*1*1
s(3,jsf)=y(3,k)-y(3,k-1)-2.0*h5*(xfunc(rho)
$-t*ss*n1*n3/(1*1)-g*n1/(1*1)-g1/rho)
s(3,indexv(1))=h5/(1*1)*(t*ss*n3+g)
s(3,indexv(2))=h5*t*ss*n1/(1*1)
s(3,indexv(3))=-1.0+h5/rho
s(3,indexv(4))=0.0
s(3,indexv(1)+4)=s(3,indexv(1))

```

```

s(3,indexv(2)+4)=s(3,indexv(2))
s(3,indexv(3)+4)=1.0+h5/rho
s(3,indexv(4)+4)=0.0
s(4,jaf)=y(4,k)-y(4,k-1)-2.0*h5/(l*1)*
$(g*d*n1-ss*n3*(n3-n1)-g2*l*1/rho)
s(4,indexv(1))=-h5/(l*1)*(g*d+ss*n3)
s(4,indexv(2))=h5/(l*1)*2.0*ss*n3
s(4,indexv(3))=0.0
s(4,indexv(4))=-1.0+h5/rho
s(4,indexv(1)+4)=s(4,indexv(1))
s(4,indexv(2)+4)=s(4,indexv(2))
s(4,indexv(3)+4)=0.0
s(4,indexv(4)+4)=1.0+h5/rho
endif
return
end

```

**OUTHEADER.F.** This opens the files and prints out header information.

```

subroutine outheader(outfile1,outfile2,conv)
character outfile1*20,outfile2*20
real*8 conv
open(7,STATUS='UNKNOWN',FILE=outfile1)
open(8,STATUS='UNKNOWN',FILE=outfile2)
open(9,STATUS='UNKNOWN',FILE='nextit.for')
c  rewind(9)
write(7,2000)conv
write(7,2001)
2000 format('Tolerance on relaxation is ',1pg10.3)
2001 format('x',10x,'n1',10x,'n2',10x,'ne',10x,'g1',10x,'g2',10x,'ge')
end

```

**OUTPUT.F.** This prints out the results.

```

subroutine output(numseg,y,numout)
include 'comparm.f'
include 'common.f'
integer numout,numseg,i,counter,j
real*8 y(ndy,ndx),l3,l4,ne0,s4,xfunc,n1,n2,n0
external ti,xfunc
write(9,*)numseg
n1 = y(1,1)
n2 = y(2,1)-n1
n0 = y(2,1)
counter = max((numseg-1)/numout,1)
do 10 i=1,numseg,counter
write(7,1000)x(i),y(1,i),(y(2,i)-y(1,i)),y(2,i),
1 y(3,i),y(4,i),(y(3,i)+y(4,i))

```

```

        write(8,1000)x(i),y(1,i)/n1,(y(2,i)-y(1,i))/n2,y(2,i)/n0,
1 y(3,i),y(4,i),(y(3,i)+y(4,i))
10 continue
    do 20 i=1,numseg
20 write(9,3000)x(i),(y(j,i),j=1,ne)
    return
3000 format(f6.4,x,5(1pg20.9,x))
1000 format(f6.2,x,8(1pg10.3,x))
end

```

**TIFUNC.F.** Although the name is the same as the files that contain the temperature variation for the other versions, this file contains only the function that determines the functional form of the external source. The name was not changed because changing it would have required numerous changes to the makefile. The functional form is exactly Wunderer's.

```

function xfunc(rho)
real*8 rho,rhob,xfunc
common /extsrce/rhob
xfunc=exp(-(rho/rhob)**2.2)
return
end

```

**MAKEFILE.** This is the makefile for the program.

```

recipepath = $(HOME)/recipes/
ext: ext.o getparms.o defprms.o outheader.o \
    output.o difeq.o $(recipepath)solvde.o \
    $(recipepath)red.o $(recipepath)pinvs.o $(recipepath)bksub.o \
    $(recipepath)zbrent.o tifunc.o common.f
ftn -O -f -o ext ext.o difeq.o getparms.o \
    defprms.o outheader.o output.o \
    $(recipepath)solvde.o $(recipepath)red.o $(recipepath)pinvs.o \
    $(recipepath)bksub.o $(recipepath)zbrent.o tifunc.o
ext.o: ext.f common.f
ftn -O -f -c ext.f
difeq.o: difeq.f common.f
ftn -O -f -c difeq.f
tifunc.o: tifunc.f common.f
ftn -O -f -c tifunc.f
$(recipepath)solvde.o: $(recipepath)solvde.f
ftn -O -f -c $(recipepath)solvde.f
$(recipepath)pinvs.o: $(recipepath)pinvs.f
ftn -O -f -c $(recipepath)pinvs.f
$(recipepath)red.o: $(recipepath)red.f
ftn -O -f -c $(recipepath)red.f

```

```
$(recipepath)bksub.o: $(recipepath)bksub.f
    ftm -O -f -c $(recipepath)bksub.f
$(recipepath)zbrent.o: $(recipepath)zbrent.f
    ftm -O -f -c $(recipepath)zbrent.f
getparms.o: getparms.f common.f
    ftm -O -f -c getparms.f
defprms.o: defprms.f common.f
    ftm -O -f -c defprms.f
output.o: output.f common.f
    ftm -O -f -c output.f
outhead.o: outhead.f common.f
    ftm -O -f -c outhead.f
```

### Bibliography

- Allis, W. P., and Rose, K. J. "The Transition for Free to Ambipolar Diffusion," *Physical Review* 93: 84-93 (January 1, 1954).
- Belousova, L. E. "Application of the Galerkin Method to Several Problems of Positive Column Theory," *Soviet Physics - Technical Physics* 13: 337-339 (September, 1968)
- Boeschoten, F. "Review of Experiments on the Diffusion of Plasma Across a Magnetic Field", *Plasma Physics (Journal of Nuclear Energy Part C)* 6: 339-388. (1964).
- Braithwaite, N. St. J., and Allen, J. E. "Boundaries and probes in electronegative plasmas," *Journal of Physics D: Applied Physics* 21: 1733-1737 (1988).
- Brown, Sanborn C. *Introduction to Electrical Discharges in Gases*. New York: Wiley, 1966.
- Chen, Francis F. *Introduction to Plasma Physics and Controlled Fusion, Volume 1: Plasma Physics* (Second Edition). New York: Plenum Press, 1984.
- Clouse, Christopher J. *Schottky Theory of Three Component Plasmas*. MS Thesis, AFIT/GNE/EN/85M-3. School of Engineering, Air Force Institute of Technology (AU), Wright-Patterson AFB OH, January 1985.
- Cohen, Ira M., and Kruskal, Martin D. "Asymptotic Theory of the Positive Column of a Gas Discharge," *The Physics of Fluids* 8: 920-934 (May 1963).
- Cohen, Ira M. and Whitman, Alan M. "Unified positive column theory of gas discharges," *The Physics of Fluids* 16: 307-314 (February, 1973).
- Dorgela, H. B., Alting, H., and Boers, J. *Physic. Haag* 2: 939 (1935).
- Ecker, G. "Theory of the Positive Column," *Proc. Phys. Soc. B*, 67: 485-491 (1954).
- Ecker, G. "Gas Discharge Theory," *Rendiconti S.I.F. XXV*: (Approximately 1967).
- Edgley, P. D., and von Engel, A. "Theory of positive columns in electronegative gases," *Proc R. Soc. Lond. A*, 370: 375-387 (1980).
- Ferreira, C. M., Gousset, G., and Touzeau, M. "Quasi-neutral theory of positive columns in electronegative gases," *Journal of Physics D*, 21: 1403-1413 (1988).

- Forrest, J. R., and Franklin, R. N. "The theory of the positive column including space-charge effects," *Brit. J. Appl Phys (J. Phys. D)*, 2: (1) 1357-1368 (1968).
- Frommhold, Lothar, and Biondi, Manfred A. "A Mathematical Study of the Electron Decay in Diffusion and Recombination Controlled Afterglows", *Annals of Physics*, 48: 407-440 (1968).
- Godyak, V. A., and Khanneh, A. S. "Ion Bombardment Secondary Electron Maintenance of Steady RF Discharge," *IEEE Transactions on Plasma Science*, PS-14: 112-123 (April 1986).
- Golant, V.E., Zhilinsky, A. P., Sakharov, I. E., and Brown, S. C. *Fundamentals of Plasma Physics*. New York: John Wiley & Sons, 1980.
- Golubovskii, Yu. B., and Lyagushchenko, R. I. "Limiting current in a steady-state diffusion-recombination discharge," *Soviet Physics Technical Physics*, 22: 1073-1078 (September 1977).
- Ingold, J. H. "Diffusion Theory of the Positive Column with Two Stage Ionization and Collisional Deexcitation", *Zeitschrift zur Physik*, 233: 89-93 (1970).
- Kieffer, L. J. *A Compilation of Electron Collision Cross Section Data for Modeling Gas Discharge Lasers*. JILA Information Report 13. Boulder, Colorado: Joint Institute for Laboratory Astrophysics, University of Colorado, 1973.
- Labuda, E. F., and Gordon, E. I. "Microwave Determination of Average Electron Energy and Density in He-Ne Discharges," *Journal of Applied Physics*, 35: 1647-1648 (1964).
- McDaniel, E. W. *et alia*. *Compilation of Atomic and Molecular Data Relevant to Gas Lasers, Volume VII*. Technical Report RH-81-4. Redstone Arsenal, Alabama: US Army Missile Command, December 1980.
- Mitchner, Morton and Kruger, Jr., Charles. *Partially Ionized Gases*. New York: Wiley-Interscience, 1973.
- Oskam, H. J. "Microwave Investigations of Disintegrating Gaseous Discharge Plasmas", *Phillips Research Report*, 13: 335-400 (1958).
- Phelps, A. V. "The Diffusion of Charged Particles in Collisional Plasmas: Free and Ambipolar Diffusion at Low and Moderate Pressures," *Journal of Research of the National Institute of Standards and Technology*, 95 : 407-431 (July-August 1990).
- and Brown, Sanborn C. "Positive Ions in the Afterglow of a Low Pressure Helium Discharge," *Physical Review*, 86: 102-105 (April 1, 1952).

- Press, William H., Flannery, Brian P., Teukolsky, Saul A., and Vetterling, William T. *Numerical Recipes The Art of Scientific Computing (FORTRAN Version)*. Cambridge: Cambridge University Press, 1989.
- Riemann, K-U. "The Bohm criterion and sheath formation," *Journal of Physics D: Applied Physics*, 24: 493-518 (1991).
- Seshadri, S. R. *Fundamentals of Plasma Physics*. New York: American Elsevier Publishing Company, Inc, 1973.
- Schmidt, Martin. "Massenspektrometrische Untersuchungen an der positiven Säule der Stickstoff-Glimmentladung," *Beiträge der Plasmaphysik*, 11: 147-163 (1965).
- Schottky, E. "Diffusionstheorie der positiven Säule," *Physik. Zeitschr.* 25: 635-640 (1924).
- Shapiro, D. A., and Valentini, H.-B. "Hydrodynamic Theory of Low-Pressure Multi-Component Discharges with Neutral Gas Depletion," *Contributions to Plasma Physics* 31: 391-409 (1991).
- Simon, A. *Phys. Rev.* 98: 317 (1955).
- Smith, D., and Adams, N. G. "Temperature Dependences of Positive-Ion Molecule Reactions," *Swarms of Ions and Electrons in Gases*, edited by W. Lindinger, T.D Märk, and F. Howorka. New York: Springer-Verlag, 1984.
- Solunskii, V. I., and Timan, B. L. "Volume Recombination in the Presence of Ambipolar Diffusion in a Gas-Discharge Plasma", *Soviet Physics-Technical Physics*, 9, (2): 207-209 (August, 1964).
- Spenke, Eberhard. "Die Diffusionstheorie der positiven Säule mit Berücksichtigung der stufenweisen Ionisierung," *Zeitschrift zur Physik*, 127: 221-242 (1950).
- Thompson, J. B. "Negative Ions in the Positive Column of the Oxygen Discharge," *Proc. Royal Society*, 73: 818-821 (1959).
- Tonks, L., and Langmuir, I. "A General Theory of the Plasma of an Arc," *Physical Review* 34: 876-922 (September, 1929).
- Valentini, H.-B. "Theoretical Description of the Radial Distributions of the Ions and of the Electrons in the Subnormal Positive Column," *Beiträge aus der Plasma-Physik* 19: 221-231 (1979).
- Valentini, H.-B. "Unified System of Differential Equations for Plasma and Boundary Layers," *Beiträge aus der Plasma-Physik* 20: 39-59 (1980).

- Valentini, H.-B. "The Calculations of the Concentrations, of the Radial Distributions, and of the Radial Particle Currents of Excited and of Doubly Charged Ions in Low Pressure Discharges," *Beiträge aus der Plasma-Physik* 20: 243-263 (1980).
- Valentini, H.-B. "Removal of singularities in the hydrodynamic description of plasmas including space-charge effects, several species of ions and non-vanishing ion temperature," *Journal of Physics D* 21: 311-321 (1988).
- von Engel, A. *Ionized Gases* (Second Edition). Oxford: Clarendon Press, 1965.
- Young, R. T. "Calculation of Average Electron Energies in He-Ne Discharges," *Journal of Applied Physics*, 36: 2324-2325 (1965).
- Whitaker, Marlin, Biondi, Manfred A., and Johnsen, Rainer. "Electron-temperature dependence of dissociative recombination of electrons with  $N_2^+ \cdot N_2$  dimer ions," *Physica Review A*, 24: 743-745 (August 1981).
- Wunderer, B. M. "Ambipolar Diffusion in a Nonuniform (sic) Plasma Containing Positive Ion Components," *IEEE Transactions of Plasma Science*, PS-6: 406-416 (December 1978).



## **VITA**

Major Thomas E. Gist was born on 12 December 1949 in Dallas, Texas. He graduated from high school in Fort Worth, Texas, in 1968, and attended Texas Christian University from which he received the degree of Bachelor of Science in Physics, Magna Cum Laude, in May 1972. Upon graduation, he received a commission in the USAF through the ROTC program. He served in the North American Air Defense Command Spacetrack and Missile Warning systems until his entry into the School of Engineering, Air Force Institute of Technology (AFIT), in June, 1972. He received the degree of Master of Science in Engineering Physics from AFIT in December, 1978. From AFIT he went to the Air Force Weapons Laboratory, where he performed laser diagnostics on various high energy lasers. In July, 1981, he returned to AFIT to enter the PhD program in Physics. In June, 1984, he arrived at the USAF Academy, where he taught physics and performed research in educational technology. In August, 1988, he became the Technical Area Manager (TAM) of the Advanced Plasma Physics Group at what is now the Wright Laboratory. He later served as the TAM for the Applied Electromagnetics Group, also at Wright Laboratory.

Permanent Address: 6021 Worrell Avenue

Fort Worth

Texas 76133

## REPORT DOCUMENTATION PAGE

17. APPROVAL  
18. DATE

1. AGENCY USE ONLY (Leave blank)

REPORT DATE

REPORT TYPE AND DATES COVERED

July 1992

Doctoral Dissertation

3. TITLE AND SUBTITLE

FUNDING NUMBERS

Multi-Ion Ambipolar Diffusion

5. AUTHOR(S)

Thomas E. Gist, Major, USAF

6. PERFORMING ORGANIZATION NAME(S) AND ADDRESS(ES)

PERFORMING ORGANIZATION  
REPORT NUMBER

Air Force Institute of Technology, WPAFB OH 45433-6583

AFIT/DS/ENP/92-1

9. SPONSORING/MONITORING AGENCY NAME(S) AND ADDRESS(ES)

SPONSORING/MONITORING  
AGENCY REPORT NUMBER

11. SUPPLEMENTARY NOTES

12a. DISTRIBUTION AVAILABILITY STATEMENT

12b. DISTRIBUTION CODE

Approved for public release; distribution unlimited

13. ABSTRACT (Maximum 200 words)

The continuity and momentum equations for electrons and multiple ion species are solved analytically and numerically using a new model for ambipolar diffusion. The general form of the model is valid for any quasi-neutral plasma for which the diffusion approximation is appropriate, including positive or negative ions, arbitrary geometries, and time dependence. The model provides criteria for determining when single ion diffusion theory is appropriate for describing multi-ion discharges, when a multi-ion proportional model is appropriate, and when a multi-ion nonproportional model is necessary. An expression is developed which provides a necessary condition for proportionality and provides the proportionality constant from the net source terms. Proportional analytic solutions are determined for uniform external ionization or single-step ionization by the bulk electrons in planar and cylindrical geometries, and double-exponential external ionization or bulk ionization and nonresonant charge transfer in planar geometries. Numerical comparisons are made to previous experimental and theoretical determinations of electron temperature, particle flux, or particle number densities. Numerical solutions for generic two-ion plasmas with recombination or charge transfer as volume losses and external or electron impact ionization sources provide scaling relationships for the effects of multiple ions on discharge parameters.

14. SUBJECT TERMS

Diffusion; plasmas (physics); diffusion coefficient; electron mobility; gas discharges; glow discharges; ambipolar diffusion

15. NUMBER OF PAGES

333

16. PRICE CODE

17. SECURITY CLASSIFICATION  
OF REPORT

Unclassified

18. SECURITY CLASSIFICATION  
OF THIS PAGE

Unclassified

19. SECURITY CLASSIFICATION  
OF ABSTRACT

Unclassified

20. LIMITATION OF ABSTRACT

UL